Biopharmaceutical characterization and formulation development of poorly water-soluble phytochemicals using *in vivo* predictive biphasic dissolution

Dissertation

zur

Erlangung des Doktorgrades (Dr. rer. nat.)

der

Mathematisch-Naturwissenschaftlichen Fakultät

der

Rheinischen Friedrich-Wilhelms-Universität Bonn

vorgelegt von

Marvin Benedikt Brenner

aus

Bremen

Bonn 2024

Angefertigt mit Genehmigung der Mathematisch-Naturwissenschaftlichen Fakultät
der Rheinischen Friedrich-Wilhelms-Universität Bonn

Gutachter/ Betreuer: Prof. Dr. Karl G. Wagner
Gutachter: Prof. Dr. Matthias Wüst

Tag der Promotion: 03.05.2024
Erscheinungsjahr: 2024

Meiner Familie

Die Dinge sind nie so, wie sie sind.

Sie sind immer das,

was man aus ihnen macht

Jean Anouilh

Abstract

Nature offers a vast variety of different substances, some of which are known to have health-beneficial effects on humans. Thus, many of these compounds are frequently used as dietary supplements or herbal medicinal products. However, biological effects are often limited by low water solubility and resulting insufficient bioavailability. Consequently, a need for the development of bioavailability-enhanced formulations arises.

To ensure efficient and cost-effective formulation development, researchers rely on *in vivo* predictive *in vitro* methods to determine the impact of different formulation principles on bioavailability. Addressing this issue, human pharmacokinetic data of five phytochemicals and their corresponding bioavailability-enhanced formulations was used to implement an *in vivo* predictive biphasic dissolution method (BiPHa+). BiPHa+ was applied for the characterization of 19 different curcumin (CUR), resveratrol, coenzyme Q10 (CoQ10), quercetin and astaxanthin (ASX) formulations.

Despite analyzing structurally diverse model extracts and regardless of the formulation principles tested, dissolution results in excellent agreement with the human pharmacokinetic data were obtained for all formulations. A comparison with conventional monophasic dissolution methods emphasized the advantages of the BiPHa+ in terms of powerful prediction. For the resveratrol, CoQ10, and ASX formulations the combination of aqueous non-sink dissolution with an overlaying organic absorption sink proved to be the optimal approach, as conventional methods failed to provide *in vivo* relevant dissolution data.

Upon analyzing commercial formulations of CoQ10 and ASX only slight improvements in bioavailability were found, highlighting the need for further development of improved formulations. Addressing this drawback, BiPHa+ was utilized as an *in vivo* relevant screening tool for subsequent formulation development.

Initially, CoQ10 was used as a model compound, and a screening process was conducted to identify the optimal polymers for manufacturing of solid dispersions. Kollidon® VA64 and hydroxypropyl cellulose (HPC)-SSL were found to be the most effective options. However, the combination of VA64 with Eudragit® EPO in ternary solid dispersions further improved the effect, resulting in 6-7 times higher CoQ10 concentration in the organic absorption sink of BiPHa+ compared to the commercial formulations.

Since none of the investigated polymers could stabilize CoQ10 in the amorphous state, the use of Syloid® XDP 3050 and Silsol® 6035 as mesoporous carriers for drug loading was identified as an alternative formulation principle. In order to investigate the effect of loading into silica for different lipophilic compounds, formulations containing CoQ10, ASX, probucol and lumefantrine were produced.

Using incipient wetness impregnation, drug loads up to 50% could be achieved. Shake flasks experiments revealed that an increase in drug load led to a significant increase in biorelevant medium solubility. This effect was consistent across all model compounds tested, resulting in an increase by a factor of up to 180. The use of both mesoporous carriers facilitated the stabilization of active ingredients in a non-crystalline form, while BiPHa+ measurements demonstrated a marked increase in the partitioning rate into the organic absorption sink.

List of publications

Parts of this thesis have been published or submitted for publication in peer-reviewed journals or as abstracts for poster/oral presentation.

Research articles:

- Brenner, M.B.; Flory, S.; Wüst, M.; Frank, J.; Wagner, K. Novel biphasic *in vitro* dissolution method correctly predicts the oral bioavailability of curcumin in humans. *J. Agric. Food Chem.*, **2023**, 71, 15632-15643, https://doi.org/10.1021/acs.jafc.3c04990
- Brenner, M.B.; Wüst, M.; Frank, J.; Wagner, K.G. *In vivo* predictive dissolution of the lipophilic phytochemicals *trans*-resveratrol, coenzyme Q10 and quercetin. *J. Drug Deliv. Sci. Technol.*, **2024**, 95, 105561, https://doi.org/10.1016/j.jddst.2024.105561
- Brenner, M.B.; Wüst, M.; Kuentz, M.; Wagner, K.G. High loading of lipophilic compounds in mesoporous silica for improved solubility and dissolution performance. *Int. J. Pharm*., **2024**, 654, 123946, https://doi.org/10.1016/j.ijpharm.2024.123946

Conference abstracts for oral presentation:

- Brenner, M.B.; Wüst, M.; Frank, J.; Wagner, K.G. Biphasische Freisetzung als Screening Plattform zur Abschätzung von Bioverfügbarkeitsunterschieden unterschiedlicher Curcuma-Formulierungen. 51. Deutsche Lebensmittelchemietage Bonn, **2023**, *Lebensmittelchemie*, 77, S3-019-S3-019, https://doi.org/10.1002/lemi.202359015

Conference abstracts for poster presentation:

- Brenner, M.B.; Wagner, K.G. Highly loaded mesoporous silica particles as an alternative formulation strategy for lipophilic compounds. 14th Pharmaceutics, Biopharmaceutics and Pharmaceutical Technology World Meeting, **2024**, Vienna, Austria

Acknowledgments

I wrote this thesis under the guidance of Professor Dr. Karl Gerhard Wagner at the Department of Pharmaceutics at the University of Bonn.

I would like to express my gratitude towards my doctoral supervisor, Prof. Wagner, for accepting me into his working group and assigning me an exciting topic. I am particularly thankful for the freedom he gave me, the numerous constructive discussions we had, and his helpful and intensive support in preparing this thesis.

Additionally, I would like to thank Prof. Dr. Matthias Wüst for being a reviewer of my doctoral thesis and allowing me to conduct the entire HPLC-based analysis in his laboratory. His feedback was always helpful and I would like to thank him for his general support.

I am also grateful to Prof. Dr. Andreas Schieber and Prof. Dr. Marc Hübner for their willingness to participate in the doctoral committee.

Prof. Dr. Jan Frank from the University of Hohenheim I would like to thank for providing the curcumin formulations and for the pleasant cooperation.

Furthermore, special thanks to Prof. Dr. Martin Kuentz from the University of Applied Sciences and Arts Northwestern Switzerland for his valuable scientific contribution and for the performance of the *in-silico* calculations of drug-silica interactions.

Many thanks to Dr. Katharina Dauer, Dr. Kristina E. Steffens and Tim Becker for the scientific discussions we had and the review of the manuscripts.

I would like to thank Dr. Maike Passon and Fabian Maretzky for their technical support, especially for the repairs of the HPLC.

A special thanks also goes to my office colleagues Jan Appelhaus, Maike Hafels, Alicia Stakemeier and Sebastian Klaus. Even though I wasn't there that often, the conversations in the office were always very funny and the regular visits to the cafeteria also helped to break up the working day. The meetings for a “Bürobier” also provided an opportunity to relax and chat. Dear Jan, your enthusiasm for this remains unsurpassed.

Moreover, I am very grateful to the working group for the warm welcome and the support whenever help was needed.

Personally, I would like to thank my friends and family who have always supported me through the years and gave me the motivation that was needed to finish this thesis.

Table of contents

List of abbreviations

Abbreviation	Definition
ACN	Acetonitrile
API	Active pharmaceutical ingredient
ASD	Amorphous solid dispersion
ASX	Astaxanthin
AUC	Area under the plasma concentration-time curve
BA	Bioavailability
BDMC	Bisdemethoxycurcumin
Bi-FaSSIF-V2	Biphasic dissolution adapted- fasted state simulated intestinal fluid-V2
BiPHa+	Fully automated, small-scale biphasic dissolution setup
CE	Capillary electrophoresis
CoQ10	Coenzyme Q10
CSD	Crystalline solid dispersion
CUR	Curcumin
DAD	Diode array detector
DCM	Dichloromethane
DL	Drug load
DMC	Demethoxycurcumin
DMSO	Dimethyl sulfoxide
DSC	Differential scanning calorimetry
DW	Detection wavelength
EPO	Eudragit® EPO
FaSSIF	Fasted state simulated intestinal fluid
FID	Flame ionization detector
GC	Gas chromatography
HCl	Hydrochloric acid
HPC	Hydroxypropyl cellulose
HPLC	High performance liquid chromatography
HPMC AS	Hydroxypropyl methylcellulose acetate succinate

HS	Headspace
i.v.	Intravenous application
IVIVR	*In vitro-in vivo* relationship
K12PF	Kollidon® 12 PF
L100-55	Eudragit® L 100-55
LLPS	Liquid – liquid phase separation
LU	Lumefantrine
MeOH	Methanol
MS	Mass spectrometry
MW	Molecular weight
NIR	Near-infrared spectroscopy
NMR	Nuclear magnetic resonance
P407	Kolliphor® P407
PB	Probucol
PhEur	European Pharmacopeia
PPM	Parts per million
PTFE	Poly-(tetrafluoroethylene)
Rf	Retarding-front
RP	Reversed phase
SD	Standard deviation
SEDDS	Self-emulsifying drug delivery system
SL	Stock solution
TLC	Thin layer chromatography
TOPS	Total outer surface area
TRIS	Tris(hydroxymethyl)aminomethane
USP	United States Pharmacopeia
VA 64	Kollidon® VA 64
WD	Water dispersible
XRPD	X-ray powder diffraction

List of figures

List of tables

1. General introduction

1.1. Natural products with biological activity in humans

Natural products are an essential source of compounds with biological activity in humans [1,2]. In many regions of the world, they form an important basis in the primary healthcare of people and are regularly taken as medicine or dietary supplement [3]. In particular, plants and extracts produced from plant parts are of central importance due to their extraordinary diversity of different ingredients. Nonetheless, a wide array of organisms generate primary and secondary metabolic products with remarkable biological properties. Among these, microorganisms, fungi, algae, and marine animals have gained considerable attention too [4–7]. Focusing on the vast variety of substances and substance classes produced by the aforementioned organisms, a need arises to systematically classify them. The most important substance classes with some example compounds are listed below.

Table 1: Most important substance classes occurring in natural products used for treatment of various diseases, including some example compounds

Substance class	Example compounds
Alkaloids [8,9]	Capsaicin, Morphine, Nicotine, Vincristine, Caffeine
Carbohydrates [10]	Glucosamine, Hyaluronic acid, Heparin, Mannitol
Fatty acids [11,12]	Eicosapentaenoic acid, Docosahexaenoic acid
Peptides and Proteins [13,14]	Exenatide, Ziconotide, Bromelain
Polyketides and	Curcumin, Gingerol, Hyperforin
Polyphenols [15,16]	Daidzein, Resveratrol, Quercetin, Theaflavin
Steroids and	Brassicasterole, Boswellic acid, Withaferine A
Terpenes [17–19]	Coenzyme Q10, Astaxanthin, β-Carotene

Owing to the wide variety of substance classes and their diverse properties, it comes as no surprise that purified natural substances or extracts are utilized to treat numerous common diseases. These treatments are predominantly aimed at addressing metabolic and cardiovascular diseases, neurologic and neurodegenerative diseases, cancer, and anti-infective applications [8,11,12,15,20].

1.1.1. Comparative analysis of extracts versus conventional active pharmaceutical ingredients

When comparing conventional active pharmaceutical ingredients (API)s to natural products or extracts from natural sources, noticeable distinctions evolve. In general, conventional APIs contain only one or a small number of active ingredients with a precisely known identity, structure, and purity. Prior to the manufacturing of the final drug product, the active ingredient(s) usually undergo various purification steps to eliminate impurities from the production process, and the efficiency of these procedures is confirmed analytically [21]. As a result, the biological effects caused by the application can be precisely attributed to one (or few) active ingredient(s) or their metabolites [22].

Extracts are often complex mixtures that consist of numerous substances, sometimes even containing over 20 structurally related components. For example, when examining astaxanthin-containing extracts from microalgae, a study by Miao et al. found the presence of 23 different astaxanthin derivatives in the extract [23]. This makes it challenging, if not impossible, to determine the effects of individual compounds when *in vivo* studies are conducted. While not all extracts contain such a large number of structurally related active ingredients, they are derived from natural sources like plant parts, which contain both the desired substances, usually in low concentrations, and various other matrix components in much higher quantities [2].

Furthermore, the extraction process applied significantly affects the range of different substances present in the crude extract. This means that using different solvents, such as organic ones with different polarities or solvent mixtures, can result in entirely different crude extracts from a single source material [24]. Determining the pharmacological impact of each individual component found in an extract can often be a challenging task. As a result, extracts are frequently utilized as a combination of their components, which are then recognized as the "active ingredient" for therapeutic purposes. Often extracts are then evaluated by the content of substances with known biological activity and adjusted to a defined concentration of these compounds [25,26]. In such instances, it is critical to maintain strict control over the extraction process and the conditions applied to ensure optimal and reproducible results [24]. In addition, the content of active ingredients in the starting material depends on environmental influences such as the availability of nutrients or external stress factors on the source organism [27].

1.2. Analytical characterization of complex mixtures

As elucidated in chapter 1.1.1, natural products and extracts made thereof usually consist of complicated matrices, wherein the desired substance(s) are present in comparatively low concentrations, alongside other components that are not relevant to the biological activity [2]. While these matrix components themselves may not affect the biological activity, they can complicate analytical processes. Furthermore, when multiple active substances with comparable structures are present, due to similarities in their UV/VIS spectra it can be difficult to differentiate between them using basic detection methods such as UV/VIS spectrophotometry. This often results in them being classified as sum parameters [28]. To overcome this difficulty and conduct a comprehensive analysis, it is essential to use chromatographic separation techniques, followed by the detection and quantification of individual constituents. High performance liquid chromatography (HPLC), gas chromatography (GC) or capillary electrophoresis (CE) hyphenated with a suitable detector (e.g. UV/VIS diode array detector (DAD), flame-ionization-detector (FID) or mass spectrometer (MS)) are often used for this purpose [29]. Mass spectrometry offers a distinct advantage over other detection techniques as it allows for detection limits to reach very low levels owing to the high sensitivities of the detector. Additionally, it enables the definite identification of the compounds separated in the chromatographic process by their characteristic fragmentation pattern [30]. (High performance) Thin-layer chromatography (TLC) is a method that primarily offers qualitative information. Nonetheless, it is highly suitable as a simple and rapid screening technique for ensuring identity for example of a new batch [31,32].

Nevertheless, most chromatographic analysis, at least in the field of target analytics, are based on the principle that the substances of interest are known. However, in cases where the identity of at least some substances in the sample is not known, extracts can alternatively be assessed by evaluating the sum of all its ingredients with respect to specific individual properties. For example, the total antioxidant activity of an extract can be evaluated as a sum parameter using *in vitro* assays [33].

Apart from the chromatographic and *in vitro* techniques aforementioned, nuclear magnetic resonance (NMR), near-infrared spectroscopy (NIR) or biosensors can also be utilized for the purpose of capturing data on the composition of the sample [33–35].

1.3. Bioavailability assessment of multi-component extracts in humans

Oral bioavailability (BA) of extracts, also referred as nutraceuticals is commonly defined as the fraction of the ingested biocomponent that reaches the systemic circulation to be distributed to organs and tissues and finally achieve the bioactivity [36,37].

$$BA = F_C \; x \; F_{B*} \; x \; F_{A*} \; x \; F_{T*} \qquad \text{(Equation 1)}$$

Whereby F_C is the fraction of a biocomponent in the ingested nutraceutical, F_{B*} is the fraction accessible to intestinal absorption (bioaccessibility), F_{A*} is the fraction absorbed through the intestinal wall, and F_{T*} is the fraction left after chemical and enzymatic transformation that enters the systemic circulation [37,38].

Typically, BA is measured in *in vivo* pharmacokinetic studies by comparing the relative percentage of the area under the curve (AUC) after oral application of a formulation to that after intravenous (i.v.) application [37]. Therefore, blood samples are collected at predefined timepoints and subjected to laboratory analysis to ascertain the concentrations of active substances or their metabolites. Due to their typically low concentrations, chromatographic separation techniques hyphenated with sensitive detectors such as fluorescence detectors or MS are essential [39]. Additionally, some natural products undergo extensive metabolism upon absorption, such as glucuronidation or sulfation, leading to a reduction in the concentration of free active substance below limit of detection. Therefore, enzymatic cleavage is necessary prior to quantification [40,41].

When using i.v. application, the active ingredients enter the bloodstream directly without any release, absorption, or metabolization occurring beforehand. Therefore, the AUC_{iv} serves as a reference point with BA assumed to be 100% [42]. However, i.v. application is not always safe for natural products, making it difficult to measure BA after oral application relative to i.v. reference data. In these cases, a reference formulation is first applied orally, which is assumed to exhibit no BA improvement, such as the native and unformulated extract. After an appropriate washout period, the bioavailability-enhanced reference formulation is applied to the same subject, and the AUCs of both formulations, at the same oral dosage, are compared with each other. The increase in AUC is reported as the fold difference and is subsequently used to evaluate the performance of the formulation developed [40,43,44].

1.4. Formulation strategies for bioavailability impaired poorly soluble extracts

Since many natural products exhibit low BA in humans as a result of their poor solubility, susceptibility to degradation within the gastrointestinal tract, or rapid metabolization, it is necessary to develop formulations with improved BA to enlarge their therapeutic potential [40,45,46]. A wide variety of different strategies are described in the literature. Nevertheless, there exist two primary approaches for enhancing the BA of natural products. The first method involves improving water solubility to elevate absorption via the enterocytes, thereby heightening BA [40,43,45].

Table 2: Formulation principles targeting an improvement of water solubility.

Formulation principle	Example market formulations
Micellar inclusion complexes	NovaSOL® Vineatrol, NovaSOL® Curcumin
Cyclodextrin inclusion complexes	Cavacurmin®, CavaQ10®
Liposomes/ Phytosomes	Meriva®, Quercefit®, Longvida®
Nanoparticles	Nano Quercetin, Theracurmin®
Amorphous formulation	curcuRouge®

The second method entails inhibiting metabolizing enzymes in enterocytes and/or hepatocytes or efflux transporters in enterocytes to amplify the proportion of unconjugated active substances in the blood stream, which is typically responsible for the biological effect [47–49].

Table 3: Formulation principles targeting the inhibition of metabolic enzymes or efflux transporters.

Formulation principle	Example market formulations
Addition of Piperine	Resveratrol- Piperine, Pro Curmin Complete II
Addition of Turmeric oils	BCM-95®

It has been reported that the principle of inhibiting metabolizing enzymes may not be the most efficient in terms of BA enhancement, when compared to solubility improvement [41]. Furthermore, there exist specific formulation approaches, particularly for highly lipophilic compounds like tetraterpenes, that seek to achieve absorption through the lymphatic pathway in parallel with dietary lipids, via the inclusion of lipids into the formulation, and thereby enhance the absorption characteristics [43].

1.5. *In vivo* predictive *in vitro* methods for bioavailability assessment

During the development of BA - enhanced formulations, a reliable testing system that can accurately estimate the impact of different formulation principles on the *in vivo* bioavailability of active ingredients is crucial. Evaluating bioavailability *in vivo* can be both costly and time-consuming, making it impractical for assessing formulations in their developmental phase. Consequently, several *in vitro* techniques have been invented to predict *in vivo* outcomes [37].

The United States Pharmacopeia (USP) enumerates several dissolution techniques such as the paddle or basket apparatus, which may be potential candidates for such predictive assays [50]. However, these systems only represent the human gastrointestinal tract in a very simplified way, which results in a loss of *in vivo* predictivity [28].

To overcome these limitations, testing methods which better reflect *in vivo* conditions in terms of pH values, solvent volume and residence time have been developed, such as *in vitro* digestion models [41,51] or biphasic dissolution approaches [28,52,53]. *In vitro* digestion models use sequential mouth, gastric, and intestinal digestion phases to simulate the conditions in the human gut. In this experimental procedure, a medium similar to the conditions of the human digestive system is prepared through the manual addition of buffer and enzyme solutions. Subsequently, the dissolution behavior of the target molecule is studied. These models can be single or multiple-compartment static, semi-dynamic or fully dynamic systems [54].

In contrast, during biphasic dissolution, samples are introduced into a biorelevant aqueous medium under non-sink conditions. During the dissolution measurement the pH value of the medium is adjusted and an absorption-sink is created by covering the aqueous medium with an organic medium, which is assumed to be predictive for the *in vivo* conditions in the small intestine [28,52].

Apart from the aforementioned techniques, simulating of permeation directly through biological barriers, specifically the intestinal wall, by using cell models based on Caco-2 monolayers is also a possible option [41]. Furthermore, combination models that enable the recording of active substance dissolution in biorelevant medium while simultaneously monitoring the process of diffusion across the intestinal wall have been introduced [55].

2. Evaluation of analytical and physicochemical properties of poorly soluble extracts of natural origin

2.1. Introduction

The diversity of substance classes found in nature (consider section 1.1) makes it difficult to classify them. Nevertheless, by focusing solely on their water solubility, we can distinguish between two categories: those that readily dissolve in the solvent volume present in the gastrointestinal tract and those with restricted solubility in water. The latter type of compounds tends to have lower BA compared to their more soluble counterparts, due to their inability of crossing the intestinal membrane in undissolved state.

Polyphenols are a diverse and widely distributed group of natural products that have gathered considerable interest in science and development (**Table 4**) [56]. This is predominantly related to their antioxidant properties, which have been widely studied. Additionally, polyphenols demonstrate a multitude of other properties, which makes them interesting for health care applications. However, a significant challenge associated with some polyphenols is their limited water solubility [57].

Table 4: Classification of polyphenols, including substance class name, basic structure and carbon framework, and some example compounds.

Substance class	General structure	Carbon framework	Example compounds
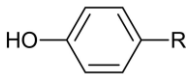	Simple phenols	C_6, C_6C_1, C_6C_2	Arbutin, Hydroquinone
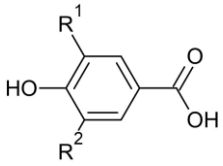	Phenol carboxylic acids	C_6C_1	Gallic acid, Vanillic acid
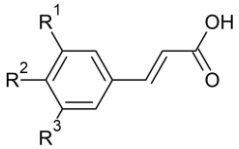	Phenylpropanoids	C_6C_3	Coumaric acid, Ferulic acid, Curcumin (Dimer)
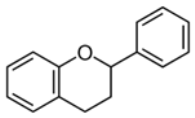	Flavonoids	$C_6C_3C_6$	Quercetin, Naringenin
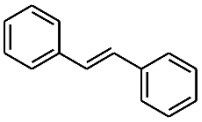	Stilbenes	$C_6C_2C_6$	Resveratrol ε-Viniferine

In **Table 4**, various structural types of polyphenols are presented, of which flavonoids, stilbenes, and some phenylpropane derivatives are particularly interesting for health care applications. Substances like curcumin (CUR), quercetin, and *trans*-resveratrol (refer **Figure 1** and **Figure 2**) are widely used as nutritional supplements and herbal medicinal products to assist with a range of health issues. Their antioxidant, anti-inflammatory, and anticancer properties are of particular interest [58–60].

However, before using extracts enriched with polyphenols as nutritional supplements or herbal medicinal products it is crucial to properly analyze and characterize them. This analysis provides information about the active phenols present and especially about glycosylation patterns and oligomerization, which helps determine their therapeutic value. To effectively separate the polyphenols, reversed-phase (RP)-HPLC is commonly used, with standard C18 columns (also in the form of core-shell particles or monolithic columns) and water-containing eluent mixtures being the preferred options [61]. To detect the polyphenols, various detectors are available, including DAD and fluorescence detectors, as well as mass spectrometers (MS). Tandem MS, in particular, can provide additional structural information about the analytes and is thereby the preferred option by many laboratories [30,61].

Besides polyphenols, terpenoid compounds and quinones, like astaxanthin and coenzyme Q10 (CoQ10) (refer **Figure 2**), are also recognized for their antioxidant properties and having various health beneficial effects [62]. Due to their structure related very high lipophilicity, these substances experience poor water solubility [63]. In addition, terpenoid compounds often occur in nature as complex mixtures of unesterified and esterified compounds with various fatty acids, including single and double esterified molecules [64]. Due to the presence of a long, conjugated polyene system, cis/trans isomerism is also of distinct interest. To quantify individual substances in these complex mixtures, chromatographic separation techniques, such as liquid chromatographic methods (HPLC) using C18 RP phases, are frequently used. In this instance, low-temperature stability concerns hinder the use of GC methods [64]. The coupling of HPLC with DAD detectors plays a unique role in detecting cis-trans isomerism. In addition, MS, in particular tandem MS, is used for structure elucidation. By combining both detection techniques, Etzbach et al. (2018) achieved optimal delineation of the individual substances and isomers [65].

The objective of this chapter was to provide a comprehensive overview of 19 extract-based formulations used in this thesis and their analytical properties. These comprised eight curcumin-formulations, four *trans*-resveratrol formulations, three coenzyme Q10 formulations, two quercetin formulations, and two astaxanthin formulations.

To achieve this, all formulations were dissolved in a suitable solvent, and their active substance content was analyzed using C18 RP-HPLC coupled with a UV/VIS detector. Furthermore, important physicochemical properties of the pure active substances (structures shown in **Figure 1** and **Figure 2**) were analyzed, including solubility behavior in various media, pK_a values, and log $D_{7.4}$, using HPLC and shake flask methods.

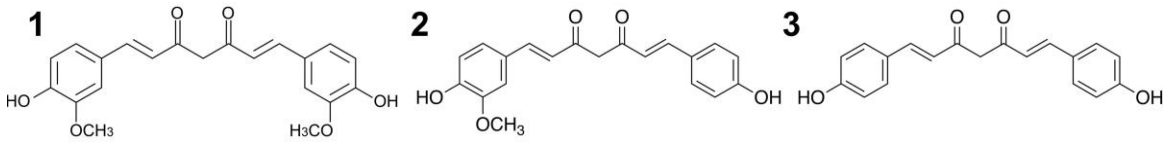

Figure 1: Chemical structures of pure curcumin (CUR) (**1**), demethoxycurcumin (DMC) (**2**) and bisdemethoxycurcumin (BDMC) (**3**).

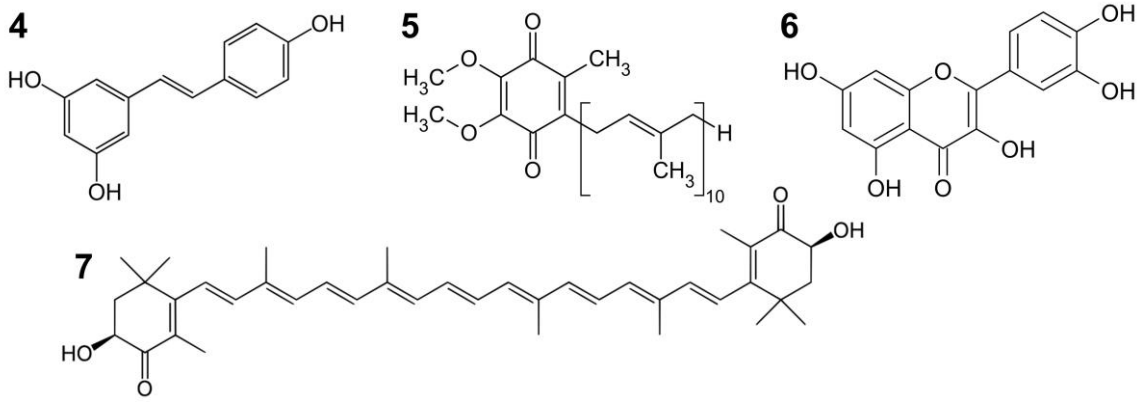

Figure 2: Chemical structures of pure *trans*-resveratrol (**4**), coenzyme Q10 (CoQ10) (**5**), quercetin (**6**) and astaxanthin (ASX) (**7**) (shown as unesterified molecule; the *Haematococcus pluvialis* extract contains mainly mono- and diesters).

2.2. Analytical characterization of model extracts and formulations based thereof in terms of active substance content

Parts of this chapter have been published in peer-reviewed research articles [28,66]. Each figure was created by the thesis author. Taking or adapting of figures is marked in the corresponding figure.

2.2.1. Curcuma formulations

All Curcuma formulations contained varying proportions of the three main curcuminoids: curcumin (CUR), demethoxycurcumin (DMC), and bisdemethoxycurcumin (BDMC) (see **Figure 3** and **Table 5**). These are biosynthesized by *Curcuma longa* L. and, due to their very similar structure and physicochemical properties, were usually extracted together. The percentage of CUR ranged from 74.5% to 89.2%, while DMC ranged from 10.5% to 22.0%, and BDMC varied from 0.3% to 3.6%. The γ-cyclodextrin complex, extract with adjuvants, and submicron-particles had higher CUR fractions (80.1%, 82.8%, and 89.2%, respectively) and lower DMC and BDMC fractions. The total curcuminoid content varied extensively across formulations, ranging from 62.7 mg/g in the micellar curcumin to 877.6 mg/g in the native extract. Generally, the water-solubility optimized formulations contained less curcuminoids (62.7 mg/g to 301.6 mg/g) due to the functional excipients used in these formulations [28].

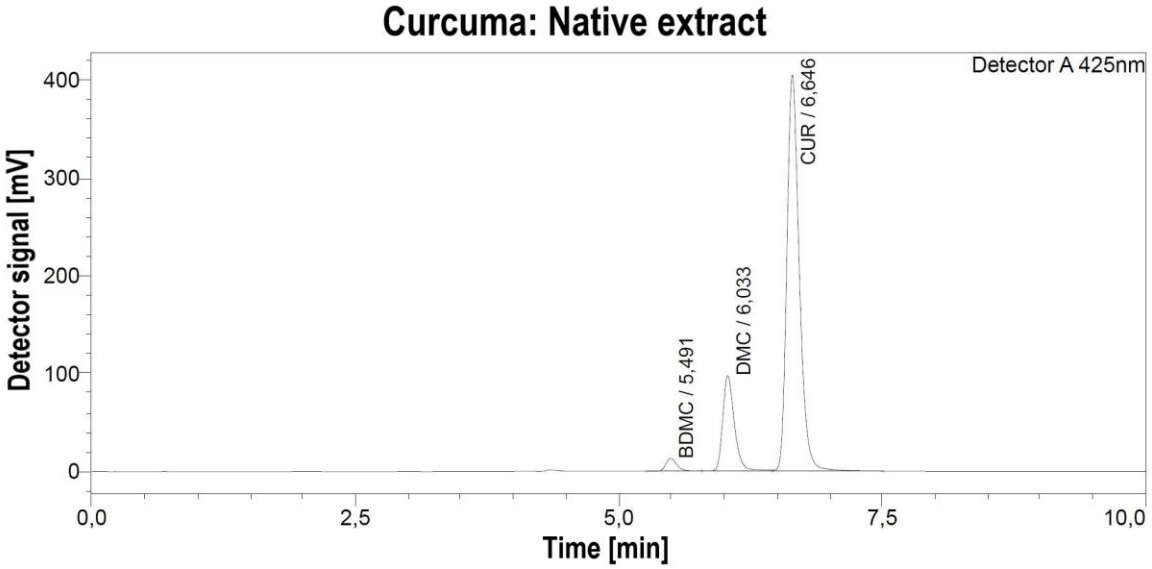

Figure 3: Example chromatogram of native Curcuma extract (10 mg in 200.0 mL MeOH; 10 µL injection volume); CUR = curcumin, DMC = demethoxycurcumin, BDMC = bisdemethoxycurcumin.

Table 5: Curcuma extracts/ formulations used for dissolution experiments, including their absolute [mg/g] and relative (%) content (mean ± SD) of curcumin (CUR); demethoxycurcumin (DMC) and bisdemethoxycurcumin (BDMC). Adapted from Brenner et al., 2023 [28]. Copyright 2023 American Chemical Society.

Formulation	**CUR [mg/g]**	**DMC [mg/g]**	**BDMC [mg/g]**	**Total [mg/g]**
	relative amount (%)			
Micelles	47.3 ± 0.2 (75.4 ± 0.4)	13.2 ± 0.1 (21.0 ± 0.1)	2.2 ± 0.0 (3.6 ± 0.0)	62.7 ± 0.3
Cyclodextrin	120.2 ± 6.2 (80.1 ± 4.1)	26.5 ± 1.4 (17.6 ± 0.9)	3.4 ± 0.2 (2.3 ± 0.1)	150.1 ± 7.8
Phytosomes	143.2 ± 1.1 (77.0 ± 0.6)	38.3 ± 0.4 (20.6 ± 0.2)	4.4 ± 0.1 (2.4 ± 0.0)	186.0 ± 1.6
Submicron particle	269.1 ± 2.5 (89.2 ± 0.8)	31.6 ± 0.3 (10.5 ± 0.1)	0.8 ± 0.0 (0.3 ± 0.0)	301.6 ± 2.8
Native extract	662.6 ± 17.2 (75.5 ± 2.0)	192.9 ± 5.3 (22.0 ± 0.6)	22.0 ± 0.7 (2.5 ± 0.1)	877.6 ± 23.2
Adjuvants	236.0 ± 7.5 (82.8 ± 2.6)	40.4 ± 1.4 (14.2 ± 0.5)	8.6 ± 0.4 (3.0 ± 0.2)	285.0 ± 9.2
Turmeric oils	650.4 ± 22.3 (74.5 ± 2.6)	193.2 ± 6.7 (22.1 ± 0.8)	29.8 ± 1.0 (3.4 ± 0.1)	873.4 ± 30.0
Liposomes	178.9 ± 2.4 (76.7 ± 1.0)	48.6 ± 0.7 (20.8 ± 0.3)	5.7 ± 0.1 (2.4 ± 0.0)	233.2 ± 3.2

2.2.2. Resveratrol formulations

The *trans*-resveratrol contents of the tested formulations differed considerably. Veri-te™ resveratrol had the highest content at 989.0 mg/g, while grapevine-shoot extract micelles had the lowest at 4.4 mg/g (**Table 6**). Along with *trans*-resveratrol monomers, the grapevine-shoot extract and its corresponding micellar formulation also contained oligomers, mainly *trans*-ε-viniferine, along with some other resveratrol oligomers [40]. Although the oligomers were partially visible at the deception wavelength of 306 nm (small peak at 6 min), they were not quantified (**Figure 4**). Similar to Curcuma formulations, water-solubility optimized formulations contained less resveratrol due to the functional excipients required for solubility optimization. In particular, the quantities of surfactant (polysorbate 80 and polysorbate 20) required for micellization led to a noticeable reduction in resveratrol content from 110.3 to 4.4 mg/g.

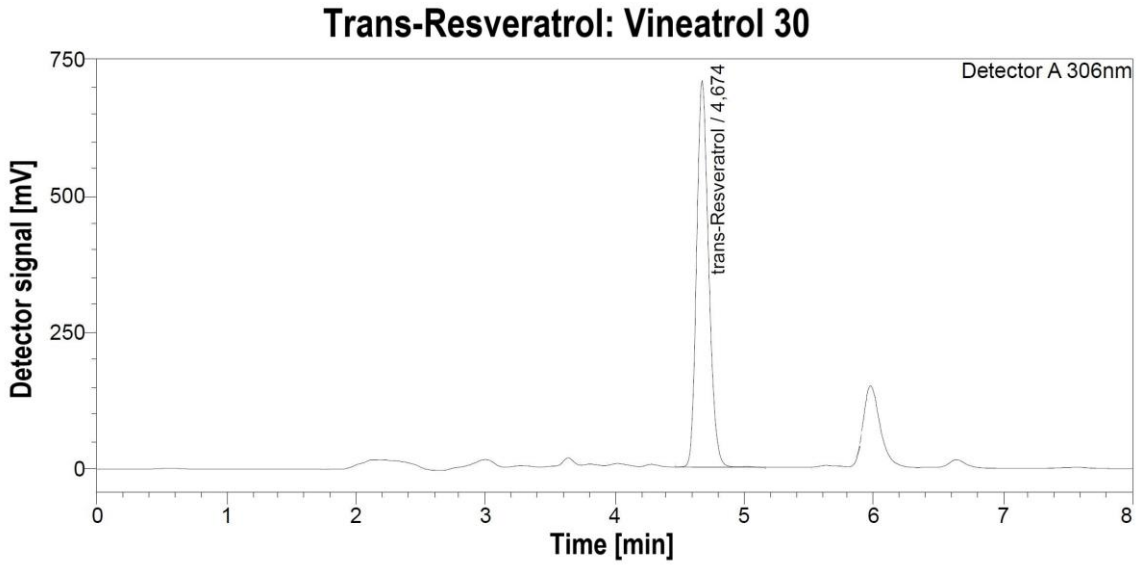

Figure 4: Example chromatogram of Vineatrol® 30 (*trans*-resveratrol containing grapevine-shoot extract; 30 mg in 50.0 mL MeOH; 10 µL injection volume).

Table 6: *Trans*-resveratrol content of the extracts/ formulations used for dissolution experiments (mean ± SD). Partially adapted from Brenner et al., 2024 [66].

Name	Formulation	Content [mg/g]
Vineatrol® 30	Grapevine-shoot extract	110.3 ± 0.8
Vineatrol® 30 micelles	Grapevine-shoot extract micelles	4.4 ± 0.0
VeriSperse™	water dispersible (WD) *trans*-resveratrol	915.8 ± 8.4
Veri-te™	purified *trans*-resveratrol	989.0 ± 6.3

2.2.3. Coenzyme Q10 formulations

Similar to the previously mentioned formulations, the coenzyme Q10 (CoQ10) containing formulations also utilized an extract of natural origin. However, the extract underwent extensive purification to ensure that only a small number of accompanying substances was present. Consequently, the non-formulated CoQ10 extract contained a high active ingredient content of 976.5 mg/g and the HPLC chromatogram did not show any peaks related to impurities (**Figure 5**). The formulation as micellar inclusion complex reduced the CoQ10 content to 53.3 mg/g, whereas the oily dispersion formulation still had a content of 334.5 mg/g (see **Table 7**).

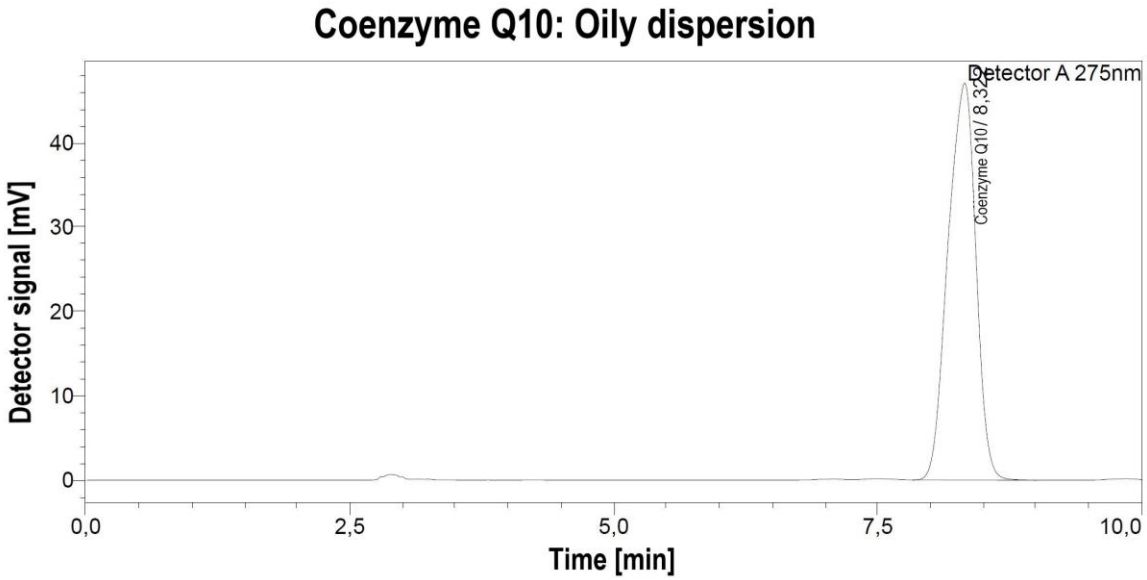

Figure 5: Example chromatogram of coenzyme Q10 oily dispersion (20 mg in 50.0 mL DCM; 10 µL injection volume).

Table 7: Coenzyme Q10 (CoQ10) content of the extracts/ formulations used for dissolution experiments (mean ± SD). Partially adapted from Brenner et al., 2024 [66].

Name	Formulation	Content [mg/g]
Coenzyme Q10	Purified CoQ10	976.5 ± 15.9
Nature Made® CoQ_{10}	Oily dispersion	334.5 ± 15.3
NovaSOL® Q	CoQ10 micelles	54.3 ± 0.3

2.2.4. Quercetin formulations

Considering the quercetin formulations, highly purified quercetin with a purity of 976.6 mg/g was used as the unformulated reference compound. However, the phytosomes contained an extract sourced from the flower buds of *Sophora japonica* L [67]. This extract also contains a small amount of other flavonoids like rutin that can be detected at 370 nm (as depicted in **Figure 6**) [68]. As a result of the incorporation of sun flower lecithin and other food-grade excipients, the quercetin content in the phytosomes formulation has been reduced to 372.8 mg/g (refer to **Table 8**).

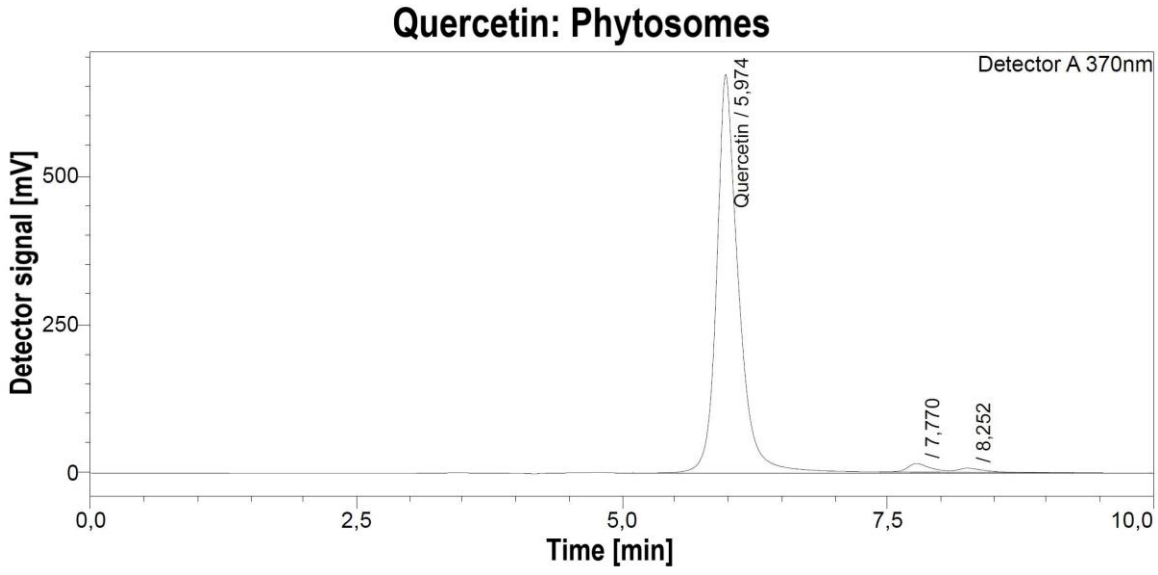

Figure 6: Example chromatogram of quercetin Phytosomes® (20 mg in 50.0 mL MeOH; 10 µL injection volume).

Table 8: Quercetin content of the extracts/ formulations used for dissolution experiments (mean ± SD). Partially adapted from Brenner et al., 2024 [66].

Name	Formulation	Content [mg/g]
Quercetin	crystalline quercetin	976.6 ± 0.2
Quercefit®	quercetin Phytosomes®	372.8 ± 8.8

2.2.5. Astaxanthin formulations

Among all analyzed extracts and formulations made therefrom, those containing astaxanthin (ASX) were the most complex in composition. **Figure 7** displays the chromatogram of the oleoresin obtained from the marine microalgae *Haematococcus pluvials* through supercritical CO_2 extraction. This extract was found to be comprised of various compounds with maximum absorption at 474 nm, including mono- and diesters of ASX with different dietary fatty acids of varying chain lengths [23]. To simplify, the ASX content was presented as the sum of mono- and diesters of ASX (sum of area of all peaks eluting from 20 min onwards) (**Table 9**). As unformulated extract contained 101.0 mg/g ASX, the micellar inclusion complex produced thereof consisted of only 15.0 mg/g ASX.

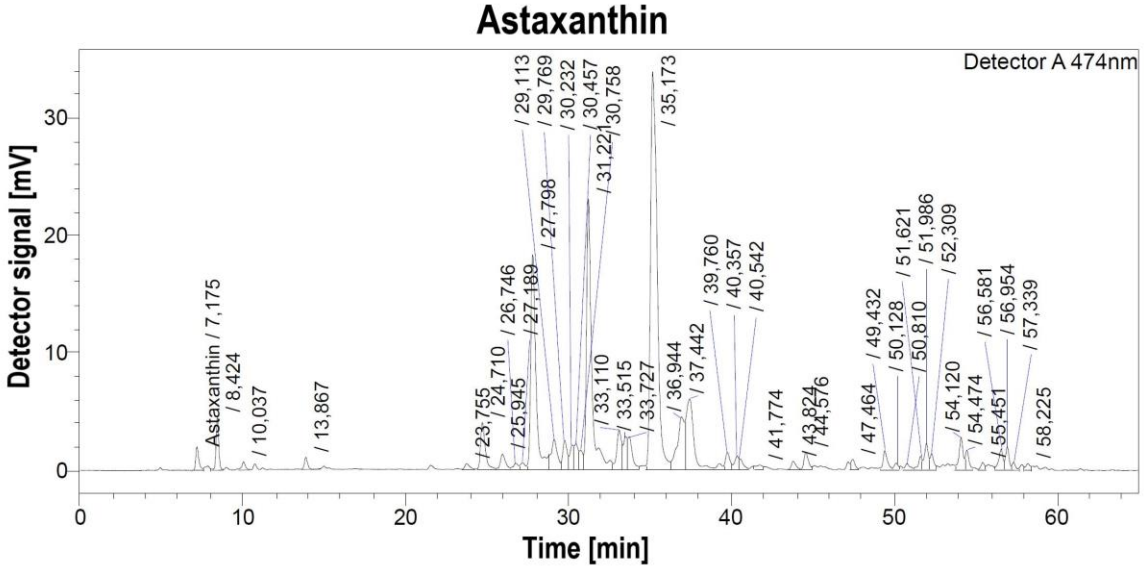

Figure 7: Example chromatogram of astaxanthin (astaxanthin enriched *Haematococcus pluvialis* oleoresin; 100 mg in 50.0 mL DCM; 1 µL injection volume); quantified by the sum of astaxanthin mono- and diesters eluting from 20 min onwards.

Table 9: Astaxanthin content of the extracts/ formulations used for dissolution experiments (mean ± SD).

Name	Formulation	Content [mg/g]
Astafit® Oleoresin	Astaxanthin enriched *Haematococcus pluvialis* oleoresin	101.0 ± 2.7 [a]
Oleoresin micelles	Astaxanthin micelles	15.0 ± 0.5 [a]

[a] both formulations contained a mixture of mono- and diesters (content is given as sum)

2.3. Determination of physicochemical properties of the active ingredients underlying the poorly soluble model extracts

Apart from quantifying active ingredients utilizing HPLC, we also conducted an analysis of basic physicochemical characteristics such as solubility in various media, pK_a value, and log $D_{7.4}$ value of the ingredients mentioned in section 2.2. **Table 10** and **Table 11** contain the results of these measurements. All three curcuminoids (CUR, DMC, BDMC), *trans*-resveratrol, and quercetin possessed pK_a values, and thus proteolysis properties, that were of relevance in the physiological pH range of up to 7. Accordingly, their ionization at varying pH levels is presented in **Figure 8** - **Figure 10**.

Table 10: pK_a values (calculated), saturation solubility in various media (0.1 N HCl, phosphate buffer pH 6.8, Bi-FaSSIF-V2 pH 6.8 and 1-decanol; determined by shake flask method), log $D_{7.4}$ (determined by HPLC) and detection wavelength of CUR = curcumin, DMC = demethoxycurcumin and BDMC = bisdemethoxycurcumin. Adapted from Brenner et al., [69]. Copyright 2023 American Chemical Society.

Parameter	CUR	DMC	BDMC
pK_a [a]	(1) 6.8 (2) 8.6 (3) 9.1	(1) 6.6 (2) 8.5 (3) 9.0	(1) 6.8 (2) 8.7 (3) 9.2
S (0.1 N HCl) [µg/mL]	0.2 ± 0.0	0.2 ± 0.1	0.3 ± 0.1
S (Buffer pH 6.8) [µg/mL]	0.3 ± 0.1	0.2 ± 0.1	0.2 ± 0.1
S (Bi-FaSSIF-V2) [µg/mL]	0.5 ± 0.1	0.4 ± 0.1	0.7 ± 0.3
S (1-decanol) [µg/mL]	1036.0 ± 23.3	331.0 ± 19.0	66.3 ± 7.5

Parameter	CUR	DMC	BDMC
Log $D_{7.4}$	3.50	3.58	3.64
wavelength (aqueous medium) [nm]	430	430	430
wavelength (1-decanol) [nm]	440	440	440

[a] pK_a values were calculated by ADMET predictor 9.5 (Simulations Plus Inc., Lancaster, CA)

The data presented in **Table 10** indicates that all curcuminoids had physiologically relevant pK_a values ranging between 6.6 and 9.2. Due to their limited water solubility and instability at alkaline pH levels, all pK_a values were predicted. At neutral pH values, the proton of the vinylogous carboxylic acid dissociates first. The deprotonation leads to a color change of the molecule from yellow to red. At the same time, the decomposition rate increases sharply due to chain cleavage [70]. When the pH of the medium increases further, first one and then both phenolic groups were deprotonated (**Figure 8**).

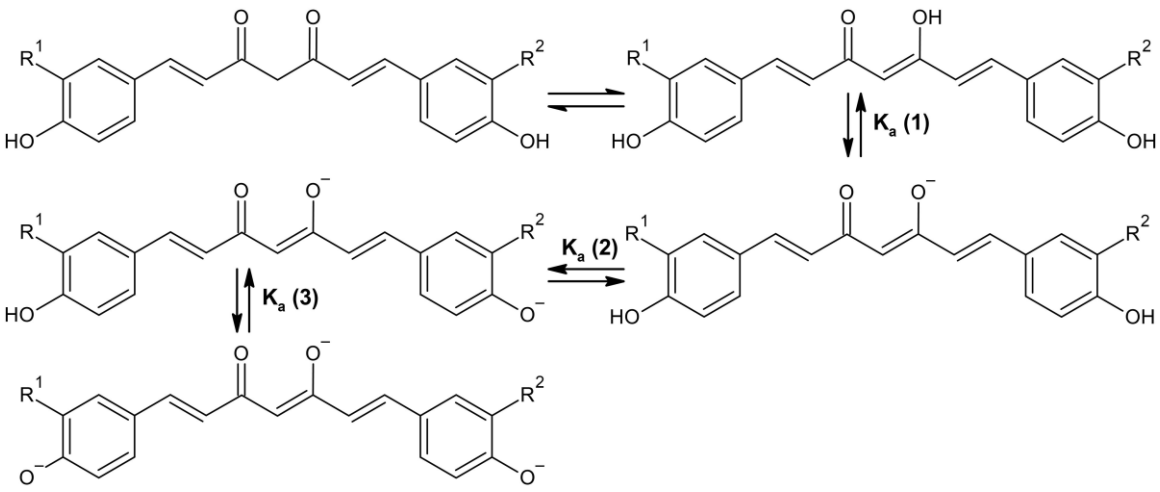

Figure 8: Keto-enol tautomerism and ionization of curcuminoids (curcumin: R^1, R^2 = OCH_3; demethoxycurcumin: R^1 = OCH_3, R^2 = H; bisdemethoxycurcumin R^1, R^2 = H) as a function of the pH of the medium (see pK_a values 1-3) in **Table 10**.

Related to the structural similarity of all three curcuminoids, their log $D_{7.4}$ values were comparable and ranged from 3.50 to 3.64. The high lipophilicity of the curcuminoids limited their water solubility. Thus, the aqueous solubility was measured to be less than 1 µg/mL for CUR, DMC, and BDMC and ranged from 0.2 to 0.3 µg/mL in surfactant free medium. No pronounced pH dependent solubility shift was observed. In the presence of sodium-taurocholate and lecithin (Bi-FaSSIF-V2), micellization occurred and the solubility

of curcuminoids was 2-3 times higher than in a surfactant-free medium [41]. However, all aqueous media provided solubility-limited non-sink dissolution conditions, as aqueous solubility remained below 1 µg/mL even when biorelevant surfactants were added.

In contrast, the 1-decanol solubility was much higher. CUR dissolved up to 1036.0 µg/mL in 1-decanol, while DMC dissolved up to 331.0 µg/mL and BDMC reached concentrations of up to 66.3 µg/mL (**Table 10**).

The absorption maximum of all three curcuminoids was at 430 nm in the aqueous medium and was shifted to a slightly higher wavelength of 440 nm in 1-decanol.

Table 11: pK_a values, saturation solubility in various media (0.1 N HCl, phosphate buffer pH 6.8, Bi-FaSSIF-V2 pH 6.8 and 1-decanol; determined by shake flask method), log $D_{7.4}$ and detection wavelength of *trans*-resveratrol, coenzyme Q10, quercetin and astaxanthin (mixture of mono- and diesters). Partially obtained from Brenner et al., 2024 [66].

Parameter	***trans*-Resveratrol**	**Coenzyme Q10**	**Quercetin**	**Astaxanthin**
published pK_a [71–74]	(1) 9.1 (2) 9.7 (3) 10.5	13.3	(1) 7.1 (2) 9.1 (3) 11.1	10.6
S (0.1 N HCl) [µg/mL]	44.5 ± 2.7	0.1 ± 0.0	16.7 ± 3.7	0.3 ± 0.1
S (Buffer pH 6.8) [µg/mL]	49.5 ± 1.3	0.1 ± 0.0	20.3 ± 5.0	0.4 ± 0.2
S (Bi-FaSSIF-V2) [µg/mL]	52.2 ± 0.2	5.5 ± 2.3	29.6 ± 6.3	1.1 ± 1.4
S (1-decanol) [µg/mL]	> 5000	> 5000	> 5000	> 5000
Log $D_{7.4}$	2.70	published value: 14.72 [75]	1.60	published value: 8.05 [76]
wavelength (aqueous medium) [nm]	315	282	370	480
wavelength (1-decanol) [nm]	320	287	375	490

The pk_a values of CoQ10 and ASX (unesterified compound) were reported to be 13.3 and 10.6, respectively. Therefore, no protolyzes in the physiological pH range was expected.

Related to their polyphenolic structure, quercetin and *trans*-resveratrol both showed three different pK_a values, as highlighted in **Table 11**. The pK_a values, ranging from 7.1 to 11.1, were consistent with the expected range for phenolic protons [77]. For quercetin, with a lowest reported pK_a of 7.1, dissociation occurred during dissolution measurements under physiological pH conditions (as illustrated in **Figure 9**). With increasing pH of the aqueous medium, phenolic protons dissociate until finally a triple negatively charged molecule is present.

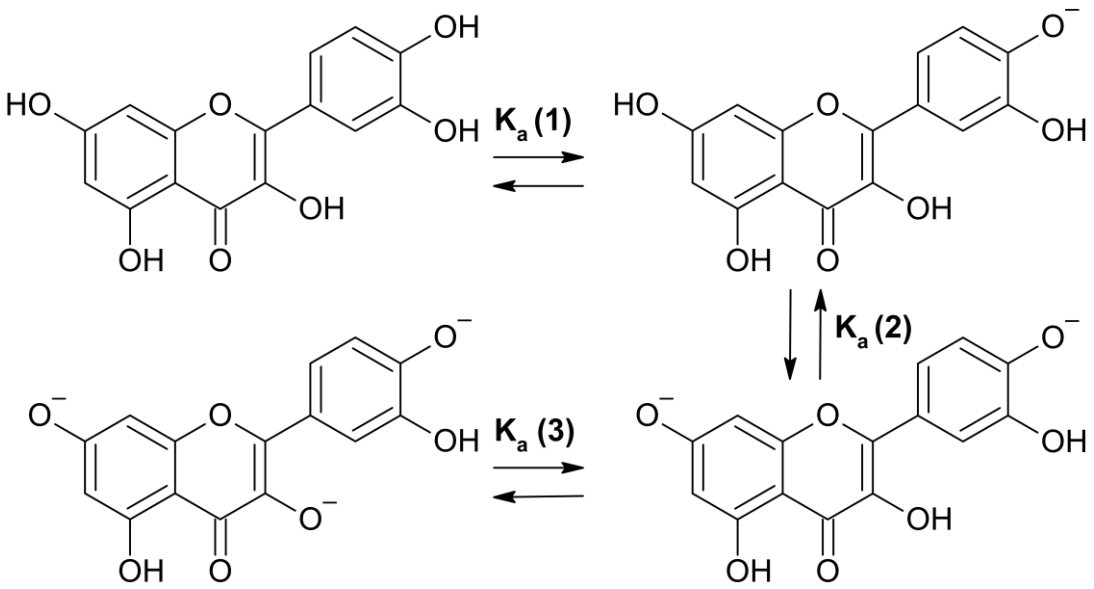

Figure 9: Ionization of quercetin as a function of the pH of the medium (see pK_a values 1-3) in **Table 11**. Obtained from Brenner et al., 2024 [66].

A comparable dissociation pattern has been described for *trans*-resveratrol (**Figure 10**). At first, the phenolic proton of the aromatic ring with just one phenol group dissociates. With increasing alkalinity of the medium, the first phenolic OH group of the second aromatic ring is eventually deprotonated, followed by dissociation of the second phenolic OH group, leading to a molecule with a triple negative charge.

However, the lowest pK_a was reported to be 9.1. Consequently, a dominant proteolysis is not expected to occur at neutral pH values.

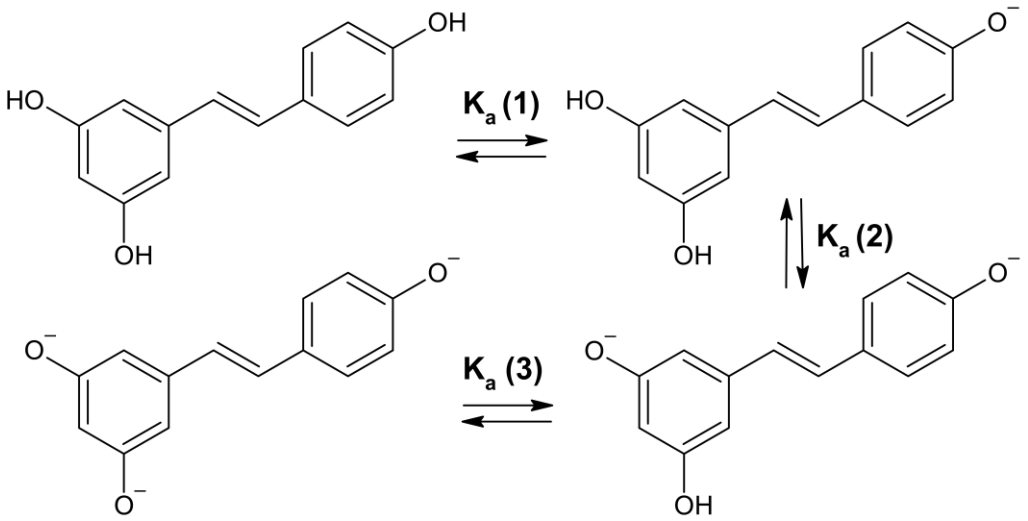

Figure 10: Ionization of *trans*-resveratrol as a function of the pH of the medium (see pK_a values 1-3) in **Table 11**. Obtained from Brenner et al., 2024 [66].

According to their dissociation behavior, the aqueous solubility of quercetin and *trans*-resveratrol increased with an increase in pH (**Table 11**). However, CoQ10 and ASX were almost insoluble in water, and their concentration remained below 1 µg/mL regardless of the media pH. Nevertheless, when biorelevant surfactants sodium-taurocholate and lecithin were present, the solubility of all compounds increased. Especially CoQ10 showed a significant increase in solubility by a factor of 55, likely attributed to increased wettability and micellization of the hydrophobic compound in the presence of surfactants [78]. In consequence, all aqueous media provided solubility-limited non-sink dissolution conditions for CoQ10 and ASX, even with surfactant. Sink conditions were only present in 1-decanol, where all substances reached concentrations greater than 5000 µg/mL.

The Log $D_{7.4}$ values for *trans*-resveratrol and quercetin were 2.70 and 1.60, respectively. In contrast, owing to their long isoprenoid chains [76], CoQ10 and ASX both are very lipophilic compounds with Log $D_{7.4}$ values reported to be 14.72 and 8.05 (unesterified molecule), respectively [75,76].

Trans-resveratrol, quercetin and CoQ10 had their absorption maximum in the UV range between 282 and 375 nm. Due to the large conjugated polyene system ASX and its esters are red in color and their absorption maximum was measured to be between 480 nm and 490 nm [62], depending on the solvent. In 1-decanol, all compounds showed an absorption maximum shifted by 5 nm to 10 nm into the higher wavelength range.

2.4. Conclusion

All formulations, despite having structurally different active components and accompanying substances in the matrix, were successfully analyzed for their active ingredient content using HPLC-UV/VIS.

Formulations containing ASX were the most complex in composition and a separation into specific individual substances was not carried out, instead the ASX content was given as the sum parameter of all mono- and diesters.

In contrast, the formulations containing CoQ10 had the lowest matrix load. The active ingredient content in the formulations ranged from 4.4 mg/g to 989.0 mg/g, with formulations with optimized water solubility having a reduced active ingredient content due to the necessary addition of functional excipients like surfactants or γ-cyclodextrins.

The physicochemical properties of the respective pure substances were analyzed, and it was found that the polyphenolic compounds CUR and *trans*-resveratrol exhibited pK_a values that indicated proteolysis phenomena to occur in the physiologically relevant pH range up to 7. The pK_a values of the terpenoid compounds CoQ10 and ASX were higher, which means they were present undissociated in aqueous media at neutral pH.

Despite the structural diversity of the compounds, all had limited water solubility. Only *trans*-resveratrol and quercetin achieved concentrations above 10 µg/mL. Concerning all other ingredients, even in surfactant-containing media, concentrations remained below 1 µg/mL. However, solubility was significantly increased in 1-decanol.

The solubility behavior of the substances might be associated with their high lipophilicity. Attributed to their long isoprenoid chains, the log $D_{7.4}$ values of CoQ10 and ASX ranged between 8.05 and 14.72, whereas the log $D_{7.4}$ values of the polyphenolic compounds ranged between 1.60 and 3.64.

3. Comparison of biorelevant biphasic dissolution with monophasic dissolution approaches in terms of *in vivo* relevant formulation characterization

3.1. Introduction

Dissolution testing was originally developed by the pharmaceutical industry to ensure the consistency of drug release in aqueous media, which was assumed to be the rate-limiting step [79]. Nowadays, the application has also been adopted by the food industry and dissolution testing is used to develop for example food supplements with improved bioavailability [80]. Additionally, dissolution measurements performed during formulation and process development can provide further information to evaluate the impact of various formulation principles on *in vivo* performance [79].

Typically, the characterization of dissolution properties requires sink conditions present in the dissolution medium, where the saturation solubility of the investigated compound is at least three to five times higher than the maximal ingredient concentration achieved when the applied dose is completely dissolved [81,82]. However, the aqueous solubility of some compounds is limited, which presents a challenge in developing dissolution methods since dissolution and not release might evolve artificially to the rate-limiting step. To overcome these limitations different approaches were developed, for example sink conditions can be achieved by using large volumes of dissolution medium, by addition of surfactants or inclusion of cosolvents, such as ethanol, to the dissolution medium [83]. However, these modifications lead to a distinct deviation from the conditions present in the human gastrointestinal tract and may thereby reduce *in vivo* predictivity.

Commonly used dissolution devices are basket and paddle apparatuses, and flow-through cells (refer to **Figure 11**). The basket (apparatus 1, USP (United States Pharmacopeia) and PhEur (European Pharmacopoeia)) and paddle (apparatus 2, USP and PhEur) apparatuses both consist of cylindrical, round bottom vessels (**Figure 11**), containing a volume of 500 – 2000 mL dissolution medium temperate to 37 °C. Considering apparatus 2, a metal paddle is used as the stirring device, under which the formulation is placed during the measurements. In the basket apparatus, the formulation is placed in a rotating basket, used for generation of sufficient hydrodynamics [84,85].

The flow-through cell assay (apparatus 4, USP, and PhEur) consists of a pump, applying standard flow rates between 4 and 16 mL of medium per minute, and a flow-through cell, in which the formulation is placed during the measurement. Using this assay, dissolution studies can be performed in closed or open loop modus, where increased volume of dissolution medium can compensate for a compound´s poor solubility [84,85].

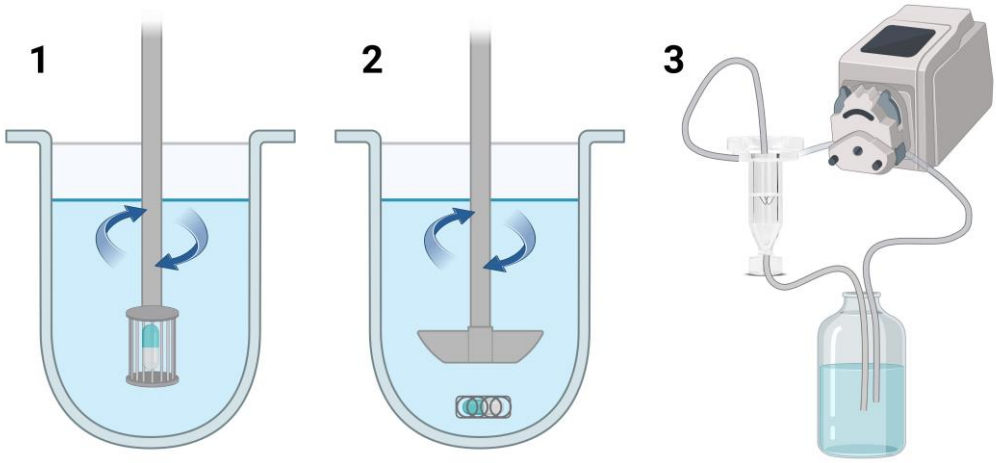

Figure 11: Overview of standard dissolution apparatuses described in the United States Pharmacopeia (USP); **1)** basket apparatus, **2)** paddle apparatus, **3**) flow-through cell (closed loop), Created with BioRender.com.

The presented methods are mostly used in quality control. However, biorelevant dissolution systems usually require a more complex design in order to properly imitate the gastrointestinal conditions. As no standardized methods are currently available, many biorelevant dissolution apparatuses are customized devices [86].

Biorelevant dissolution assays can be categorized as single-phase aqueous models and absorption sink models [87]. Single-phase aqueous models simulate the gastrointestinal passage with biorelevant media, pH changes and/or transfer models. These assays are conducted under non-sink conditions to evaluate the effect of enabling formulations of poorly soluble compounds on dissolution. A major disadvantage of single-phase aqueous assays is the establishment of an equilibrium of dissolved and undissolved active ingredient species, which sometimes lead to insufficient formulation characterization [83]. To address this limitation, absorption assays like the BiPHa+ from Denninger et al. are developed [52]. The BiPHa+ assay consists of an aqueous donor phase, where the active ingredient dissolves under non-sink conditions, and an acceptor compartment, in which sink conditions are present. Typically, not water miscible organic solvents like 1-decanol or 1-octanol are used as organic absorption compartments [52,88–90]. In contrast to the

paddle apparatus, the BiPHa+ uses cylindrical vessels with a flat bottom and a magnetic stirrer to ensure sufficient hydrodynamics. Furthermore, the device is built in small scale and uses only 50 mL each of aqueous and organic medium (refer to **Figure 12**).

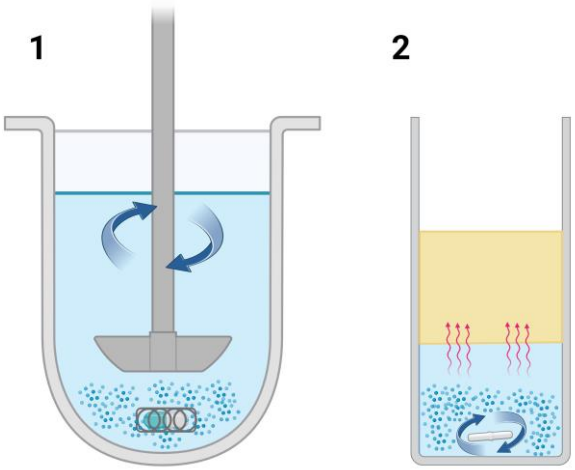

Figure 12: Comparison of vessel shape and stirring device between: **1)** a conventional paddle apparatus and **2)** the BiPHa+ apparatus built by Denninger et al., Created with BioRender.com.

The aqueous medium simulates the gastrointestinal passage, whereas intestinal absorption is mimicked by the organic layer. Though the combination of aqueous non sink dissolution with an artificial absorption compartment biphasic dissolution setups achieve a high degree of *in vivo* predictivity for various compounds [28,52,53].

In order to assess the *in vivo* predictivity of various dissolution methods, all formulations outlined in chapter 2 were analyzed using three distinct apparatuses. All these methods utilized online UV/VIS diode array detectors (DAD) to measure the quantity of active ingredient that dissolved/ partitioned in the dissolution medium. Since, the extracts measured were comprised of complex mixtures of multiple substances, the accuracy of the quantification method for recording the dissolution process needed to be proven. Therefore, the results of online UV/VIS quantification were compared with concentration levels determined by previously validated HPLC methods.

Subsequently, conventional monophasic dissolution measurements using a paddle apparatus with 900 mL phosphate buffer pH 6.8 were conducted. Additionally, dissolution measurements utilizing a fully automated small scale dissolution setup (containing 50 mL of dissolution medium) with pH shift and biorelevant medium were performed. Lastly, biphasic dissolution studies employing the BiPHa+ fully automated device were executed.

3.2. Analytical comparison of online UV/VIS quantification during dissolution measurements and concentration determination using HPLC

Parts of this chapter have been published in peer-reviewed research articles [28,66]. Each figure and table were created by the thesis author. Taking or adapting of figures or tables is indicated in the corresponding position.

In order to evaluate the comparability of online UV/VIS detection and HPLC quantification, the concentrations of the active ingredients measured after 270 min in both, the aqueous and organic medium, of the BiPHa+ were taken as reference points. The results of each method can be found in **Figure 13** - **Figure 17**, with y-axes scaled to 100% for consistency. However, due to some formulations reaching low concentrations that cannot be read at this scale, separate tables (**Table 12** - **Table 16**) were created to show the concentrations in each medium. Multiple t-tests were conducted to determine if there were any significant differences in the concentrations obtained by both measurement methods. The significance level was set at 0.05.

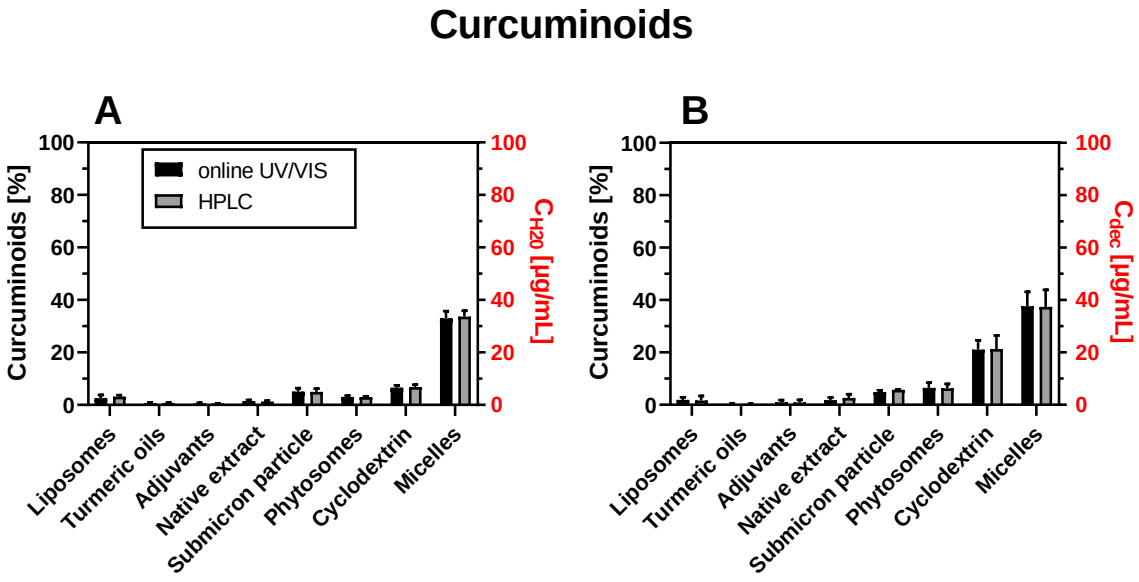

Figure 13*:* Comparison of the released amount of curcuminoids (sum of curcumin, demethoxycurcumin and bisdemethoxycurcumin; mean ± SD) in **A)** the aqueous medium and **B)** the partitioned amount in the 1-decanol layer determined by HPLC and online UV/VIS detection, data refers to the end of biorelevant biphasic dissolution (BiPHa+) at 270 min.; (100% corresponds to 100 µg/mL). In case of very low solubilities, concentrations cannot be displayed in this figure and the reader is referred to **Table 12**. Adapted from Brenner et al., 2023 [69]. Copyright 2023 American Chemical Society.

Table 12: Concentrations of released/ partitioned curcuminoids (sum of curcumin, demethoxycurcumin and bisdemethoxycurcumin; mean ± SD) in the aqueous medium and the 1-decanol layer at the end of biorelevant biphasic dissolution (BiPHa+) measurement at 270 min (determined by HPLC and online UV/VIS detection), no significant differences were detected between both methods ($\alpha = 0.05$).

Formulation	**aqueous medium [%]**		**1-decanol [%]**	
	online UV/VIS	**HPLC**	**online UV/VIS**	**HPLC**
Liposomes	2.6 ± 1.3	3.1 ± 0.6	1.9 ± 0.9	1.6 ± 1.8
Turmeric oils	0.6 ± 0.3	0.7 ± 0.1	0.2 ± 0.2	0.3 ± 0.0
Adjuvants	0.5 ± 0.3	0.6 ± 0.0	0.9 ± 0.9	0.9 ± 1.0
Native extract	1.5 ± 0.4	1.2 ± 0.4	1.8 ± 1.0	2.3 ± 1.4
Submicron particle	5.0 ± 1.3	4.9 ± 1.3	4.9 ± 0.6	5.2 ± 0.2
Phytosomes	3.0 ± 0.5	2.9 ± 0.4	6.5 ± 2.0	6.3 ± 1.8
Cyclodextrin	6.5 ± 0.9	6.8 ± 1.2	21.1 ± 3.6	21.3 ± 5.1
Micelles	32.9 ± 2.8	33.6 ± 2.3	37.6 ± 5.5	37.4 ± 2.8

The results of the method comparison between online UV/VIS detection und HPLC quantification of the eight investigated Curcuma formulations are shown in **Figure 13** and **Table 12**.

As described in chapter 2.2, all formulations tested contained the three structurally closely related curcuminoids CUR, DMC, and BDMC. Due to their structural relationship, however, they also exhibited absorption maxima at the same wavelength. Consequently, online UV/VIS detection could not distinguish between them. This detection method does not have the capability to separate the substances before detection [91]. As a result, we considered the curcuminoids as a sum of all three compounds.

Nevertheless, employing HPLC coupled with UV/VIS detection each compound could be quantified separately. To compare both methods, the individual concentrations of CUR, DMC, and BDMC determined by HPLC were summarized to receive the total concentration of curcuminoids. As shown in **Table 12**, no significant difference between the two quantification methods was discovered. Therefore, the release and dissolution behavior of curcuminoids, regardless of the formulation principle applied, could be determined using online UV/VIS detection.

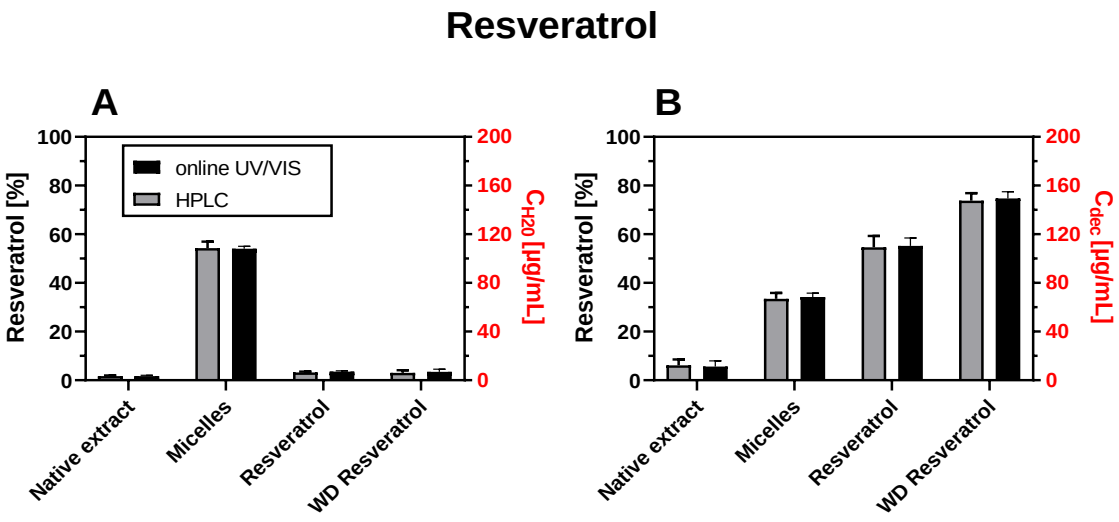

Figure 14*:* Comparison of the released amount of *trans*-resveratrol (mean ± SD) in **A)** the aqueous medium and **B)** the partitioned amount in the 1-decanol layer determined by HPLC and online UV/VIS detection, data refers to the end of biorelevant biphasic dissolution (BiPHa+) measurement at 270 min.; (100% corresponds to 200 µg/mL). In case of very low solubilities, concentrations cannot be displayed in this figure and the reader is referred to **Table 13**.

Table 13: Concentrations of released/ partitioned *trans*-resveratrol (mean ± SD) in the aqueous medium and the 1-decanol layer at the end of biorelevant biphasic dissolution (BiPHa+) measurement at 270 min (determined by HPLC and online UV/VIS detection), no significant differences were detected between both methods (α = 0.05).

Formulation	**aqueous medium [%]**		**1-decanol [%]**	
	online UV/VIS	**HPLC**	**online UV/VIS**	**HPLC**
Native extract	1.6 ± 0.4	1.7 ± 0.3	5.6 ± 2.3	6.1 ± 2.5
Micelles	54.1 ± 1.0	54.3 ± 2.6	34.1 ± 1.6	33.5 ± 2.5
Resveratrol	3.6 ± 0.3	3.2 ± 0.4	55.2 ± 3.3	54.6 ± 4.7
WD Resveratrol	3.5 ± 1.1	3.0 ± 1.1	74.7 ± 2.8	73.8 ± 3.1

WD = water dispersible

Figure 14 and **Table 13** display the *trans*-resveratrol concentrations determined after 270 min in the aqueous medium and the 1-decanol layer of biorelevant biphasic dissolution. Since the native extract and its corresponding micellar formulation not only contained *trans*-resveratrol, but also oligomeric compounds like *trans*-ε-viniferine (refer to section 2.2), having similar absorption characteristics like resveratrol, online UV/VIS detection might be impaired [40]. However, dissolution in the aqueous medium and especially partitioning into the 1-decanol layer of these compounds was found to

occur in reduced quantities compared to *trans*-resveratrol. Our results were supported by the fact, that *trans*-ε-viniferine is known to exhibit extremely poor water solubility and a high sensitivity towards UV radiation, combined with its low intestinal absorption through the intestinal membrane, resulting in very low bioavailability in humans [40,92]. Thus, it was possible to determine the resveratrol concentration in both media not only by means of HPLC, but also by online UV/VIS detection. Similar to the Curcuma formulations, no significant difference was observed between the two methods, indicating that online UV/VIS detection is a suitable way to monitor the release and dissolution of resveratrol-containing formulations.

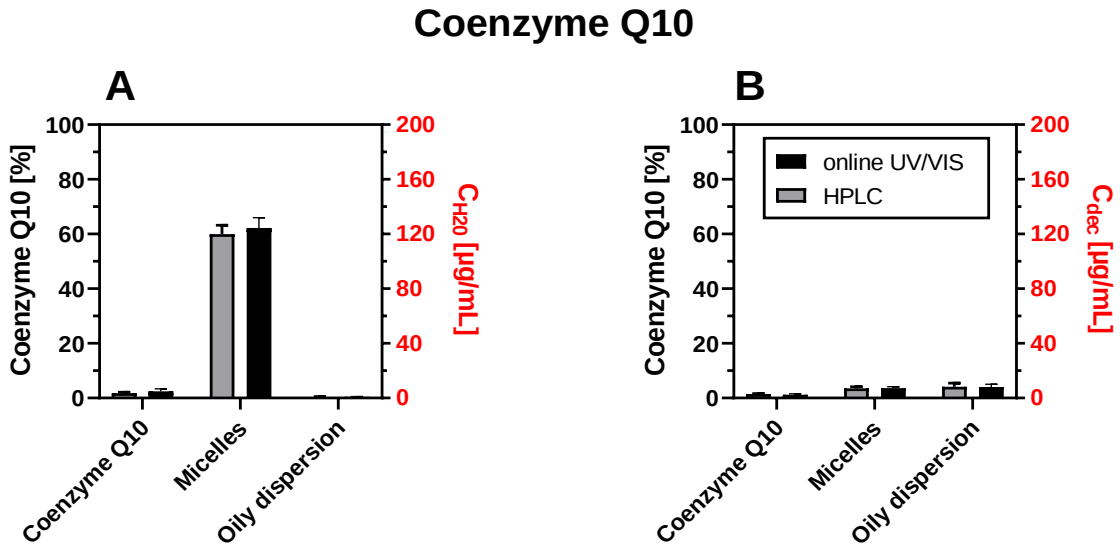

Figure 15: Comparison of the released amount of coenzyme Q10 (mean ± SD) in **A)** the aqueous medium and **B)** the partitioned amount in the 1-decanol layer determined by HPLC and online UV/VIS detection, data refers to the end of biorelevant biphasic dissolution (BiPHa+) measurement at 270 min.; (100% corresponds to 200 µg/mL). In case of very low solubilities, concentrations cannot be displayed in this figure and the reader is referred to **Table 14**.

Table 14: Concentrations of released/ partitioned coenzyme Q10 (mean ± SD) in the aqueous medium and the 1-decanol layer at the end of biorelevant biphasic dissolution (BiPHa+) measurement at 270 min (determined by HPLC and online UV/VIS detection), no significant differences were detected between both methods (α = 0.05).

Formulation	**aqueous medium [%]**		**1-decanol [%]**	
	online UV/VIS	**HPLC**	**online UV/VIS**	**HPLC**
Coenzyme Q10	2.5 ± 0.9	2.0 ± 0.4	1.2 ± 0.3	1.5 ± 0.2
Micelles	62.2 ± 3.8	60.0 ± 3.2	3.6 ± 0.5	3.6 ± 0.6
Oily dispersion	0.5 ± 0.1	0.4 ± 0.1	4.1 ± 0.9	4.0 ± 1.3

Based on the results shown in section 2.2, the CoQ10 formulations were found to have almost no impurities. As a result, quantification using online UV/VIS detection was not affected. Since there were no accompanying substances that needed to be separated, lack of chromatographic separation was not a disadvantage. Thus, as displayed in **Figure 15** and **Table 14**, the concentrations obtained via online UV/VIS detection were comparable to those obtained through HPLC measurements and no significant difference was found.

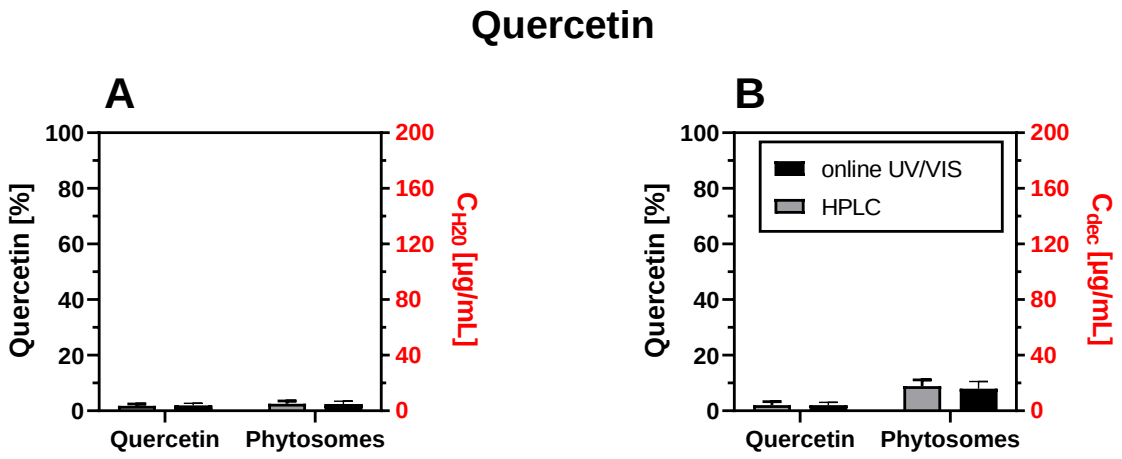

Figure 16*:* Comparison of the released amount of quercetin (mean ± SD) in **A)** the aqueous medium and **B)** the partitioned amount in the 1-decanol layer determined by HPLC and online UV/VIS detection, data refers to the end of biorelevant biphasic dissolution (BiPHa+) measurement at 270 min.; (100% corresponds to 200 µg/mL). In case of very low solubilities, concentrations cannot be displayed in this figure and the reader is referred to **Table 15**.

Table 15: Concentrations of released/ partitioned quercetin (mean ± SD) in the aqueous medium and the 1-decanol layer at the end of biorelevant biphasic dissolution (BiPHa+) measurement at 270 min (determined by HPLC and online UV/VIS detection), no significant differences were detected between both methods (α = 0.05).

Formulation	**aqueous medium [%]**		**1-decanol [%]**	
	online UV/VIS	**HPLC**	**online UV/VIS**	**HPLC**
Quercetin	1.9 ± 0.8	1.8 ± 0.6	2.0 ± 1.0	1.9 ± 1.3
Phytosomes	2.4 ± 1.0	2.5 ± 1.3	8.0 ± 2.5	8.9 ± 2.2

The two quercetin formulations showed a low matrix load (see section 2.2) and reached maximum concentrations of less than 10% in both media (refer to **Figure 16** and **Table 15**). This prevented the presence of other flavonoids, like rutin, in the phytosomes from hindering online UV/VIS detection. The UV/VIS detection approach proved effective in

monitoring the flavonoid release and dissolution of quercetin-containing formulations, and no significant disparity was observed between both quantification methods.

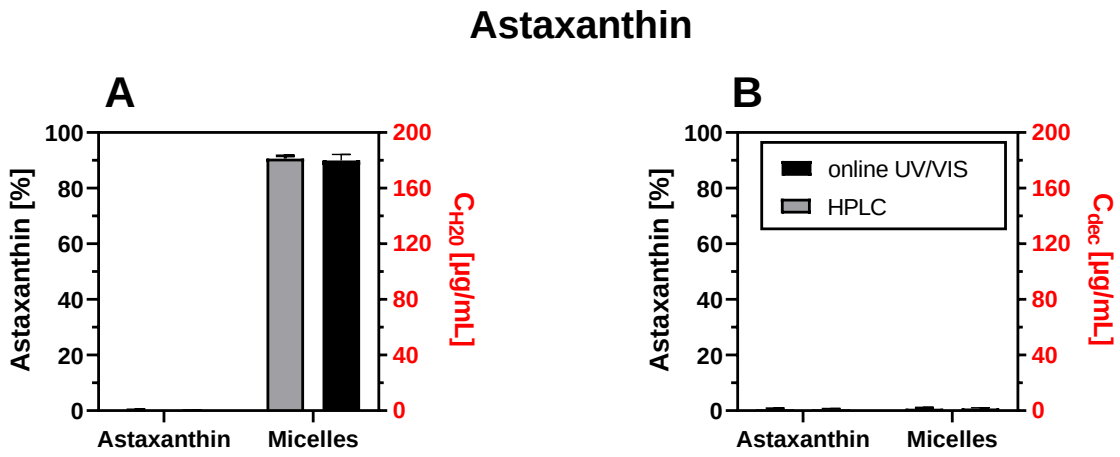

Figure 17*:* Comparison of the released amount of astaxanthin (sum of mono- and diesters; mean ± SD) in **A)** the aqueous medium and **B)** the partitioned amount in the 1-decanol layer determined by HPLC and online UV/VIS detection, data refers to the end of biorelevant biphasic dissolution (BiPHa+) measurement at 270 min.; (100% corresponds to 200 µg/mL). In case of very low solubilities, concentrations cannot be displayed in this figure and the reader is referred to **Table 16**.

Table 16: Concentrations of released/ partitioned astaxanthin (sum of mono- and diesters; mean ± SD) in the aqueous medium and the 1-decanol layer at the end of biorelevant biphasic dissolution (BiPHa+) measurement at 270 min (determined by HPLC and online UV/VIS detection), no significant differences were detected between both methods (α = 0.05).

Formulation	**aqueous medium [%]**		**1-decanol [%]**	
	online UV/VIS	**HPLC**	**online UV/VIS**	**HPLC**
Astaxanthin	0.2 ± 0.1	0.2 ± 0.1	0.5 ± 0.3	0.4 ± 0.3
Micelles	90.0 ± 2.1	90.7 ± 1.0	0.8 ± 0.3	0.7 ± 0.2

The two ASX formulations were derived from an extract obtained from the microalgae *Haematococcus pluvialis*, which contained a multifaceted blend of mono- and diesters of ASX (refer section 2.2). In consequence of this complex composition, the concentration of ASX determined by both quantification methods was only indicated as a sum of all mono- and diesters. The findings are depicted in **Figure 17** and **Table 16**. However, despite the complexity of the formulations, no significant difference in the determined ASX concentration between both quantification methods was detected and online UV/VIS detection was found to be suitable.

3.3. Dissolution results obtained for the *Curcuma* formulations

Parts of this chapter have been published in a peer-reviewed research article [28]. Each figure and table were created by the thesis author. Taking or adapting of figures or tables is indicated in the corresponding position.

In chapter 3.1, various dissolution methods were presented, such as conventional methods and biorelevant models. The aim of the following section was to investigate the effect of different methods on the dissolution characteristics of the eight Curcuma formulations described in chapter 2.2.1. The study utilized three different systems, namely a conventional paddle system (apparatus 2, USP, and PhEur) with 900 mL phosphate buffer pH 6.8 (monophasic non-sink dissolution; **Figure 18**), a monophasic dissolution model with biorelevant medium and pH shift (pH shift dissolution with biorelevant medium; **Figure 19**), and a biorelevant biphasic dissolution system (BiPHa+; **Figure 20**). The latter two systems each used 50 mL of biorelevant aqueous medium.

The y-axes were scaled to 100% for consistency, but since some formulations only dissolved small amounts, the curcuminoid concentrations achieved by each formulation at the end of the dissolution experiment were also presented in **Table 17** - **Table 19**.

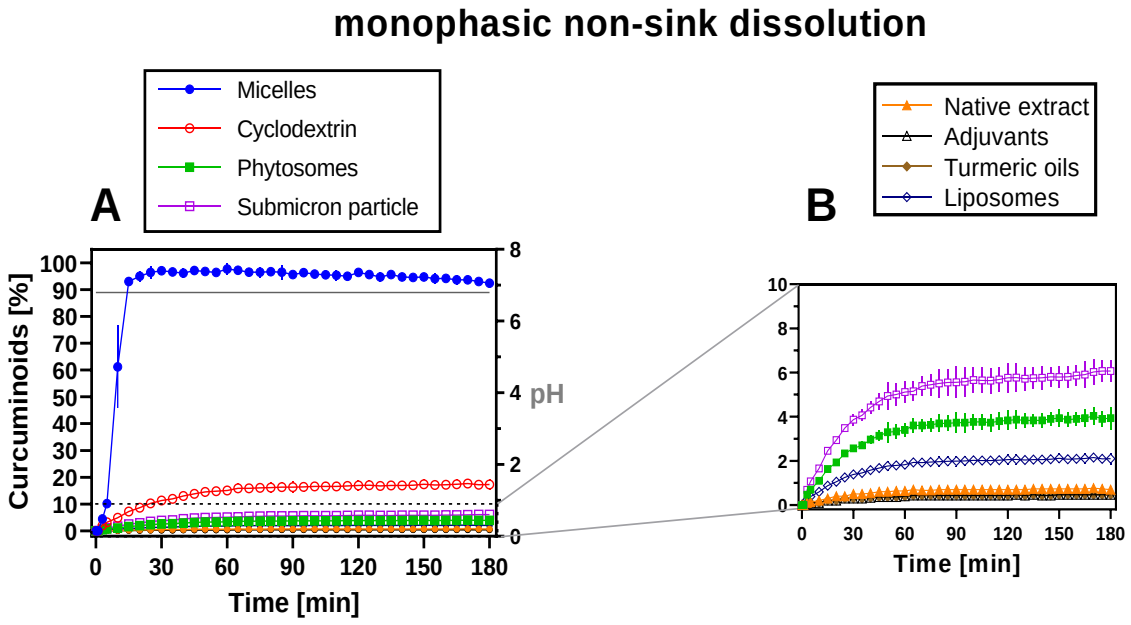

Figure 18: Dissolved amount of curcuminoids (sum of curcumin, demethoxycurcumin and bisdemethoxycurcumin; mean ± SD) during monophasic non-sink dissolution, **A)** full y-scale, **B)** y-scale zoom (0-10%) excluding micelles and cyclodextrin complex; the pH profile in the aqueous medium is represented by the grey line, (100% corresponds to 6 µg/mL). Adapted from Brenner et al., 2023 [69]. Copyright 2023 American Chemical Society.

Table 17: Concentrations of dissolved curcuminoids (sum of curcumin, demethoxycurcumin and bisdemethoxycurcumin; mean ± SD) at the end of monophasic non-sink dissolution at 180 min (determined by HPLC).

Formulation	Endpoint concentration [%]
Liposomes	2.1 ± 0.3
Turmeric oils	0.5 ± 0.1
Adjuvants	0.5 ± 0.1
Native extract	0.7 ± 0.1
Submicron particle	6.1 ± 0.5
Phytosomes	3.9 ± 0.5
Cyclodextrin	17.3 ± 2.1
Micelles	92.4 ± 1.5

The native extract and the formulations with adjuvants and turmeric oils generated a release of 0.5 - 0.7% (**Figure 18B**). The last two formulations mentioned were designed to target post-absorptive mechanisms, such as the inhibit of phase II enzymes or intestinal membrane transporters [47,48,93]. However, these formulations were not optimized for solubility, which might explain why they were not effective in enhancing the dissolution rate compared to the native extract. Higher release was observed for liposomes and phytosomes, which released 2.1% and 3.9%, respectively. Submicron particles showed 6.1% curcuminoid release, which represented an improvement by the factor of 12.2 compared to the native extract. As the size of the particles decreases, drug particles have a higher degree of interaction with the solvent, leading to an increase in solubility [94,95]. The Noyes-Whitney equation (equation 2) states that when the particle size is reduced, the total effective surface area of the drug particle is increased, which results in an enhancement of the dissolution rate.

$$\frac{d_C}{d_t} = D\ x\ A\ x\ \frac{c_s - c}{h} \qquad \text{(Equation 2)}$$

Where, d_c/d_t is the dissolution rate of the drug particles, D is the diffusion coefficient, A is the effective surface area of the drug particles, h is the thickness of the diffusion layer around each drug particle, c_s is the saturation solubility of the drug and c the concentration of the drug present in the dissolution medium.

Along with the submicron particles, both the cyclodextrin and the micellar formulation had decisively increased dissolution rates. The cyclodextrin complex revealed the second highest dissolution performance, with a maximum release of 17.3%. Micelles achieved almost complete curcuminoid release within the first 15 minutes (92.4%) and maintained a high level of release throughout the dissolution test. Both, self-emulsifying drug delivery systems (SEDDS), e.g., the micellar formulation, and cyclodextrin inclusion complexes are well known and studied formulation strategies to enhance the solubility and bioavailability of poorly soluble compounds [96,97].

Basically, the dissolution profiles of all formulations were similar in shape, with a gradual increase in concentration at the beginning and a subsequent plateau from 60 - 180 min (**Figure 18**). All the formulations except those containing adjuvants and turmeric oils achieved a higher concentration after 180 min than the native extract, leading to supersaturation without any curcuminoid precipitation. This could be explained by the formulations' ability to stabilize supersaturation, and the large solvent volume of 900 mL, which resulted in low absolute concentrations of curcuminoids in the dissolution medium. In order to ensure consistency across different dissolution techniques, a fixed dose of 5 mg curcuminoids per formulation was used, resulting in a maximum theoretical concentration of 6 µg/mL. The lower the degree of supersaturation, the less likely precipitation will occur [82].

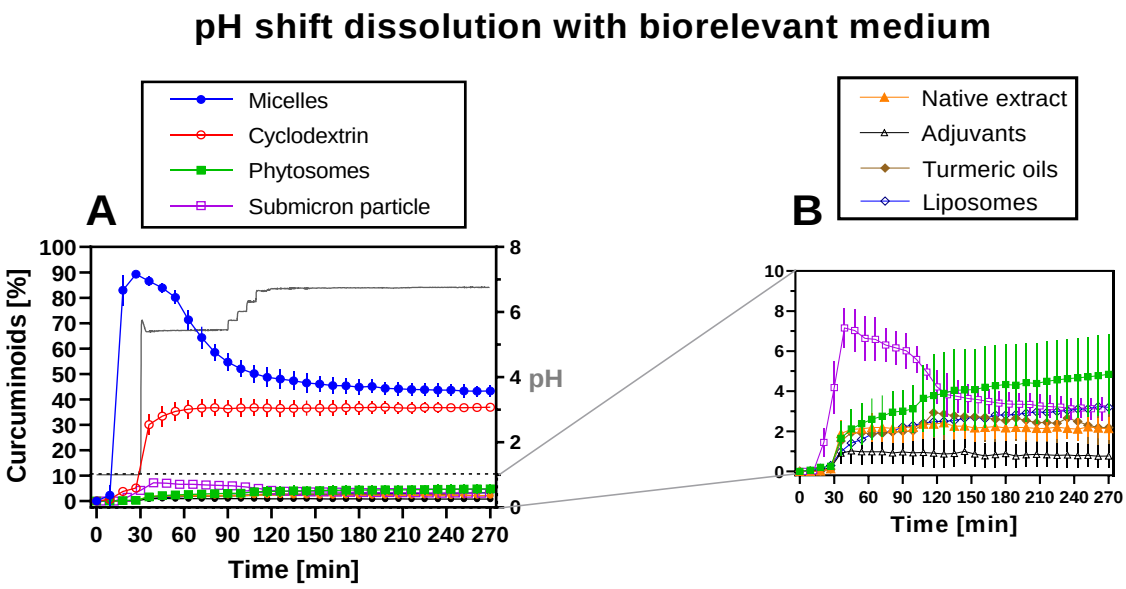

Figure 19: Dissolved amount of curcuminoids (sum of curcumin, demethoxycurcumin and bisdemethoxycurcumin; mean ± SD) during monophasic non-sink dissolution with pH shift and biorelevant medium, **A)** full y-scale, **B)** y-scale zoom (0-10%) excluding micelles and cyclodextrin complex; the pH profile in the aqueous medium is represented by the grey line, (100% corresponds to 0.1 mg/mL). Adapted from Brenner et al., 2023 [69]. Copyright 2023 American Chemical Society.

Table 18: Concentrations of dissolved curcuminoids (sum of curcumin, demethoxycurcumin and bisdemethoxycurcumin; mean ± SD) at the end of monophasic non-sink dissolution with pH shift and biorelevant medium at 270 min (determined by HPLC).

Formulation	Endpoint concentration [%]
Liposomes	3.2 ± 0.5
Turmeric oils	2.2 ± 1.0
Adjuvants	0.8 ± 0.6
Native extract	2.1 ± 0.6
Submicron particle	3.1 ± 0.6
Phytosomes	4.8 ± 2.0
Cyclodextrin	36.9 ± 1.3
Micelles	43.3 ± 2.3

In contrast to monophasic non-sink dissolution, the pH shift dissolution with biorelevant medium works with changing pH values in the medium during dissolution measurements. A distinction can be made between a gastric stage lasting 30 minutes at pH 1, a subsequent stage at pH 5.5 lasting 60 minutes (simulating the jejunum), and a final stage at pH 6.8 (simulating the ileum).

During the gastric stage, the release of curcuminoids from various formulations, including liposomes, extracts with adjuvants or turmeric oils, and phytosomes was found to be below 0.5% (as shown in **Figure 19B** and **Table 18**). The addition of biorelevant surfactants at 30 min led to an increase in concentration to 0.8% for the extract with adjuvants, while the other formulations achieved about 2%. The use of a biorelevant medium led to higher end concentrations in the dissolution medium when compared to monophasic non-sink dissolution, even though only 50 mL of medium were used. The biorelevant surfactants enabled maintaining higher concentrations of curcuminoids in the solution through micellization, which particularly benefitted the non-solubility-enhanced formulations [98]. The concentration of dissolved curcuminoids remained stable from 30 - 270 min for the native extract and adjuvants formulation. However, the dissolution of curcuminoids from the liposomes and phytosomes steadily increased until the maximum of 3.1% and 4.8% was achieved at the end of the dissolution test.

Only the submicron particles, cyclodextrin complex, and micelles displayed a noticeable release of curcuminoids during the gastric stage (**Table 19 A/B**). Submicron particles released up to 4.2% within 30 min, which subsequently increased to 7.2% after adding biorelevant surfactants. However, the formulation could not stabilize curcuminoid supersaturation, and gradual precipitation occurred, which led to a concentration of 3.2% at the end of the dissolution test. The increase in dissolution rate might be attributed to the increased specific surface area of the nanoparticles, resulting in a high degree of supersaturation [95]. But a reduction in particle size without the addition of precipitation inhibitors like polymers did not yield in a stabilization of dissolved curcuminoids in the supersaturated solution [99]. Thus, the high degree of supersaturation caused precipitation, resulting in a decrease in the concentration of curcuminoids to a level that corresponds to their equilibrium solubility in biorelevant medium.

The cyclodextrin complex released 5.6% in the gastric stage, which subsequently increased to 36.9%, and then remained constant until the end of the test at 270 min. The combination of cyclodextrins and surfactants produced a remarkable synergistic effect, which notably enhanced the solubility of curcuminoids beyond that of the pure cyclodextrin complex. Chakravarthy et al. also noted a substantial improvement in the dissolution rate of quercetin when it was prepared with cyclodextrins and Tween 80 [100].

In comparison to the other formulations, the micelles showed a high degree of release within the first 30 min (90.0%). Related to the high surfactant content of the formulation, the addition of biorelevant medium had no influence on dissolution behavior. However, like the submicron particles, the supersaturation of curcuminoids in solution could not be sustained throughout the dissolution test, leading to precipitation [101]. Between 60 - 120 min, the dissolved amount decreased from 79.2% to 43.3%, until a plateau was reached, and the concentration remained constant.

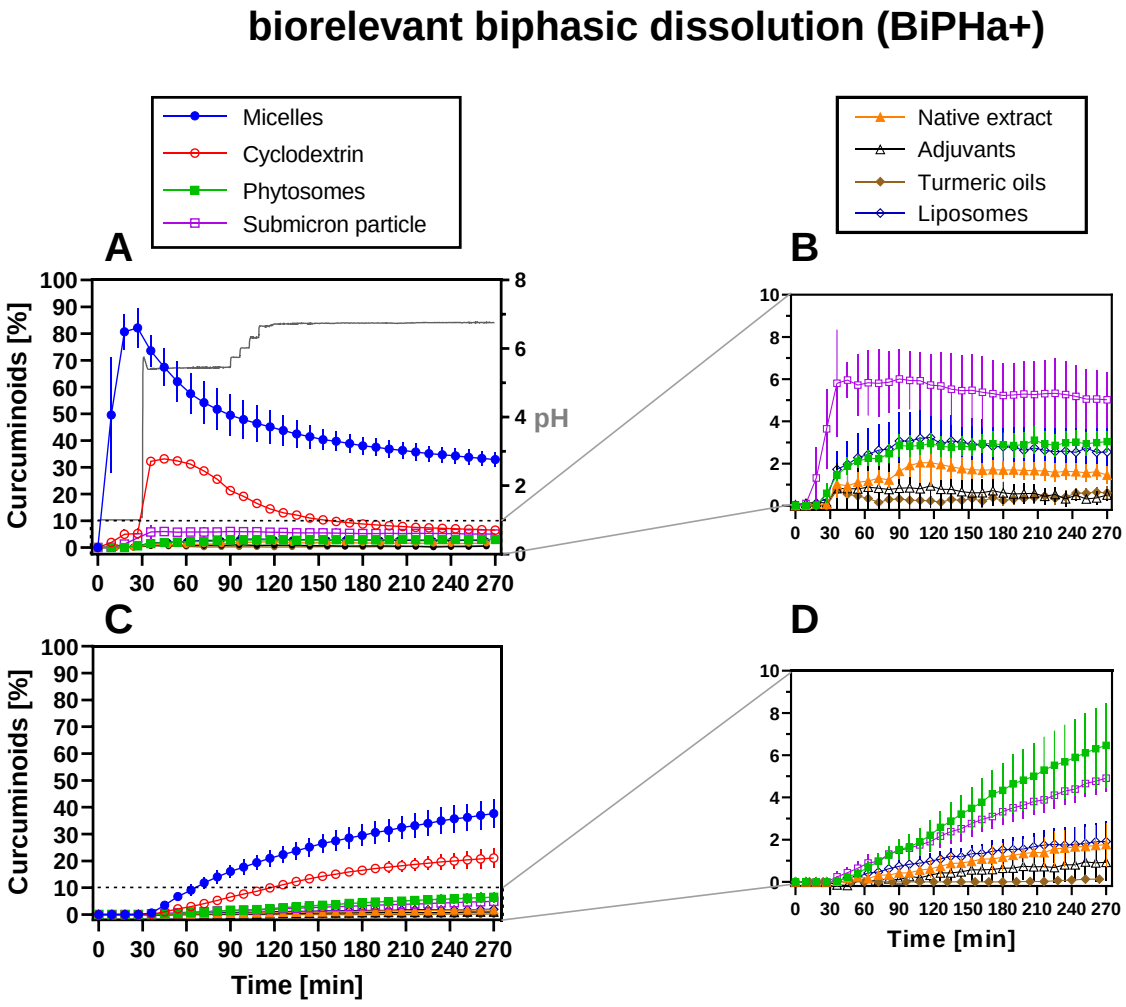

Figure 20: Dissolved/partitioned amount of curcuminoids (sum of curcumin, demethoxycurcumin and bisdemethoxycurcumin; mean ± SD) during biorelevant biphasic dissolution (BiPHa+) measurements, **A)** aqueous medium full y-scale, **B)** aqueous medium y-scale zoom (0-10%) excluding micelles and cyclodextrin complex, **C)** 1-decanol layer full y-scale, **D)** 1-decanol layer y-scale zoom (0-10%) excluding micelles and cyclodextrin complex; the pH profile in the aqueous medium is represented by the grey line, (100% corresponds to 0.1 mg/mL). Adapted from Brenner et al., [69]. Copyright 2023 American Chemical Society.

Table 19: Concentrations of dissolved/ partitioned curcuminoids (sum of curcumin, demethoxycurcumin and bisdemethoxycurcumin; mean ± SD) in the aqueous medium and the 1-decanol layer at the end of biorelevant biphasic dissolution (BiPHa+) at 270 min (determined by HPLC).

Formulation	**Endpoint concentration [%]**	
	aqueous medium	**1-decanol**
Liposomes	3.1 ± 0.6	1.6 ± 1.8
Turmeric oils	0.7 ± 0.1	0.3 ± 0.0
Adjuvants	0.6 ± 0.0	0.9 ± 1.0
Native extract	1.2 ± 0.4	2.3 ± 1.4
Submicron particle	4.9 ± 1.3	5.2 ± 0.2
Phytosomes	2.9 ± 0.4	6.3 ± 1.8
Cyclodextrin	6.8 ± 1.2	21.3 ± 5.1
Micelles	33.6 ± 2.3	37.4 ± 2.8

The results of the biorelevant biphasic dissolution studies indicated that liposomes, Curcuma extracts with turmeric oils or with adjuvants, and the native extract did not release curcuminoids during the gastric stage (**Figure 20 A/B** and **Table 19**). However, after adding biphasic dissolution adapted- fasted state simulated intestinal fluid-V2 (Bi-FaSSiF-V2) surfactants at 30 min, a small proportion of curcuminoids, approximately 1-2%, dissolved in the aqueous phase. Despite the gradual increase in pH value to 6.8 during the dissolution runs, no increase in the release rate was observed, and the released amount remained at the same level throughout the entire dissolution run. Notably, the Curcuma extracts with adjuvants and turmeric oils provided a curcuminoid dissolution of up to 0.7%, the native extract released 1.2%, and the liposomes delivered a release of 3.1%.

Similarly, as in the aqueous medium, no pH-dependent increase in partitioning rate could be detected (**Figure 20 C/D**). The partitioned amount of curcuminoids in the 1-decanol layer was low, with 0.3% for the turmeric oils formulation, 0.9% for the Curcuma extract with adjuvants, and 1.6 - 2.3% for the liposomes and native extract, respectively.

During biphasic dissolution, it is necessary for the active ingredient to dissolve in the aqueous medium first and then cross the aqueous-organic interface before accumulating in the organic phase. As a result, formulations containing adjuvants, turmeric oils, and liposomes did not perform differently from the native extract (see **Table 19**). In all of these formulations, the quantity of dissolved curcuminoids in the aqueous medium was

insufficient for increased partitioning into the 1-decanol layer [52]. Denninger et al. (2021) similarly observed limited partitioning into the organic phase for itraconazole due to low itraconazole concentrations in the aqueous medium [53]. This may explain why formulations targeting post-absorptive mechanisms, such as inhibiting phase II enzymes with adjuvants (e.g., piperine) [47,93] or intestinal membrane transporters (e.g., with turmeric oils) [48], were not effective as these inhibitors would only impact curcumin that had already been absorbed. However, due to poor dissolution, absorption was limited.

Although the aqueous dissolution profiles of the phytosomes and the liposomes were comparable (approximately 3% release), the partitioning in the 1-decanol layer was much more pronounced for the phytosomes, with 6.5% after 270 min. Furthermore, phytosomes exhibited a 3.5-fold higher release than the native extract, but the concentration at the endpoint of the dissolution test in the aqueous medium only increased by a factor of 2. Curcuminoid-phospholipid complexes, which were known to form lipid-compatible molecular complexes, may allow for higher drug partitioning into the 1-decanol layer than neat curcuminoids of the same concentration [102,103]. While liposomes also consist partially of phospholipids, namely soy lecithin, their dissolution performance in all three investigated dissolution methods was worse than that of the phytosomes. It appears that despite similar vesicles needing to form *in situ*, the extent of that formation was different. During pH shift dissolution with a biorelevant medium, liposomes released 3%, whereas phytosomes released nearly 5% (**Table 18**). This might be attributed to the superior *in situ* formation of phytosome vesicles compared to liposomes.

In comparison to the aforementioned formulations, the submicron particles demonstrated a gradual release of curcuminoids during the gastric stage, without a distinct increase following the addition of surfactants. At the 39-minute mark, 6.0% of curcuminoids were released in the aqueous medium, which decreased to 5.2% after 270 min. After 270 min 5.2% of curcuminoids partitioned into the 1-decanol layer. Thus, submicron particle-based formulations showed a slight improvement in dissolution, likely due to their increased specific surface area (see section 3.3).

The cyclodextrin complex allowed for the dissolution of curcuminoids up to 5.3% during the gastric stage. However, after the addition of Bi-FaSSIF-V2, there was a significant increase to 33.0%, followed by a decrease to 6.8%. The decrease might partially be related to precipitation of dissolved curcuminoids between 60 - 120 min, which then decreased

in the subsequent time of the dissolution measurement. In addition, the aqueous concentration was reduced by partitioning of active ingredient into the 1-decanol absorption phase, until between 210 and 270 min, almost no further reduction in concentration was detected. In the organic medium, a rapid partitioning of curcuminoids was observed, which gradually decreased during the dissolution process. However, the partitioned amount of 21.3% in the 1-decanol layer was higher than all other formulations except for the micelles. The micellar formulation exhibited the highest dissolution rate, with 82.4% of dissolved curcuminoids detected during the gastric stage, followed by a decrease to 33.6%. Compared to all other formulations, the micelles released curcuminoids quickly and almost entirely during the gastric stage, achieving the most efficient partitioning in the 1-decanol layer of 37.4% (**Figure 20 C/D**).

The biorelevant biphasic dissolution studies revealed, that only curcumin micelles and curcumin-cyclodextrin complexes demonstrated decisively improved dissolution in the aqueous medium and improved partitioning into the 1-decanol layer (**Table 19**). This findings were in agreement with the fact that both exhibit superior oral bioavailability in humans too [41,45,104]. To enhance the bioavailability of poorly soluble compounds, self-emulsifying drug delivery systems generated using surfactants or the formation of cyclodextrin inclusion complexes were commonly used [96,97].

3.3.1. Analysis of relative and absolute curcuminoid distribution in the aqueous and organic medium

Apart from focusing on differences in dissolution and partitioning behavior of curcuminoids from various formulations, the curcuminoid distribution ratios were also examined. At specific intervals throughout each dissolution measurement (30, 90, 120, 210, and 270 minutes), samples were collected, filtered through 0.22 µm PTFE filters, and directly introduced into the HPLC system (for experimental details refer to section 2.2.1.). Overall, the ratios of CUR, DMC, and BDMC remained consistent throughout the dissolution measurements, with no significant changes detected in the organic phase. However, certain formulations exhibited a minor decrease in concentration of CUR in the aqueous medium. The relative amounts of CUR, DMC, and BDMC in the aqueous medium after biphasic dissolution measurements of all eight Curcuma formulations are shown in **Table 20** and **Table 21**.

Table 20: **1.** Relative amount (mean ± SD) of curcumin (CUR), demethoxycurcumin (DMC) and bisdemethoxycurcumin (BDMC) after 30, 90, 120, 210 and 270 min in the aqueous medium of biorelevant biphasic dissolution (BiPHa+) (determined by HPLC). Adapted from Brenner et al., [69]. Copyright 2023 American Chemical Society.

		Amount in the aqueous medium [%]			
	Time [min]	Liposomes	Turmeric oils	Adjuvants	Native extract
CUR	30	38.4 ± 10.4	70.5 ± 1.2	70.0 ± 9.2	60.1 ± 6.5
	90	34.3 ± 9.8	63.2 ± 0.7	64.9 ± 11.8	60.3 ± 6.8
	120	31.7 ± 10.6	61.5 ± 0.6	63.7 ± 10.6	58.0 ± 7.0
	210	35.3 ± 7.1	59.9 ± 3.3	60.7 ± 8.6	56.7 ± 7.2
	270	32.8 ± 8.4	57.4 ± 4.6	62.8 ± 10.9	57.1 ± 8.3
DMC	30	48.6 ± 7.4	20.0 ± 0.2	22.6 ± 6.8	29.7 ± 4.6
	90	51.9 ± 7.0	21.2 ± 0.5	22.9 ± 6.1	29.2 ± 1.7
	120	53.9 ± 7.2	21.9 ± 0.8	21.6 ± 3.5	30.0 ± 1.5
	210	51.4 ± 4.6	24.5 ± 1.5	22.1 ± 4.0	31.9 ± 1.1
	270	53.2 ± 5.1	25.7 ± 1.6	22.2 ± 5.1	32.2 ± 2.2
BDMC	30	13.0 ± 3.1	9.6 ± 1.0	7.4 ± 2.4	10.2 ± 2.6
	90	13.7 ± 2.8	15.6 ± 0.7	12.2 ± 5.7	10.5 ± 5.1
	120	14.5 ± 3.5	16.6 ± 1.1	14.7 ± 7.1	12.0 ± 5.5
	210	13.4 ± 2.5	15.6 ± 4.6	17.2 ± 4.8	11.4 ± 6.3
	270	14.0 ± 3.3	16.9 ± 3.2	15.1 ± 6.1	10.6 ± 6.1

The relative distribution of the three curcuminoids in the 1-decanol layer is shown in **Table 22** and **Table 23**.

A comparison between Curcuma extracts with turmeric oils and adjuvants revealed that both formulations had comparable profiles in the aqueous medium and the 1-decanol layer. In the aqueous medium, the percentage of CUR detected was 70.0 - 70.5% at 30 min, which decreased to 57.4 - 62.8% after 270 min. As a result, the DMC and BDMC fractions increased (**Table 20**).

Table 21: **2.** Relative amount (mean ± SD) of curcumin (CUR), demethoxycurcumin (DMC) and bisdemethoxycurcumin (BDMC) after 30, 90, 120, 210 and 270 min in the aqueous medium of biorelevant biphasic dissolution (BiPHa+) (determined by HPLC). Adapted from Brenner et al., [69]. Copyright 2023 American Chemical Society.

		Amount in the aqueous medium [%]			
	Time [min]	**Submicron particle**	**Phytosomes**	**Cyclodextrin**	**Micelles**
CUR	30	86.9 ± 0.8	46.2 ± 7.6	71.4 ± 2.3	69.0 ± 1.0
	90	87.8 ± 1.3	42.2 ± 20.1	71.1 ± 1.0	69.3 ± 0.5
	120	87.3 ± 0.8	40.4 ± 22.5	70.2 ± 1.5	68.4 ± 0.5
	210	88.0 ± 0.6	37.6 ± 20.6	69.7 ± 1.3	67.6 ± 0.8
	270	87.4 ± 1.0	40.0 ± 24.2	69.8 ± 1.2	67.6 ± 1.0
DMC	30	12.2 ± 0.7	44.9 ± 6.2	24.7 ± 1.6	25.5 ± 0.5
	90	11.9 ± 1.0	47.9 ± 15.6	24.9 ± 0.7	25.3 ± 0.3
	120	11.8 ± 0.7	49.4 ± 15.6	25.5 ± 0.9	25.9 ± 0.3
	210	11.3 ± 0.5	51.7 ± 15.9	25.9 ± 0.7	26.5 ± 0.5
	270	11.7 ± 0.8	49.5 ± 19.4	26.1 ± 0.5	26.6 ± 0.6
BDMC	30	0.9 ± 0.1	8.9 ± 1.5	3.9 ± 0.6	5.5 ± 0.5
	90	0.8 ± 0.3	9.9 ± 4.5	4.0 ± 0.3	5.4 ± 0.2
	120	0.9 ± 0.1	10.2 ± 5.1	4.3 ± 0.6	5.6 ± 0.2
	210	0.7 ± 0.1	10.8 ± 4.7	4.4 ± 0.6	5.9 ± 0.3
	270	0.9 ± 0.2	10.5 ± 4.8	4.1 ± 0.7	5.9 ± 0.4

In the 1-decanol layer, the turmeric oils and adjuvants formulation showed a stable ratio of 71.4 - 69.8% and 74.1 - 72.5%, respectively (**Table 22**). However, the adjuvants formulation exhibited higher variance. For the native extract, the CUR proportions were 60.1% at 30 min, reducing to 57.1% after 270 min in the aqueous medium and 69.4% at 90 min, reducing to 65.2% after 270 min in the 1-decanol layer. The liposomes and phytosomes formulations exhibited a reduced CUR fraction in both media, especially when compared to the undissolved formulations. Additionally, both formulations showed a considerable variance concerning the CUR proportion, especially the phytosomes, which subsequently affected the organic phase. The liposomes showed a CUR fraction of 60.5 - 58.3% in the organic medium, while the phytosomes showed relative amounts of 48.4 - 46.1%.

Conversely, formulations with increased dissolution performance showed more stable CUR fractions. For the micellar, cyclodextrin complex, and submicron particle formulations, stable proportions of the three curcuminoids throughout the test were determined. Focusing on the submicron particles, the study found an increased CUR fraction of 86.9 - 87.4% in the aqueous medium and 85.4 - 85.8% in the 1-decanol layer, which corresponded to the high CUR amount in the raw material. The micelles released 69.0 - 67.6% into the aqueous medium and 73.9 - 72.7% partitioned in the organic medium, while the cyclodextrin-complex released 71.4 - 69.8% in the aqueous medium and 73.7 - 71.7% partitioned in the 1-decanol layer, respectively (**Table 21** and **Table 23**). In general, a formulation-independent shift in the 1-decanol layer towards a higher proportion of CUR with a simultaneous reduction in the proportion of other curcuminoids was observed.

Table 22: **1.** Relative amount (mean ± SD) of curcumin (CUR), demethoxycurcumin (DMC) and bisdemethoxycurcumin (BDMC) after 90, 120, 210 and 270 min in the 1-decanol layer of biorelevant biphasic dissolution (BiPHa+) (determined by HPLC). Adapted from Brenner et al., [69]. Copyright 2023 American Chemical Society.

		Amount in the 1-decanol layer [%]			
	Time [min]	**Liposomes**	**Turmeric oils**	**Adjuvants**	**Native extract**
CUR	90	60.5 ± 20.2	71.4 ± 4.9	74.1 ± 8.1	69.4 ± 3.2
	120	58.2 ± 20.5	70.9 ± 5.1	72.9 ± 9.5	68.3 ± 4.6
	210	57.6 ± 20.4	69.3 ± 5.9	72.0 ± 10.0	65.7 ± 5.9
	270	58.3 ± 18.8	69.8 ± 4.9	72.5 ± 10.0	65.2 ± 6.6
DMC	90	33.0 ± 15.3	19.5 ± 0.4	18.3 ± 4.2	25.1 ± 1.2
	120	34.2 ± 15.5	19.7 ± 0.2	19.5 ± 5.6	26.1 ± 2.5
	210	34.1 ± 15.6	19.9 ± 0.3	18.9 ± 5.2	27.8 ± 2.6
	270	35.2 ± 14.3	20.5 ± 0.6	18.9 ± 5.2	27.9 ± 2.9
BDMC	90	6.5 ± 4.9	9.1 ± 4.8	7.6 ± 3.9	5.5 ± 2.0
	120	7.6 ± 4.9	9.4 ± 5.1	7.6 ± 3.9	5.5 ± 3.1
	210	8.3 ± 4.8	10.8 ± 5.6	9.1 ± 4.9	6.5 ± 3.3
	270	6.5 ± 4.5	9.7 ± 4.4	8.6 ± 5.4	6.9 ± 1.4

Table 23: **2.** Relative amount (mean ± SD) of curcumin (CUR), demethoxycurcumin (DMC) and bisdemethoxycurcumin (BDMC) after 90, 120, 210 and 270 min in the 1-decanol layer of biorelevant biphasic dissolution (BiPHa+) (determined by HPLC). Adapted from Brenner et al., [69]. Copyright 2023 American Chemical Society.

		Amount in the 1-decanol layer [%]			
	Time [min]	**Submicron particle**	**Phytosomes**	**Cyclodextrin**	**Micelles**
CUR	90	85.4 ± 0.6	48.4 ± 17.8	73.7 ± 0.5	73.9 ± 1.0
	120	85.3 ± 0.5	47.0 ± 16.6	73.8 ± 0.5	73.1 ± 1.1
	210	85.5 ± 0.2	45.6 ± 20.2	71.9 ± 0.5	72.0 ± 1.1
	270	85.8 ± 0.1	46.1 ± 19.8	71.7 ± 0.6	72.7 ± 1.2
DMC	90	13.6 ± 0.5	44.3 ± 14.7	23.1 ± 0.4	22.2 ± 0.7
	120	13.7 ± 0.4	45.4 ± 13.8	22.9 ± 0.4	22.7 ± 0.8
	210	13.6 ± 0.1	46.7 ± 16.7	24.2 ± 0.4	23.5 ± 0.7
	270	13.4 ± 0.1	46.0 ± 16.3	24.0 ± 0.4	22.7 ± 0.7
BDMC	90	1.0 ± 0.2	7.3 ± 3.1	3.2 ± 0.1	3.9 ± 0.3
	120	1.0 ± 0.1	7.6 ± 2.9	3.3 ± 0.1	4.2 ± 0.3
	210	0.9 ± 0.1	7.7 ± 3.5	3.9 ± 0.1	4.5 ± 0.3
	270	0.8 ± 0.0	7.9 ± 3.5	4.3 ± 0.1	4.6 ± 0.3

3.3.2. Determination of the *in vivo* relevance of each dissolution method based on the establishment of *in vitro – in vivo* relationships

Generally, a dissolution method should not only be able to distinguish between various formulations and yield different dissolution rates for them, but the dissolution profiles should also be predictive towards the actual absorption kinetic *in vivo* and the expectable bioavailability in humans.

To accurately assess the predictive value of the three different dissolution methods presented in section 3.3 towards the bioavailability observed *in vivo, in vitro - in vivo* relationships were computed. **Figure 21** showcases the results. Unfortunately, due to a lack of intravenous reference data, it was not possible to subtract the *in vivo* fractions absorbed from the oral plasma concentration-time curves. As a substitute, the CUR $AUC_{0\text{-}24h\ in\ vivo}$ determined by Flory et al. [41] was used to estimate relative *in vivo* absorption and correlated with the CUR concentrations (determined through HPLC) at the end of the various dissolution tests. The correlation coefficient r^2 was used to assess linearity.

Focusing on biphasic measurements, with a particular emphasis on the organic absorption sink, a high degree of linearity as indicated by an r^2 value of one (1.00) was revealed (**Figure 21A**). The liposomes, the native extract, and formulations containing adjuvants or turmeric oils exhibited only minor partitioning rates into the 1-decanol layer and thus concentrations at the end of the dissolution test remained low (0.3 – 2.3%). The partitioned fraction of the submicron particles and phytosomes was higher (5.2%, 6.3%, respectively), with the cyclodextrin complex (21.3%) and the micelles (37.4%) showing the highest partitioned amount. The submicron particles and phytosomes could be differentiated from the four least-performing formulations based on their partitioned fraction. The BiPHa+ method facilitated a clear differentiation between the micelles and the cyclodextrin complex, enabling an accurate ranking of the formulations in the order of their bioavailability observed in humans.

However, compared to the biphasic data, the pH shift dissolution method with biorelevant medium had a lower r^2 value (0.92). The method underestimated the bioavailability of the submicron particles. According to their dissolution performance (3.1%), no differentiation could be made against the liposomes (3.2%) (**Figure 21B**). Moreover, the phytosomes

dissolution performance (4.8%) was worse than expected based on the pharmacokinetic data. However, the difference between the dissolution data and the human pharmacokinetic data was most evident for the two formulations with significantly improved bioavailability [41]. The amount released from the cyclodextrin complex (36.9%) was much higher, i.e., overestimated, compared to the micelles (43.3%). The pH-shift dissolution method with biorelevant medium was able to rank the formulations mostly correctly; however, it was not able to accurately display the bioavailability differences.

Regarding the r^2 value, the monophasic non-sink dissolution method performed the worst (0.89) (**Figure 21C**). Although the $AUC_{0\text{-}24h}$ *in vivo* of the phytosomes exceeded that of the submicron particles, the release at the endpoint of the dissolution test of the submicron particles was higher. However, the difference between the cyclodextrin complex (17.3%) and the micelles (92.4%) could not be accurately portrayed. Therefore, an accurate assessment of the bioavailability differences was not possible.

By utilizing both, an aqueous non-sink dissolution in combination with an organic absorption sink, a precise assessment of the differences in bioavailability among various formulations could be achieved. Frank et al. (2014) discovered that a monophasic non-sink dissolution process was able to differentiate between four dipyridamole formulations. However, a biphasic approach was necessary to generate biorelevant dissolution profiles [89]. Solubilization techniques such as micellization or complexation with cyclodextrins may compromise solubility enhancement by reducing transepithelial permeability [82,105]. A characterization based solely on water solubility proved to be less accurate, as indicated by the reduced degree of linearity in established Level C *in vitro - in vivo* relationships for the pH shift dissolution with biorelevant medium, and the monophasic, non-sink dissolution. The combination of aqueous non-sink dissolution with a biorelevant medium and an organic sink compartment provided an accurate estimation of bioavailability differences among various CUR formulations. The BiPHa+ was equally predictive regardless of the tested formulation principle and could be a valuable contribution in preclinical formulation development.

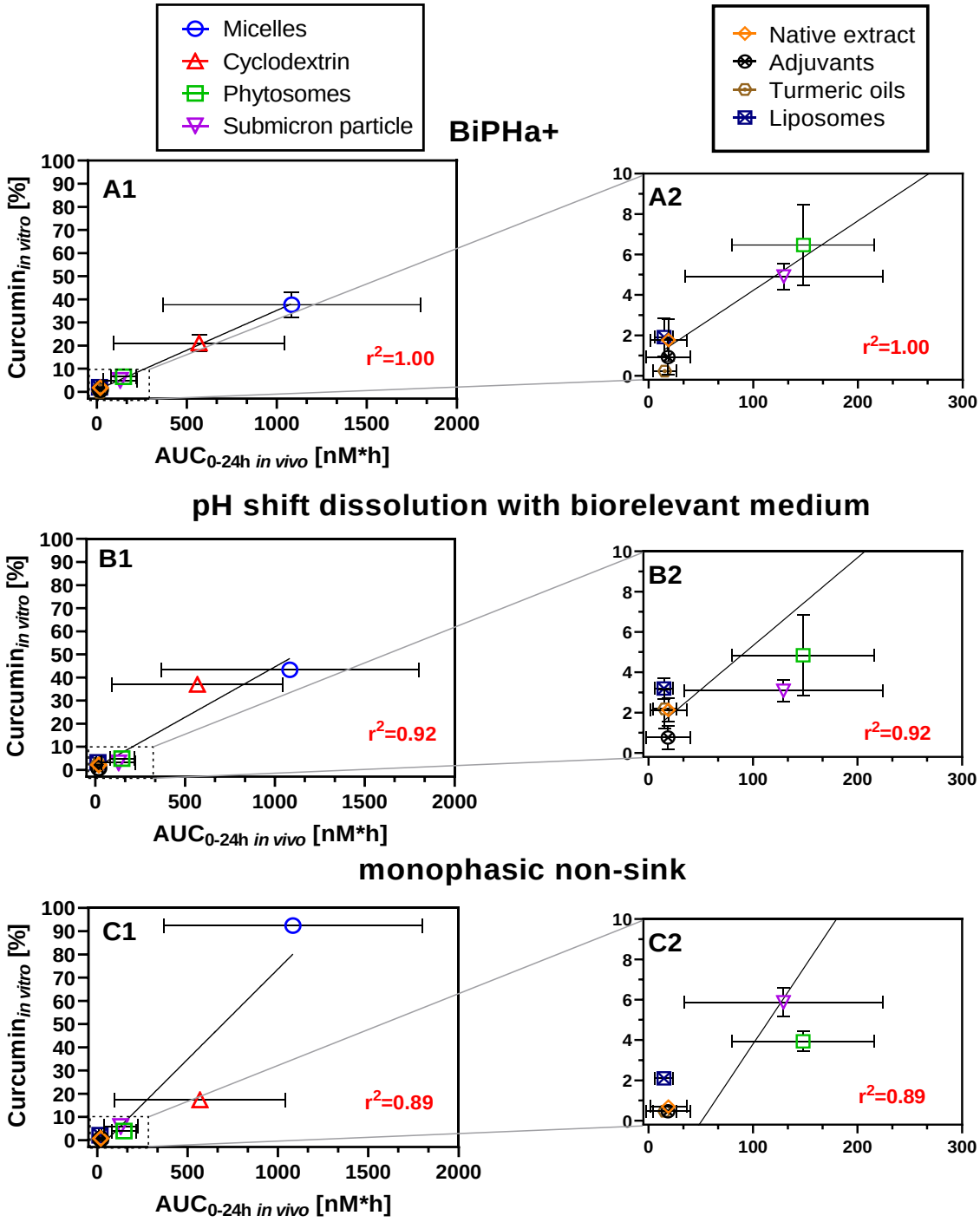

Figure 21: *In vitro-in vivo* relationships between the $AUC_{0\text{-}24h\ in\ vivo}$ [41] (mean ± SD) and the dissolved/partitioned amount of curcumin (mean ± SD, determined by HPLC) at the end of the dissolution test, **A1)** biorelevant biphasic dissolution (BiPHa+), 270 min runtime, full y-scale, **A2)** biorelevant biphasic dissolution (BiPHa+) y-scale zoom (0-10%) excluding micelles and cyclodextrin complex**, B1)** pH shift dissolution with biorelevant medium, 270 min runtime, full y-scale, **B2)** pH shift dissolution y-scale zoom (0-10%) excluding micelles and cyclodextrin complex, **C1)** monophasic non-sink dissolution (pH 6.8), 180 min runtime, full y-scale, **C2)** non-sink dissolution y-scale zoom (0-10%) excluding micelles and cyclodextrin complex. Adapted from Brenner et al., 2023 [69]. Copyright 2023 American Chemical Society.

3.4. Dissolution results obtained for the *trans-resveratrol* formulations

Parts of this chapter have been published in a peer-reviewed research article [66]. Each figure and table were created by the thesis author. Taking or adapting of figures or tables is indicated in the corresponding position.

Similar to the results presented in section 3.3, the influence of different dissolution methods on formulation characterization was investigated, this time using four different *trans*-resveratrol formulations (refer to section 2.2.2). The same three dissolution devices as previously mentioned were used, namely a conventional paddle system (apparatus 2, USP, and PhEur) with 900 mL phosphate buffer pH 6.8 (monophasic dissolution; **Figure 22**), a monophasic (non-sink) dissolution model with biorelevant medium and pH shift (pH shift dissolution with biorelevant medium; **Figure 23**), and a biorelevant biphasic dissolution system (BiPHa+; **Figure 24**). The latter two systems each used 50 mL of biorelevant aqueous medium. In contrast to the Curcuma formulations, however, the dose was set to an amount of equivalent to 10 mg resveratrol, as its solubility in 1-decanol was not limited (refer to section 2.3).

For consistency, the y-axes were scaled to 100%. Since some formulations only dissolved small amounts, the resveratrol concentrations achieved by each formulation at the end of the dissolution experiment were also presented in **Table 24** - **Table 26**.

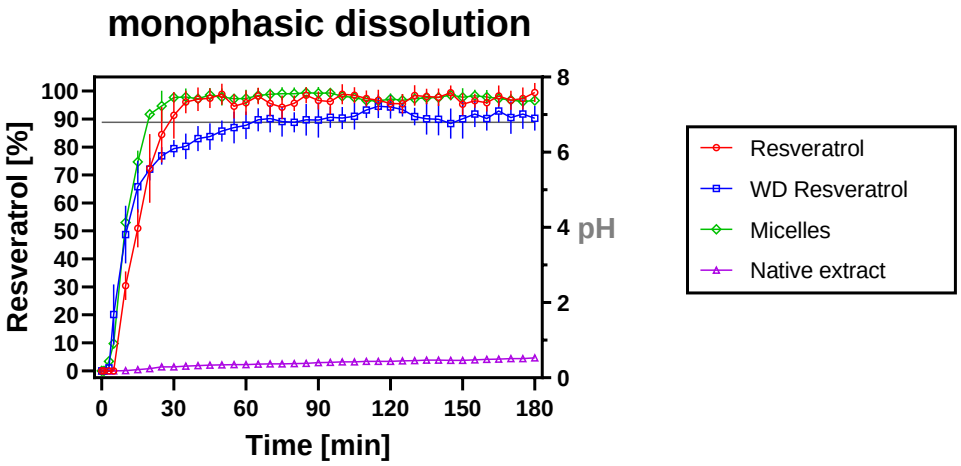

Figure 22: Dissolved amount of *trans*-resveratrol (mean ± SD) during monophasic dissolution; the pH profile in the aqueous medium is represented by the grey line, (100% corresponds to 0.01 mg/mL). Adapted from Brenner et al., 2024 [66].

Table 24: Concentrations of dissolved *trans*-resveratrol (mean ± SD) at the end of monophasic dissolution at 180 min (determined by HPLC).

Formulation	Endpoint concentration [%]
Native extract	4.6 ± 0.3
Micelles	96.6 ± 1.3
Resveratrol	99.5 ± 3.4
Water dispersible (WD) Resveratrol	90.3 ± 4.4

As mentioned above, during monophasic dissolution measurements, each vessel contained a solvent volume of 900 mL phosphate buffer pH 6.8, while the dose per vessel remained constant at 10 mg resveratrol. This resulted in a maximum possible resveratrol concentration of 0.01 mg/mL. According to this low maximum concentration of resveratrol, sink conditions were present (refer to section 2.3).

Corresponding to this large solvent volume, resveratrol and the self-emulsifying micellar formulation (micelles) achieved complete resveratrol dissolution within the first 30 min (illustrated in **Figure 22** and **Table 24**). Water dispersible (WD) resveratrol, on the contrary, was able to release over 90% of resveratrol within 60 min. At the end of the dissolution experiment at 180 minutes, the resveratrol concentrations of all three formulations were comparable (resveratrol: 98.1%; WD resveratrol: 91.6%; micelles: 96.6%). However, the native extract differed from the other formulations, releasing only 4.6% of resveratrol. Likely attributed to the swelling of matrix components in the presence of water, resveratrol dissolution was hindered. Limited by the hydrodynamics present in the dissolution vessel, the matrix components could not be brought into solution. As a consequence, the inflow of fresh dissolution medium was restricted, leading to an increased concentration of resveratrol in the local area. This caused a lower tendency for further dissolution of resveratrol from the powder reservoir. [106]. Thus, the increased volume of the dissolution medium could not affect the dissolution of resveratrol from this formulation.

Applying large solvent volumes, while maintaining the dose of active substance low (i.e., sink conditions) was not beneficial and the formulations could not be distinguished, although different formulation principles were investigated.

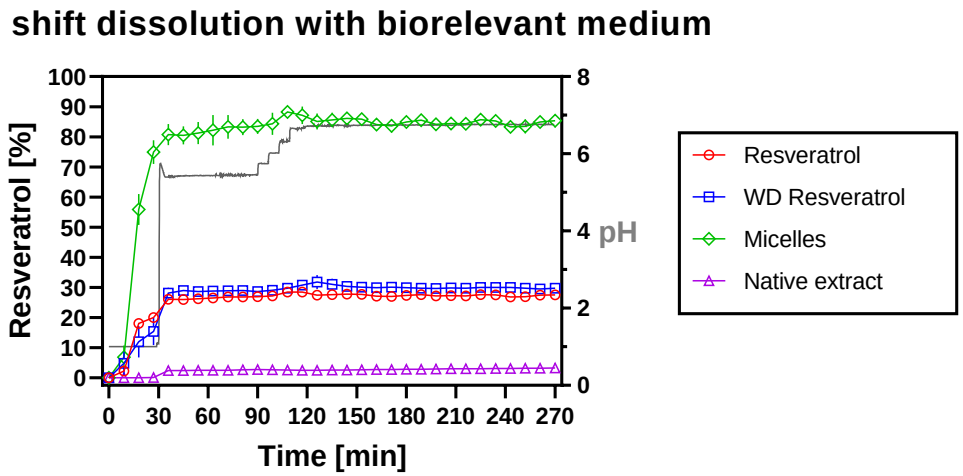

Figure 23: Dissolved amount of *trans*-resveratrol (mean ± SD) during monophasic non-sink dissolution with pH shift and biorelevant medium; the pH profile in the aqueous medium is represented by the grey line, (100% corresponds to 0.2 mg/mL). Adapted from Brenner et al., 2024 [66].

Table 25: Concentrations of dissolved *trans*-resveratrol (mean ± SD) at the end of monophasic non-sink dissolution with pH shift and biorelevant medium at 270 min (determined by HPLC).

Formulation	Endpoint concentration [%]
Native extract	4.6 ± 0.5
Micelles	85.3 ± 2.2
Resveratrol	27.5 ± 0.7
Water dispersible (WD) resveratrol	29.7 ± 0.5

Despite the presence of biorelevant surfactants, attributed to the reduced volume of dissolution medium (50.0 mL), non-sink dissolution conditions were present during pH shift dissolution with biorelevant medium.

The dissolution studies revealed, that the unformulated native extract did not release any resveratrol during the first 30 min of the dissolution test (**Figure 23**). However, the addition of biorelevant surfactants increased the concentration to 4.6%, which remained constant for the duration of the dissolution measurement. Comparable with the monophasic dissolution (apparatus 2, USP, and PhEur) results, swelling of matrix components (e.g., resveratrol oligomers [40]) limited the inflow of fresh medium and thus restricted the dissolution of resveratrol from the extract [106].

By contrast, resveratrol and WD resveratrol formulations reached concentrations of 15 - 20% in the first 30 min, with a distinct increase to nearly 30% through the addition of

Bi-FaSSIF-V2 surfactants. This concentration was equivalent to the equilibrium solubility of resveratrol in the biorelevant medium (see section 2.3). As a result, there was no further increase in concentration of resveratrol, and a plateau was formed. Both formulations reached comparable release of 27.5% and 29.7%, respectively, and were indistinguishable based on this dissolution method (**Table 25**).

Only the self-emulsifying micellar formulation achieved an extensive release of resveratrol (78.7%) during the first 30 min, even without the addition of biorelevant surfactants. This was due to the formulation already containing significant amounts of surfactant [40]. Despite being higher than the equilibrium solubility of resveratrol in biorelevant medium, the concentration remained stable at 85.3% until the end of the dissolution test. The micelles were able to stabilize resveratrol in the supersaturated state without any precipitation.

By limiting the volume of dissolution medium while providing solubility limited non-sink dissolution conditions, the resveratrol micelles could be differentiated from the other formulations. However, resveratrol and WD resveratrol remained indistinguishable.

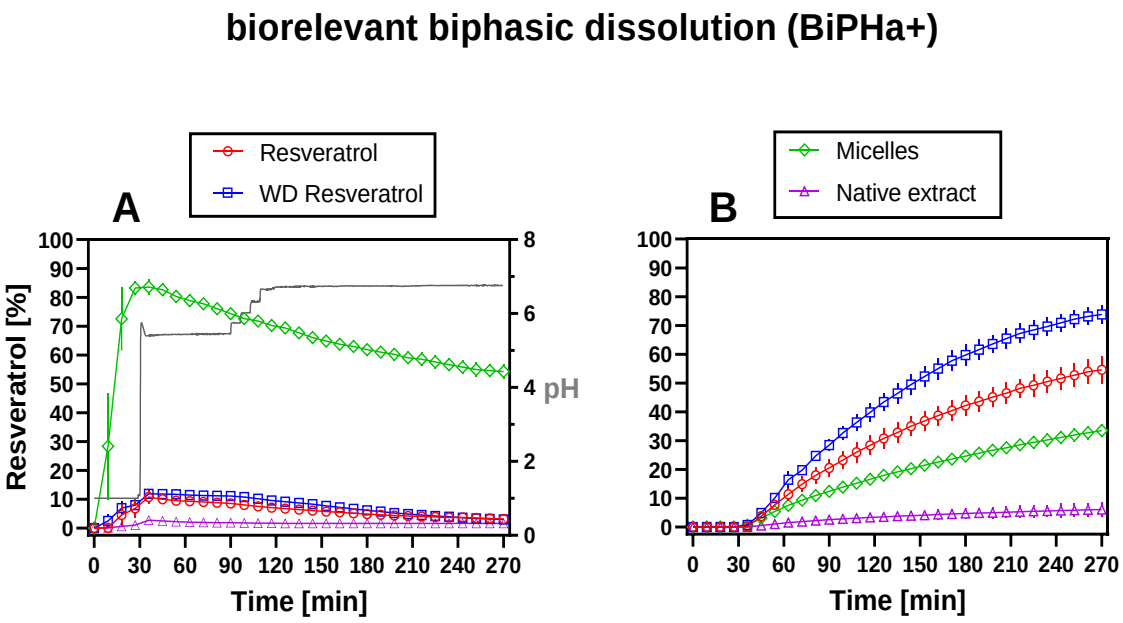

Figure 24: Dissolved/partitioned amount of *trans*-resveratrol (mean ± SD) during biorelevant biphasic dissolution (BiPHa+) measurements; **A)** aqueous medium, **B)** 1-decanol layer; the pH profile in the aqueous medium is represented by the grey line, (100% corresponds to 0.2 mg/mL). Adapted from Brenner et al., 2024 [66].

Table 26: Concentrations of dissolved/ partitioned *trans*-resveratrol (mean ± SD) in the aqueous medium and the 1-decanol layer at the end of biorelevant biphasic dissolution (BiPHa+) at 270 min (determined by HPLC).

Formulation	**Endpoint concentration [%]**	
	aqueous medium	**1-decanol**
Native extract	1.7 ± 0.3	6.1 ± 2.5
Micelles	54.3 ± 2.6	33.5 ± 2.4
Resveratrol	3.2 ± 0.4	54.6 ± 4.7
Water dispersible (WD) resveratrol	3.0 ± 1.1	73.8 ± 3.1

Results revealed that the native extract released 1.0 % resveratrol during the gastric phase of biphasic dissolution (**Figure 24A**). Subsequent to the addition of Bi-FaSSIF-V2 at 30 min, the concentration increased to 2.9%, followed by a decrease to approximately 1.7% in the progress of the dissolution measurement. Resveratrol and WD resveratrol formulations showed comparable dissolution profiles in the aqueous medium. During the gastric stage, resveratrol released 6.8% and for WD resveratrol a release of 7.2% was detected. After the addition of surfactant, the concentration increased to 12 - 13%, followed by a gradual decrease to 3.2% and 3.0%, respectively. The highest dissolution was observed for the micellar formulation of the native extract, which exhibited 85.0% dissolution during the first 30 min. No influence of surfactant addition was detected. Subsequently, the concentration gradually decreased to 54.3% (**Table 26**). Similar to the previously described monophasic dissolution methods, the micellar formulation formed an emulsion *in situ* and resveratrol was trapped in the micelles and thus kept in solution [107].

After 30 min the aqueous medium was covered with 50.0 mL 1-decanol to simulate intestinal absorption. The organic layer acted as an artificial sink, and dissolved resveratrol was removed from the water phase. Consequently, the dissolution profiles in the aqueous phase showed a gradual reduction in concentration for all formulations (**Figure 24B**). However, due to the declining concentration in the aqueous phase and the resulting reduced pull into the 1-decanol phase, the partitioning rate into the organic layer continuously decreased, reaching the maximum concentration at 270 min.

Comparable to the dissolution of resveratrol in the aqueous medium, it was found that the native extract had the lowest partitioning rate and a concentration of 6.1% was

measured after 270 min. Typically, in biphasic dissolution experiments, the active ingredient is first dissolved in an aqueous medium and then crosses the aqueous-organic interface, finally accumulating in the organic phase. If the aqueous concentration generated by the formulation is to low, reduced partitioning into the organic absorption phase will occur [52].

For the micellar formulation the decisively increased water solubility of resveratrol, even under non-sink conditions, partially led to an increased partitioning rate and 33.5% resveratrol were detected in the 1-decanol layer after 270 min.

While the WD resveratrol and resveratrol formulations had reduced water solubility compared to micelles, they exhibited a higher partitioning rate into the organic phase, with 73.8% and 54.6% of the applied doses detected in the 1-decanol layer after 270 min, respectively. This may seem contradictory at first, but depending on the stability and lipophilicity of the surfactants used, micellar inclusion complexes may hinder partitioning into the organic phase. If stable complexes were formed, the active ingredient can at least partially be retained in the aqueous medium, as the amount of free active ingredient in the solution decreases, and only free active ingredient is available for partitioning into the organic layer [85,103].

Active ingredient which was released by the resveratrol or WD resveratrol formulations dissolved in the aqueous phase without forming inclusion complexes and was therefore directly available for partitioning into the organic phase. While association with the biorelevant surfactants lecithin and taurocholate might be possible, the micelles formed were not stable enough to hinder the transition into the organic phase.

3.4.1. Assessment the *in vivo* relevance of each dissolution method based on comparison with human pharmacokinetic data

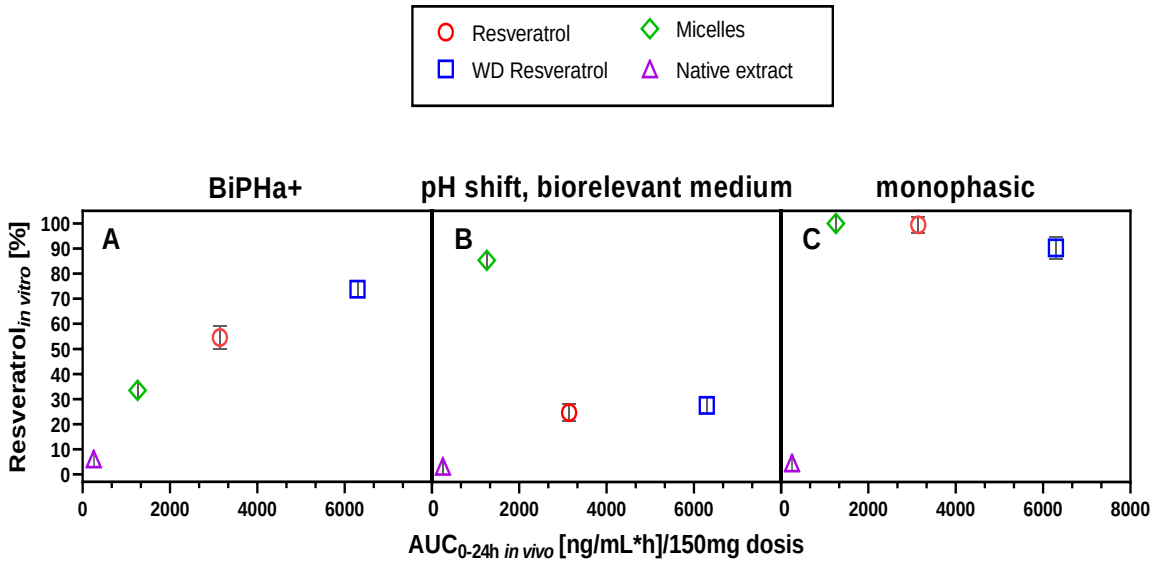

Figure 25: Comparison of *in vitro* dissolution results of *trans*-resveratrol (mean ± SD) with the $AUC_{0\text{-}24h\ in\ vivo}$ values [40,44], **A)** biorelevant biphasic dissolution (BiPHa+), 270 min runtime, organic layer, **B)** monophasic non-sink dissolution with pH shift and biorelevant medium, 270 min runtime, **C)** monophasic dissolution (pH 6.8), 180 min runtime. Adapted from Brenner et al., 2024 [66].

To compare the predictive value of the three different investigated dissolution methods (**Figure 22** - **Figure 24**), consideration of pharmacokinetic data from strictly controlled human trials is essential. As there is a lack of intravenous (i.v.) reference data, the area under the curve (AUC) has been used as a surrogate for relative *in vivo* absorption and compared with *in vitro* dissolution results. In the case of resveratrol, data from two pharmacokinetic trials were available, each comparing two different formulations [40,44].

The biphasic dissolution assay accurately reproduced the 5.0-fold increase in AUC observed in the comparison of the native extract and the micelles by Calvo-Castro et al. (2018), revealing a 5.5-fold superiority of the micelles (**Figure 25A**). However, both the monophasic non-sink dissolution with pH shift and biorelevant medium and the monophasic dissolution overestimated the performance of the micelles and failed to predict the *in vivo* results correctly.

SEDDS are known to enhance the bioavailability of poorly soluble natural compounds [40,41,43,45]. However, the improvement in water solubility often does not correspond to an equally high increase in bioavailability. Otherwise, any self-emulsifying system that

enables dissolving of the applied dose completely in a glass of water (250 mL) would have to be 100% bioavailable.

The relative bioavailability of resveratrol and water dispersible (WD) resveratrol was studied by Briskey and Rao (2020), determining a 2-fold superiority of the WD resveratrol formulation. Our study revealed a 1.4-fold increase in the partitioned amount of WD resveratrol in biphasic dissolution, and thus, the results corresponded quantitatively to the results of Briskey and Rao [44]. The other investigated dissolution methods either failed to differentiate between both formulations (**Figure 25B**) or revealed a superiority of the resveratrol formulation (**Figure 25C**). This suggests that relying only on water solubility for formulation characterization is inadequate, and an organic absorption sink should be included to achieve a meaningful formulation characterization.

These findings align with Frank et al. (2014), who reported that a biphasic approach is required for generating biorelevant partitioning profiles, while monophasic non-sink dissolution could only differentiate qualitatively between the dipyridamole formulations investigated [89].

In addition to comparing formulations within studies, the results of two separate pharmacokinetic studies were linked. Resveratrol and WD resveratrol studied by Briskey and Rao showed higher AUCs, when compared to the native extract and the corresponding micellar formulation. However, these results could only be reproduced by biphasic dissolution measurements (**Figure 25A**). In contrast, the monophasic non-sink dissolution method with pH shift and biorelevant medium underestimated the performance of resveratrol and WD resveratrol, while overestimating the performance of the micelles (**Figure 25B**). Lastly, related to the large volume of dissolution medium used, monophasic dissolution failed to differentiate between three of the four investigated formulations, namely the micelles, resveratrol, and water dispersible resveratrol (**Figure 25C**) and proofed to be inadequate for formulation characterization.

3.5. Dissolution results obtained for the *coenzyme Q10* formulations

Parts of this chapter have been published in a peer-reviewed research article [66]. Each figure and table were created by the thesis author. Taking or adapting of figures or tables is indicated in the corresponding position.

For consistency, the y-axes were scaled to 100%. Since some formulations only dissolved small amounts, the CoQ10 concentrations achieved by each formulation at the end of the dissolution experiment were also presented in **Table 27** - **Table 29**. In the case of monophasic non-sink dissolution (**Figure 26**) and monophasic non-sink dissolution with pH shift and biorelevant medium (**Figure 27**), a y-scale zoom 0 - 10% is additionally shown in order to display the dissolution results obtained for the not water-solubility optimized formulations.

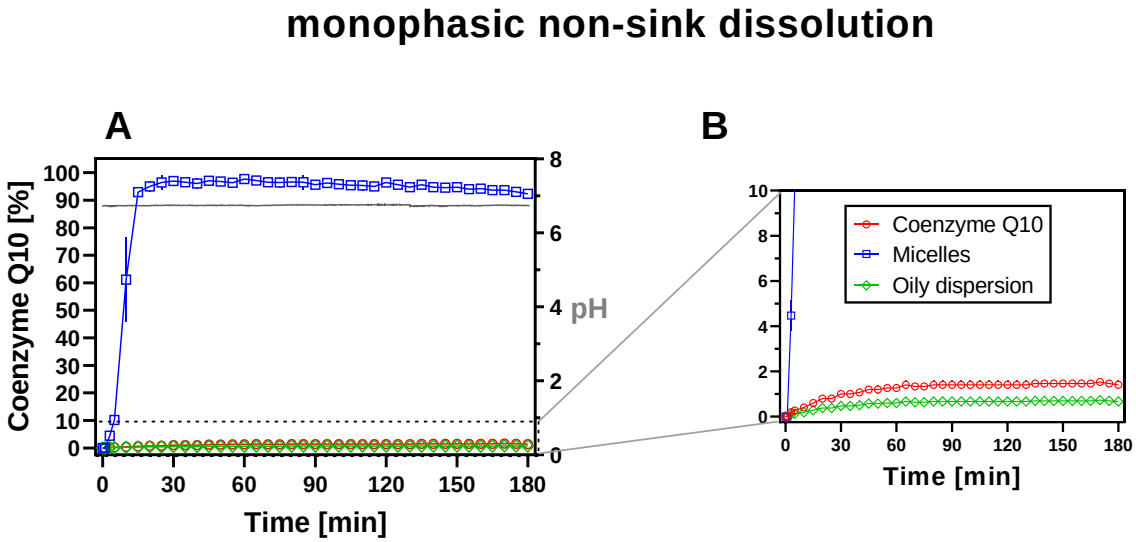

Figure 26: Dissolved amount of coenzyme Q10 (mean ± SD) during monophasic non-sink dissolution, **A)** full y-scale, **B)** y-scale zoom (0-10%) excluding micelles; the pH profile in the aqueous medium is represented by the grey line, (100% corresponds to 0.01 mg/mL).

Table 27: Concentrations of dissolved coenzyme Q10 (mean ± SD) at the end of monophasic non-sink dissolution at 180 min (determined by HPLC).

Formulation	Endpoint concentration [%]
Coenzyme Q10	1.4 ± 0.2
Micelles	92.4 ± 1.5
Oily dispersion	0.7 ± 0.1

Despite using a large volume of 900 mL phosphate buffer, while maintaining the dose per vessel at 10 mg active ingredient, the pH independent low solubility of CoQ10 in water resulted in non-sink conditions being present during monophasic dissolution (apparatus 2, USP, and PhEur) measurements.

Consequently, the release of CoQ10 from the oily dispersion formulation and the unformulated compound were limited and concentrations of 0.7 - 1.4% were measured (**Figure 26** and **Table 27**). Since the oily dispersion formulation aimed to increase CoQ10 bioavailability through absorption in combination with dietary fats via the lymphatic pathway, the formulation has not been optimized for water solubility [43]. Accordingly, a concentration at the end of the dissolution test, that does not differ significantly from that of unformulated CoQ10 has to be expected.

In contrast, the self-emulsifying micellar formulation dissolves CoQ10 quickly and quantitative. By incorporating the highly hydrophobic CoQ10 together with lipids in a micellar inclusion complex, almost 100% release was achieved within 30 min. The formulation stabilized the high concentration in the aqueous medium until the end of the dissolution test, and no precipitation occurred.

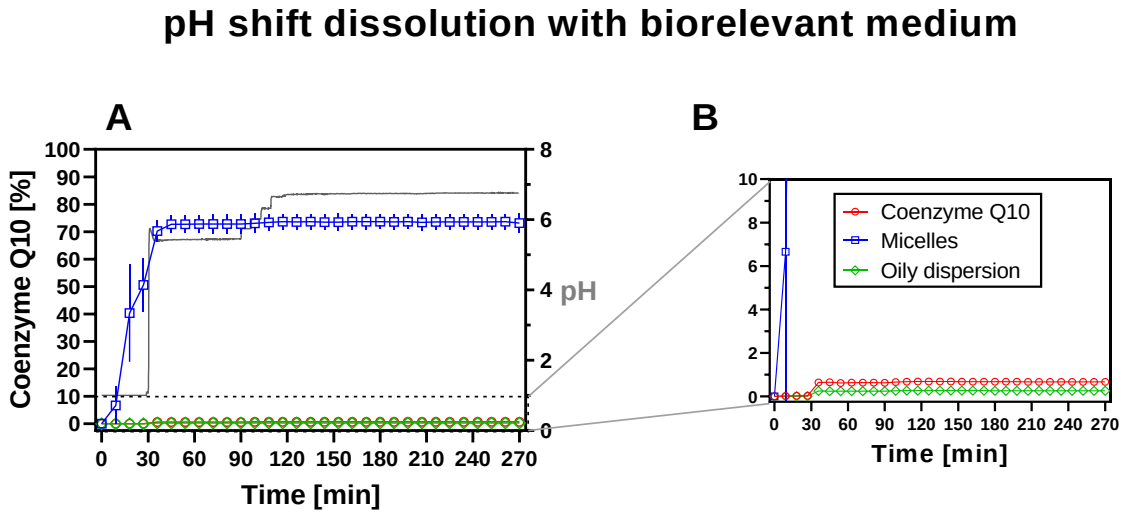

Figure 27: Dissolved amount of coenzyme Q10 (mean ± SD) during monophasic non-sink dissolution with pH shift and biorelevant medium, **A)** full y-scale, **B)** y-scale zoom (0-10%) excluding micelles; the pH profile in the aqueous medium is represented by the grey line, (100% corresponds to 0.2 mg/mL). Adapted from Brenner et al., 2024 [66].

Table 28: Concentrations of dissolved coenzyme Q10 (mean ± SD) at the end of monophasic non-sink dissolution with pH shift and biorelevant medium at 270 min (determined by HPLC).

Formulation	Endpoint concentration [%]
Coenzyme Q10	0.7 ± 0.1
Micelles	73.1 ± 3.5
Oily dispersion	0.3 ± 0.0

Comparable to the monophasic non-sink dissolution (apparatus 2, USP, and PhEur) results, unformulated CoQ10 and the oily dispersion formulation reached only deficient CoQ10 concentrations in the aqueous medium during monophasic non-sink dissolution with pH shift and a biorelevant medium (**Figure 27**). After the addition of biorelevant surfactants at the 30-minute mark, a slight increase in the CoQ10 concentration was detected for both formulations. However, the oily dispersion formulation only achieved 0.3% release after 270 min, while the unformulated CoQ10 achieved 0.7% release. Even though surfactants were added to the dissolution medium, due to its reduced volume compared to the monophasic non-sink dissolution, CoQ10 concentrations remained even lower.

The micelles achieved approx. 70% release after 45 min, further dissolution was not achieved. After 270 min, a CoQ10 concentration of 73.1% was reached (**Table 28**). Precipitation of already dissolved active ingredients was not observed.

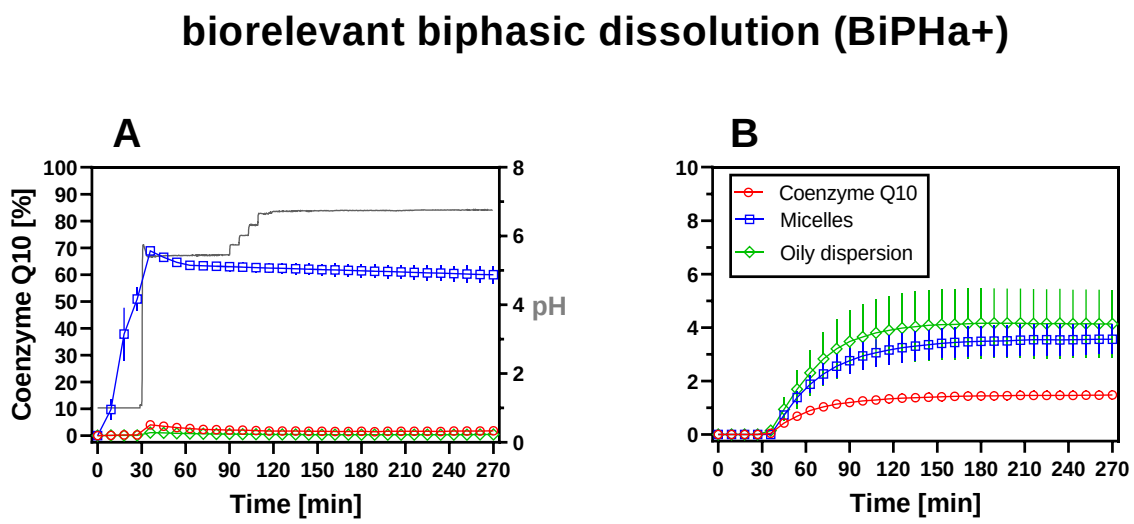

Figure 28: Dissolved/partitioned amount of coenzyme Q10 (mean ± SD) during biorelevant biphasic dissolution (BiPHa+) measurements; **A)** aqueous medium**, B)** 1-decanol layer; the pH profile in the aqueous medium is represented by the grey line, (100% corresponds to 0.2 mg/mL). Adapted from Brenner et al., 2024 [66].

Table 29: Concentrations of dissolved/ partitioned coenzyme Q10 (mean ± SD) in the aqueous medium and the 1-decanol layer at the end of biorelevant biphasic dissolution (BiPHa+) at 270 min (determined by HPLC).

Formulation	**Endpoint concentration [%]**	
	aqueous medium	**1-decanol**
Coenzyme Q10	2.0 ± 0.3	1.5 ± 0.2
Micelles	60.0 ± 3.2	3.6 ± 0.6
Oily dispersion	0.4 ± 0.1	4.0 ± 1.3

Comparable to the self-emulsifying formulations of CUR and resveratrol, the CoQ10 micelles released the highest amount during biorelevant biphasic dissolution, as depicted in **Figure 28**. In the first 30 min, up to 70% of CoQ10 was released, which then decreased to 60.0%. This decline may have resulted from the transfer of CoQ10 into the organic absorption sink.

In contrast, neat CoQ10 and the oily dispersion showed reduced water solubility. During the gastric stage (first 30 min), less than 1% release was detected, increasing to 1.2% for the oily dispersion and 4.3% for neat CoQ10, respectively. At the end of the dissolution test, the concentration of neat CoQ10 in the aqueous medium decreased to 2.1%, which corresponds to the equilibrium solubility in Bi-FaSSIF-V2 (refer to section 2.3).

According to the results presented in **Figure 28B** and **Table 29**, the partitioned amount of CoQ10 in the 1-decanol layer was 1.5% for neat CoQ10, 4.0% for the oily dispersion, and 3.6% for the micelles, respectively. While the micelles had significantly higher water solubility (20 times), the partitioned amount of CoQ10 only increased by a factor of 2.4. This was likely attributed to the *in situ* formation of stable micellar inclusion complexes, which restricted the amount of free active ingredient available for partitioning into the organic layer [90,108].

Conversely, the oily dispersion showed reduced water solubility, but experienced a higher partitioning rate into the organic medium. This could be explained by their lipophilic matrix, including the dissolved/suspended CoQ10 fraction, being capable of directly partitioning into the organic layer, since the oil components exhibited a high 1-decanol solubility. When bile salts emulsify tiny droplets of the formulation, these droplets could directly pass into the organic phase. This improved the partitioning rate, even though the

actual CoQ10 concentration in the aqueous medium remained low [109]. Thus, the BiPHa+ was also able to simulate increased absorption of lipophilic compounds via the lymphatic pathway. However, only a small fraction of the formulation gets emulsified *in situ*, which limits the total CoQ10 amount available for transfer into the organic phase and after 270 min of dissolution, only a concentration of 4.1% CoQ10 was detected in the 1-decanol layer.

3.5.1. Determination of the *in vivo* relevance of each dissolution method based on the establishment of *in vitro – in vivo* relationships

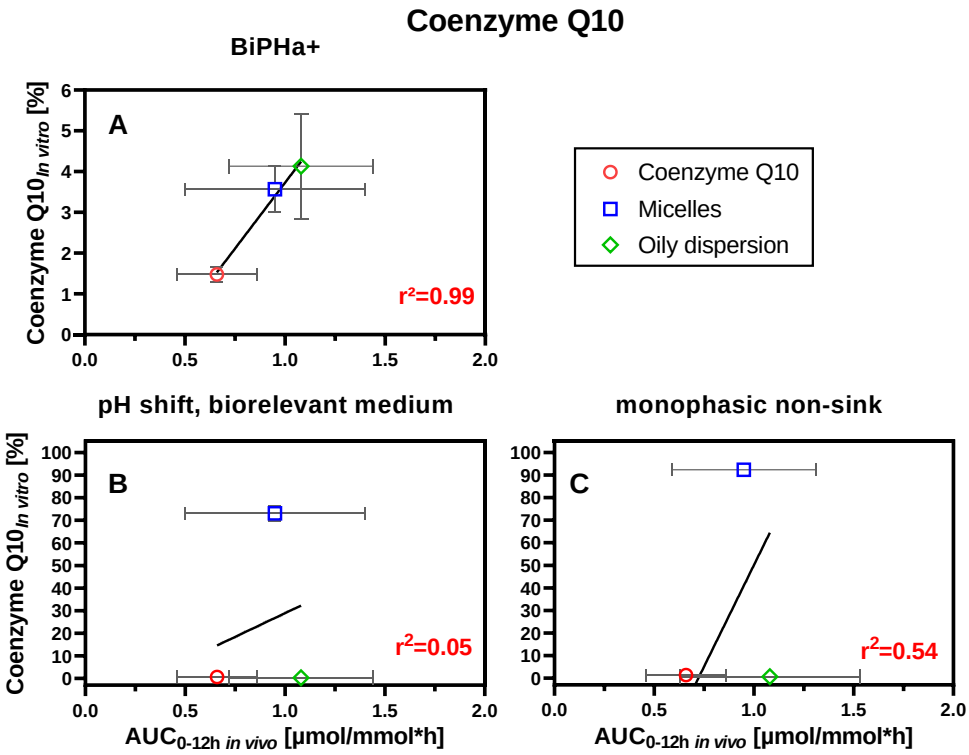

Figure 29: *In vitro-in vivo* relationship between the $AUC_{0\text{-}24h\ in\ vivo}$ [43] (mean ± SD) and the dissolved/partitioned amount of coenzyme Q10 (mean ± SD) at the end of the dissolution test, **A**) biorelevant biphasic dissolution (BiPHa+), 270 min runtime, organic layer, **B**) monophasic non-sink dissolution with pH shift and biorelevant medium, 270 min runtime, **C**) monophasic non-sink dissolution (pH 6.8), 180 min runtime. Partially adapted from Brenner et al., 2024 [66].

To compare the predictive value of the three different dissolution methods investigated (**Figure 26** - **Figure 28**), it is crucial to consider pharmacokinetic data from strictly controlled human trails. Since there was no i.v. reference data available, the $AUC_{0\ -\ 12h\ in\ vivo}$ has been utilized as an alternative for quantification of relative *in vivo* absorption and compared with *in vitro* dissolution results. *In vitro – in vivo* relationships

for CoQ10 were established, using the correlation coefficient r^2 for determination of linearity.

The study conducted by Schulz et al. in 2006 has been used to obtain human pharmacokinetic data of different CoQ10 formulations for reference [43].

The biphasic dissolution results revealed a linear relationship between the $AUC_{0\text{-}12h}$ *in vivo* and the concentration measured in the 1-decanol layer at the end of dissolution measurements. Based on this relationship, all three formulations were ranked according to their expected bioavailability in humans and their differences in bioavailability were accurately reproduced (as shown in **Figure 29A**). Thus, the correlation coefficient r^2 was calculated to be 0.99 for the *in vitro – in vivo* relationship.

However, in the case of monophasic non-sink dissolution with pH shift and a biorelevant medium, the concentration values at the end of dissolution measurements did not correlate with the $AUC_{0\text{-}12h}$ *in vivo* values. The correlation coefficient in this case was found to be low ($r^2 = 0.05$) (as shown in **Figure 29B**). The micelles were overestimated and the oily dispersion and neat CoQ10 were indistinguishable.

The results of the monophasic non-sink dissolution studies showed a similar outcome (**Figure 29C**). The efficacy of the micellar formulation in improving the bioavailability of CoQ10 was considerably overestimated, while differentiating between the unformulated CoQ10 and the oily dispersion formulation was impossible. Unfortunately, the differences in bioavailability among the various formulations could not be accurately measured neither quantitatively nor qualitatively.

As a result, only biphasic dissolution was able to evaluate the bioavailability differences of the formulations. Both monophasic dissolution approaches failed in generating *in vivo* relevant data.

3.6. Dissolution results obtained for the *quercetin* formulations

Parts of this chapter have been published in a peer-reviewed research article [66]. Each figure and table were created by the thesis author. Taking or adapting of figures or tables is indicated in the corresponding position.

For consistency, the y-axes were scaled to 100%. Since some formulations only dissolved small amounts, the quercetin concentrations achieved by each formulation at the end of the dissolution experiment were also presented in **Table 30** - **Table 32**. The dissolution results obtained for monophasic dissolution, monophasic non-sink dissolution with pH shift and a biorelevant medium and biorelevant biphasic dissolution are shown in **Figure 30** - **Figure 32**.

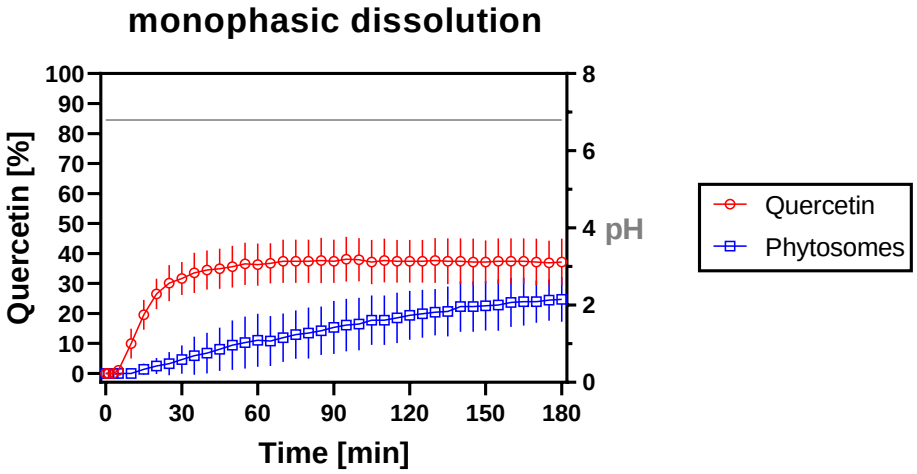

Figure 30: Dissolved amount of quercetin (mean ± SD) during monophasic dissolution; the pH profile in the aqueous medium is represented by the grey line, (100% corresponds to 0.01 mg/mL). Adapted from Brenner et al., 2024 [66].

Table 30: Concentrations of dissolved quercetin (mean ± SD) at the end of monophasic dissolution at 180 min (determined by HPLC).

Formulation	Endpoint concentration [%]
Quercetin	37.1 ± 7.8
Phytosomes	24.7 ± 7.5

During monophasic dissolution measurements, it was found that neat quercetin dissolved at a faster rate and to a higher extent than the phytosomes, when 900 ml of phosphate

buffer at pH 6.8 (1.8x sink) were used as dissolution medium (**Figure 30**). Neat quercetin dissolution was measured as 37.1% after 60 min, followed by a plateau formation until the end of the 180-min dissolution test. Attributed to the increased solvent volume, no precipitation occurred. Conversely, the phytosomes showed a continuous increase in concentration over time, reaching a maximum concentration of 24.7% at 180 min (**Table 30**). The decreased dissolution speed of the phytosomes could be attributed to their larger particle size. Neat quercetin was in the form of fine powder, whereas the phytosomes were manufactured in the form of granules. Larger particles have less surface area available for interaction with the solvent, when compared to smaller particles of the same mass. As a result, lower dissolution rates were achieved. Neuwith et al. (2023) discovered a linear relationship between the total outer surface area (TOPS) and the dissolution rate of amorphous solid dispersions (ASD) produced by spray drying or pellet coating. The smaller the particle size, the larger was the TOPS and the higher was the dissolution rate of the model drugs ketoconazole and loratadine [110].

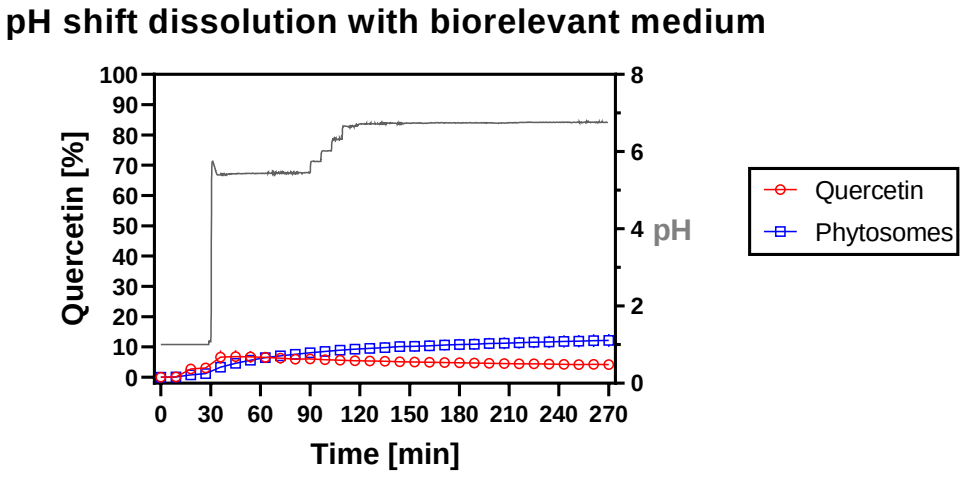

Figure 31: Dissolved amount of quercetin (mean ± SD) during monophasic non-sink dissolution with pH shift and biorelevant medium; the pH profile in the aqueous medium is represented by the grey line, (100% corresponds to 0.2 mg/mL). Adapted from Brenner et al., 2024 [66].

Table 31: Concentrations of dissolved quercetin (mean ± SD) at the end of monophasic non-sink dissolution with pH shift and biorelevant medium at 270 min (determined by HPLC).

Formulation	Endpoint concentration [%]
Quercetin	4.2 ± 0.9
Phytosomes	12.2 ± 2.2

During monophasic non-sink dissolution with a pH shift and biorelevant medium, the amount of quercetin released from the phytosomes steadily increased until the end of the dissolution test, resulting in a maximum dissolved amount of 12.2% at 270 min (**Figure 31** and **Table 31**). As the formulation contains phospholipids that act as emulsifiers and form quercetin inclusion complexes, no effect of Bi-FaSSIF-V2 addition was observed [46]. However, neat quercetin displayed a strong dependence on surfactant concentration. At the 30-minute mark of dissolution, only 3.0 % of quercetin was released, with an increase to 6.8% after Bi-FaSSIF-V2 addition. Afterwards, due to quercetin precipitation, the concentration decreased to 4.2%.

In a manner similar to monophasic dissolution, the unformulated quercetin exhibited a faster initial dissolution rate owing to its smaller particle size. Nevertheless, the limited solvent volume of 50.0 mL and the low solubility of quercetin in biorelevant medium prevented further dissolution beyond the 10% mark. However, the phytosomes proved to be effective in enhancing the solubility of quercetin, enabling it to dissolve continuously without precipitation. Phytosomal inclusion complexes have already demonstrated their ability to increase bioavailability and dissolution rate of various phytoconstituents via *in situ* formation of drug delivery vehicles [46,111,112].

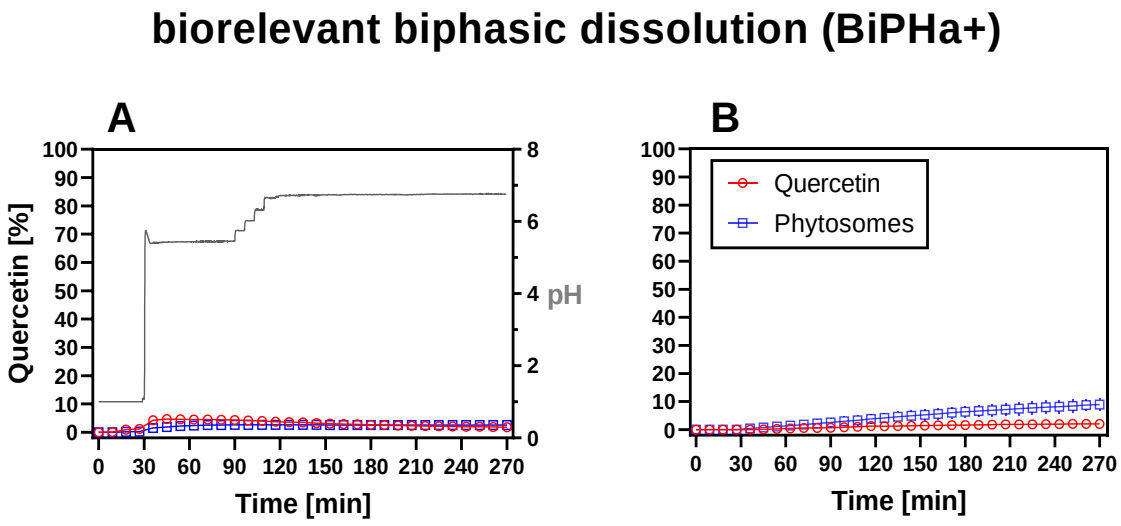

Figure 32: Dissolved/partitioned amount of quercetin (mean ± SD) during biorelevant biphasic dissolution (BiPHa+) measurements; **A)** aqueous medium, **B)** 1-decanol layer; the pH profile in the aqueous medium is represented by the grey line, (100% corresponds to 0.2 mg/mL). Adapted from Brenner et al., 2024 [66].

Table 32: Concentrations of dissolved/ partitioned quercetin (mean ± SD) in the aqueous medium and the 1-decanol layer at the end of biorelevant biphasic dissolution (BiPHa+) at 270 min (determined by HPLC).

Formulation	**Endpoint concentration [%]**	
	aqueous medium	**1-decanol**
Quercetin	1.8 ± 0.6	1.9 ± 1.3
Phytosomes	2.5 ± 1.3	8.9 ± 2.2

The biorelevant biphasic dissolution measurements, found that both neat quercetin and the phytosomes released less than 3% in the first 30 min. However, the addition of Bi-FaSSIF-V2 resulted in an increase in concentration to 4.6% and 2.5%, respectively, as depicted in **Figure 32A**. Throughout the test, the amount of quercetin dissolved by the phytosomes remained constant, while for neat quercetin the concentration reduced to 1.8% due to partitioning into the organic layer (**Table 32**). Nevertheless, the concentration of quercetin in the aqueous medium was too low to facilitate higher partitioning of quercetin in the artificial 1-decanol absorption compartment (refer to section 3.3).

Despite comparable concentrations in the aqueous medium, the phytosomes experienced continuous partitioning into the 1-decanol layer, resulting in a concentration of 8.9% at the dissolution endpoint (**Figure 32B**). This might be attributed to a dynamic equilibrium formed wherein the dissolution speed from the undissolved powder reservoir was as high as the partitioning rate into the 1-decanol layer [53].

The partitioning rate for neat quercetin into the organic phase was less pronounced, with only 1.9% measured after 270 min. However, phytosomes showed an enhanced partitioning rate into the 1-decanol layer, which could be related to the *in situ* formation of lipid-compatible molecular complexes with improved absorption behavior [102,103]. The formation of quercetin-phospholipid complexes may facilitate partitioning into the 1-decanol layer compared to neat quercetin at the same concentration.

3.6.1. Assessment of the *in vivo* relevance of each dissolution method based on comparison with human pharmacokinetic data

Table 33: Comparison of *in vitro* dissolution results (concentration at the end of the dissolution test; mean ± SD) with *in vivo* pharmacokinetic parameters of quercetin and quercetin phytosomes (mean ± SD; *n* = 12) obtained by Riva et al. (2018) [46]. Adapted from Brenner et al., 2024 [66].

Parameter	Quercetin	Phytosomes
$AUC_{0\text{-}24h\ in\ vivo}$ [µg x h/mL] [46]	4774.9 ± 1190.6	96,163.9 ± 9291.3
Difference (n-fold)	**20.1**	
Biorelevant biphasic dissolution (BiPHa+) [%]	1.9 ± 1.3	8.9 ± 2.2
Difference (n-fold)	**4.7**	
Monophasic non-sink dissolution with pH shift and biorelevant medium [%]	4.2 ± 0.9	12.2 ± 2.2
Difference (n-fold)	**2.9**	
Monophasic dissolution [%]	37.1 ± 7.8	24.7 ± 7.5
Difference (n-fold)	**0.7**	

The results of the quercetin dissolution studies were compared with human pharmacokinetic data. Since there was no available i.v. reference data, the $AUC_{in\ vivo}$ has been utilized as an alternative for quantification of relative *in vivo* absorption and compared with *in vitro* dissolution results.

Riva et al. (2018) conducted a strictly controlled human pharmacokinetic trial that revealed a 20-fold increase in $AUC_{0\text{-}24h}$ when phytosomes were applied [46]. Even though none of the dissolution methods were able to reproduce a difference of that scale, biphasic dissolution demonstrated a 4.7 times higher partitioning in the 1-decanol layer for the phytosomes (**Table 33**). This particular method showed the greatest difference between both formulations and most closely matched the *in vivo* results. Non-sink dissolution with pH shift and biorelevant medium showed a 2.9-fold increase. However, conventional monophasic dissolution did not provide dissolution profiles that were relevant to *in vivo* results, and phytosomes were estimated to have 0.7 times inferior bioavailability. Thus, the use of a 1-decanol absorption sink was not necessary for this set of formulations, but beneficial in terms of estimating bioavailability differences. Whereas using a non-biorelevant dissolution medium resulted in a loss of distinguishability between formulations and, therefore, *in vivo* relevance of the dissolution method.

3.7. Dissolution results obtained for the *astaxanthin* formulations

For consistency, the y-axes were scaled to 100%. Since the unformulated *Haematococcus pluvialis* extract (oleoresin) only dissolved small amounts, the ASX concentrations (sum of mono- and diesters) achieved by each formulation at the end of the dissolution experiment were also presented in **Table 30** - **Table 32**.

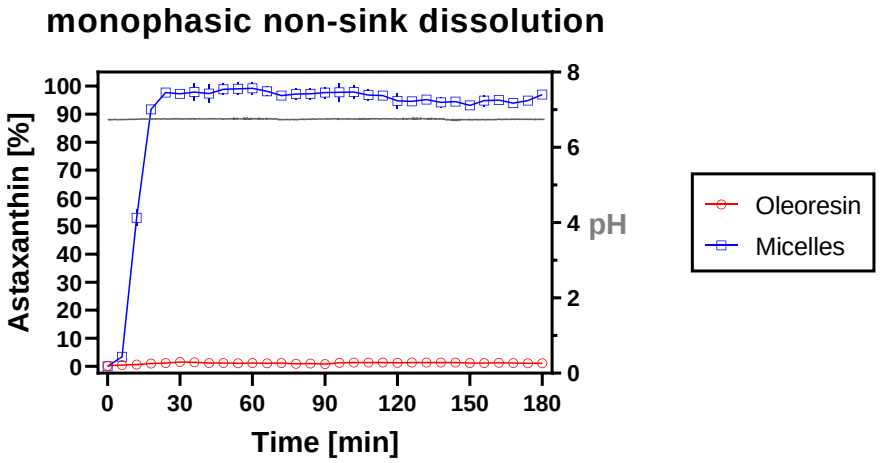

Figure 33: Dissolved amount of astaxanthin (sum of mono- and diesters; mean ± SD) during monophasic non-sink dissolution; the pH profile in the aqueous medium is represented by the grey line, (100% corresponds to 0.01 mg/mL).

Table 34: Concentrations of dissolved astaxanthin (sum of mono- and diesters; mean ± SD) at the end of monophasic non-sink dissolution at 180 min (determined by HPLC).

Formulation	Endpoint concentration [%]
Oleoresin	1.1 ± 1.0
Micelles	97.0 ± 1.0

The self-emulsifying micellar ASX formulation exhibited a high dissolution rate, with complete dissolution achieved within 30 min (**Figure 33**). The initially reduced dissolution speed resulted from the hard gelatine capsule (necessary for proper dosing and introduction of the formulation into the dissolution vessels) needing to dissolve first to than release the formulation. As already demonstrated for CoQ10 and other hydrophobic natural compounds, maintaining a high concentration of ASX in solution required a self-emulsifying drug delivery system that kept the active substance enclosed in the lipophilic core of the micelles formed *in situ* (see sections 2.2.1 to 2.2.3) [113]. Throughout the

dissolution measurement, the concentration of ASX remained stable at 97.0%, demonstrating the effectiveness in enhancing water solubility of this delivery system. However, the unformulated microalgae extract (oleoresin) had a semi-solid paste-like composition that resulted in the formation of large droplets in the dissolution medium. Concerning their mass, theses droplets had minimal surface area, which is needed for interaction with the solvent, leading to a low ASX concentration of 1.1% at the end of the measurement at 180 min (**Table 34**) [114]. The concentration aligned with its expected value based on saturation solubility in water at pH 6.8.

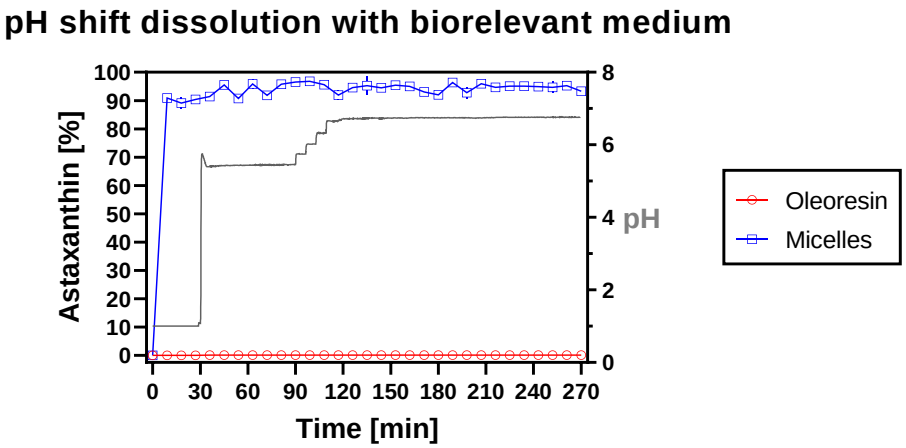

Figure 34: Dissolved amount of astaxanthin (sum of mono- and diesters; mean ± SD) during monophasic non-sink dissolution with pH shift and biorelevant medium; the pH profile in the aqueous medium is represented by the grey line, (100% corresponds to 0.2 mg/mL).

Table 35: Concentrations of dissolved astaxanthin (sum of mono- and diesters; mean ± SD) at the end of monophasic non-sink dissolution with pH shift and biorelevant medium at 270 min (determined by HPLC).

Formulation	Endpoint concentration [%]
Oleoresin	0.1 ± 0.1
Micelles	93.3 ± 0.7

Likely attributed to the low solvent volume, in combination with limited saturation solubility of ASX in biorelevant medium, there was minimal release observed from the oleoresin during monophasic non-sink dissolution with pH shift and biorelevant medium (**Figure 34**). After 270 min, only a concentration of 0.1% was measured (**Table 35**). When the oleoresin was introduced to an aqueous medium, it formed large droplets with

minimal surface area. Accordingly, no increase in the dissolution rate occurred with the addition of biorelevant surfactants. The overall surface area in contact with the aqueous dissolution medium was too low to enable the surfactants to emulsify larger proportions of the oleoresin formulation.

However, the self-emulsifying micellar formulation dissolved ASX entirely (95%) within 30 min and the concentration remained stable throughout the dissolution measurement, even though a high concentration of near to 0.2 mg/mL was reached (saturation solubility of ASX in biorelevant medium: 0.001 mg/mL). The addition of biorelevant surfactants did not affect the dissolution rate due to the high surfactant content of the formulation [115]. Generally, the dissolution rate of ASX generated by both formulations was found to be pH-independent.

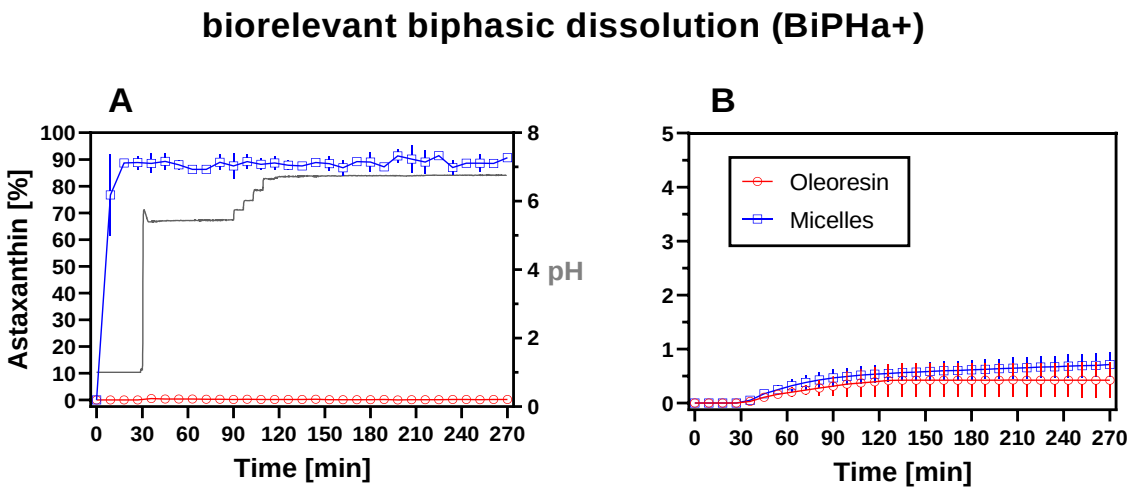

Figure 35: Dissolved/partitioned amount of astaxanthin (sum of mono- and diesters; mean ± SD) during biorelevant biphasic dissolution (BiPHa+) measurements; **A)** aqueous medium, **B)** 1-decanol layer; the pH profile in the aqueous medium is represented by the grey line, (100% corresponds to 0.2 mg/mL).

Table 36: Concentrations of dissolved/ partitioned astaxanthin (sum of mono- and diesters; mean ± SD) in the aqueous medium and the 1-decanol layer at the end of biorelevant biphasic dissolution (BiPHa+) at 270 min (determined by HPLC).

Formulation	**Endpoint concentration [%]**	
	aqueous medium	**1-decanol**
Oleoresin	0.2 ± 0.1	0.4 ± 0.3
Micelles	90.7 ± 1.0	0.7 ± 0.2

In line with previously described dissolution results, the self-emulsifying ASX formulation achieved a high dissolution of over 90% in the aqueous medium of the BiPHa+ within the first 30 min (**Figure 35A**). Likewise, the microalgae oleoresin formulation behaved as expected and a deficient concentration of 0.2% ASX was measured in the aqueous medium after 270 min.

The addition of bile salts after the first 30 min of the dissolution measurement did not impact the dissolution rate. Hence, dissolution results for both formulations were comparable to monophasic non-sink dissolution with pH shift and biorelevant medium.

Remarkably, no reduction in concentration in the aqueous phase, due to partitioning of active ingredient into the 1-decanol absorption sink, was detected. This was particularly surprising for the micelles, as they reached a high concentration in the aqueous medium. The solubility of ASX in 1-decanol was not a limiting factor, as the shake flask experiment showed ASX concentrations in 1-decanol of over 5 mg/mL (refer to section 2.3).

The concentration profiles obtained in the organic absorption sink were comparable, while both formulations failed to generate sufficient partitioning rates and ASX concentrations of 0.4% and 0.7% were received after 270 min (**Table 36**). This represented a negligible difference. Thus, the self-emulsifying drug delivery system could achieve high concentrations of ASX in the aqueous medium, but the ASX – micellar inclusion complexes formed were too stable to allow for transfer of ASX into the organic phase [108,116]. Nearly 100% of the applied ASX dose was entrapped into the lipophilic core of the *in situ* formed micelles and thereby the amount of free drug available for partitioning into the organic layer was limited.

Although pure ASX released from the oleoresin formulation was not prevented from crossing the aqueous-organic interface, the amount and speed of its dissolution were too low, resulting in an insufficient concentration of active ingredient available for partitioning into the organic phase.

3.7.1. Assessment of the *in vivo* relevance of each dissolution method based on comparison with human pharmacokinetic data

Table 37: Comparison of *in vitro* dissolution results (concentration at the end of the dissolution measurement; mean ± SD) with *in vivo* pharmacokinetic parameters of astaxanthin containing oleoresin and astaxanthin micelles (mean ± SD; *n* = 12) obtained by Teaima et al. (2024) [117].

Parameter	Oleoresin		Micelles
$AUC_{0\text{-}72h\ in\ vivo}$ [ng x min/mL] [117]	104.27		116.75
Difference (n-fold)		**1.1**	
Biorelevant biphasic dissolution (BiPHa+) [%]	0.4 ± 0.3		0.7 ± 0.2
Difference (n-fold)		**1.8**	
Monophasic non-sink dissolution with pH shift and biorelevant medium [%]	0.1 ± 0.1		93.3 ± 0.7
Difference (n-fold)		**933.0**	
Monophasic non-sink dissolution [%]	1.1 ± 1.0		97.0 ± 1.0
Difference (n-fold)		**88.2**	

The results of all three ASX dissolution methods applied were compared with human pharmacokinetic data (**Table 37**). Since there was no available i.v. reference data, the $AUC_{\ in\ vivo}$ has been utilized as an alternative for quantification of relative *in vivo* absorption and compared with *in vitro* dissolution results. Teaima et al. compared 2019 the relative oral bioavailability of an ASX containing oleoresin and a self-emulsifying drug delivery system (micelles) made thereof in a strictly controlled pharmacokinetic trial [117].

The study revealed a 1.1-time superiority of the micelles. These *in vivo* results were precisely reproduced by the BiPHa+, which showed a 1.8-fold superiority of the micelles. The two other methods used to determine the relative oral bioavailability of both formulations failed. They drastically overestimated the effect of the increased water solubility of the micelles on bioavailability in humans.

Hence, the monophasic non-sink dissolution method with pH shift and biorelevant medium demonstrated that the micelles were superior by a factor of 933, signifying a bioavailability close to 100%. Although the monophasic non-sink dissolution method also overestimated the micelles, the extent was reduced (factor 88.2). These findings suggest that an organic absorption sink is necessary to accurately estimate the expected bioavailability of micellar formulations in humans.

3.8. Conclusion

The purpose of the present chapter was to assess the effects of different dissolution methods on the release patterns of a range of plant-based model extracts. Specifically, the study examined eight curcumin formulations, four *trans*-resveratrol formulations, three CoQ10 formulations, and two quercetin and ASX formulations, respectively.

Dissolution measurements were conducted using three different methods: a conventional monophasic (compound dependent presence of non-sink conditions) dissolution (apparatus 2, USP, and PhEur) with 900 mL phosphate buffer pH 6.8, a monophasic non-sink dissolution with pH shift and biorelevant medium using 50.0 mL biorelevant medium (Bi-FaSSIF-V2), and a biorelevant biphasic dissolution (BiPHa+) using 50.0 mL biorelevant medium (Bi-FaSSIF-V2) and 50.0 mL 1-decanol.

Online UV/VIS spectrophotometric detection was utilized across all methods to quantify the proportion of active ingredients released/partitioned in the aqueous/organic medium. At first the suitability of this method to quantify the active ingredients (either as single compounds or as a sum parameter of several structurally related compounds) needed to be proven. To achieve this, the results of online UV/VIS detection were compared with concentrations determined by validated HPLC methods (refer to section 3.2). Despite the challenges posed by diverse extracts and formulations, such as ASX containing multicomponent extracts, online UV/VIS quantification proved to be applicable and provided accurate concentrations of active ingredients that did not differ significantly from HPLC measurements (see section 3.2). In addition, upon completion of each dissolution measurement, samples were taken, filtered and analyzed via HPLC.

This way, for the curcumin formulations it was possible to identify the CUR content in the various dissolution media, which could afterwards be used for comparison with human pharmacokinetic data.

Subsequently, the dissolution results (sorted by the respective active ingredients e.g., CUR, resveratrol etc.) obtained from the three different dissolution methods were compared. The objective was to evaluate the relevance of these results towards the conditions present *in vivo* by comparing them with published oral bioavailability data from strictly controlled human pharmacokinetic trails [40,41,43,46,117].

In vitro - *in vivo* relationships were established whenever possible (CUR and CoQ10) and their linearity was evaluated by calculating the correlation coefficient r^2.

If such relationships could not be established (resveratrol, quercetin and ASX formulations), the dissolution results were expressed as fold differences relative to the non-bioavailability-enhanced extracts. Subsequently, these differences were compared with the bioavailability distinctions observed *in vivo*.

The fully automated BiPHa+ biphasic dissolution method has shown great success in predicting the bioavailability of various natural products. Regardless of the investigated extract or formulation manufactured thereof, the dissolution device was equally predictive and the correlation coefficients of the established *in vitro* - *in vivo* relationships always showed the highest linearity. Based on the present data, BiPHa+ could in future be used not only for formulation development but also for bioavailability assessment of existing formulations for which no human pharmacokinetic data is available. This way, advertising claims made by manufacturers of food supplements, that can be classified as unrealistic, could be critically reviewed [118].

Apart from the Curcuma formulations, where a dose reduction was necessary (1-decanol sink limitations), this method employed a single set of parameters for all compounds and formulations tested, resulting in partitioning profiles that were of great relevance to *in vivo* conditions. When conventional dissolution methods have failed in characterizing formulations, biphasic dissolution offers an accurate approach to assess expected differences in bioavailability. In particular, the assessment of self-emulsifying micellar formulations with regard to their expected bioavailability in humans showcased the limitation of conventional monophasic (non-sink) dissolution methods.

Comparing both monophasic (non-sink) dissolution methods, it was found that limiting the solvent volume, while providing solubility limited non-sink dissolution conditions was advantageous in order to better differentiate between various formulation principles. If the volume of aqueous dissolution medium becomes too large and sink conditions were present, the effect of resveratrol micelles on bioavailability was compromised due to other formulations dissolving to an equal amount. A similar phenomenon has been observed for quercetin formulations.

4. Development of bioavailability improved formulations based on biorelevant biphasic dissolution results

4.1. Introduction

Low water solubility often hinders the development of new active pharmaceutical ingredients (APIs) [119,120]. Within the pharmaceutical industry, screening programs have revealed that over 40% of new chemical entities face formulation developmental challenges, largely related to hydrophobic molecular properties [121,122]. This challenge is not only limited to conventional APIs, but also to a variety of phytopharmaceuticals and food supplements, where reduced water solubility is a common issue for natural products used in these preparations [123,124]. To overcome this limitation, various strategies have been developed in recent years. There are several possible formulation approaches that can enhance water solubility, including complexation of active molecules with for example cyclodextrins, utilization of emulsion formation, micelles and microemulsions, particle size reduction technologies, pharmaceutical salts, prodrugs, solid-state alternation technique, soft gel technology, nanocrystals, solid dispersion methods, and crystal engineering techniques [121,125].

In the group of phytopharmaceuticals and food supplements, complexation of active molecules with cyclodextrins, self-(nano)-emulsifying drug delivery systems, particle size reduction technologies, the formation of liposomes, solid-state alternation techniques and metabolic absorption enhancers like piperine are used to enhance absorption [41].

Although the aforementioned formulation principles have been proven to impact the water solubility of various active molecules and enhance their bioavailability, not all formulation principles are universally applicable. For example, self-emulsifying micellar formulations are highly effective for CUR and *trans*-resveratrol containing extracts, but have minimal impact on CoQ10 and nearly none on ASX bioavailability (refer to chapter 3) [40,41,43,117]. To evaluate a formulation's suitability for a particular active ingredient prior to clinical testing in animals or humans, biorelevant *in vitro* test systems are necessary.

Chapter 1.5 outlined a variety of *in vitro* methods that may be appropriate for this purpose. Of the methods mentioned, the BiPHa+ fully automated small-scale biorelevant biphasic dissolution method proved particularly advantageous. The *in vivo* relevance of

the resulting partitioning profiles in the organic absorption sink has already been demonstrated for various pharmaceutical formulations and natural extracts [53,66,69,126]. Monophasic dissolution systems can provide *in vivo* relevant data, especially if biorelevant media and a pH profile reflecting the conditions in the human gastrointestinal tract, were used [121,127]. However, these systems are limited by the lack of an absorption step, as the enhancement of water solubility generated by different enabling formulation principles does not always directly translate into increased bioavailability (see sections 3.3 - 3.7.1).

4.2. Coenzyme Q10 as bioavailability impaired naturally occurring model compound

Natural substances that are used as phytopharmaceuticals and food supplements but suffer from poor bioavailability are widely studied [62,128,129]. These substances belong to a variety of different substance classes, including polyisoprenes like coenzyme Q10 (CoQ10). CoQ10, also known as ubiquinone, is a key component of the mitochondrial respiratory chain [130]. Researchers have uncovered its complex structure, which includes a redox-active benzoquinone ring and a long isoprenoid side chain (**Figure 36**) [131]. CoQ10 is the only lipid-soluble antioxidant that is produced endogenously. It can be found in high- and low-density lipoproteins, as well as in all cellular membranes and blood. By transporting electrons in mitochondrial and extramitochondrial membranes, CoQ10 plays a vital role in cellular metabolism. It also serves to protect membranes and lipoproteins from protein oxidation and lipid peroxidation [132,133]. Due to its substantial effects on the human metabolism, it is widely used for the treatment of various diseases including cardiovascular diseases such as chronic heart failure and hypertension, diabetes and neurodegenerative disorders [132].

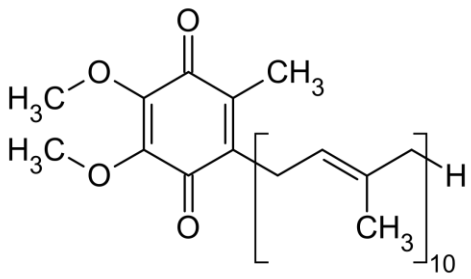

Figure 36: Chemical structure of coenzyme Q10 (CoQ10), including a redox-active benzoquinone ring and a long (10x isoprene) side chain.

Although numerous studies have been conducted regarding the various metabolic effects of CoQ10, its low oral bioavailability has hindered significant therapeutic breakthroughs thus far [132]. The substance's molecular structure is highly hydrophobic (**Figure 36**), leading to decreased water solubility as indicated in **Table 38**. Even in biorelevant, surfactant containing, medium, the solubility does not exceed 5.5 µg/mL.

Table 38: Solubility in various media (0.1 N HCl, phosphate buffer pH 6.8 and Bi-FaSSIF-V2 pH 6.8) and log $D_{7.4}$ value of coenzyme Q10. Adapted from Brenner et al., 2024 [66].

Parameter	Coenzyme Q10
S (0.1 N HCl) [µg/mL]	0.1 ± 0.0
S (Buffer pH 6.8) [µg/mL]	0.1 ± 0.0
S (Bi-FaSSIF-V2) [µg/mL]	5.5 ± 2.3
Log $D_{7.4}$	published value: 14.72 [75]

Several formulations have been developed and launched on the market to enhance CoQ10 bioavailability. These formulations include self-emulsifying micellar systems and oily dispersions. However, as depicted in **Figure 37**, the currently available commercial formulations have not demonstrated a noteworthy enhancement in bioavailability in comparison to pure crystalline CoQ10 yet [43].

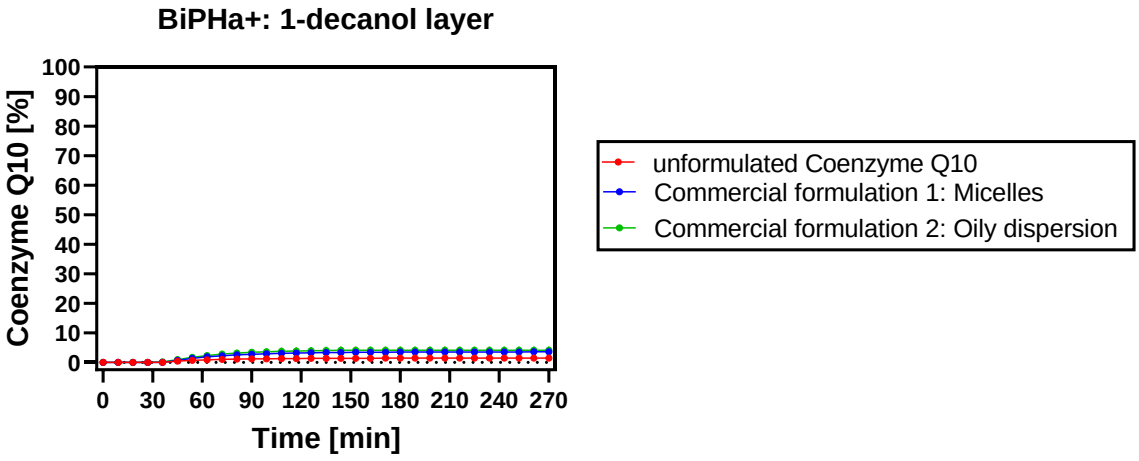

Figure 37: Partitioning profiles (mean ± SD) of coenzyme Q10 into the 1-decanol absorption sink of biorelevant biphasic dissolution (BiPHa+) shown for unformulated coenzyme Q10 and two commercial formulations (1. micelles; 2. oily dispersion); 100% corresponds to 0.2 mg/mL. Adapted from Brenner et al., 2024 [66].

Given the limited success of previous commercial formulations, the aim was to identify alternative formulation strategies that could be expected to improve bioavailability of CoQ10 beyond the commercial formulations. Since it was not feasible to directly evaluate the effectiveness of the formulations in humans or animals, the end concentration in the 1-decanol absorption compartment of biorelevant biphasic dissolution (BiPHa+) was used as the target parameter. Chapter 3.5.1 demonstrated that BiPHa+ yields partitioning profiles for various CoQ10 formulations with excellent alignment to the human pharmacokinetic data generated by Schulz et al. in 2006.

4.2.1. Biorelevant biphasic dissolution performance of coenzyme Q10 – polymer dispersions

A commonly used approach to improve the dissolution performance of different drugs is to embed them in a polymer matrix, resulting in crystalline (CSD) or amorphous solid dispersions (ASD) [120,134,135].

In line with this, CoQ10 polymer dispersions were developed, applying eight of the most common polymers in pharmaceutical industry (Eudragit® EPO and L100-55, Kollidon® VA64 and K12PF, Kolliphor® P407, hydroxypropyl cellulose (HPC) - SSL, hydroxypropyl methylcellulose acetate succinate (HPMC AS), and Soluplus®), with a drug load of 20% (*w/w*). All dispersions were manufactured using the solvent evaporation technique in combination with an appropriate organic solvent (see section 5.2.9). For a detailed overview of the investigated polymers, including their chemical structure and general physicochemical properties, refer to section 5.1.3.

The study involved comparing the biphasic dissolution performance of these dispersions with that of pure CoQ10, while also analyzing the influence of different polymers on the process. The results of biphasic dissolution studies are displayed in (**Figure 38**).

Since unformulated CoQ10 and some polymer dispersions only reached low concentrations in both dissolution media, the concentrations in the aqueous medium and the 1-decanol layer at the end of BiPHa+ measurements at 270 min were additionally shown in **Table 39**.

Furthermore, we investigated the influence of drug load on dissolution performance (**Figure 39**) and the effect of polymer combinations into ternary CoQ10 solid dispersions (**Figure 40** and **Table 40**)

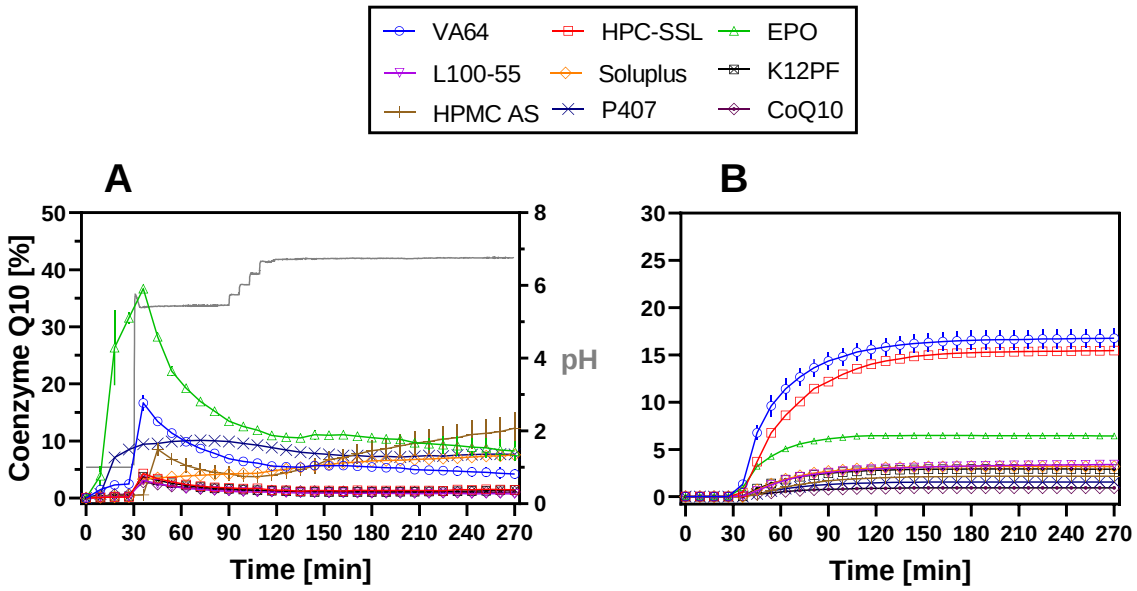

Figure 38: Dissolved/partitioned amount of coenzyme Q10 (mean ± SD) during biorelevant biphasic dissolution (BiPHa+) measurements of unformulated coenzyme Q10 (reference) and binary coenzyme Q10 – polymer dispersions (20% drug load (*w/w*); **A)** aqueous medium, **B)** 1-decanol layer; the pH profile in the aqueous medium is represented by the grey line, (100% corresponds to 0.2 mg/mL).

Table 39: Concentrations of dissolved/ partitioned coenzyme Q10 (CoQ10) (mean ± SD) from binary CoQ10 polymer dispersions (20% drug load) in the aqueous medium and the 1-decanol layer at the end of biorelevant biphasic dissolution (BiPHa+) at 270 min (determined by HPLC).

Formulation	**Endpoint concentration [%]**	
	aqueous medium	**1-decanol**
Coenzyme Q10	**2.0 ± 0.3**	**1.5 ± 0.2**
CoQ10 – P407	7.6 ± 0.4	1.5 ± 0.1
CoQ10 – HPMC AS	12.2 ± 2.7	2.2 ± 0.1
CoQ10 – K12PF	1.4 ± 0.2	2.9 ± 0.1
CoQ10 – Soluplus	7.6 ± 0.7	3.2 ± 0.3
CoQ10 – L100-55	0.7 ± 0.0	3.4 ± 0.3
CoQ10 – EPO	8.2 ± 1.8	6.4 ± 0.2
CoQ10 – HPC-SSL	**1.4 ± 0.6**	**15.5 ± 0.4**
CoQ10 – VA64	**4.2 ± 0.9**	**16.8 ± 1.0**

In the initial 30 min of the dissolution test, neat crystalline CoQ10 did not dissolve in the aqueous medium of the BiPHa+ (**Figure 38**). However, after the addition of biorelevant surfactants, approximately 2.8% of CoQ10 dissolved. This resulted in a low concentration of dissolved active substance available for transfer into the 1-decanol layer, with only 1.5% of the dose being dissolved in the organic medium after 270 min.

CoQ10 polymer dispersions had varying effects on solubility in the aqueous medium and partitioning into the 1-decanol layer, depending on the polymer used for embedding. When Eudragit® L100-55, HPC-SSL, or Kollidon® K12PF were used as polymers for embedding, the dispersions formed showed no increase in CoQ10 concentration in the aqueous medium, compared to pure active ingredient. No CoQ10 dissolved in the first 30 min, and even after the addition of biorelevant surfactants, concentrations of less than 5% were achieved. At the end of the dissolution tests, the CoQ10 concentrations were approximately 1 - 2% (**Table 39**).

However, the measured concentration profiles were different in the organic medium. The K12PF and L100-55 dispersions achieved a CoQ10 concentration of 2.9% and 3.4%, respectively. This is approximately double the concentration of the unformulated compound. Contrarily, the HPC-SSL dispersion meaningfully improved the partitioning of CoQ10 into the organic phase, with a concentration of 15.5% observed after 270 min. The presence of HPC-SSL increased the dissolution rate of CoQ10, even though a low absolute concentration in the aqueous medium was present. A dynamic equilibrium was achieved, resulting in a constant outflow of CoQ10 into the organic medium. Onoue et al. also observed a significant increase in the bioavailability of CoQ10 in rats when it was formulated as a crystalline solid dispersion (CSD) with HPC-SSL [136].

In general, the concentration profiles in the organic absorption sink showed similar trajectories for all CoQ10-polymer dispersions prepared. A rapid initial partitioning rate of CoQ10 occurred, with a subsequent constant reduction. From minute 150, there was practically no change in concentration until the end of the dissolution measurement.

During BiPHa+ dissolution studies, the use of polymers such as Soluplus®, P407, or HPMC-AS resulted in an increase in CoQ10 concentrations in the aqueous medium. Specifically, the dispersion using P407 and Soluplus® both achieved an end concentration of 7.6%, while for the HPMC-AS dispersion a concentration of 12.2% was measured. As HPMC-AS is a pH-dependent soluble polymer, its dissolution starts at a pH value of

5.5 - 6.8, depending on the degree of substitution of the polymer. As a result of this property, an increase in CoQ10 concentration in the aqueous medium was observed over time (with increasing media pH), with the maximum concentration being reached after 270 min.

Unfortunately, none of the formulations achieved a major increase in the partitioning rate into the organic phase. 1-Decanol concentrations of 1.5% - 3.2% were measured, which only corresponds to an increase by a factor of 2 (compared to neat CoQ10) in the case of the Soluplus® dispersion. For *in situ* micelle-forming polymers such as P407 and Soluplus®, micellar inclusion complexes formed from CoQ10 and polymer hindered partitioning into the organic phase due to their increased hydrophilicity. This effect has already been described for Soluplus® by Lopez Marmol in 2021 [137].

Upon analyzing the effects of Kollidon® VA 64 and Eudragit® EPO on water solubility of CoQ10, it was discovered that both had a positive impact. The addition of biorelevant surfactants led to an increase in concentration, with CoQ10 - EPO exhibiting the most prominent effect as it achieved a concentration of 36.7% after 30 min. The VA64 dispersion achieved a maximum CoQ10 release of 16.7%.

After the addition of the 1-decanol absorption sink, both formulations showed a decrease in concentration in the aqueous medium. But even after 270 min, 8.2% and 4.2% CoQ10 were still dissolved (**Table 39**). The reduction in concentration for the EPO dispersion could mainly be attributed to the precipitation of active substance, while for VA64 - CoQ10, the reduction was mostly attributed to partitioning of CoQ10 into the organic medium. This resulted in a concentration of 16.8% after 270 min, which was the best result achieved among all formulations.

Out of the eight polymers tested, VA64 was found to be the most effective for CoQ10 embedding as it allowed for supersaturation in the aqueous medium without hindering transfer into the organic medium. This observation was consistent with the literature where VA64 is described as an effective polymer to improve the solubility and bioavailability of CoQ10 in rats [138,139].

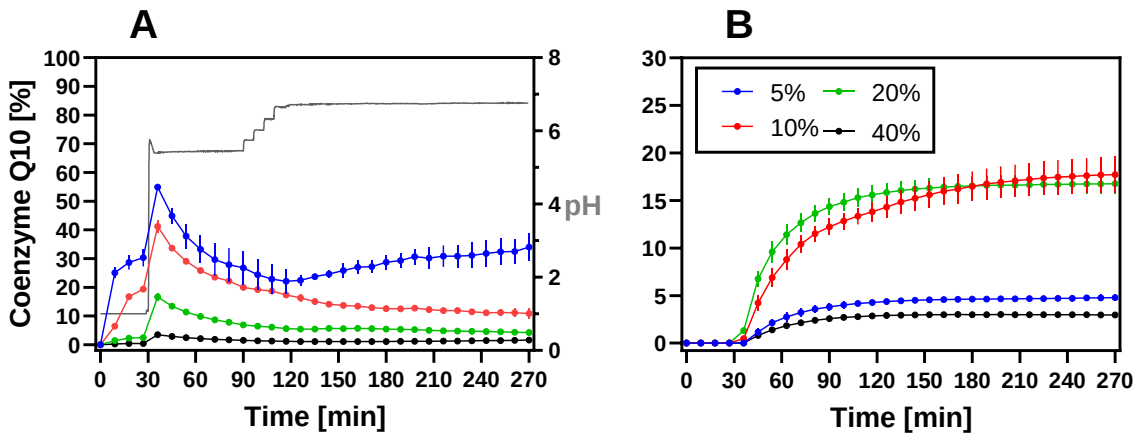

Figure 39: Evaluation of drug load dependent (5%, 10%, 20%, 40%; *w/w*) dissolution/ partitioning of coenzyme Q10 during biorelevant biphasic dissolution (BiPHa+) of coenzyme Q10 – VA64 polymer dispersions; **A)** aqueous medium, **B)** 1-decanol layer; the pH profile in the aqueous medium is represented by the grey line, (100% corresponds to 0.2 mg/mL).

Through the research, it was found that VA64 was the optimal polymer for manufacturing of CoQ10 solid dispersions. To determine the ideal drug load for the polymer formulations, dispersions with various drug loads were prepared, including 5%, 10%, and 40% (*w/w*), in addition to the 20% dispersions used in the initial screening (**Table 38**). As illustrated in **Figure 39**, the drug load quantity affected the dissolution/partitioning profiles of CoQ10 during biorelevant biphasic dissolution. Basically, the concentration of CoQ10 in the aqueous medium increased as the polymer concentration in the dispersion increased/ the drug load decreased. For the 5% dispersion, a release of 54.9% was achieved after 30 min. Comparable to the 20% dispersion, the other formulations also showed an apparent effect of adding biorelevant surfactants, and the highest concentrations were reached after 30 min. With the exception of the 40% dispersion, the concentration decreased after reaching its peak due to the outflow of active substance into the organic medium. The decrease was lowest for the 40% dispersion as only low CoQ10 concentrations were achieved in the aqueous medium due to an insufficient polymer concentration.

For many polymers, it is known that a certain minimum concentration must be present in aqueous solution to achieve a stable supersaturation of the active substance. Monschke et al. observed a noteworthy decrease in dissolution performance for ketoconazole – L100-55 ASDs when the drug load was increased from 10 to 25% [140].

For the 5% dispersion a concentration reduction was observed after 30 min, which could be related to precipitation of CoQ10 and partitioning into the organic phase until the concentration stabilized at around 35% after 150 min.

Considering partitioning from the aqueous medium into the organic absorption sink, the concentration of the polymer had various effects. The 5% and 40% dispersions had different compositions but both resulted in low CoQ10 concentrations (4.7% and 3.0%, respectively) after 270 min in the 1-decanol layer. For the 40% dispersion, a low concentration in the organic phase was expected, given the low polymer content and the resulting low CoQ10 concentration in the aqueous medium (**Figure 39A**).

However, the 5% dispersion showed a higher CoQ10 concentration in the aqueous medium, which did not translate into a higher partitioning rate in the organic phase, as the transfer of active ingredient might be hindered by high polymer-CoQ10 interactions in the aqueous medium [137]. Additionally, dissolved CoQ10 precipitated after 30 min due to the high maximum concentration reached, which reduced the concentration further.

Increasing the concentration of the active ingredient from 10% to 20% did not result in a higher CoQ10 concentration, with both formulations achieving approx. 17% (**Figure 39B**). Consequently, the ideal drug load was determined to be 20%.

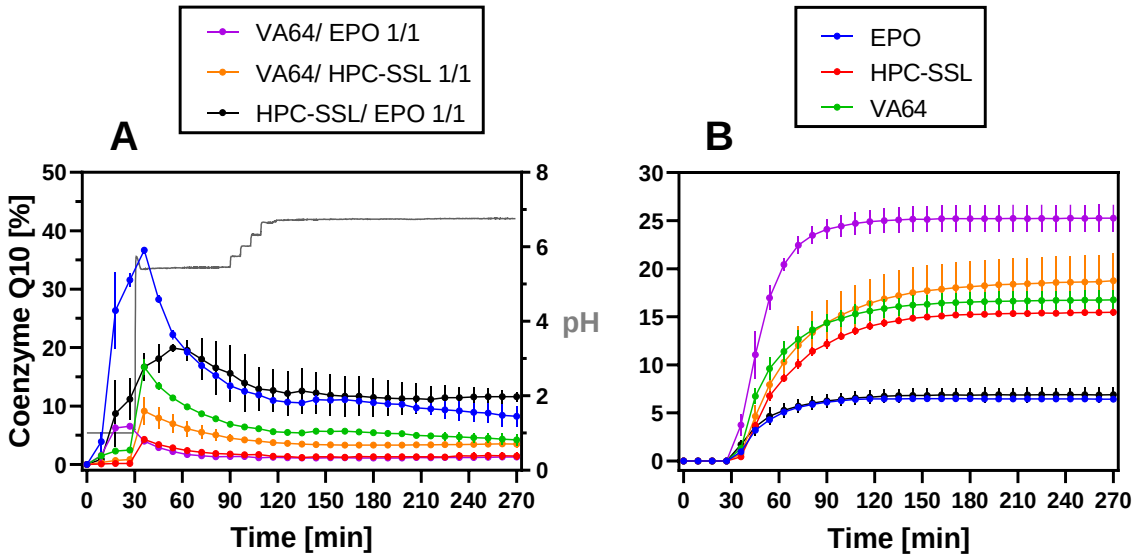

Figure 40: Dissolved/partitioned amount of coenzyme Q10 (mean ± SD) during biorelevant biphasic dissolution (BiPHa+) measurements of binary and ternary (1/1 (*w/w*) polymer mixtures) polymer dispersions (20% drug load (*w/w*); **A)** aqueous medium, **B)** 1-decanol layer; the pH profile in the aqueous medium is represented by the grey line, (100% corresponds to 0.2 mg/mL).

Table 40: Concentrations of dissolved/ partitioned coenzyme Q10 (CoQ10) (mean ± SD) from binary and ternary polymer dispersions (20% drug load)/ commercial formulations in the aqueous medium and the 1-decanol layer at the end of biorelevant biphasic dissolution (BiPHa+) at 270 min (determined by HPLC).

Formulation	Endpoint concentration [%]	
	aqueous medium	1-decanol
Coenzyme Q10	**2.0 ± 0.3**	**1.5 ± 0.2**
CoQ10 - EPO	8.2 ± 1.8	6.4 ± 0.2
CoQ10 - HPC-SSL	1.4 ± 0.6	**15.5 ± 0.4**
CoQ10 - VA64	4.2 ± 0.9	**16.8 ± 1.0**
CoQ10 - VA64/ EPO (1/1)	1.3 ± 0.3	**25.3 ± 1.4**
CoQ10 - VA64/ HPC-SSL (1/1)	3.5 ± 0.6	**18.7 ± 2.8**
CoQ10 - HPC-SSL/ EPO (1/1)	11.6 ± 0.9	6.9 ± 0.8
Commercial formulations		
1. Micelles	60.0 ± 3.2	**3.6 ± 0.6**
2. Oily dispersion	0.4 ± 0.1	**4.0 ± 1.3**

In order to investigate the impact of polymer combinations on BiPHa+ dissolution performance, ternary solid dispersions were manufactured. A target drug load of 20% (*w/w*) was chosen, similar to binary dispersions (**Figure 39**). Analysis revealed that polymers VA64 and HPC-SSL exhibited the greatest increase in CoQ10 partitioning rate, while EPO decisively enhanced water solubility (**Table 39**). Using these results, combinations of two of the mentioned three polymers (equal mass fractions) were prepared employing the solvent evaporation technique and assessed in the BiPHa+ (**Figure 40**). To facilitate comparison, the end concentrations in both media of BiPHa+ were additionally presented in **Table 40**.

The combination of HPC-SSL and EPO did not yield benefits in terms of improving the 1-decanol partitioning rate, despite its ability to enhance the water solubility of CoQ10 (**Figure 40A**). While the concentration of CoQ10 in the aqueous medium increased to 11.6% after 270 min, the partitioning rate (6.9%) was comparable to that of the binary EPO dispersion (6.4%).

The combination of VA64 and HPC-SSL also did not show a synergistic effect, and the concentration achieved was 18.7%, which was comparable to the respective binary

dispersions (**Table 40**). Accordingly, the CoQ10 concentration detected in the aqueous medium was in the same range as the CoQ10 concentrations generated by the binary HPC-SSL and VA64 dispersions.

However, when the polymers VA64 and EPO were combined, a remarkable synergistic effect was observed, resulting in a final concentration of 25.3% in 1-decanol. This corresponds to a 150% increase compared to the binary VA64 dispersion and a 17-fold increase compared to pure CoQ10 (**Figure 40B**).

Throughout the course of the dissolution measurement, only a minor increase in the concentration of CoQ10 in the aqueous medium was observed and the dissolution profile was generally similar to the CoQ10 dissolution profile of the binary HPC-SSL dispersion. However, during the gastric stage at pH 1, there was an evident dissolution of the formulation, resulting in a CoQ10 concentration of 6.5%. The dissolution was not impacted by the addition of biorelevant surfactants at 30 min. Given the high lipophilicity of CoQ10, the ternary VA64/EPO dispersion demonstrated a rapid partitioning rate, with 24.1% CoQ10 already present in the organic phase after 90 min. By the end of the dissolution measurement, an equilibrium had been established, leading to an unchanged concentration between 120 and 270 min.

The use of ternary solid dispersions in pharmaceutical formulation is a recent development that already showed great promise [141,142]. By combining a polymer with a surfactant, another polymer or active ingredient, or a carrier substance, this technique has been shown to enhance the dissolution performance and bioavailability of a range of active ingredients [135,141,143]. In addition, it assists with overcoming the limitations that can restrict the effectiveness of a single drug-polymer combination. Pötges et al. have noted that L100-55 can stabilize a distinct level of supersaturation of celecoxib in the short term before precipitation occurs. When HPC-SSL is used, celecoxib can be kept in solution at lower concentrations, but the supersaturation remained stable throughout the whole assay (180 min). When these two polymers were combined, a synergistic effect occurred and celecoxib was stabilized in the solution to a greater extent and for a longer period than with individual polymers [134].

4.2.2. Solid state characterization in terms of crystallinity of neat coenzyme Q10 and polymer dispersions made thereof

The solid state of CoQ10 polymer dispersions, both binary and ternary, were examined using differential scanning calorimetry (DSC) and X-ray powder diffraction (XRPD) measurements. The results of the analysis are shown in **Figure 41** (XRPD) and **Figure 42** (DSC). In accordance with the results from section 4.2.1, only the three polymers with the best BiPHa+ performance (VA64, HPC-SSL, EPO) and the corresponding ternary dispersions were examined.

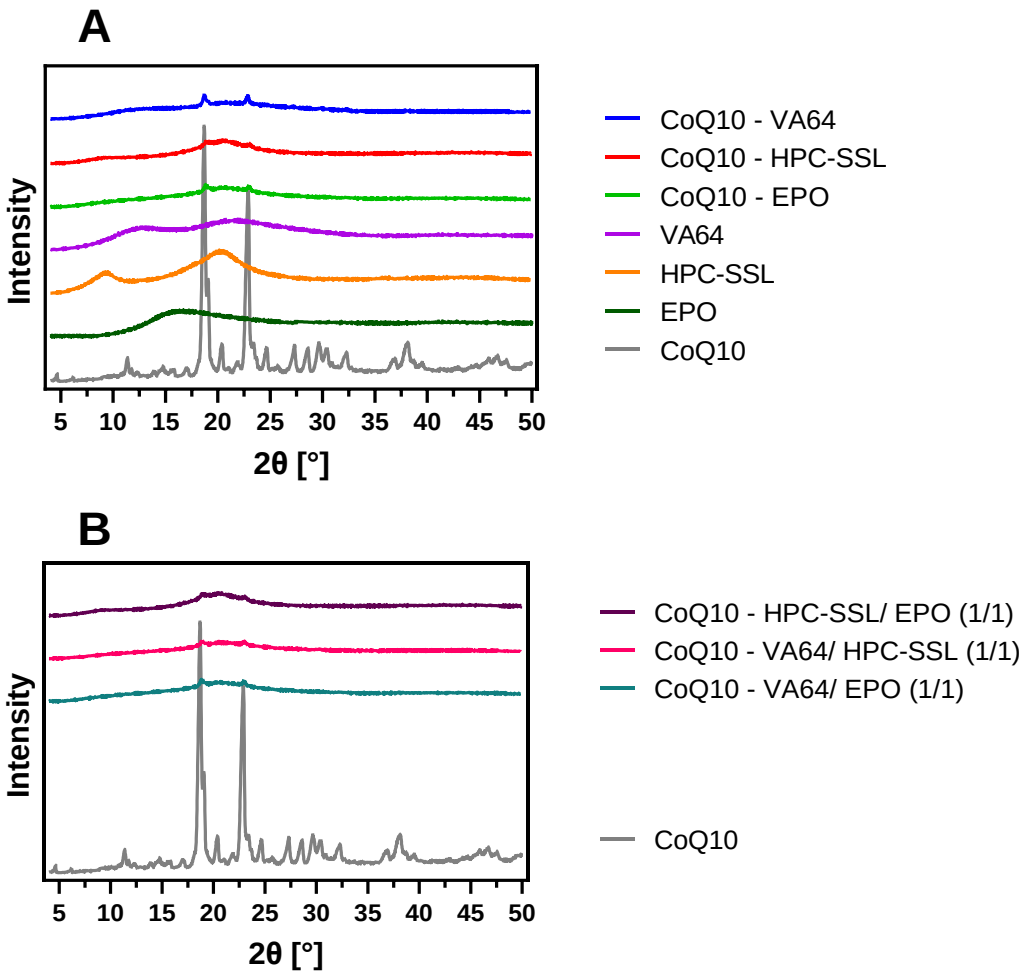

Figure 41: X-Ray powder diffractograms of **A)** binary (including neat coenzyme Q10 (CoQ10), VA64, HPC-SSL and EPO for reference) and **B)** ternary (including neat coenzyme Q10 for reference) coenzyme Q10 – polymer dispersions (20% drug load (*w/w*).

The XRPD analysis of pure CoQ10 revealed its crystalline nature, with sharp reflection peaks observed at 18.7° and 22.9° 2θ (**Figure 41**). In contrast, the neat polymers displayed an amorphous state with no identifiable reflection peaks.

Despite this, residual crystallinity was still noticeable in all three binary polymer dispersions, as evidenced by the sharp reflection peaks at 18.7° and 22.9° 2θ. Consequently, none of the polymers was able to permanently stabilize CoQ10 in an amorphous state (**Figure 41A**).

This may be attributed to the highly lipophilic nature of the CoQ10 molecule, which cannot be dissolved in the polymer to a sufficient concentration, leading to the presence of a crystalline phase alongside amorphous CoQ10 dissolved in the polymer matrix. Accordingly, Onoue et al. described that the combination of CoQ10 with VA64 resulted in crystalline solid dispersions [136]. Reducing the drug load to decrease the concentration of active ingredients in the polymer matrix might be an option. However, based on biphasic dissolution studies (refer to section 4.2.1), it has been observed that reducing the drug load had either no effect (10%) or it had a negative effect (5%) on the partitioning rate into the organic medium.

In light of the inability of the neat polymers to stabilize CoQ10 (at a 20% drug load (*w/w*) in the amorphous state, ternary dispersions also exhibited sharp reflection peaks at 18.7° and 22.9° 2θ, indicating the presence of crystallinity (**Figure 41B**).

Confirmation of the XRPD measurements was obtained through DSC measurements (**Figure 42**). Neat CoQ10 demonstrated a sharp melting peak at 50.1 ± 0.8 °C, while the neat polymers VA64, HPC-SSL and EPO did not display a melting peak. Instead, glass transition was observed for VA64 and EPO. In line with previous research, for HPC-SSL no glass transition temperature could be determined [134].

The melting peaks observed in the binary polymer dispersions, ranging from 49 - 51°C, were attributed to the presence of crystalline CoQ10, as illustrated in **Figure 42A**. DSC measurements indicated the existence of a crystalline CoQ10 phase alongside the amorphous polymer-CoQ10 matrix, supporting the XRPD measurements. In accordance with the inability of the single polymers to stabilize CoQ10 in the amorphous state, sharp melting peaks at 49.8 ± 1.2 °C were detected for the ternary solid dispersions too (**Figure 42B**).

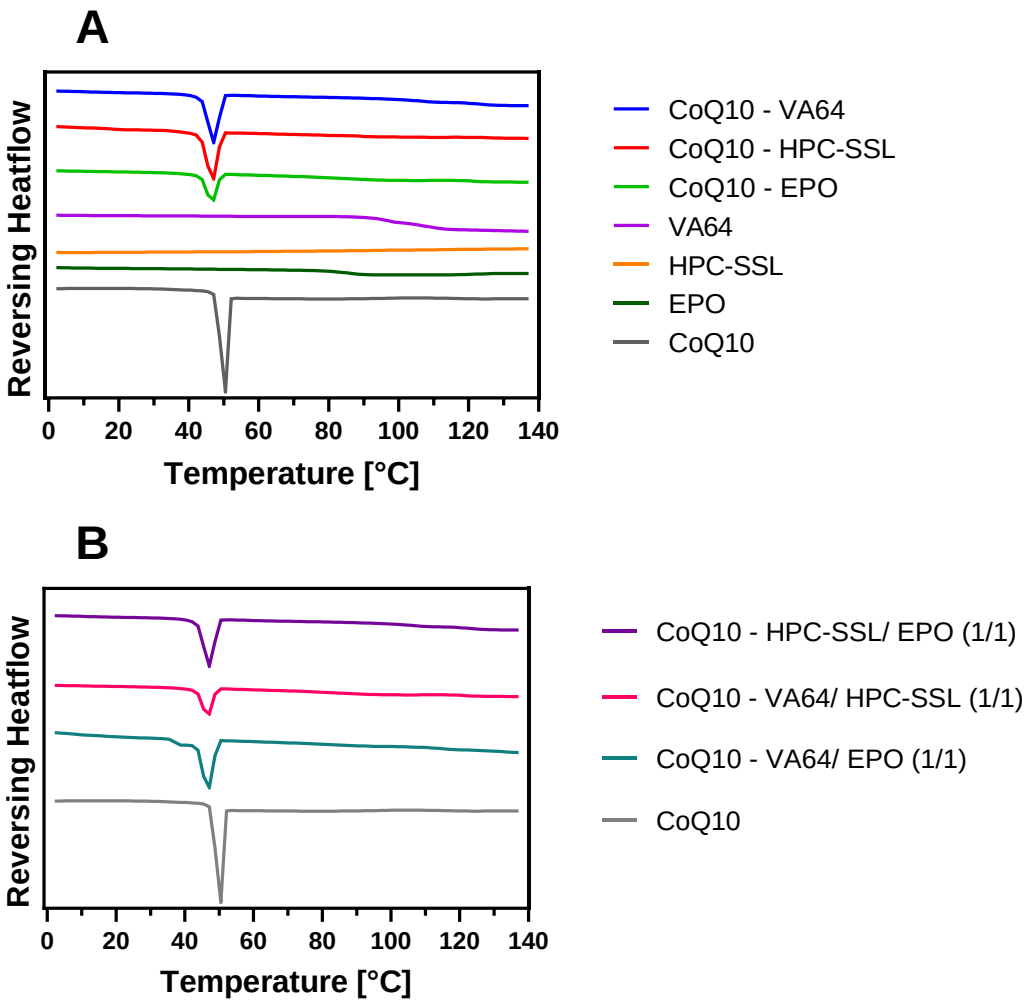

Figure 42: Differential scanning calorimetry thermograms (exo up) of **A)** binary (including neat coenzyme Q10 (CoQ10), VA64, HPC-SSL and EPO for reference) and **B)** ternary (including neat coenzyme Q10 for reference) coenzyme Q10 – polymer dispersions (20% drug load (*w/w*).

4.3. Highly loaded mesoporous silica particles as an alternative formulation strategy for the lipophilic model compounds coenzyme Q10, astaxanthin, probucol and lumefantrine

Parts of this chapter have been published in a peer-reviewed research article [63]. Each figure and table were created by the thesis author. Taking or adapting of figures or tables is indicated in the corresponding position.

The formulation of the lipophilic natural product CoQ10 with different polymers in the form of binary or ternary solid dispersion has led to a decisive improvement in the partitioning rate into the organic 1-decanol absorption sink of the BiPHa+, whereby the extent of the improvement was strongly dependent on the polymer type chosen (refer to section 4.2.1). However, XRPD and DSC measurements revealed (see section 4.2.2) that none of the polymers used could generate an amorphous system, as residual crystallinity was always present. This may result in complete recrystallization, as amorphous systems are in a metastable transition state with higher chemical potential and low physical stability [144]. Transitioning from the amorphous to the crystalline form can alter the dissolution behavior of a formulation, as amorphous material exhibits higher solubilities and faster dissolution compared to the corresponding crystalline molecular composition [145]. Dissolving of amorphous material does not require breaking of the crystal lattice structure, which usually results in enhanced interactions with solvent molecules and an exceedance of the thermodynamic solubility [113].

The upper limit of drug load that could be achieved without risk of crystallization is determined by the solid-state solubility of the drug within the polymer matrix. As long as the drug content remains below its solid-state solubility, the solid dispersion formed can be regarded as stable [146].

The very lipophilic molecular structure of CoQ10 limited its polymer solubility and thus restricted the maximal drug load achievable without the formation of an undissolved crystalline phase within the solid dispersions. However, the analysis of the optimal drug load revealed that a drug load below 10% led to a reduction in the partitioning rate into the organic phase and accordingly a reduction in formulation efficacy (**Figure 39**).

As a result, creating a bioavailability improved formulation of CoQ10 via embedding in various polymers faced several limitations.

An alternative formulation principle was required that could both improve the biorelevant biphasic dissolution performance of the model compound and stabilize it in a non-crystalline form. One such alternative could be the utilization of mesoporous silica.
Different mesoporous silica with various pore diameters and volumes have been shown to stabilize various drugs in a non-crystalline form and thereby improve the solubility and bioavailability of these drug [147–149].
The small diameter of the mesopores could prevent recrystallization of the active ingredients, as if the diameter falls below an active ingredient-dependent maximum value, spatial/nano confinement could suppress undesired crystallization [150,151]. Consequently, there is not surrounding polymer matrix needed as in case of ASDs, which appears beneficial for enabling the use of highly lipophilic/ poorly soluble APIs.

The study presented in the following chapter had two primary goals. Firstly, to examine the effectiveness of drug loaded mesoporous silica in increasing the solubility of CoQ10 (**Figure 46**). Secondly, to assess the feasibility of this method for creating solubility enhanced formulations of structurally different lipophilic active ingredients (**Figure 46**). Thus, CoQ10, as well as the astaxanthin-rich microalgae extract described in section 2.2.5, probucol, and lumefantrine were used as naturally occurring and synthetic lipophilic model compounds. Their chemical structures are illustrated in **Figure 43**.

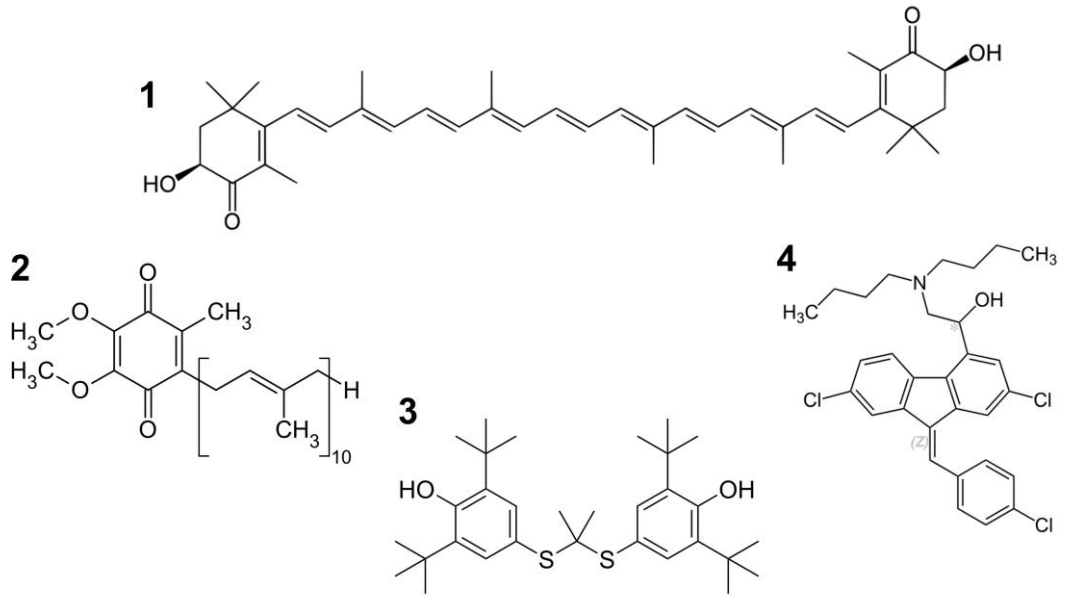

Figure 43: Chemical structures of astaxanthin (**1**) (shown as unesterified molecule; the *Haematococcus pluvialis* extract contains mainly mono- and diesters), coenzyme Q10 (**2**), probucol (**3**) and lumefantrine (**4**).

Before manufacturing drug-loaded mesoporous silica, it was essential to evaluate some key physicochemical parameters of the model compounds, particularly their molecular weight and solubility in various aqueous and organic media (0.1 N HCl, phosphate buffer pH 6.8, Bi-FaSSIF-V2 pH 6.8 and 1-decanol). The literature was consulted to obtain the pK_a and log $D_{7.4}$ values due to the high lipophilicity and low solubility of the model compounds.

Table 41: Molecular weight, pK_a values, saturation solubility in 0.1 N HCl, phosphate buffer pH 6.8, Bi-FaSSIF-V2 pH 6.8 and 1-decanol (determined by HPLC) and log $D_{7.4}$ of coenzyme Q10, astaxanthin, probucol and lumefantrine (mean ± SD). Adapted from Brenner et al., 2024 [63].

Parameter	Coenzyme Q10	Astaxanthin	Probucol	Lumefantrine
Molecular weight [g/mol]	863.3	596.8	516.8	528.9
published log $D_{7.4}$ [76,152–154]	14.7	8.1	10.9	8.3
published pK_a [74,155–157]	13.3	10.6	10.3	8.2
S (0.1N HCl) [µg/mL]	0.1 ± 0.0	0.3 ± 0.1	3.3 ± 0.4	1.5 ± 0.2
S (Buffer pH 6.8) [µg/mL]	0.1 ± 0.0	0.4 ± 0.2	0.9 ± 0.3	0.2 ± 0.1
S (Bi-FaSSIF-V2) [µg/mL]	5.5 ± 2.3	1.1 ± 1.4	2.0 ± 1.2	2.1 ± 0.1
S (1-decanol) [µg/mL]	> 5000	> 5000	> 5000	> 5000

The molecular weight of the model compounds ranged from 516.8 to 863.3 g/mol, whereby the molar mass of naturally occurring ASX could increase to up to 1200 g/mol due to ester formation with fatty acids (**Table 41**). In accordance with the selection of very lipophilic model compounds, the log $D_{7.4}$ values were observed to be very high, ranging from 8.3 to 14.7. Due to their long isoprenoid chains [155,158], the natural substances CoQ10 and ASX showed higher log $D_{7.4}$ values in contrast to the synthetic active pharmaceutical ingredients PB and LU. The pK_a values of the model compounds ranged from 8.2 to 13.3, therefore being predominantly not relevant to proteolysis phenomena occurring in the physiologically acidic to neutral pH range. Only the basic nitrogen atom of lumefantrine (LU) was expected to be protonated along the gastrointestinal pH (basic pK_a 8.2; **Figure 43**), introducing a charge into the molecule and increasing solubility.

Accordingly, the solubility in 0.1 N HCl was 7.5 times higher than at pH 6.8. Probucol (PB) solubility also showed minor pH dependence. CoQ10 and astaxanthin (ASX) showed no pH dependent solubility behavior.

In general, low concentrations of 0.1 - 3.3 µg/mL were measured in aqueous media for all tested compounds. The addition of the biorelevant surfactants lecithin and taurocholate increased solubility, with CoQ10 showing the most prominent effect with a 55-fold increase. However, even surfactant addition only resulted in low absolute concentrations of active ingredient in the medium (1.1 - 5.5 µg/mL). Consequently, all media provided solubility limited non-sink dissolution conditions (BiPHa+). In contrast, the model compounds showed solubility above 5 mg/mL in 1-decanol, establishing sink conditions in the absorption compartment during BiPHa+ biorelevant biphasic dissolution.

Table 42: Preparation of mesoporous silica formulations, including the maximum achievable compound concentration in the dichloromethane (DCM) stock solution (applied solvent volume for drug loading: 1.50 mL/g (XDP 3050) and 0.75 mL/g (Silsol® 6035)) and the total drug load (*w/w*) of the obtained formulation (determined by HPLC), Obtained from Brenner et al., 2024 [63].

Formulation	Concentration: DCM stock solution [mg/mL]	Total drug load [%]
CoQ10: Silsol 6035	670	33.1
CoQ10: XDP 3050	670	49.8
ASX: Silsol 6035 [a]	67	3.3
ASX: XDP 3050 [a]	67	5.9
PB: Silsol 6035	290	17.8
PB: XDP 3050	290	30.3
LU: Silsol 6035	290	17.9
LU: XDP 3050	290	30.1

[a]: ASX content of *Haematococcus pluvialis* extract used for silica loading was 10.1% (*w/w*), therefore the maximum achievable drug load was reduced

After analyzing the physicochemical properties of the model compounds, different silica formulations with varying drug loads were created. To load the mesoporous carriers, Syloid® XDP 3050 and Silsol® 6035 (obtained from Grace), incipient wetness impregnation was utilized [159].

Le et al. discovered that the dissolution performance of felodipine and furosemide loaded XDP 3050 increased with an increase in drug load [160]. In consequence, silica formulations with drug loads of 1%, 5%, 10%, 15%, and (formulation and silica dependent) 20%, 30%, and 50% (*w/w*) were prepared to evaluate loading-dependent effects on solubility in biorelevant medium and partitioning rate into the 1-decanol absorption sink of BiPHa+. For the ASX formulations, only drug loads of 0.1%, 1%, 2.5%, and 5% (*w/w*) were possible since the ASX content of the extract was only 10.1%. Drug load was evaluated by HPLC. The maximum possible drug loads were restricted by the solubility in dichloromethane (DCM) in combination with the pore volume of the mesoporous silica. To achieve the highest possible drug load of silica formulations, an organic solvent was necessary. DCM was found to provide the best results among all tested solvents due to its high solution capability for the model compounds.

Table 42 displays the maximum possible DCM concentrations for each model compound. 1.5 mL/g DCM was used for loading Syloid® XDP 3050, while 0.75 mL/g was used for loading Silsol® 6035.

Under continuous stirring, the DCM stock solutions were added stepwise to the silica powder in a beaker. Stirring was continued until all the liquid was absorbed into the pores and a seemingly dry powder was obtained. Subsequently, the formulations were protected from light and the solvent was evaporated under atmospheric conditions for 24 h in a drying oven. However, it is important to note that, related to the toxicological side effects, DCM has a limit value of 600 ppm in oral pharmaceutical formulations (ICH guideline Q3C [161]). Therefore, the residual amount of DCM in the formulations with the highest achievable drug load was quantified using a headspace (HS) - gas chromatography (GC) - flame ionization detector (FID) method after drying the formulations. The results of the residual solvent determination are presented in **Table 43**.

Table 43: Residual dichloromethane (DCM) (determined by HS-GC-FID) in coenzyme Q10, astaxanthin, probucol and lumefantrine loaded XDP 3050 and Silsol® 6035 formulations with the highest possible drug load; *n* = 6. Obtained from Brenner et al., 2024 [63].

Active substance	Residual dichloromethane [ppm]	
	Silsol® 6035	Syloid® XDP 3050
Coenzyme Q10	< 10	< 10
Astaxanthin	< 10	< 10
Probucol	99.2 ± 15.3	< 10
Lumefantrine	< 10	< 10

The recovery of the HS - GC - FID method was tested across three different concentration levels: 40 ppm, 200 ppm, and 600 ppm. It was determined to be 105.6 ± 1.7%. Accordingly, the method was suitable for reliably detecting low quantities of DCM.

The residual amount of DCM measured in the CoQ10, ASX, and LU formulations was found to be less than 10 ppm. These values are well below the maximum permitted level of 600 ppm, complying with the ICH guideline. Accordingly, no further optimization of the drying process was necessary. However, for Silsol® 6035 loaded with PB, a residual quantity of 99.2 ± 15.3 ppm was detected, which equals around one-sixth of the limit value. Thus, for further reduction of the residual solvent content, extending the drying period for PB-containing formulations to 48 h could be an option. Although the extended drying phase is not mandatory, it enhances the formulation's safety since DCM is classified as solvent which should be limited because of its inherent toxicity [161].

4.3.1. Solid state of lipophilic model compounds as a function of loading onto mesoporous silica

Differential scanning calorimetry (DSC) (**Figure 44**) and X-ray powder diffraction (XRPD) (**Figure 45**) techniques were employed to investigate the solid-state properties of the silica formulations that were loaded with the lipophilic model compounds. For simplicity, only the results for the formulations with the highest possible drug load were shown. All formulations with a lower drug load did not differ from the maximally loaded formulations in terms of their solid state.

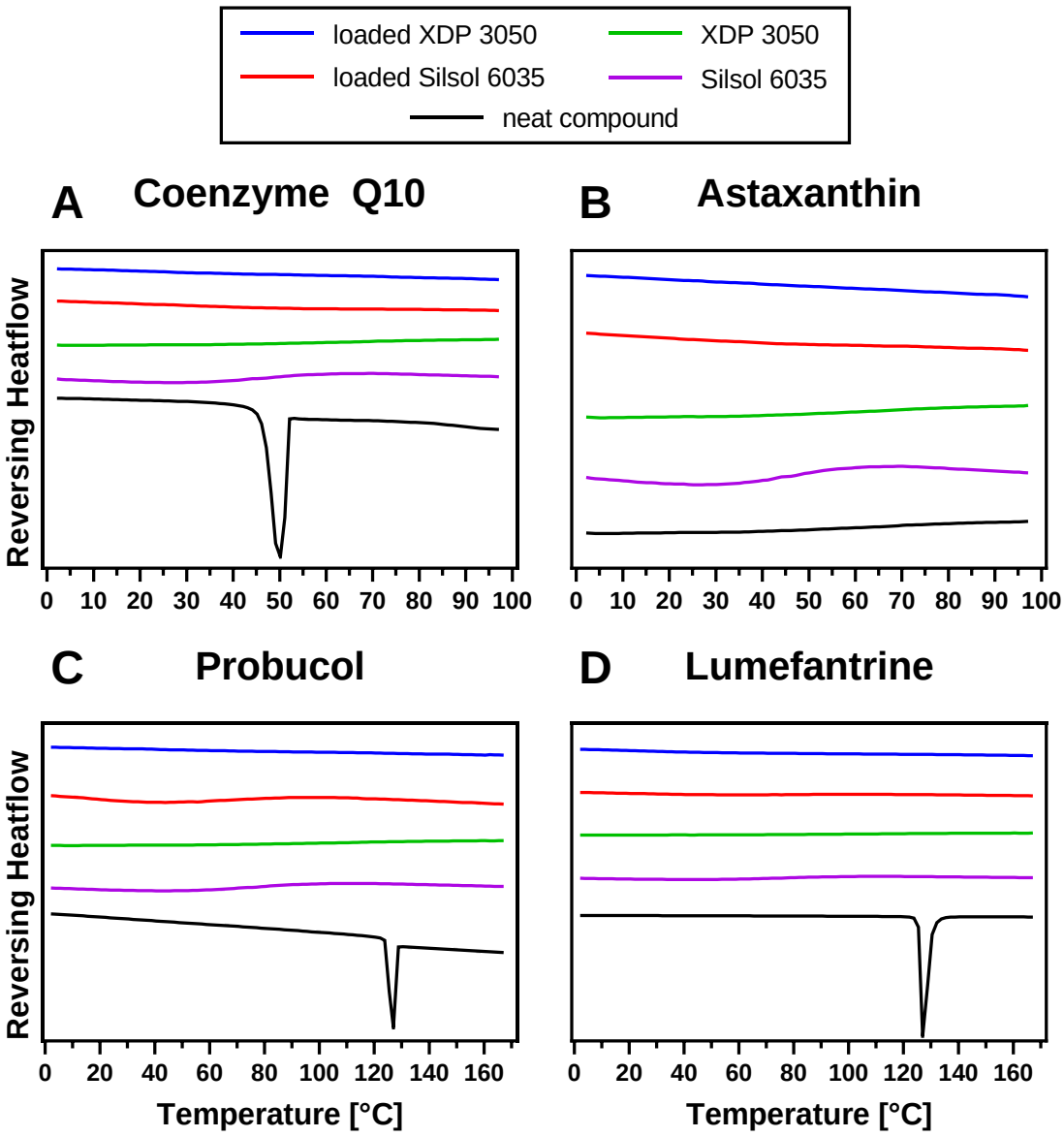

Figure 44: Differential scanning calorimetry thermograms (exo up) of **A)** coenzyme Q10, **B)** astaxanthin, **C)** probucol, **D)** lumefantrine, XDP 3050, Silsol® 6035 and the highly loaded mesoporous silica formulations. Obtained from Brenner et al., 2024 [63].

None of the highly loaded silica formulations showed crystallinity during the DSC experiments, although all model compounds (except the ASX extract) were crystalline (**Figure 44**). Neither the loaded silica formulations nor the pure mesoporous silica displayed any glass transitions, which is consistent with the findings of Kissi et al. The researchers noticed that DSC failed to detect glass transition temperatures for amorphous carvedilol and ibuprofen loaded onto mesoporous Parteck SLC [162].

CoQ10 demonstrated a sharp melting peak at 50.1 ± 0.8 °C (**Figure 44A**). Since the ASX containing *Haematococcus pluvialis* extract was obtained by supercritical fluid extraction of microalgae cells, ASX was dissolved in a lipid-containing, semi-solid extract matrix [163]. This resulted in the absence of any crystallinity detectable during the DSC experiments (**Figure 44B**). On the other hand, probucol (PB) and lumefantrine (LU) exhibited sharp melting peaks at 127.2 ± 1.0 °C and 126.9 ± 1.3 °C, respectively (**Figure 44C/ D**).

Insufficient space within the mesopores, which ranged in diameter from 6 nm to 25 nm for Syloid® XDP 3050 and Silsol® 6035 [164–166], may be the cause of the lack of crystallinity. The small diameter of the mesopores could prevent recrystallization of the active ingredients as if the diameter falls below an active ingredient-dependent maximum value, spatial/nano confinement could suppress undesired crystallization. According to the theory of homogeneous nucleation, only nuclei larger than a critical nucleation size can grow and cause formulation instability. If the pore size is smaller than about 12 times the molecular size of the drug, it is estimated that drug would be sufficiently confined in the nanopores to remain in a non-crystalline form [167]. In that case, no recrystallization can occur, although it would be thermodynamically favored [150].

Usually, a monomolecular surface coverage of the silica particles is targeted to harness the molecular interactions with the silica surface. However, Le et al. conducted experiments in which they achieved complete amorphization of ibuprofen by loading it on Syloid® XDP 3050. Even with a maximum surface coverage of 300%, the active ingredient remained non-crystalline [160]. In addition, Hate et al. achieved non-crystalline formulations of atazanavir loaded mesoporous SBA-15 with drug loads of up to 50% (*w/w*) [168]. This indicated, that even with multi-layer adsorption of drug within the pores, the mechanism of nanoconfinement could prevented recrystallization [169].

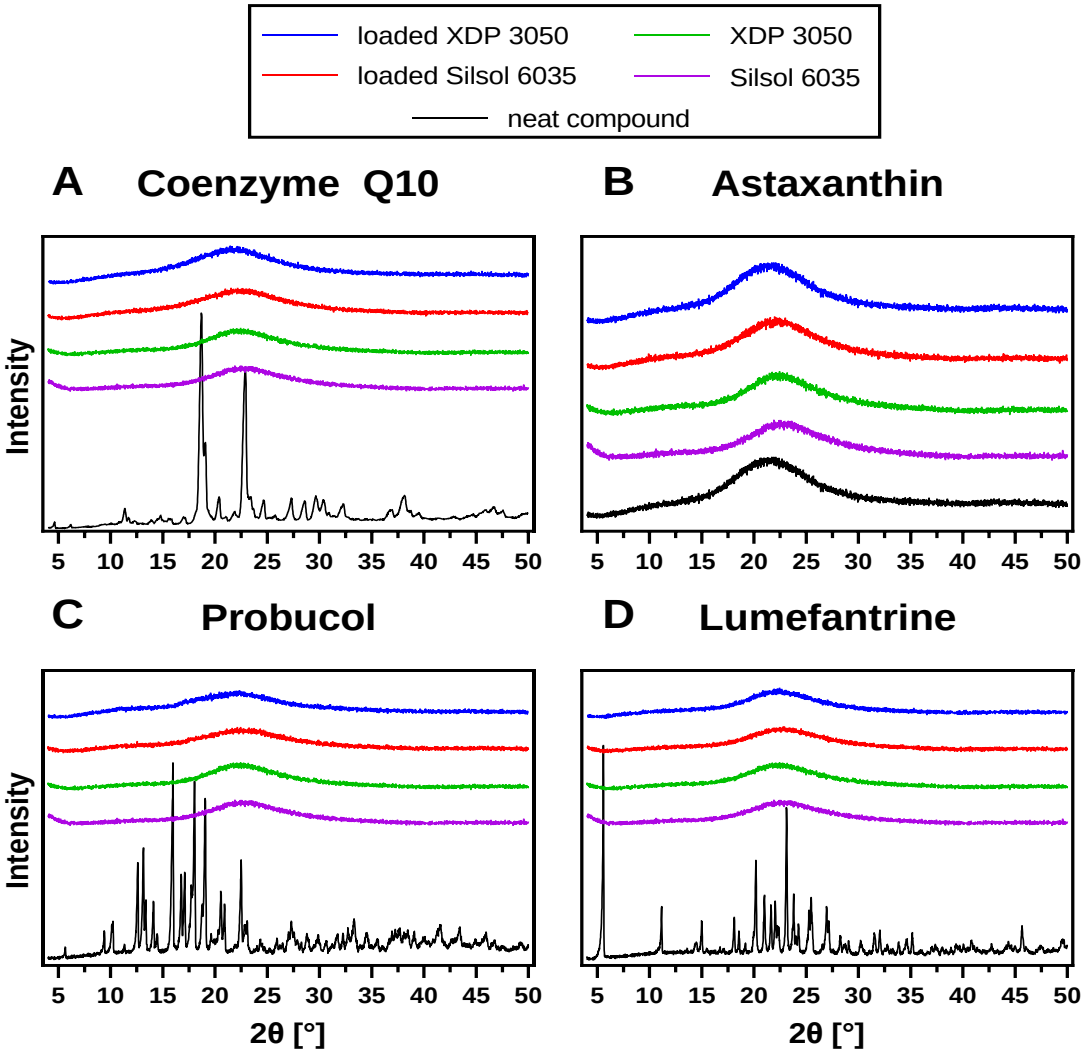

Figure 45: X-Ray powder diffractograms of **A)** coenzyme Q10, **B)** astaxanthin, **C)** probucol, **D)** lumefantrine, XDP 3050, Silsol® 6035 and the highly loaded mesoporous silica formulations. Obtained from Brenner et al., 2024 [63].

The DSC results were confirmed by XRPD measurements (**Figure 45**). It was observed that the pure mesoporous silica and the highly loaded formulations did not exhibit any crystallinity, regardless of the lipophilic model compound or silica investigated.

However, pure CoQ10 showed crystallinity, with sharp reflection peaks at 18.7° and 22.9° 2θ, along with other less intense peaks (**Figure 45A**). As mentioned previously, attributed to the lipid containing extract matrix ASX did not exhibit any remaining crystallinity (**Figure 45B**). In their unformulated state, both PB and LU showed sharp reflection peaks similar to CoQ10. The highest intensity peaks for PB were observed at 16.0°, 18.0°, and 19.1° 2θ (**Figure 45C**), while for LU, they were observed at 5.6°, 21.0° and 23.1° 2θ (**Figure 45D**).

4.3.2. Drug load-dependent equilibrium solubility in various media

The drug load dependent equilibrium solubility of all four model compounds was investigated in phosphate buffer pH 6.8 (**Table 44** and **Table 45**) and biorelevant medium (Bi-FaSSIF-V2) (**Figure 46**).

Despite the model compounds facing low water solubility (**Table 41**), ranging from 0.1 to 0.9 µg/mL at pH 6.8, the higher-loaded silica formulations did exhibit some active substance release in phosphate buffer, as evidenced by visible precipitate in the flasks. Unfortunately, due to the lack of precipitation inhibitors or surfactants in the medium, stable supersaturation was not achieved. Accordingly, after 48 hours, the concentrations measured in the aqueous medium were found to be only marginally increased when compared to the equilibrium solubility of the pure active ingredients.

Table 44: Evaluation of drug load-dependent solubility (48 h shake flask; determined by HPLC) of coenzyme Q10, astaxanthin, probucol and lumefantrine loaded mesoporous XDP 3050 in 0.1 M phosphate buffer pH 6.8. Obtained from Brenner et al., 2024 [63].

	Concentration in PBS pH 6.8 [µg/mL]			
Syloid® XDP 3050 Drug load (*w/w*)	**Coenzyme Q10**	**Astaxanthin**	**Probucol**	**Lumefantrine**
unformulated	0.1 ± 0.0	0.4 ± 0.2	0.9 ± 0.3	0.2 ± 0.1
0.1%	-	ND	-	-
1%	ND	0.2 ± 0.1	0.1 ± 0.0	ND
2.5%	-	0.4 ± 0.2	-	-
5%	ND	2.6 ± 1.5	0.7 ± 0.6	0.1 ± 0.1
10%	ND	-	0.5 ± 0.0	0.1 ± 0.2
20%	0.1 ± 0.0	-	0.9 ± 0.1	0.2 ± 0.1
30%	0.2 ± 0.1	-	1.2 ± 0.6	0.4 ± 0.2
50%	0.4 ± 0.3	-	-	-

ND = not detectable

Table 45: Evaluation of drug load-dependent solubility (48 h shake flask; determined by HPLC) of coenzyme Q10, astaxanthin, probucol and lumefantrine loaded mesoporous Silsol® 6035 in 0.1 M phosphate buffer pH 6.8. Obtained from Brenner et al., 2024 [63].

	Concentration in PBS pH 6.8 [µg/mL]			
Silsol® 6035 Drug load (*w/w*)	**Coenzyme Q10**	**Astaxanthin**	**Probucol**	**Lumefantrine**
unformulated	0.1 ± 0.0	0.4 ± 0.2	0.9 ± 0.3	0.2 ± 0.1
0.1%	-	ND	-	-
1%	ND	0.4 ± 0.1	ND	ND
2.5%	-	1.1 ± 0.7	-	-
5%	ND	-	0.1 ± 0.1	0.1 ± 0.1
10%	0.1 ± 0.1	-	0.5 ± 0.3	0.2 ± 0.0
15%	0.1 ± 0.0	-	1.0 ± 0.2	0.2 ± 0.1
20%	0.2 ± 0.1	-	1.3 ± 0.5	0.3 ± 0.3
30%	0.4 ± 0.2	-	-	-

ND = not detectable

Contrastingly, the equilibrium solubility of all four model compounds in biorelevant medium relied on the drug load of the mesoporous silica, except for a compound dependent loading quantity that had no effect on solubility (**Figure 46**). In general, the solubility was observed to increase linearly with the loading quantity. However, the increase was dependent on the chosen model compound and the silica type. Silsol® 6035 exhibited a greater extent of solubility improvement compared to the XDP 3050 formulations.

For CoQ10 the greatest impact on solubility was detected (**Figure 46A**). The maximum-loaded Silsol® formulation exceeded the equilibrium solubility in a biorelevant medium of 5.5 µg/mL by a factor of 128 (703.3 µg/mL), whereas the maximum-loaded XDP 3050 formulation exceeded it by a factor of 107 (588.6 µg/mL). While the XDP 3050 formulations with 1 - 15% (*w/w*) CoQ10 drug load had no effect on solubility, only the 1% loaded formulation of Silsol® 6035 achieved no effect.

Due to the high matrix content of the ASX-enriched extract, lower drug loads were achieved compared to CoQ10 (0.1 - 5.9%). However, all loaded silica formulations decisively improved solubility except for the 0.1% drug load formulation (**Figure 46B**).

Related to the limited achievable drug loads, the loading capacity of XDP 3050 exceeds that of Silsol® by a factor of approximately two, resulting in the greatest increase in solubility (180x; 198.3 µg/mL) being measured for the 5% loaded XDP 3050 formulation. For Silsol® a maximal solubility improvement by a factor of 93 (102.4 µg/mL) was measured.

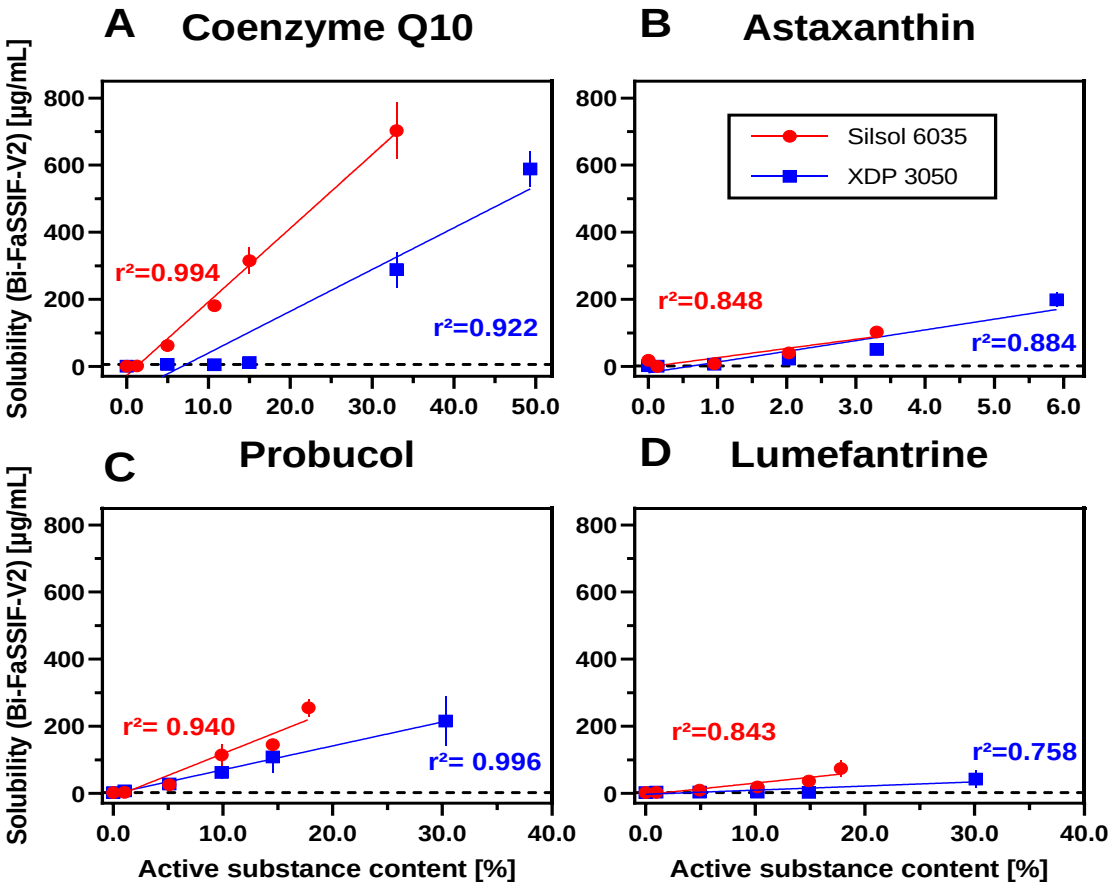

Figure 46: Evaluation of drug load-dependent solubility (determined by HPLC) of **A)** coenzyme Q10, **B)** astaxanthin, **C)** probucol and **D)** lumefantrine loaded mesoporous XDP 3050 and Silsol® 6035 in biorelevant medium (48 h shake flask, 20.0 mL Bi-FaSSIF-V2, pH 6.8); the dashed line represents the equilibrium solubility (48 h) of the unformulated compounds (shake flask method). Adapted from Brenner et al., 2024 [63].

However, for PB, the 1%-loaded silica formulations did not have an impact on solubility, while positive results were observed for all other drug loads (**Figure 46C**). Silsol® showed an improvement factor of 128 (255.3 µg/mL), whereas XDP 3050 improved the solubility of PB by a factor of 108 (215.1 µg/mL).

LU formulations exhibited the least impact on solubility in biorelevant medium (**Figure 46D**). For XDP 3050, only the maximum loaded formulation achieved an effect, resulting in an improvement by a factor of 20 (73.8 µg/mL). Silsol® performed better, with a maximum improvement factor of 35 (41.9 µg/mL).

Depending on the specific model compound, the concentrations of active ingredient obtained in the biorelevant medium varied. However, upon examining the enhancement in relation to the equilibrium solubility of the pure substances, it becomes evident that, with the exception of LU, all model compounds experienced a silica dependent 100 - 200 times improvement of solubility.

As evidenced in section 4.2.2 (solid state characterization) all tested model compounds remained in a non-crystalline form after being loaded onto the mesoporous carrier particles, even at high drug loads. Unlike the crystalline form, dissolving non-crystalline material does not involve breaking the crystal lattice structure. This allows for better interactions with solvent molecules, resulting in an increased solubility and exceedance of the thermodynamic solubility [170]. As a result, loaded silica formulations demonstrated a significant increase in equilibrium solubility. The literature describes the ability to generate supersaturated solutions for various silica and active ingredient combinations [148,160,171,172]. However, depending on the model compound and silica carrier used, there was a drug load-dependent threshold value below which no improvement in equilibrium solubility occurred. This might be related to the formation of a dynamic adsorption equilibrium between the silica surface and the drug molecules. Dening and Taylor described the adsorption of ritonavir to SBA-15, which was used as a mesoporous carrier, as the reason for the incomplete release of ritonavir from these formulations [171]. Assuming that a model compound and a silica-specific amount of active ingredient would stay adsorbed on the silica surface, an increased drug load could compensate for the adsorbed fraction and increase dissolution.

An ingress of water may lead to competitive interactions of the active ingredients with water molecules on the silica surface, leading to a displacement of the active ingredients. If non-crystalline active ingredient gets released from the mesopores, it could be directly solubilized by the surfactants lecithin and taurocholate present in the biorelevant medium.

Thereby, the released fraction is stabilized in solution, even at high concentrations. This leads to a visible increase in the degree of turbidity of the aqueous medium, particularly for highly loaded silica formulations.

However, if a medium without surfactants, such as phosphate buffer, is used, the released active ingredient cannot be stabilized and precipitated out of the solution (refer to **Table 44** and **Table 45**).

The different pore sizes of mesoporous silica carriers can lead to differences in the concentration of the model compound. Silsol 6035 (6 nm) has smaller pores that enable high concentrations at lower drug loads compared to XDP 3050, which has an average pore size of 23 nm [164].

However, the extent of solubility improvement depends on the model compound studied, with CoQ10 showing the most significant effect. The equilibrium solubility improvement differences might be related to the interactions between the model compounds and silica surface on one hand and the interactions between the drug molecules themselves (i.e., self-cohesion) on the other hand. The strength of interaction can be represented by the enthalpy of mixing ΔH_{mix} (**Table 46**), with CoQ10 having a decisively lower enthalpy of -4.35 kJ/mol compared to other model compounds, indicating a higher tendency to dissolve in solution.

Table 46: Rf-values measured on silica gel thin layer chromatography (TLC) plates (10 cm x 10 cm) eluted with petroleum ether - ethyl acetate - acetic acid 70:20:10 (*v/v/v*) and COSMOquick enthalpy of mixing at 37 °C obtained for coenzyme Q10, astaxanthin, probucol and lumefantrine. Obtained from Brenner et al., 2024 [63].

Active ingredient	Rf-Value	ΔH_{mix} [kJ/mol]
Coenzyme Q10	0.85	- 4.35
Astaxanthin	0.88	- 12.68
Probucol	0.89	- 9.63
Lumefantrine	0.40	- 9.25

Conversely, the lowest equilibrium solubility-enhancing effect among all formulations was observed for LU. Results from TCL experiments revealed a lower Rf value of 0.40 for LU, indicating a stronger interaction with the silanol groups on the silica surface compared to other model compounds (which had an Rf value between 0.85 and 0.89), as shown in **Table 46**.

The combination of theoretical calculations and the experimental chromatographic screening method proved to be a promising approach in estimating molecular drug-silica interactions. While the binary ΔH_{mix} calculations were based on a sound quantum-chemical and thermodynamic level of theory, the values were based on simplified binary drug-silica interactions in the bulk. The water phase on the surface was neglected. Therefore, ΔH_{mix} can be considered a measure of intrinsic drug affinity to silica. This was complemented by the chromatographic screening method, where a mobile phase was present to capture further solvation effects or possible ionization, such as possibly for LU. However, the usefulness of these pre-formulation approaches would have to be demonstrated with further compounds to draw firm conclusions.

4.3.3. Investigation of apparent solubility/ kinetic concentration in comparison to monophasic dissolution profiles of highly loaded mesoporous silica formulations

To investigate the apparent solubility (i.e., kinetic concentration) of the model compounds in a biorelevant medium, solvent shift experiments were conducted. A concentrated acetone stock solution (SL; 40 mg/mL) was introduced to 50.0 mL of Bi-FaSSIF-V2 (pH 6.8) and the changes in active ingredient concentration were monitored for 270 min (see **Figure 47**). The apparent solubility profiles of the non-crystalline model compounds (obtained by solvent shift) over time were then compared with the equilibrium solubility (48 h shake flask; see section 4.3) of the pure (crystalline) substances. The impact of pre-suspended silica in the aqueous medium on the apparent solubility profiles was additionally examined.

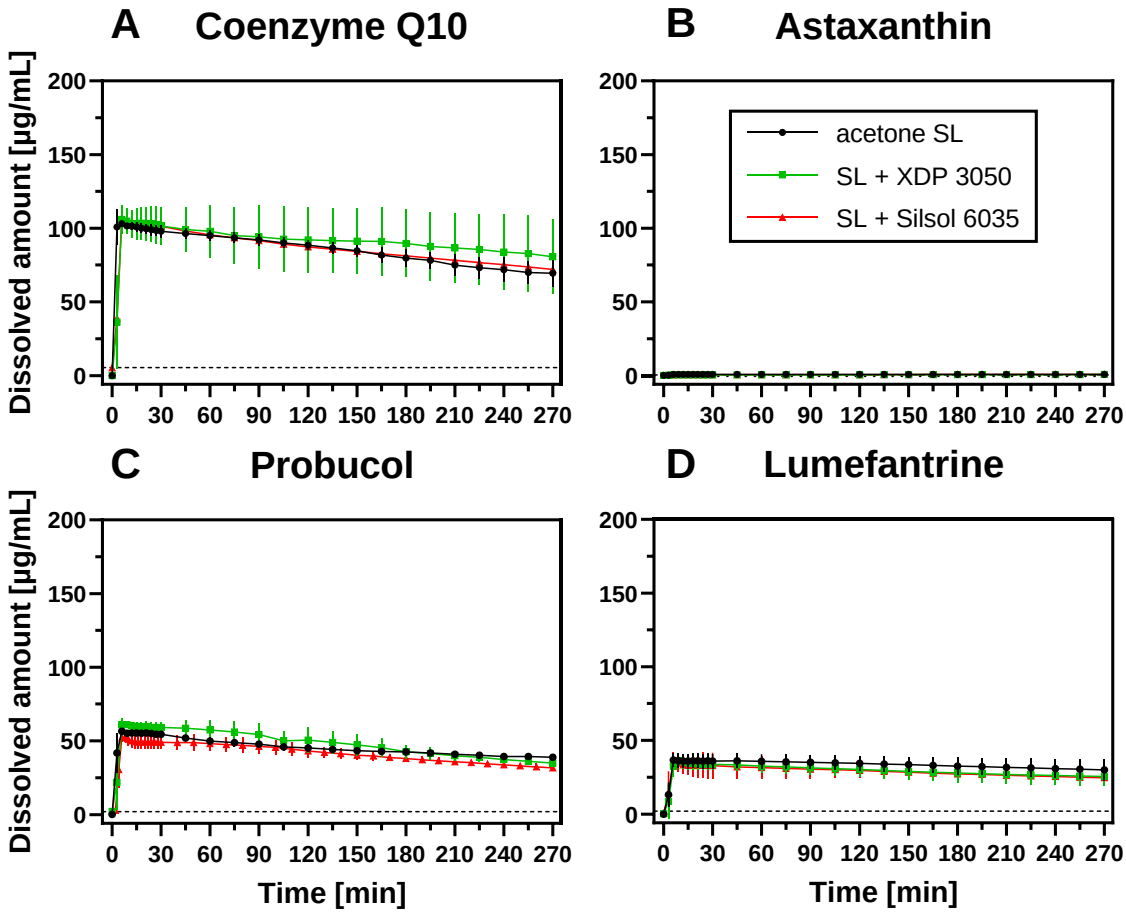

Figure 47: Apparent solubility (250 µL acetone stock solution (40 mg/mL)) of **A)** coenzyme Q10, **B)** astaxanthin, **C)** probucol and **D)** lumefantrine in biorelevant medium (50.0 mL Bi-FaSSIF-V2, pH 6.8) without and in the presence of mesoporous XDP 3050 and Silsol® 6035, (100% corresponds to 0.2 mg/mL); the dashed line represents the equilibrium solubility (48h) of the unformulated compounds (shake flask method). Adapted from Brenner et al., 2024 [63].

CoQ10, PB, and LU exhibited comparable apparent solubility profiles in biorelevant medium (**Figure 47**). The initial concentration attained was 18 - 28 times greater than the equilibrium solubility. Thereby, the presence of suspended silica (Silsol® 6035 or XDP 3050) in the aqueous medium had no impact on the concentration profiles and no surface absorption was detected.

Subsequently, a gradual decline over time occurred due to precipitation of dissolved active ingredient, resulting in the lowest concentration after 270 min. Nevertheless, the concentration still remained above the equilibrium solubility (**Figure 46**). As the supersaturated state has a significantly higher free energy than a saturated solution, the system is driven to return to its stable state through crystallization and/or precipitation [173]. Precipitation can thereby occur in crystalline or amorphous state [174]. The degree of precipitation varied based on the active ingredient.

The experiments revealed that CoQ10 achieved the highest concentration among all model compounds tested, which was comparable to the shake flask results of highly loaded mesoporous silica (see **Figure 46**). The measurement of 103 µg/mL of CoQ10 after 6 min displayed an 18.7-times increase in solubility in contrast to crystalline CoQ10. Subsequently, the concentration decreased to 69.5 µg/mL (270 min) (**Figure 47A**).

On the contrary, ASX remained consistent at approx. 1 µg/mL for the entire test duration (**Figure 47B**). For the semi-solid ASX containing oleoresin, which is paste-like at room temperature, it was found that when the acetone SL was added to the aqueous medium, the extract immediately precipitated out again. This resulted in the formation of large droplets which did not dissolve due to their small surface area and high lipophilicity [175]. As a result, the apparent solubility of ASX could not be displayed by solvent shift experiments.

PB reached a concentration of 56.6 µg/mL after 6 min, which represents an increase by a factor of 28.3 compared to the crystalline substance (**Figure 47C**). Subsequently, the concentration declined to 38.9 µg/mL.

LU solubility was improved by a factor of 17.5, and after 6 min, a concentration of 36.7 µg/mL was reached, which reduced to 30.0 µg/mL during the experiment (**Figure 47D**).

The boosted solubility of the active ingredient can be credited to its non-crystalline form resulting from the solvent shift. As a result, the active ingredient lacks a crystal lattice, which reduces the interaction forces between individual molecules and eliminates the need for solvation energy for the solvent to dissolve the active ingredient. Consequently, a stronger interaction between the solvent and the active ingredient is achieved, leading to a significantly higher solubility than the crystalline form [176,177].

Furthermore, the apparent solubility profiles of the non-crystalline model compounds (solvent shift) were compared with monophasic dissolution profiles in biorelevant medium (Bi-FaSSIF-V2) of the highly loaded mesoporous silica formulations (**Figure 48**).

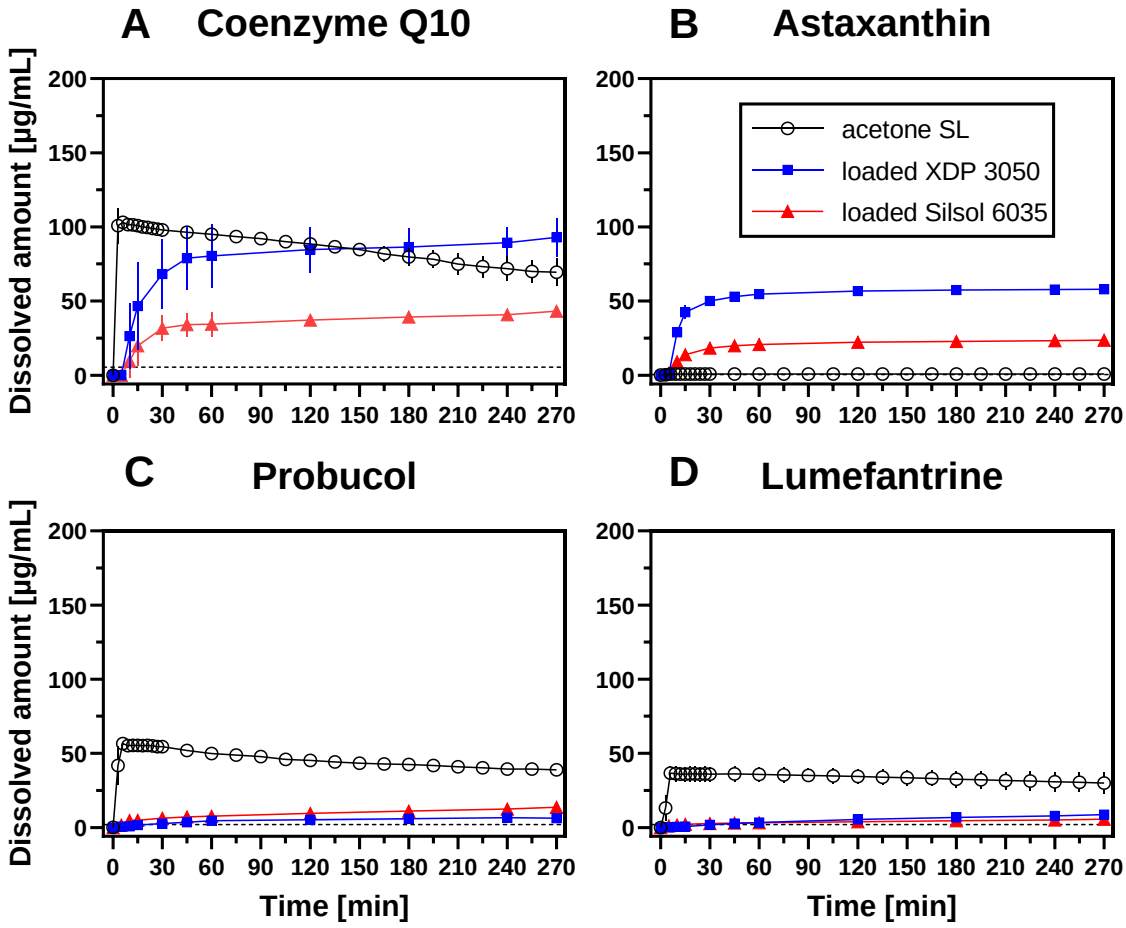

Figure 48: Apparent solubility (250 µL acetone stock solution (40 mg/mL)) in biorelevant medium (50.0ml Bi-FaSSIF-V2, pH 6.8) of **A)** coenzyme Q10, **B)** astaxanthin, **C)** probucol, **D)** lumefantrine and monophasic dissolution (biorelevant medium) of their corresponding loaded mesoporous XDP 3050 and Silsol® 6035 formulations, (100% corresponds to 0.2 mg/mL); the dashed line represents the equilibrium solubility (48h) of the unformulated compounds (shake flask method). Adapted from Brenner et al., 2024 [63].

Since shake flask experiments revealed, that model compound solubility increased with increasing drug load (as depicted in **Figure 46**) for all compounds, only the formulations with the highest possible drug load were examined.

The data showed that, similar to the results of shake flask experiments, there was a substantial increase in release rate of CoQ10 generated from the loaded XDP 3050 and Silsol® 6035 formulations, when compared to the crystalline compound (**Figure 48A**). Under the hydrodynamic conditions present in the BiPHa+ cylindrical vessels, the concentration of CoQ10 increased rapidly for both mesoporous silica formulations. With 80.3 µg/mL already released for loaded XDP 3050 and 34.4 µg/mL for loaded Silsol® after 60 min and thereby notably exceeding the equilibrium solubility (5.5 µg/mL). However, the release rate slowed down significantly thereafter, with the CoQ10 concentration rising slowly. After 270 min, XDP 3050 released 93.0 µg/mL of CoQ10, while Silsol® 6035 released 43.2 µg/mL.

Silica loaded with the ASX containing microalgae extract showed similar effects compared to CoQ10. Initially, a high release rate was observed which decreased decisively over time, reaching a plateau after 60 min. The XDP 3050 formulation released 58.0 µg/mL, while the Silsol® formulation released 23.6 µg/mL (**Figure 48B**). Both concentrations significantly exceeded the equilibrium solubility of ASX in biorelevant medium (1.1 µg/mL). However, unlike CoQ10, both loaded silica formulations surpassed the apparent solubility of ASX as determined in the solvent shift experiment and there was no evidence of precipitation of extract released from the pores with subsequent droplet formation.

When investigating the release of PB and LU formulations, a different situation occurred (**Figure 48C/ D**). The silica formulations for both model compounds did not achieve the release rates of the CoQ10 and ASX formulations and no rapid release kinetics could be detected. However, there was a slow release with steadily increasing PB and LU concentrations. Nevertheless, the equilibrium solubility (PB: 2.0 µg/mL / LU: 2.1 µg/mL) was already exceeded after 120 min for both active ingredients. For PB loaded XDP 3050, 6.3 µg/mL was reached after 270 min, and for PB loaded Silsol®, 13.7 µg/mL was detected. This represented an increase by 3.2 - 6.9 compared to the unformulated compound. XDP 3050 and Silsol 6035 formulations loaded with LU increased solubility by a factor of 4.1 - 2.7 and achieved 8.7 µg/mL and 5.6 µg/mL, respectively.

In general, however, decisively lower concentrations of all model compounds were measured during the monophasic dissolution studies than during the 48 h shake flask experiments. This can be attributed to the fact that besides the loading quantity of the silica carrier particles (refer to **Figure 46**), the model compound solubility in biorelevant medium was additionally influenced by the amount of loaded silica formulation per solvent volume (**Figure 49**).

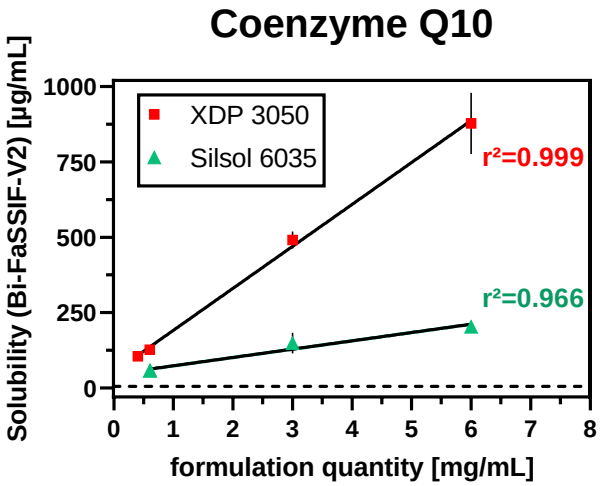

Figure 49: Evaluation of the effect of formulation quantity of highly loaded coenzyme Q10 - XDP 3050 /Silsol® 6035 formulations on coenzyme Q10 solubility (determined by HPLC) in biorelevant medium (Bi-FaSSIF-V2, pH 6.8) determined by shake flask experiments; the dashed line represents the equilibrium solubility (48 h) of the unformulated compound (shake flask method). Obtained from Brenner et al., 2024 [63].

As formulation quantity per mL aqueous solvent volume increased, the concentration of CoQ10 in solution increased linearly for both types of silica. The impact was particularly evident with XDP 3050, where the resulting CoQ10 concentrations in solution were significantly higher than those achieved with loaded Silsol® 6035 using the same quantity of formulation. Notably, the disparity in CoQ10 concentration achieved by both mesoporous carriers increased with larger amounts of formulation used.

During biorelevant monophasic/ biphasic dissolution measurements the amount of formulation used was between 0.4 mg/mL and 1 mg/mL, depending on the drug load of the investigated formulation. By contrast, during shake flask experiments significantly larger quantities of formulation were used (formulation excess of at least 20 times the equilibrium solubility of the model compound in biorelevant medium which corresponds to up to 10 mg/mL).

The 270 min monophasic dissolution measurements (**Figure 48**) were followed up with 24-hour measurements to investigate the stability of the supersaturation achieved by the silica formulations (**Figure 50**).

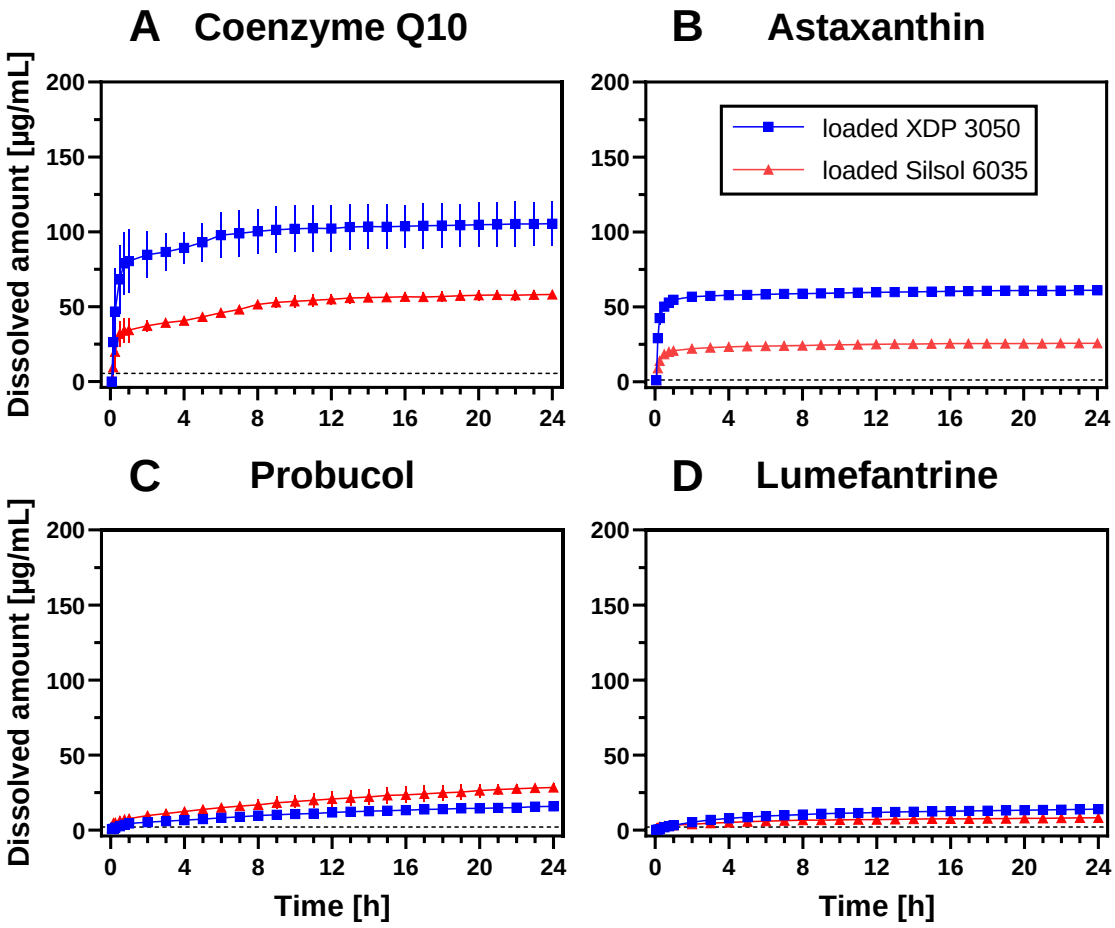

Figure 50: 24 h solubility profile in biorelevant medium (50.0ml Bi-FaSSIF-V2, pH 6.8) of **A)** coenzyme Q10, **B)** astaxanthin, **C)** probucol and **D)** lumefantrine loaded mesoporous XDP 3050 and Silsol® 6035; the dashed line represents the equilibrium solubility (48h) of the unformulated compounds (shake flask method). Adapted from Brenner et al., 2024 [63].

The generated supersaturation remained stable for a period of 24 h without any precipitation occurring. For CoQ10, a dynamic equilibrium was reached in about 10 h and after 24 h concentrations of 105.4 µg/mL were reached by the XDP 3050 formulation and 58.1 µg/mL by the Silsol® formulation, respectively. For ASX, the equilibrium was achieved in just one hour and end concentrations of 61.0 µg/mL (XDP 3050) and 25.6 µg/mL (Silsol® 6035) were measured. The concentration of PB consistently increased at a steady rate (C_{max} XDP 3050: 15.9 µg/mL / Silsol® 6035: 28.4 µg/mL), but for LU, the plateau was reached after eight hours (C_{max} XDP 3050: 13.9 µg/mL / Silsol® 6035: 8.2 µg/mL).

4.3.4. Biorelevant biphasic dissolution results

Prior to investigating the biorelevant biphasic dissolution (BiPHa+) performance of the highly loaded mesoporous silica formulations for each model compound, studies to examine how the drug load affected the partitioning rate into the organic absorption sink were performed. As part of this investigation, XDP 3050 formulations that were loaded with CoQ10 were selected exemplarily. For detailed findings on the BiPHa+ measurements, please refer to **Figure 51**.

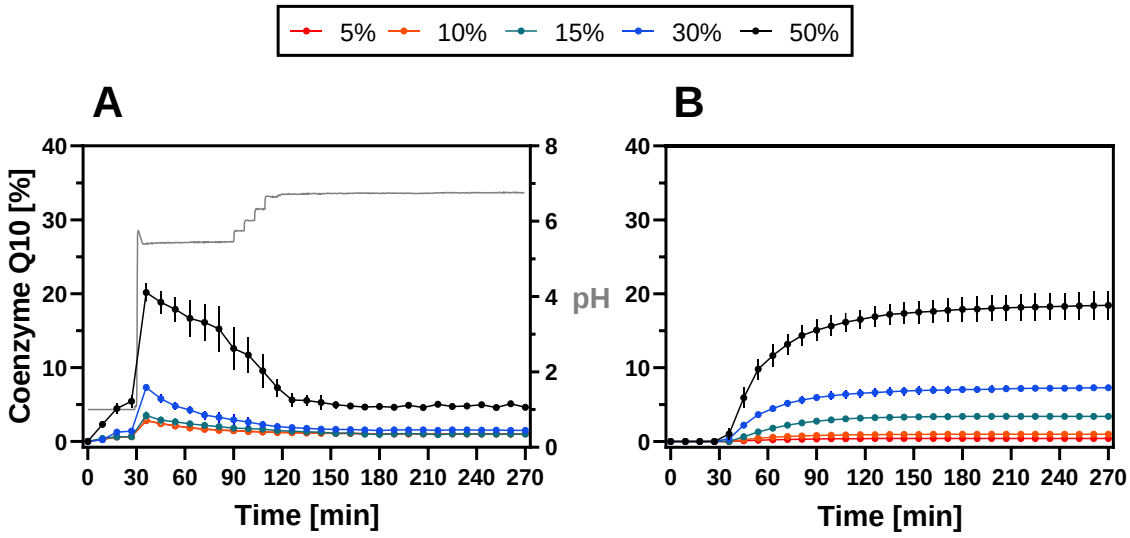

Figure 51: Dissolved/ partitioned amount of coenzyme Q10 (mean ± SD) as a function of loading quantity on XDP 3050 (5%, 10%, 15%, 30% and 50% drug load; *w/w*) during biorelevant biphasic dissolution (BiPHa+); **A)** aqueous medium, **B)** 1-decanol layer; the pH profile in the aqueous medium is represented by the grey line, (100% corresponds to 0.2 mg/mL). Obtained from Brenner et al., 2024 [63].

Initially, focusing on the aqueous medium, comparable concentration profiles for the XDP 3050 formulations with drug loads of 5%, 10%, and 15% (*w/w*) were obtained (**Figure 51A**). Only about 0.7% of the drug was released in the first 30 min, followed by a sudden increase to approximately 3% after biorelevant surfactants were added. Subsequently, the concentration declined and finally stabilized at 1%. This concentration profile was equal to the profile received for unformulated CoQ10, but the rate of partitioning into the organic 1-decanol phase varied between the different formulations (**Figure 51B**). The 5% formulation achieved an end concentration (270 min) of 0.4%, while the 10% formulation had an end concentration of 0.9%. This represented a slight reduction in concentration compared to unformulated CoQ10. At low loading levels, CoQ10

remained in the mesoporous matrix of XDP 3050, which reduced its interaction with the dissolution medium [178,179]. For various active ingredients, it is known that a fraction of the loaded drug molecules could be tightly bound to the silica surface or attached to sites that were inaccessible to the dissolution medium, which led to a reduction in the released amount of active ingredient [179–182]. However, this effect was not observed for the 15% (*w/w*) loaded formulation, and a final concentration in 1-decanol of 3.4% was achieved, which was equal to twice the 1-decanol concentration achieved by the CoQ10 powder.
On the other hand, the formulation with a 30% (*w/w*) drug load achieved an increased concentration of CoQ10 already in the aqueous medium. After adding Bi-FaSSIF-V2, 7.3% of the active ingredient was released, representing a decisive increase in dissolution rate compared to unformulated CoQ10. Related to the increased water solubility and the higher amount of active ingredient available for partitioning into the 1-decanol layer, after 270 min a concentration in the organic absorption sink of 7.3% was measured [89,90].
The effect of increasing CoQ10 solubility in biorelevant medium with increasing drug load, observed during shake flask experiments (refer to section 4.2; **Figure 46A**), partially translated into an increase in partitioning rate during biorelevant biphasic dissolution. Out of all tested formulations, the one with a drug load of 50% (*w/w*) achieved the highest CoQ10 concentration in the aqueous medium at 20.2% after 30 min. However, due to partitioning across the aqueous/organic interface and accumulation in the organic absorption sink, the concentration decreased and reached a plateau of approximately 4.7% after 120 min. At the same time in the organic phase the highest partitioning rate was detected, and after 270 min, the formulation achieved a concentration of 18.4%.
The end concentration of CoQ10 achieved in the organic absorption sink by different formulations was found to be linearly dependent on the loading quantity of CoQ10. The higher the loading quantity, the higher the partitioning rate.

Based on these findings, biphasic dissolution studies were conducted analyzing the XDP 3050 and Silsol® 6035 formulations with the highest possible drug load. The experimental results were than compared with the dissolution and partitioning profiles of the unformulated model compounds. Furthermore, for CoQ10 and ASX the BiPHa+ data of the commercial formulations studied in section 3.5 and 3.7 were taken into consideration as a reference for the performance of currently available formulations.

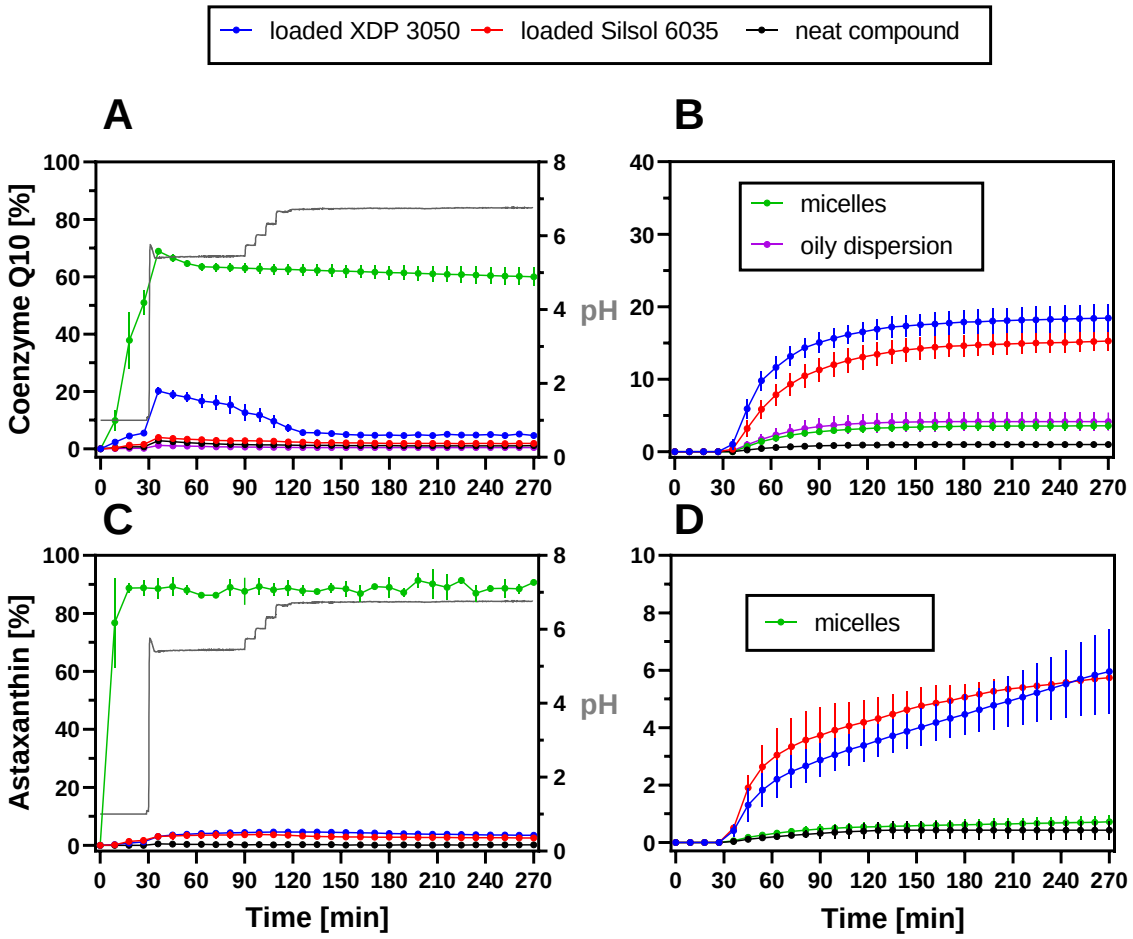

Figure 52: Dissolved/ partitioned amount of coenzyme Q10 (including micelles and oily dispersion as commercial formulation with previously studied bioavailability [183]) and astaxanthin (including micelles as commercial formulation) (mean ± SD) during biorelevant biphasic dissolution (BiPHa+); **A)** coenzyme Q10 aqueous medium, **B)** coenzyme Q10 1-decanol layer, **C)** astaxanthin aqueous medium, **D)** astaxanthin 1-decanol layer; the pH profile in the aqueous medium is represented by the grey line, (100% corresponds to 0.2 mg/mL). Obtained from Brenner et al., 2024 [63].

As previously mentioned, the degree of loading had a direct impact on the CoQ10 solubility in biorelevant medium (**Figure 51**). Accordingly, the XDP 3050 formulation achieved a notable improvement in water solubility due to its very high drug load of 50% (*w/w*) (**Figure 52A**). But among the formulations tested, the self-emulsifying micellar one (1. commercial formulation for comparison) proved to be the most effective in terms of water solubility optimization due to the high surfactant content of the formulation. It released about 70% of the active ingredient in the first 30 min [107]. On the other hand, the Silsol® 6035 and oily dispersion (2. commercial formulation for comparison) formulations did not improve solubility compared to pure CoQ10.

However, the mesoporous silica formulations stood out from the rest, as they demonstrated a marked increase in the partitioning rate into the organic phase compared to unformulated CoQ10 and commercial formulations (**Figure 52B**). While pure CoQ10 reached an end concentration of 1.5% in 1-decanol after 270 min, the two commercial formulations achieved 3.6 - 4% (**Table 47**). This represents an increase by a factor of 2.4 to 2.7 compared to the unformulated active ingredient. However, the silica formulations were substantially more effective. For the loaded Silsol® 6035 formulation, a CoQ10 concentration of 15.3% was measured in the organic phase after 270 min, representing an increase by a factor of 10 compared to the pure active ingredient and an increase of 3.8 to 4.3 compared to the commercial formulations. The increased partitioning rate compared to the commercial formulations and crystalline CoQ10 could be attributed to the rapid release kinetic of active ingredient from the mesopores of Silsol® after the addition of biorelevant surfactants (refer to **Figure 48**). As a result, CoQ10 is immediately available for transfer into the organic phase, lowering the concentration of the active ingredient in the water phase. This prompts more active ingredient to be released from the reservoir in the mesopores, creating a dynamic equilibrium that allows for a high partitioning rate into the organic phase while maintaining a low absolute concentration of CoQ10 in the aqueous medium. In their study, Denninger et al. found that ritonavir exhibited a high partitioning rate in the organic phase, while its concentration in the water phase remained low [52]. The authors attributed this to the formation of drug rich nano-droplets in the dissolution medium via liquid – liquid phase separation (LLPS). LLPS can occur for slow crystallizing drug when the amorphous solubility is exceeded in solution [184,185].

For the XDP 3050 formulation a concentration of 18.4% was measured in the organic phase. This represented the highest CoQ10 concentration among all the formulations tested and displayed a five-fold increase compared to the commercial formulations. As a result, silica formulations loaded with CoQ10 represented a suitable alternative with better performance to the currently available commercial formulations. Both mesoporous carriers experienced significantly improved performance in biorelevant test systems and allowed for a 1.5 to 9 times higher drug load than the commercial formulations.

Table 47: Concentrations of dissolved/ partitioned coenzyme Q10 (CoQ10) and astaxanthin (ASX) (mean ± SD) from the unformulated compounds, highly loaded silica formulations and commercial formulations in the aqueous medium and the 1-decanol layer at the end of biorelevant biphasic dissolution (BiPHa+) at 270 min (determined by HPLC).

Formulation	**Endpoint concentration [%]**	
	aqueous medium	**1-decanol**
Coenzyme Q10	**2.0 ± 0.3**	**1.5 ± 0.2**
CoQ10 - XDP 3050	4.6 ± 0.0	**18.4 ± 1.9**
CoQ10 - Silsol® 6035	1.8 ± 0.5	**15.3 ± 1.3**
Commercial formulations		
Micelles	60.0 ± 3.2	**3.6 ± 0.6**
Oily dispersion	0.4 ± 0.1	**4.0 ± 1.3**
Astaxanthin	**0.2 ± 0.1**	**0.4 ± 0.3**
ASX - XDP 3050	3.5 ± 0.6	**6.0 ± 1.5**
ASX - Silsol® 6035	2.5 ± 0.8	**5.7 ± 0.4**
Commercial formulation		
Micelles	90.7 ± 1.0	**0.7 ± 0.2**

Focusing on the ASX formulations, both silica formulations showed an increase in ASX solubility in the aqueous dissolution medium. The concentration profiles measured were comparable, with peak concentrations of less than 10% detected after 30 min (**Figure 52C**). However, the unformulated extract displayed minimal dissolution in water and maintained a concentration below 1% throughout the measurement. Conversely, the self-emulsifying micellar formulation (commercial formulation for comparison) dissolved quickly and completely, achieving 90% release after 30 min. However, only both silica formulations exhibited a significant increase in partitioning rate into the organic phase, with concentrations of 6.0% for XDP 3050 and 5.7% for Silsol® 6035 being measured after 270 min (**Figure 52D**). Neither the unformulated extract nor the micelles achieved end concentrations of over 1% in 1-decanol. Thus, the silica formulations improved ASX partitioning into the organic absorption sink by a factor of 8 to 15 (**Table 47**) and no measurable difference between both formulations was observed.

Comparable to the CoQ10 formulations, both silica formulations achieved higher concentration of active ingredient during biphasic dissolution studies than the commercial formulation while at the same time providing an up to 3 times higher drug load.

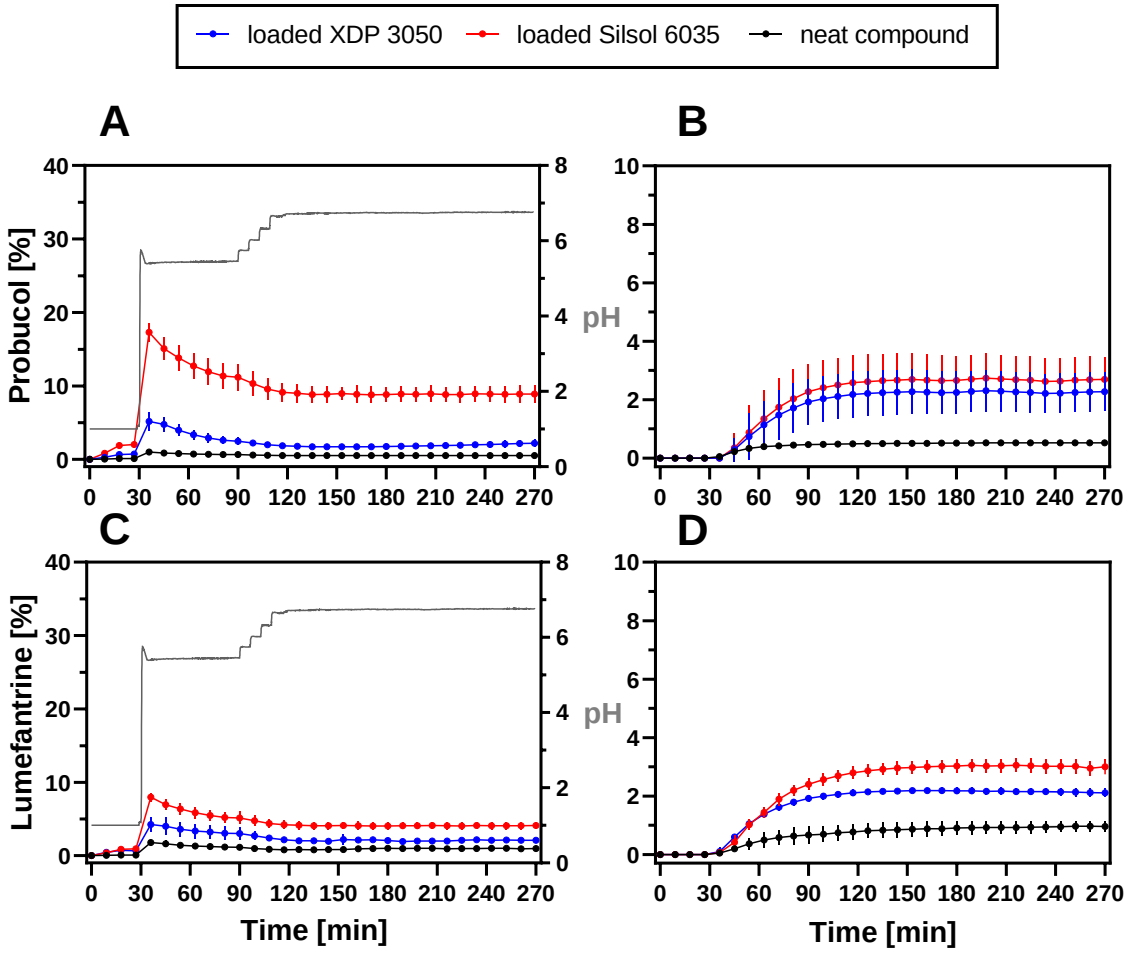

Figure 53: Dissolved/ partitioned amount of probucol and lumefantrine (mean ± SD) during biorelevant biphasic dissolution (BiPHa+); **A)** probucol aqueous medium, **B)** probucol 1-decanol layer, **C)** lumefantrine aqueous medium, **D)** lumefantrine 1-decanol layer; the pH profile in the aqueous medium is represented by the grey line, (100% corresponds to 0.2 mg/mL). Obtained from Brenner et al., 2024 [63].

Compared to the natural substances CoQ10 and ASX, no commercial formulations were available for PB and LU. Therefore, only the unformulated active ingredients were used for comparison.

Although Syloid® XDP 3050 and Silsol® 6035 formulations improved water solubility and increased the partitioning rate of both active ingredients, the effects were not as pronounced as examined for CoQ10 and ASX.

Concerning PB-containing formulations, loaded Silsol® 6035 allowed for a higher concentration of PB in the aqueous dissolution medium (**Figure 53A**). After adding biorelevant surfactants (30 min), a concentration of 17.3% was measured, which subsequently reduced to 8.9% during the dissolution measurement.

On the other hand, the pure active ingredient only reached 1% after 30 min, which further reduced to 0.5%. Using XDP 3050 as a mesoporous carrier, the PB solubility increase was minor, and after 30 min, 5.2% PB was measured in the aqueous medium.

In the organic phase, the partitioning rate was enhanced by both silica formulations, and after 270 min, 2.3% was measured for XDP 3050 and 2.7% for Silsol® (**Figure 53B**). This corresponded to a five-fold increase compared to the pure active ingredient, which reached a concentration of 0.5% at the end of the biorelevant dissolution test (**Table 48**). Although the concentration of PB in the aqueous medium was increased, the Silsol® formulation did not show a pronounced increase in the partitioning rate for PB compared to the XDP 3050 formulation. This could be related to the surfactants lecithin and taurocholate present in the biorelevant medium interacting with PB. This interaction appears to have inhibited the partitioning across the aqueous/ organic interface and thereby reduced accumulating of PB in the organic absorption sink (**Figure 54**).

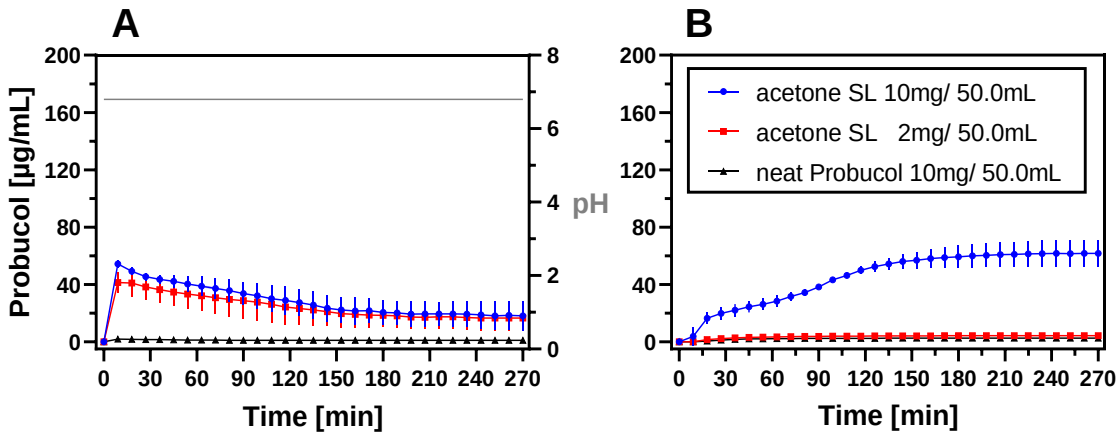

Figure 54: **A)** Supersaturation in biorelevant medium (50.0 mL Bi-FaSSIF-V2) and **B)** partitioning into the 1-decanol layer of probucol (PB) stock solutions (SL) 40 mg/mL in acetone (1. 250 µL SL = 10 mg PB, 2. 50 µL = 2 mg PB) compared to PB - dicalcium phosphate tablets (20% dug load (*w/w*), weight corresponding to 10 mg PB); (mean ± SD); the pH profile in the aqueous medium is represented by the grey line, (100% corresponds to 0.2 mg/mL). Obtained from Brenner et al., 2024 [63].

The transfer of dissolved PB across the aqueous/ organic interface in the presence of biorelevant surfactants was investigated using BiPHa+ measurements carried out with acetone stock solutions (SL) of PB (**Figure 54A**). Initially, an amount of SL (250 µL) equivalent to 10 mg active ingredient was added. The obtained concentration profile in the aqueous phase closely matched the apparent solubility profile of PB in

biorelevant medium (refer to **Figure 48C**). Nevertheless, most of the active ingredient precipitated directly after the solvent shift, and floating of the fine precipitate directly into the organic phase occurred due to the high hydrophobicity of PB (**Figure 54B**). This limitation of BiPHa+ measurements made it necessary to reduce the amount of SL to 50 µL to keep the active ingredient entirely in solution and suppress floating. Despite the dose reduction to 2 mg the aqueous concentration profile observed matched the profile of the 10 mg dose. Simultaneously precipitate formation was suppressed, and floating was not observed. Even though the concentration of PB in the aqueous medium reached up to 41.3 µg/mL (significantly higher than the 2.0 µg/mL detected for unformulated PB) there was no increase observed in the partitioning rate of the active ingredient into the organic phase. After 270 min, the supersaturated solution of PB achieved a concentration of 4.3 µg/mL, while unformulated PB only reached 2.6 µg/mL. This suggests that the presence of lecithin and taurocholate reduced the transfer of PB into the organic phase by interacting with dissolved PB. For different surfactant-active ingredient combinations it is known, that the formation of stable micellar inclusion complexes counteracts an increase in absorption *in vitro*, even if significantly higher active ingredient concentrations are present in solution [117,183,186].

Table 48: Concentrations of dissolved/ partitioned probucol (PB) and lumefantrine (LU) (mean ± SD) from unformulated compound and highly loaded silica formulations in the aqueous medium and the 1-decanol layer at the end of biorelevant biphasic dissolution (BiPHa+) at 270 min (determined by HPLC).

Formulation	**Endpoint concentration [%]**	
	aqueous medium	**1-decanol**
Probucol	**0.5 ± 0.1**	**0.5 ± 0.1**
PB - XDP 3050	2.2 ± 0.5	**2.3 ± 0.7**
PB - Silsol® 6035	8.9 ± 1.1	**2.7 ± 0.8**
Lumefantrine	**1.0 ± 0.1**	**1.0 ± 0.2**
LU - XDP 3050	2.1 ± 0.3	**2.1 ± 0.1**
LU - Silsol® 6035	4.1 ± 0.5	**3.0 ± 0.3**

Similar to the dissolution results of the PB formulations, only minor improvements in the partitioning rate into the organic phase were observed for LU loaded XDP 3050 and Silsol® 6035. However, loaded Silsol® increased the maximum LU concentration in the aqueous medium (which was reached after adding biorelevant surfactants) from 1.8% measured for unformulated LU to 8.0% (**Figure 53C**). Throughout the dissolution test, the concentration gradually decreased to 4.1%. XDP 3050 had a reduced impact on LU solubility and after 30 min, a concentration of 4.3% was measured, which subsequently decreased to 2.1%. In contrast to the PB formulations, however, the increased solubility led to an improved partitioning rate into the 1-decanol layer.

After 270 min, 3.0% and 2.1% were measured for the Silsol® and XDP 3050 formulations, respectively. This corresponded to an increase by a factor of 3 and 2.1 in comparison to unformulated LU that reached 1.0% (**Figure 53D**). However, silica loaded with LU showed overall reduced performance in terms of biorelevant biphasic dissolution.

Moreover, during monophasic dissolution measurements (refer to **Figure 48D**), LU was released at the lowest rate when compared to the other lipophilic model compounds. This might be attributed to stronger interaction of LU with the silanol groups on the surface of the mesoporous silica carrier particles, as it contains a protonatable basic amin.

Nevertheless, an increase in the partitioning rate was observed for both PB and LU loaded silica formulations and endpoint concentrations of the unformulated model compounds were surpassed by up to five times.

4.4. Conclusion

Despite the challenges presented by the unfavorable molecular properties of CoQ10, which include high lipophilicity (log $D_{7.4}$: 14.7) and low water solubility (5.5 µg/mL in Bi-FaSSIF-V2), various formulations that decisively increase its partitioning rate into the organic absorption sink of BiPHa+ have been developed. As discussed in section 3.5.1 the BiPHa+ has been proven to deliver biorelevant dissolution results for CoQ10 independent of the investigated formulation principle.

Screening experiments have identified HPC-SSL, EPO, and VA64 as suitable carrier polymers for the manufacturing of binary solid dispersions, with improved water solubility and increased partitioning rate into the 1-decanol absorption sink. The combination of VA64 and EPO (50/50) in ternary solid dispersions showed synergistic effects, resulting in a higher partitioning rate than binary solid dispersions. This formulation achieved an end concentration of CoQ10 in the organic medium that was 6 -7 times higher than that of bioavailability-enhanced formulations currently available on the food supplement market. However, achieving complete amorphization during manufacturing of the solid dispersions (drug load of 20%; *w/w*) was not possible due to the high lipophilicity of CoQ10 and its reduced solubility in the carrier polymers. A reduction of the drug load to achieve a completely amorphous formulation was not considered, as the evaluation of the optimal drug load revealed negative effects of reduced drug loads below 10%.

As a result, the use of mesoporous silica, such as Syloid® XDP 3050 and Silsol® 6035, as carrier particles for drug loading and as an alternative bioavailability improved formulation strategy was additionally investigated. For evaluation of the effect of loading onto mesoporous silica particles different lipophilic model compounds were investigated, in addition to the natural substances CoQ10 and ASX, the synthetic active pharmaceutical ingredients PB and LU were also examined.

Comparable to CoQ10, all model compounds showed low water solubility and high lipophilicity, making them unsuitable for direct use in medicinal products. To address this issue, mesoporous carriers were employed and loaded via incipient wetness impregnation with DCM as an organic solvent. This method led to high drug loads being received, with HS-GC-FID measurements showing residual solvent amounts below 100 ppm. The loaded formulations of both silica and all four model compounds showed a linear dependence of

the active ingredient solubility in biorelevant medium (shake flask) on the drug load employed, resulting in solubility improvements of up to 180 times compared to the crystalline compounds. However, this effect was only observed in biorelevant medium and not in plain buffer at pH 6.8.

Differences in solubility improvement between the model compounds could successfully be explained by *in silico* calculations of mixing enthalpy for drug and silica as well as an experimental chromatographic method to estimate molecular interactions. The given *in silico* approach was meant to characterize an intrinsic affinity of drug to silica, whereas the chromatographic method had a mobile phase that complemented the calculations by capturing possible effects of solvation and ionization in solution phase. However, to draw firm conclusions, the investigation of further compounds is necessary.

In line with the results of the shake flask experiments, increased solubilities were also measured during monophasic dissolution studies, particularly for CoQ10 and ASX. The lower concentrations observed during these experiments in comparison to the shake flask measurements could be attributed to the solubility-enhancing effect being reliant on the amount of formulation present in the dissolution medium.

When comparing polymer dispersions to mesoporous silica formulations loaded with different model compounds, the latter did not exhibit any residual crystallinity, even at high drug loads of up to 50%. Additionally, the ability of these formulations to improve solubility resulted in a marked enhancement in biorelevant dissolution performance. ASX and CoQ10 demonstrated 5 to 7 times better results compared to commercial formulations, while PB and LU showed improved dissolution when compared to the unformulated, crystalline active ingredients. However, the formulation principle was found to be less suitable for PB and LU due to certain limitations.

In summary, loading lipophilic compounds into silica carrier particles is a highly effective alternative to other formulation principles, such as self-emulsifying drug delivery systems or polymer dispersions, especially for compounds with a poly-isoprene structure like CoQ10 and ASX. This method allowed for stabilization of al model compounds in a non-crystalline form, resulting in significantly improved dissolution performance, while also providing high drug loads of 30% to 50% (*w/w*; depending on the solvent used).

5. Materials and methods

5.1. Materials

5.1.1. Extracts and formulations made thereof

Table 49: Overview of the extracts and formulations used in this thesis (including chemical structures and physicochemical properties of the respective main active ingredient, product name and manufacturer).

Curcuma formulations		
Curcumin (CUR) 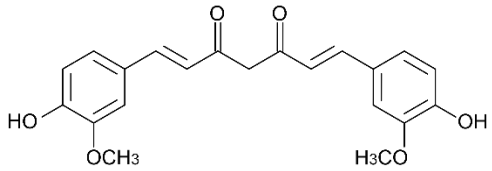 **Physicochemical properties** [28]**:** Molecular weight (MW): 368.4 g/mol Acid/ base/ neutral: weak acid pK_a: 6.8/ 8.6/ 9.1 Log $D_{7.4}$: 3.50	**Formulation:**	**Manufacturer:**
	Micelles **Product name:** NovaSOL® Curcumin	AQUANOVA AG, Darmstadt, Germany
	Cyclodextrin complex **Product name:** Cavacurmin®	Wacker Chemie, Munich, Germany
	Phytosomes **Product name:** Meriva®	Indena S.p.A., Milan, Italy
	Submicron particle **Product name:** Theracurmin®	Theravalues Corp., Tokyo, Japan
Demethoxycurcumin (DMC) 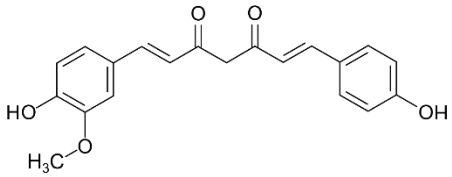 **Physicochemical properties** [28]**:** MW: 338.4 g/mol Acid/ base/ neutral: weak acid pK_a: 6.6/ 8.5/ 9.0 Log $D_{7.4}$: 3.58	Native extract **Product name:** -	Jupiter Leys, Okkal, India
	Adjuvants **Product name:** Pro Curmin Complete II	TISSO Naturprodukte, Wenden, Germany
Bisdemethoxycurcumin (BDMC) 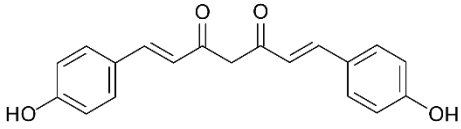 **Physicochemical properties** [28]**:** MW: 308.4 g/mol Acid/ base/ neutral: weak acid pK_a: 6.8/ 8.7/ 9.2 Log $D_{7.4}$: 3.64	Turmeric oils **Product name**: BCM-95®	Arjuna Natural Extracts, Kerala, India
	Liposomes **Product name:** Longvida®	Verdure Sciences, Noblesville, USA

Resveratrol Formulations		
***Trans*-Resveratrol** 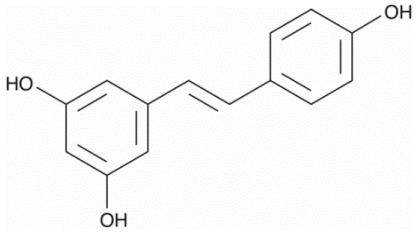 **Physicochemical properties** [66]**:** MW: 228.3 g/mol Acid/ base/ neutral: weak acid pK_a: 9.1/ 9.7/ 10.5 Log $D_{7.4}$: 2.70	**Formulation:**	**Manufacturer:**
	Grapevine-shoot extract **Product name:** Vineatrol® 30	Actichem, Montauban, France
	Grapevine-shoot extract micelles **Product name:** NovaSOL® Vineatrol 30	AQUANOA AG, Darmstadt, Germany
	Water dispersible (WD) resveratrol **Product name:** VeriSperse™	Evolva Holding SA, Reinach, Switzerland
	Purified resveratrol **Product name:** Veri-te™	Evolva Holding SA, Reinach, Switzerland
Coenzyme Q10 Formulations		
Coenzyme Q10 (CoQ10) 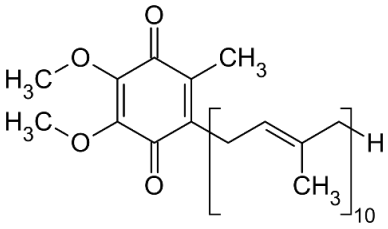 **Physicochemical properties** [66]**:** MW: 863.3 g/mol Acid/ base/ neutral: neutral pK_a: 13.3 Log $D_{7.4}$: 14.72	**Formulation:**	**Manufacturer:**
	Purified CoQ10 **Product name:** -	Kingdomway Pharmaceutics, Inner Mongolia, China
	Oily dispersion **Product name:** Nature Made® CoQ_{10}	Pharmavite®, Northridge, CA, USA
	Micelles **Product name:** NovaSOL® Q	AQUANOA AG, Darmstadt, Germany
Quercetin Formulations		
Quercetin 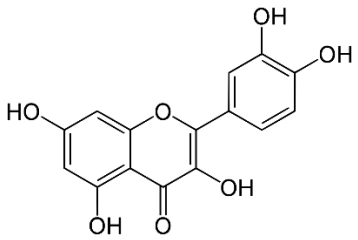	**Formulation:**	**Manufacturer:**
	Crystalline Quercetin **Product name:** -	Sigma-Aldrich, Buchs, Switzerland

Physicochemical properties [66]**:** MW: 302.2 g/mol Acid/ base/ neutral: weak acid pK_a: 7.1/ 9.1/ 11.1 Log $D_{7.4}$: 1.60	Phytosomes® **Product name:** Quercefit®	Indena S.p.A., Milan, Italy
Astaxanthin Formulations		
Astaxanthin (ASX) (unesterified) 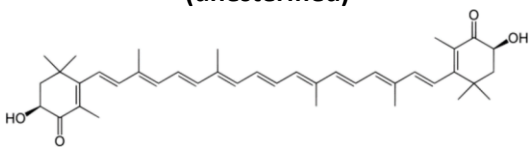 **Physicochemical properties** [63]**:** MW: 596.9 g/mol Acid/ base/ neutral: neutral pK_a: 10.6 Log $D_{7.4}$: 8.05	**Formulation:**	**Manufacturer:**
	Astaxanthin enriched *Haematococcus pluvials* extract (contains mainly mono- and diester)/ oleoresin **Product name**: AstaFit®	BDI-BioLife Science, Hartberg, Austria
	Micelles (containing mainly mono- and diester) **Product name:** NovaSOL® Astaxanthin	AQUANOVA AG, Darmstadt, Germany

5.1.2. Drug substances loaded onto mesoporous silica

Table 50: Chemical structures, manufacturer and physicochemical properties (predicted values; except molecular weight (MW) and log $D_{7.4}$) of the drugs used for mesoporous silica loading.

Lumefantrine (LU) 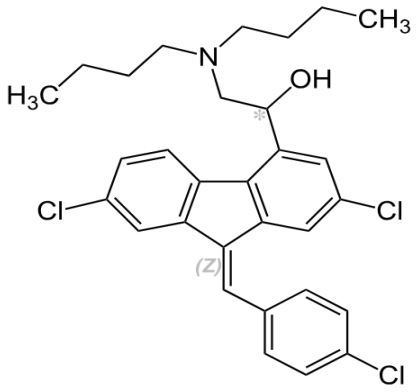 	**Manufacturer:** Swapnroop Drugs & Pharmaceuticals, Aurangabad, India **Physicochemical properties** [187]**:** MW: 528.9 g/mol Acid/ base/ neutral: weak base pK_a: 8.2 Log $D_{7.4}$: 8.3 [154] Hydrogen acceptor count: 2 Hydrogen donor count: 1
Probucol (PB) 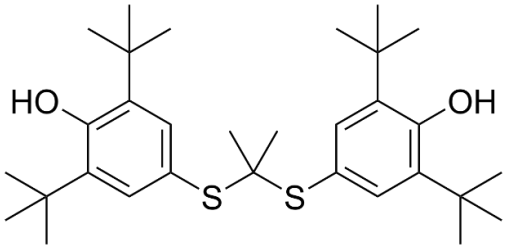 	**Manufacturer:** Swapnroop Drugs & Pharmaceuticals, Aurangabad, India **Physicochemical properties** [157]**:** MW: 516.8 g/mol Acid/ base/ neutral: neutral pK_a: 10.3 Log $D_{7.4}$: 10.9 [153] Hydrogen acceptor count: 2 Hydrogen donor count: 2

5.1.3. Polymer substances

Table 51: Molecular structures, information about the manufacturer, and relevant physicochemical properties of polymers used for production of coenzyme Q10 – polymer dispersions.

Basic butylated methacrylate copolymer (Eudragit® EPO) 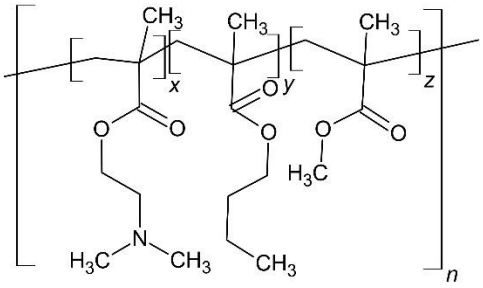	**Manufacturer:** Evonik, Darmstadt, Germany **Physicochemical properties** [188]**:** MW: 47,000 g/mol Aqueous solubility: Soluble below pH 5.0, permeable above pH 5.0
Hydroxypropyl cellulose (HPC) Grade: SSL 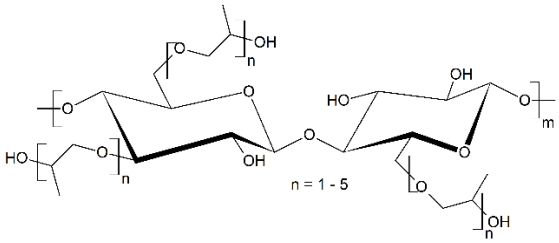	**Manufacturer:** Nippon Soda Co., Tokyo, Japan **Physicochemical properties** [189]**:** MW (HPC-SSL): 40,000 g/mol Aqueous solubility: pH-independent soluble
Hydroxypropyl methylcellulose acetate succinate (HPMC AS) 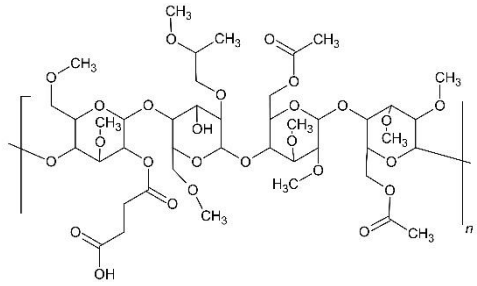	**Manufacturer:** Shin-Etsu Chemical, Tokyo, Japan **Physicochemical properties** [190]**:** MW: 17,000 g/mol Aqueous solubility: Soluble above pH 5.5
Methacrylic acid-ethyl acrylate copolymer (1:1) (Eudragit® L 100-55) 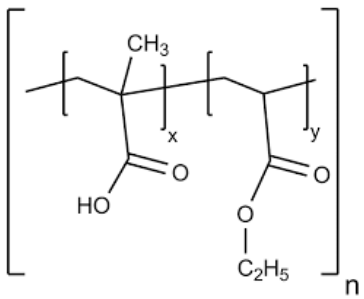	**Manufacturer:** Evonik, Darmstadt, Germany **Physicochemical properties** [188]**:** MW: 320,000 g/mol [120] Aqueous solubility: Soluble above pH 5.5

Polyoxyethlene – polyoxypropylen copolymer (2:1) Kolliphor® P407 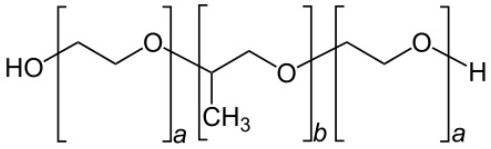	**Manufacturer:** BASF SE, Ludwigshafen, Germany **Physicochemical properties** [191]**:** MW: 10,000 – 14,600 g/mol Aqueous solubility: pH-independent soluble
Polyvinyl caprolactam – polyvinyl acetate – polyoxyethylene copolymer (Soluplus®) 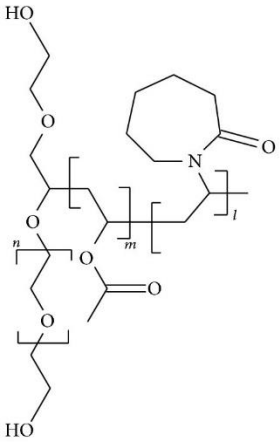	**Manufacturer:** BASF SE, Ludwigshafen, Germany **Physicochemical properties** [192]**:** MW: 90,000 – 140,000 g/mol Aqueous solubility: pH-independent soluble
Polyvinylpyrrolidone (Kollidon® K12 PF) 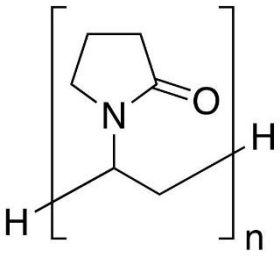	**Manufacturer:** BASF SE, Ludwigshafen, Germany **Physicochemical properties** [193]**:** MW: 2,000 – 3,000 g/mol Aqueous solubility: pH-independent soluble
Vinylpyrrolidone-vinyl acetate copolymer (Kollidon® VA 64) 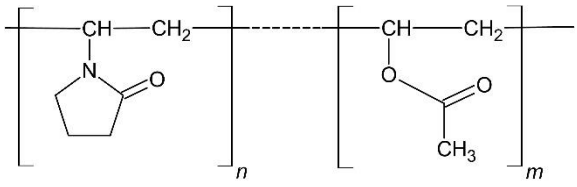	**Manufacturer:** BASF SE, Ludwigshafen, Germany **Physicochemical properties** [194]**:** MW: 45,000 – 70,000 g/mol Aqueous solubility: pH-independent soluble

5.1.4. Additional chemical substances

Table 52: Additional chemical substances used for performing various experiments of this thesis.

Excipient/ Chemical	Supplier or manufacturer
Acetone, HPLC grade	VWR International S.A.S., Fontenay-sous-Bois, France
Acetonitrile (ACN), HPLC grade	VWR Chemicals, Darmstadt, Germany
Astaxanthin (ASX) (≥ 98.0%), HPLC-Standard	Sigma-Aldrich, Buchs, Switzerland
Bisdemethoxycurcumin (BDMC) (≥ 99.5%), HPLC-Standard	Cayman Chemical, Ann Arbor, USA
Coenzyme Q10 (CoQ10) (≥ 99.9%), HPLC-Standard	Acros Organics, Geel, Belgium
Curcumin (CUR) (≥ 99.5%), HPLC-Standard	Cayman Chemical, Ann Arbor, USA
1-Decanol	VWR Chemicals, Darmstadt, Germany
Demethoxycurcumin (DMC) (≥ 99.5%), HPLC-Standard	Cayman Chemical, Ann Arbor, USA
Dichloromethane (DCM), HPLC grade	VWR International S.A.S., Fontenay-sous-Bois, France
Dimethyl sulfoxide (DMSO)	Fisher Scientific, Geel, Belgium
Di-sodium hydrogen phosphate dihydrate	Th. Geyer, Renningen, Germany
Ethanol absolute (≥ 99.8%), HPLC grade	VWR International S.A.S., Fontenay-sous-Bois, France
Formic acid	VWR International S.A.S., Fontenay-sous-Bois, France
Glacial acetic acid	VWR International S.A.S., Fontenay-sous-Bois, France
Hydrochloric acid (HCl) 0.1 N	VWR Chemicals, Darmstadt, Germany
Lecithin	VWR Chemicals, Darmstadt, Germany
Methanol (MeOH), HPLC grade	VWR International S.A.S., Fontenay-sous-Bois, France
Quercetin (≥ 97.6%), HPLC-Standard	Sigma-Aldrich, Buchs, Switzerland
Silsol® 6035	Grace, Worms, Germany
Sodium dihydrogen phosphate dihydrate	Th. Geyer, Renningen, Germany
Sodium hydroxide	VWR Chemicals, Darmstadt, Germany

Excipient/ Chemical	Supplier or manufacturer
Sodium taurocholate	VWR Chemicals, Darmstadt, Germany
Trans-Resveratrol (≥ 99.5%), HPLC-Standard	Sigma-Aldrich, Buchs, Switzerland
Tri-potassium citrate	Carl Roth, Karlsruhe, Germany
Tri-potassium phosphate	VWR Chemicals, Darmstadt, Germany
Water, HPLC grade	Fisher Chemicals, Loughborough, UK
Syloid® XDP 3050	Grace, Worms, Germany

5.2. Methods

5.2.1. High performance liquid chromatography (HPLC) measurements

For concentration determination of all investigated compounds validated HPLC methods with minor adjustments (as outlined in **Table 53**) were used [23,28,195–197]. The measurements were conducted using a Shimadzu HPLC system (LC-2010A HT, Shimadzu Corporation, Kyoto, Japan) equipped with either a LiChrospher® RP-18 column (125 mm x 4.6 mm, 5 µm particle size, Merck Millipore, Billerica, MA, USA) for PB and LU quantification or a Nucleodur® C18ec column (250 mm x 4.6 mm, 3 µm particle size, Macherey-Nagel, Düren, Germany) (used for quantification of the other compounds). The column was maintained at a temperature of 40.0 °C. Samples of the dissolution medium (aqueous/organic) were collected after each dissolution run, filtered through a 0.22 µm poly-(tetrafluoroethylene) (PTFE) syringe filter, and 10 µL were injected directly into the HPLC system. For samples containing ASX, the injection volume had to be reduced to 1 µL due to the high absorption coefficient. Fresh standard curves were prepared for each run to serve as a reference for quantification and correct peak identification. LabSolutions software (Shimadzu Corporation, Kyoto, Japan) was employed to monitor and integrate all peaks.

For the determination of active ingredient content of the formulations used for validation of the biorelevant biphasic dissolution system (BiPHa+) as well as CoQ10 – polymer dispersions and drug loaded mesoporous silica the same HPLC system and methods were used. Samples of 5 to 100 mg (depending on the expected active ingredient content) were accurately weighed into 50.0 mL amber-colored volumetric flasks and diluted with methanol or DCM (depending on which solvent was the best). After ultrasonication for 10 min, 1000 µL samples were collected, filtered through a 0.22 µm PTFE syringe filter, and directly injected into the HPLC system.

Table 53: Composition of the mobile phases (*V/V)*, solvent flow and detection wavelength (DW) used during HPLC quantification.

Active ingredient	Mobile phase A	Mobile phase B	Flow [mL/min]	Elution	DW [nm]
Curcuminoids	ACN with 0.1% formic acid (60%)	water with 0.1% formic acid (40%)	1.00	isocratic	425
Resveratrol	ACN (78%)	water with 0.05% acetic acid (22%)	1.00	isocratic	306
Coenzyme Q10	ethanol (65%)	methanol (35%)	1.00	isocratic	275
Quercetin	ACN (70%)	Water with 1% formic acid (30%)	0.60	isocratic	370
Astaxanthin	acetone (83-98%)	water (17-2%)	0.80	gradient (60 min)	474
Probucol	ACN (90%)	water (10%)	1.00	isocratic	254
Lumefantrine	ACN (90%)	water (10%)	1.00	isocratic	350

5.2.2. Determination of equilibrium solubility in biorelevant medium

The shake flask method was used to determine the equilibrium solubility of all unformulated compounds/extracts (CUR, DMC, BDMC, resveratrol, CoQ10, quercetin, ASX, PB, and LU) across various media, including 0.1 N HCl, phosphate buffer pH 6.8, Bi-FaSSIF-V2 (pH 6.8), and 1-decanol. In addition, drug load-dependent solubility in biorelevant medium (Bi-FaSSIF-V2) of CoQ10, ASX, PB, and LU loaded mesoporous silica (XDP 3050 and Silsol 6035) formulations with drug loads of 1%, 5%, 10% (*w/w*), and (if achievable; detailed in section 5.2.10) 15%, 20%, 30%, and 50% (*w/w*) was studied.

To create biphasic dissolution-adapted fasted-state simulated intestinal fluid-V2 (Bi-FaSSIF-V2), sodium taurocholate and lecithin was added to 0.1 M phosphate buffer pH 6.8. An excess of the mentioned compounds/formulations (at least 20 times) was incubated in 20.0 mL medium (aqueous/organic). The experiments were conducted using a GFL 1083 shaking incubator (Gesellschaft für Labortechnik GmbH, Burgwedel, Germany) at 37.0°C ± 0.5°C. After 48 h, 1000 µL samples were collected, filtered through a 0.22 µm PTFE syringe filter, and directly injected into the HPLC system (as detailed in section 5.2.1: HPLC method).

5.2.3. Determination of apparent solubility/ kinetic concentration in biorelevant medium

For determination of the apparent solubility (i.e., kinetic concentration) of CoQ10, ASX, PB, and LU in a biorelevant medium (Bi-FaSSIF-V2 with pH 6.8), supersaturation assays were conducted. The same dissolution apparatus used for biorelevant biphasic dissolution (BiPHa+) measurements was occupied (to ensure consistent hydrodynamics), but the organic phase was omitted (**Figure 55**). Acetone stock solutions containing 40 mg/mL of CoQ10, ASX, PB, and LU were prepared, and the assays were initiated by adding 250 µL to 50.0 mL biorelevant medium to achieve a potential concentration of 0.2 mg/mL.

Next, the apparent solubility was compared to the monophasic non-sink dissolution performance of highly loaded mesoporous silica formulations. Loaded XDP 3050 or Silsol® 6035 formulations equivalent to 10 mg of active ingredient were transferred to hard gelatin capsules (size 4) and introduced into the dissolution medium (Bi-FaSSIF-V2) by a metal sinker. Concentrations were measured for 270 min (equivalent to biphasic dissolution) using an 8454 UV/VIS DAD spectrophotometer (Agilent, Waldbronn, Germany). After 270 min concentrations present in the biorelevant medium were additionally determined by HPLC.

5.2.4. Investigation of 24 h solubility profiles of loaded mesoporous silica formulations

In order to investigate the behavior of the loaded silicate formulations in biorelevant medium (50.0 mL Bi-FaSSIF-V2 with pH 6.8) over a longer period of time, 24h release studies were carried out. For this purpose, BiPHa+ vessels were used to ensure consistent hydrodynamics, but the organic phase was omitted (**Figure 55**). A quantity of formulation equivalent to 10 mg active ingredient was encapsulated in hard gelatin capsules (size 4) and introduced into the dissolution medium with a metal sinker. The concentrations were analyzed with an 8454 UV/VIS DAD spectrophotometer (Agilent, Waldbronn, Germany). Following 24 h, HPLC was utilized to ascertain the concentrations within the biorelevant medium.

5.2.5. Log $D_{7.4}$ determination using HPLC

To determine the lipophilicity of CUR, DMC, BDMC, *trans*-resveratrol and quercetin, their octanol-water partitioning coefficients at pH 7.4 (log $D_{7.4}$) were measured using a method described in the literature [198]. The lipophilicity assessment of other compounds and extracts was deemed unattainable through the present method, owing to their excessive hydrophobicity (>>6). Consequently, literature values were utilized as a substitute.

Generally, the same HPLC system as described in section 5.2.1 was used, with the difference, that a Lichrospher® RP-18 column (50 mm x 4 mm, 5 µm particle size, Agilent Technologies, UK) maintained at 25.0 °C was used for all measurements. The mobile phase consisted of methanol (MeOH) and 20 µM trometamol (TRIS) buffer adjusted to pH 7.4, with a flow rate set to 0.8 mL/min. A linear gradient starting with 5% MeOH and ending with 95% within 5 min, which was then maintained for 1.5 min was applied, followed by an equilibrium time of 5.5 min between the runs. Detection was performed at a wavelength of 270.0 nm. After performing a calibration with 6 different drugs (log $D_{7.4}$ range: -1.38 to 6.50) with known log $D_{7.4}$ values, retention times of the analytes were used to calculate their log $D_{7.4}$ values.

5.2.6. Biorelevant biphasic dissolution

The BiPHa+ fully automated, small scale, biorelevant biphasic dissolution apparatus developed by Denninger et al. was used to conduct biphasic dissolution studies on neat compounds and all (developed) formulations [52]. The apparatus comprised of four cylindrical vessels (each containing 50.0 mL aqueous medium), with three dedicated to samples and one for the blank, placed in a water bath at 37 °C ± 0.5 °C (as depicted in **Figure 55**). Immediately before the start of dissolution measurements, an amount equivalent to 10 mg total active ingredients per formulation (due to limited 1-decanol solubility (see **Table 10**) the amount was reduced to 5 mg for measurements of Curcuma formulations) was accurately weighed into hard gelatin capsules (size 4). The capsules were then placed into metal sinkers (mesh size 1mm) above the magnetic stirring bars to ensure adequate hydrodynamics at a rotation speed of 160 rpm. To prevent fine particulate and hydrophobic neat CoQ10, quercetin, PB, and LU from directly floating into the 1-decanol layer, dicalcium-phosphate tablets with 20% drug load (*w/w*)

(equivalent to 10 mg API) were produced, grinded down using mortar and pestle and then introduced into the dissolution medium like the other compounds/formulations.

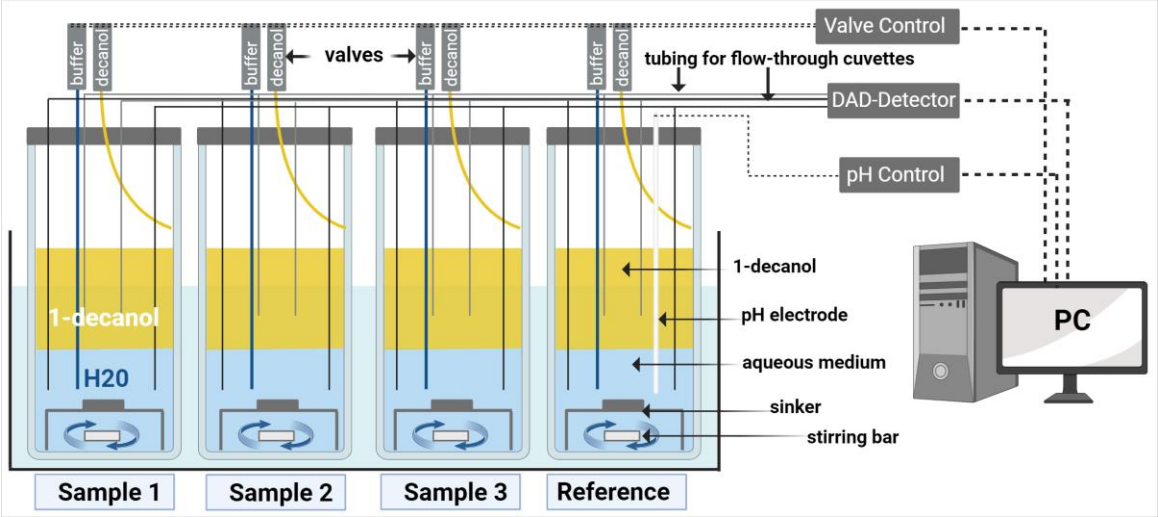

Figure 55: Scheme of the biorelevant biphasic dissolution apparatus BiPHa+, adapted from Denninger et al., 2020 [52]. Created with BioRender.com.

BiPHa+ dissolution studies were divided into three pH stages to replicate the gastrointestinal passage in a fasted state (**Figure 56**). The dissolution process began at pH 1.0 for 30 min, after which the pH was adjusted to 5.5 by adding citrate phosphate buffer concentrate (**Table 54**). Prior to the pH adjustment, an aqueous concentrate of lecithin and sodium taurocholate in deionized water was added to create the Bi-FaSSIF-V2 biorelevant medium. This medium was then covered with 50.0 mL of 1-decanol to serve as an artificial absorption compartment. After 90 min the pH was stepwise adjusted to 6.8 and remained stable until the end of the dissolution experiment (which lasted 270 min). The duration of BiPHa+ measurements is thereby mirroring the reported average gastric and small intestine transition time under fasted conditions in humans [199].

Table 54: Composition of buffer concentrate used for pH adjustments during BiPHa+ measurements and necessary volumes added to 50.0 mL 0.1N HCl to achieve the mentioned pH value (5.5 / 6.8). Adapted from Denninger et al., 2020 [52].

Composition		dV $_{pH\ 5.5}$ [mL]	dV $_{pH\ 6.8}$ [mL]
K-Citrate	0.525 M		
K-Phosphate	0.225 M	2.12	2.54
NaOH	1.7 M		

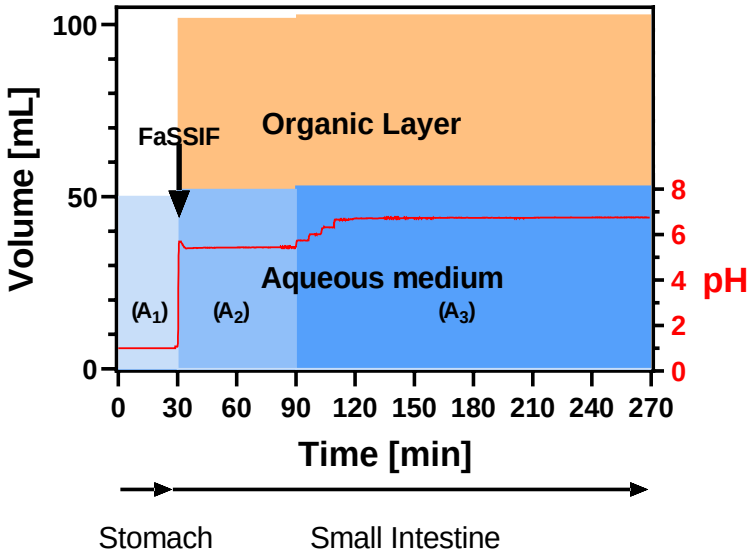

Figure 56: Media setup of the biphasic dissolution model: (**A1**) = 0.1 N HCl (pH 1.0); (**A2**) = Bi-FaSSIF-V2 (pH 5.5); (**A3**) = Bi-FaSSIF-V2 (pH 6.8), Adapted from Brenner et al., 2024 [66].

Throughout the experiment, the pH was monitored by a pH-electrode (Semi-micro VWR Collection, VWR Chemicals, Darmstadt, Germany), while a fully automated liquid dispensing system handled the pH adjustments and the 1-decanol covering.

An Agilent 8454 UV/VIS DAD spectrophotometer (Agilent, Waldbronn, Germany) with 1.0 mm flow-through cuvettes was used to measure the concentration levels of active ingredient in both media (aqueous/organic). For reduction of scattering phenomena caused by precipitate in the aqueous medium, 1 µm full-flow filters were used. Additionally, LabView® software programmed by Denninger et al., was utilized to eliminate remaining scattering during UV measurements. In addition, the endpoint concentrations in both media were determined by HPLC (see section 5.2.1).

5.2.7. Monophasic non-sink dissolution with pH shift and biorelevant medium

The monophasic non-sink dissolution experiments with pH shift and biorelevant medium were conducted under similar conditions as the biphasic experiments, utilizing the same dissolution apparatus (**Figure 55**) and media (**Figure 56**), with the exception of the absence of 1-decanol in the dissolution vessels. At the end of dissolution measurements concentrations in the dissolution medium were determined by HPLC (see section 5.2.1).

5.2.8. Monophasic (non-sink) dissolution

Conventional monophasic (non-sink) dissolution experiments (USP II apparatus as depicted in **Figure 57**) were conducted for 180 min using an AT7 dissolution apparatus made by Sotax AG (Allschwil, Switzerland). The paddle speed was set at 100 rpm, and the dissolution medium used was 900 mL of 0.1 M phosphate buffer (pH 6.8) heated to 37.0°C ± 0.5°C. To introduce the samples (equivalent to 5 or 10 mg of active ingredient), they were first weighed and placed into size 4 hard gelatin capsules. A metal sinker was then used to introduce the capsules into the dissolution medium. Concentration measurements were taken using an Agilent 8454 UV/VIS DAD spectrophotometer (Agilent, Waldbronn, Germany), which was equipped with 1 mm flow-through cuvettes. Subsequent to the completion of the measurement process, the concentrations present in the dissolution medium were determined through employment of HPLC (see section 5.2.1).

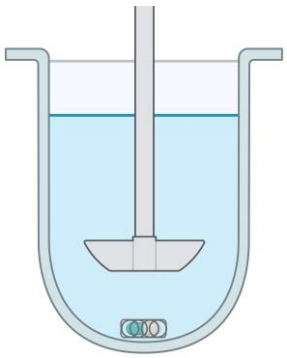

Figure 57: Scheme of USP II paddle apparatus with sample and sinker. Created with BioRender.com.

5.2.9. Preparation of coenzyme Q10 – polymer dispersions

First, the eight polymers listed in **Table 51** were used for generating CoQ10 dispersions (20% drug load; *w/w*) through solvent evaporation. This method entailed dissolving the polymer and active ingredient in a suitable organic solvent, like acetone or DCM (depending on which solvent dissolved the polymer best). The solution was then transferred to a PTFE flask and concentrated on a rotary evaporator under reduced pressure. Following the attainment of a seemingly solvent-free dispersion, post-drying was performed for a period of 2 h under vacuum to ensure any residual solvent was eliminated. Following the evaluation on how different polymers impact the biorelevant biphasic dissolution (BiPHa+) performance, the optimal drug load needed to be determined.

Kollidon® VA64 was chosen as a model polymer with good improvement of CoQ10 partitioning rate into the organic layer. Dispersions with 10%, 20%, 30%, and 40% drug load (*w/w*) were tested, ultimately discovering that a 20% drug load achieved the best balance between high active ingredient content and optimal BiPHa+ performance.

Subsequently, it was explored whether combining the most effective polymers could improve dissolution performance further than a single polymer. To test this, CoQ10 dispersions (20% drug load) were created with a blend of polymers, including Eudragit® EPO, Kollidon® VA64, and HPC-SSL, in a 1:1 (*w/w*) ratio using the solvent evaporation technique. The success of polymer combination was then evaluated using the BiPHa+.

5.2.10. Preparation of loaded mesoporous silica formulations

The process of incipient wetness impregnation was utilized to load mesoporous silica particles (**Figure 58**). Different drug loads of 1, 5, 10, 15%, and (silica and model compound dependent) 20%, 30%, and 50% (*w/w*) were produced by dissolving varying concentrations of CoQ10, ASX, PB, and LU in DCM. Due to the reduced ASX content (10.1%) of the extract, drug loads of 0.1, 1, 2.5% and 5% (*w/w*) were produced. The maximum achievable drug load was determined by the solubility of the drugs in DCM, as indicated in **Table 55**. To load the silica particles, 1.50 mL/g of DCM was used for XDP 3050, while Silsol® 6035 required 0.75 mL/g due to its reduced pore volume [164,165]. The silica powder was then added to a beaker and DCM stock solutions (SL) were gradually introduced while stirring continuously. Stirring continued until all the liquid was absorbed into the pores, resulting in a seemingly dry powder. The formulations were then protected from light and the solvent was evaporated under atmospheric conditions for 24 hours in a drying oven. Finally, the drug load was determined using HPLC (refer to section 5.2.1) and the absence of residual solvent was confirmed by means of HS-GC-FID as described in section 5.2.11.

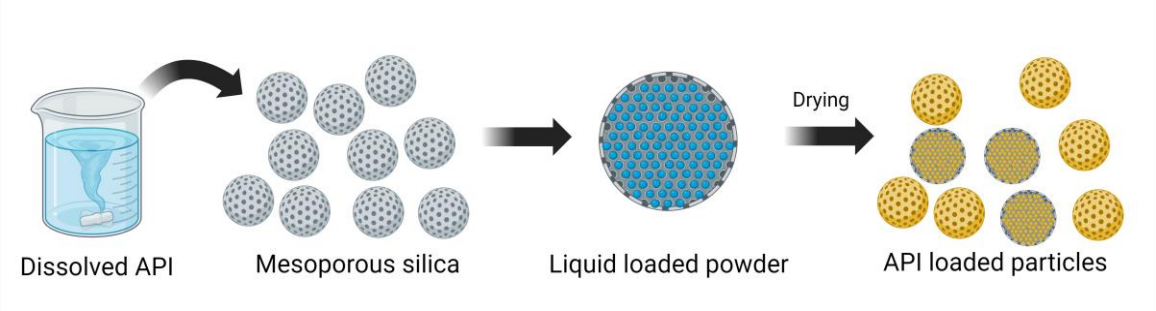

Figure 58: Loading of mesoporous silica particles by means of incipient wetness impregnation. Created with BioRender.com.

Table 55: Preparation of mesoporous silica formulations, including the maximum achievable compound concentration in the dichloromethane (DCM) stock solution (applied solvent volume for drug loading: 1.50 mL/g (XDP 3050) and 0.75 mL/g (Silsol 6035)) and the total drug load (*w/w*) of the obtained formulation (determined by HPLC), Obtained from Brenner et al., 2024 [63].

Formulation	Concentration: DCM stock solution [mg/mL]	Total Drug Load [%]
CoQ10: Silsol 6035	670	33.1
CoQ10: XDP 3050	670	49.8
ASX: Silsol 6035 [a]	67	3.3
ASX: XDP 3050 [a]	67	5.9
PB: Silsol 6035	290	17.8
PB: XDP 3050	290	30.3
LU: Silsol 6035	290	17.9
LU: XDP 3050	290	30.1

[a]: ASX content of *Haematococcus pluvialis* extract used for silica loading was 10.1%, therefore the maximum achievable drug load was reduced

5.2.11. Gas chromatographic (GC) detection of residual solvent

During preparation of loaded mesoporous silica formulations via incipient wetness impregnation, dichloromethane (DCM) was used as organic solvent, which allowed for high loading rates. DCM is toxic and has a limit value of 600 ppm in pharmaceutical formulations [200]. Therefore, the DCM residue was analyzed using a Focus GC connected to a TriPlus SH Autosampler unit by Thermo Fischer Scientific (Waltham, MA, USA). A FS_CS_624 capillary column (30 m x 0.32 mm, 1.8 µm film thickness, 6% cyanopropylpolysiloxane, CS-Chromatographie Service GmbH, Langerwehe, Germany) was used. All measurements were performed in headspace (HS) mode, with a flame ionization detector (FID) set to 240 °C for detection. To prepare the samples, approximately 50 mg was weighed and mixed with 1.0 mL DMSO. The mixture was incubated at 50 °C for 10 min, then 1.0 mL of the gas phase was injected into the GC. The column oven was heated from 50 to 140 °C at a rate of 10 °C/min, followed by a 4 min plateau at 140 °C. Nitrogen (2.0 mL/min) was used as the carrier gas, and a split flow of 1/5 was applied during injection.

5.2.12. Thin layer chromatography (TLC) measurements

In order to examine how CoQ10, ASX, PB, and LU interacted with the amorphous silica gel surface of mesoporous silica particles, thin layer chromatographic (TLC) experiments were conducted. Silica gel TLC plates with a fluorescence indicator (specifically, silica gel 60 F254 measuring 10 cm x 10 cm) manufactured by Merck (Darmstadt, Germany) were utilized for the analysis. To prepare, the compounds were dissolved in DCM (at a concentration of 1 mg/mL), and then 2 µL of each solution was carefully applied to the TLC plate, allowed to dry, and then eluted with petroleum ether - ethyl acetate - acetic acid 70:20:10 (*v/v/v*). The use of organic solvents was necessary to achieve the needed eluting power. Once the eluent was evaporated, the separated spots were marked and visualized under UV illumination at 254 nm, and the retarding-front (Rf) values were calculated.

5.2.13. *In silico* calculation of model compound and silica surface interaction

In addition to the TLC experiments, the interactions between the amorphous silica surface of Syloid XDP 3050/ Silsol 6035 and the model compounds (CoQ10, ASX, PB and LU) were accessed by simplified drug-silica bulk calculations based on the software COSMOquick (BIOVIA COSMOquick, Version 2020, Dassault systems, France). The excess enthalpy (H_{ex}) of drug and silica was estimated at 37°C as a measure of molecular drug-excipient interactions similar to Price et al [172]. H_{ex} is also referred to as the enthalpy of mixing ΔH_{mix} with the advantage that the "self-cohesion" of the pure components is taken into account, compared to other interaction energy values, for example from molecular docking:

$$\Delta H_{mix} = \sum_k x_k H^k_{mix} - \sum_k x_k H^k_{pure} \qquad \text{(Equation 3)}$$

In this general equation x_k holds for the molar fraction of a component k, H^k_{mix} is the enthalpy of compound k in the mixture, whereas H^k_{pure} represents the enthalpy of the pure component k.

The use of ΔH_{mix} as interaction parameter is a simplification as it does not take the situation on the surface with the water phase into account. However, this binary drug-excipient interaction can exhibit rank-order performance correlations [172]. For a more detailed description of the calculations performed, the reader is referred to [201].

5.2.14. Differential scanning calorimetry (DSC)

Neat compounds and processed formulations (CoQ10 – polymer dispersions and loaded mesoporous silica) were analyzed with differential scanning calorimetry. To conduct the measurements, a Mettler-Toledo DSC 2 (Gießen, Germany) was used, along with a nitrogen cooling system and nitrogen as purge gas (30 mL/min). Aluminum pans were weighed with approximately 10 mg of samples and then sealed with a pierced lid. The samples were heated using a conventional method, with a constant temperature rise of 10 °C/min, from 25 to 100 °C (CoQ10 and ASX) or to 170 °C (PB and LU) for all measurements. Due to high glass transition temperatures of some of the polymers used for the production of CoQ10 - polymer dispersions, it was necessary to apply a heating cycle ranging from 25 to 140 °C for these formulations.

5.2.15. X-Ray powder diffraction (XRPD)

Analysis of the molecular structure of neat CoQ10, ASX, PB, and LU and the formulations made thereof (CoQ10 – polymer dispersions and loaded mesoporous silica) was carried out via reflection mode X-ray powder diffraction using an X´Pert MRD Pro instrument (PANalytical, Almelo, The Netherlands) at 45 kV and 40 mA. The instrument utilized nickel filtered $CuK_{\alpha 1}$ radiation and an X´Celerator detector. The scanning range was set from 5 to 45° 2θ, with a step size of 0.017° 2θ.

Summary and outlook

Natural substances have shown great promise in treating a wide variety of different diseases. However, many compounds exhibit low solubility in water which can limit their therapeutic potential and hinder intestinal absorption, resulting in reduced bioavailability. To increase their therapeutic value, it is necessary to develop formulations with enhanced bioavailability in humans. Improving water solubility can be a suitable approach to increase bioavailability. However, enhanced solubility does not always translate directly into greater intestinal absorption. Thus, *in vivo* relevant *in vitro* methods are needed to identify promising formulation approaches prior to clinical testing. Among these methods, biorelevant biphasic dissolution systems have shown great promise.

Since many natural substances are used as extracts rather than in their pure form, HPLC based separation coupled to UV/VIS detection was used to quantify the main active ingredients in all investigated extracts and their bioavailability-enhanced formulations. The HPLC-based quantification was then used to evaluate the ability of online UV/VIS DAD detection, which is commonly applied during dissolution testing, to provide accurate information about the amount of active ingredient released/dissolved. Although simple UV/VIS DAD detection does not allow for separation into individual compounds, structurally related ingredients can be quantified as sum of individual components. Fortunately, the sum parameters closely matched the concentrations determined by HPLC, making online UV/VIS DAD quantification feasible for monitoring of extract dissolution. In addition, HPLC samples were taken at the end of each dissolution measurement to separately quantify the dissolved active ingredients.

After confirming the analytics, model extract that contained curcumin, *trans*-resveratrol, coenzyme Q10, quercetin, and astaxanthin, as well as their bioavailability-enhanced formulations were subjected to dissolution studies. The results were then compared to pharmacokinetic data obtained from strictly controlled human trials. The study evaluated three different dissolution systems: the biorelevant biphasic system BiPHa+, a monophasic non-sink dissolution method with pH shift and a biorelevant medium, and a conventional monophasic approach (apparatus II, USP, and PhEur).

It was found that BiPHa+ had clear advantages over the other two methods. Biphasic dissolution was able to characterize all formulations according to their expected

bioavailability in humans. The combination of aqueous non-sink dissolution with an overlaying organic artificial absorption sink proved to be particularly advantageous in terms of powerful prediction. Despite the different substance classes and formulations studied, with applying a single set of parameters, *in vivo* relevant partitioning profiles were obtained. The advantage of BiPHa+ was particularly evident in the assessment of the effect of self-emulsifying micellar formulations, as conventional methods failed in biorelevant characterization of CoQ10 and ASX formulations. Their effect on the bioavailability was considerably overestimated. Therefore, BiPHa+ was established as an *in vivo* relevant *in vitro* screening tool for the preclinical formulation development of multi-component extracts. This is particularly important because current commercial formulations of CoQ10 and ASX showed only minor improvements in bioavailability of the active ingredients mentioned, requiring further optimization.

Compared to existing commercial formulations, by incorporating CoQ10 into a polymer matrix within binary solid dispersions, a notable improvement in the partitioning rate into the organic absorption sink was observed. Out of the 8 commonly used pharmaceutical polymers tested, VA64, HPC-SSL, and EPO were found to be most suitable for this purpose. Notably, the combination of VA64 with EPO (50/50) into ternary solid dispersions yielded a synergistic effect, leading to a further increase in the partitioning rate. At a drug load of 20% (*w/w*), a 6 to 7-fold increase was achieved compared to formulations currently available on the food supplement market. However, neither individual polymers nor combinations of polymers were able to stabilize CoQ10 in the amorphous state, resulting in semi-crystalline systems.

As such, alternative formulation approaches were explored, with loading active ingredients on mesoporous carrier particles by incipient wetness impregnation identified as a promising strategy.

In the initial investigation, it was found that increasing the drug load had a linear effect on solubility in biorelevant medium of the highly lipophilic model compounds CoQ10, ASX, PB and LU. The highest load quantity had the greatest impact, and depending on the formulation, solubility could be improved by a factor of 35 - 180. Performance differences between the model compounds could be explained by *in silico* calculations of mixing enthalpy for drug and silica as well as an experimental chromatographic method to estimate molecular interactions between drug and carrier. By using DCM as an organic

solvent, drug loads of up to 50% could be achieved without any crystallinity detected in DSC and XRPD measurements. All active ingredients were effectively stabilized in a non-crystalline form.

In addition, the non-crystalline form in combination with the solubility-enhancing effect of the mesoporous carrier particles translated into improved monophasic and biphasic dissolution performance. During monophasic dissolution studies, even after 24 h, no precipitation of the lipophilic model compounds was observed, despite exceeding their equilibrium solubility. The improved solubility also resulted in an increased partitioning rate into the organic absorption sink during biphasic dissolution measurements, leading to a decisively higher end concentration of CoQ10 and ASX compared to market formulations. While PB and LU formulations achieved a lower effect, an increase was still achieved compared to the crystalline active ingredients.

However, the dissolution performance was not only influenced by the drug load of the investigated formulation but also depended on the amount of formulation per volume of dissolution medium. The greater the excess of formulation, the more active ingredient dissolved. Nevertheless, the underlying mechanisms of these phenomena are not yet fully understood, necessitating further research to unveil the detailed mechanistic relationships between the interactions of the mesoporous silica particles and various structurally different APIs as well as performance evaluation *in vivo*.

In addition, drug - drug interactions are particularly relevant for highly loaded formulations as an exceedance of the theoretical monolayer surface coverage has to be expected. Thus, the usefulness of *in silico* mixing enthalpy calculations and the chromatographic method would have to be demonstrated with further compounds to draw firm conclusions.

Furthermore, lipophilic substances such as CoQ10 and ASX are known to be absorbed through the lymphatic pathway in the same way as dietary lipids. Using this pathway, bioavailability of active ingredients is strongly influenced by the fat content of the ingested food. Currently, BiPHa+ can only simulate absorption in the fasted state, but it would be noteworthy to study the effect of simultaneously ingested food already during *in vitro* dissolution measurements, particularly for lipophilic active ingredients.

References

1. Newman, D.J.; Cragg, G.M. Natural Products as Sources of New Drugs from 1981 to 2014. *J. Nat. Prod.* **2016**, *79*, 629–661, doi:10.1021/acs.jnatprod.5b01055.
2. Atanasov, A.G.; Zotchev, S.B.; Dirsch, V.M.; Supuran, C.T. Natural Products in Drug Discovery: Advances and Opportunities. *Nat. Rev. Drug Discov.* **2021**, *20*, 200–216, doi:10.1038/s41573-020-00114-z.
3. Miroddi, M.; Mannucci, C.; Mancari, F.; Calapai, G.; Navarra, M. Research and Development for Botanical Products in Medicinals and Food Supplements Market. *Evid. Based Complement. Alternat. Med.* **2013**, *2013*, e649720, doi:10.1155/2013/649720.
4. DerMarderosian, A.; Beutler, J.A. The Review of Natural Products: The Most Complete Source of Natural Product Information. *Rev. Nat. Prod. Most Complete Source Nat. Prod. Inf.* **2002**.
5. Dysin, A.P.; Egorov, A.R.; Godzishevskaya, A.A.; Kirichuk, A.A.; Tskhovrebov, A.G.; Kritchenkov, A.S. Biologically Active Supplements Affecting Producer Microorganisms in Food Biotechnology: A Review. *Molecules* **2023**, *28*, 1413, doi:10.3390/molecules28031413.
6. Dufossé, L.; Fouillaud, M.; Caro, Y. Fungi and Fungal Metabolites for the Improvement of Human and Animal Nutrition and Health. *J. Fungi* **2021**, *7*, 274, doi:10.3390/jof7040274.
7. Ścieszka, S.; Klewicka, E. Algae in Food: A General Review. *Crit. Rev. Food Sci. Nutr.* **2019**, *59*, 3538–3547, doi:10.1080/10408398.2018.1496319.
8. Rampogu, S.; Balasubramaniyam, T.; Lee, J.-H. Phytotherapeutic Applications of Alkaloids in Treating Breast Cancer. *Biomed. Pharmacother.* **2022**, *155*, 113760, doi:10.1016/j.biopha.2022.113760.
9. Debnath, B.; Singh, W.S.; Das, M.; Goswami, S.; Singh, M.K.; Maiti, D.; Manna, K. Role of Plant Alkaloids on Human Health: A Review of Biological Activities. *Mater. Today Chem.* **2018**, *9*, 56–72, doi:10.1016/j.mtchem.2018.05.001.
10. Michelle Kilcoyne; Lokesh Joshi Carbohydrates in Therapeutics. *Cardiovasc. Hematol. Agents Med. Chem. Former.* **2007**, *5*, 186–197, doi:10.2174/187152507781058663.
11. Sokoła-Wysoczańska, E.; Wysoczański, T.; Wagner, J.; Czyż, K.; Bodkowski, R.; Lochyński, S.; Patkowska-Sokoła, B. Polyunsaturated Fatty Acids and Their Potential Therapeutic Role in Cardiovascular System Disorders—A Review. *Nutrients* **2018**, *10*, 1561, doi:10.3390/nu10101561.
12. Lei, E.; Vacy, K.; Boon, W.C. Fatty Acids and Their Therapeutic Potential in Neurological Disorders. *Neurochem. Int.* **2016**, *95*, 75–84, doi:10.1016/j.neuint.2016.02.014.
13. Hikisz, P.; Bernasinska-Slomczewska, J. Beneficial Properties of Bromelain. *Nutrients* **2021**, *13*, 4313, doi:10.3390/nu13124313.
14. Wang, L.; Wang, N.; Zhang, W.; Cheng, X.; Yan, Z.; Shao, G.; Wang, X.; Wang, R.; Fu, C. Therapeutic Peptides: Current Applications and Future Directions. *Signal Transduct. Target. Ther.* **2022**, *7*, 1–27, doi:10.1038/s41392-022-00904-4.

15. Tauchen, J.; Huml, L.; Rimpelova, S.; Jurášek, M. Flavonoids and Related Members of the Aromatic Polyketide Group in Human Health and Disease: Do They Really Work? *Molecules* **2020**, *25*, 3846, doi:10.3390/molecules25173846.
16. Tocci, N. Hypericum Perforatum Subsp. Angustifolium: Study of Xanthone Biosynthesis in Planta and in in Vitro Systems. **2013**, doi:10.24355/dbbs.084-201309270914-0.
17. Patel, S.S.; Savjani, J.K. Systematic Review of Plant Steroids as Potential Antiinflammatory Agents: Current Status and Future Perspectives. *J. Phytopharm.* **2015**, *4*, 121–125, doi:10.31254/phyto.2015.4212.
18. Del Prado-Audelo, M.L.; Cortés, H.; Caballero-Florán, I.H.; González-Torres, M.; Escutia-Guadarrama, L.; Bernal-Chávez, S.A.; Giraldo-Gomez, D.M.; Magaña, J.J.; Leyva-Gómez, G. Therapeutic Applications of Terpenes on Inflammatory Diseases. *Front. Pharmacol.* **2021**, *12*.
19. Paduch, R.; Kandefer-Szerszeń, M.; Trytek, M.; Fiedurek, J. Terpenes: Substances Useful in Human Healthcare. *Arch. Immunol. Ther. Exp. (Warsz.)* **2007**, *55*, 315–327, doi:10.1007/s00005-007-0039-1.
20. Fernandes, E.S.; da Silva Figueiredo, I.F.; Monteiro, C.R.A.V.; Monteiro-Neto, V. Antimicrobial and Anti-Infective Activity of Natural Products—Gaining Knowledge from Novel Studies. *Antibiotics* **2023**, *12*, 1051, doi:10.3390/antibiotics12061051.
21. Bundesministerium für Gesundheit Anlage Der Bekanntmachung Zu § 2 Nummer 3 Der Arzneimittel- Und Wirkstoffherstellungsverordnung – AMWHV – Im Bundesanzeiger Vom 27. Mai 2015_Teil II: Grundlegende Anforderungen Für Wirkstoffe Zur Verwendung Als Ausgangsstoffe 2014.
22. Liu, H.; Zhang, H.; IJzerman, A.P.; Guo, D. The Translational Value of Ligand-Receptor Binding Kinetics in Drug Discovery. *Br. J. Pharmacol. n/a*, doi:10.1111/bph.16241.
23. Miao, F.; Lu, D.; Li, Y.; Zeng, M. Characterization of Astaxanthin Esters in Haematococcus Pluvialis by Liquid Chromatography–Atmospheric Pressure Chemical Ionization Mass Spectrometry. *Anal. Biochem.* **2006**, *352*, 176–181, doi:10.1016/j.ab.2006.03.006.
24. Lefebvre, T.; Destandau, E.; Lesellier, E. Selective Extraction of Bioactive Compounds from Plants Using Recent Extraction Techniques: A Review. *J. Chromatogr. A* **2021**, *1635*, 461770, doi:10.1016/j.chroma.2020.461770.
25. Gaedcke, F. Definitionen und Probleme mit den Europäischen Arzneibuch-Monographien für pflanzliche Extrakte und ihre Konsequenzen für die Zulassung. *DPhG* **2006**.
26. *Europäisches Arzneibuch_Allgemeine Monographie: Extrakte Aus Pflanzlichen Drogen*; 11; 2022;
27. Chibarabada, T.P.; Modi, A.T.; Mabhaudhi, T. Nutrient Content and Nutritional Water Productivity of Selected Grain Legumes in Response to Production Environment. *Int. J. Environ. Res. Public. Health* **2017**, *14*, 1300, doi:10.3390/ijerph14111300.
28. Brenner, M.B.; Flory, S.; Wüst, M.; Frank, J.; Wagner, K. Novel Biphasic *In Vitro* Dissolution Method Correctly Predicts the Oral Bioavailability of Curcumin in Humans. *J. Agric. Food Chem.* **2023**, *71*, 15632–15643, doi:10.1021/acs.jafc.3c04990.
29. Muyumba, N.W.; Mutombo, S.C.; Sheridan, H.; Nachtergael, A.; Duez, P. Quality Control of Herbal Drugs and Preparations: The Methods of Analysis, Their Relevance and Applications. *Talanta Open* **2021**, *4*, 100070, doi:10.1016/j.talo.2021.100070.

30. El-Aneed, A.; Cohen, A.; Banoub, J. Mass Spectrometry, Review of the Basics: Electrospray, MALDI, and Commonly Used Mass Analyzers. *Appl. Spectrosc. Rev.* **2009**, *44*, 210–230, doi:10.1080/05704920902717872.
31. Kharade, S.S.; Samal, K.C.; Rout, G.R. High Performance Thin Layer Chromatography Fingerprint Profile of Rhizome Extracts of Five Important Curcuma Species. *Proc. Natl. Acad. Sci. India Sect. B Biol. Sci.* **2017**, *87*, 1335–1341, doi:10.1007/s40011-016-0709-z.
32. Morlock, G.E.; Ristivojevic, P.; Chernetsova, E.S. Combined Multivariate Data Analysis of High-Performance Thin-Layer Chromatography Fingerprints and Direct Analysis in Real Time Mass Spectra for Profiling of Natural Products like Propolis. *J. Chromatogr. A* **2014**, *1328*, 104–112, doi:10.1016/j.chroma.2013.12.053.
33. Oroian, M.; Escriche, I. Antioxidants: Characterization, Natural Sources, Extraction and Analysis. *Food Res. Int.* **2015**, *74*, 10–36, doi:10.1016/j.foodres.2015.04.018.
34. Duval, J.; Pecher, V.; Poujol, M.; Lesellier, E. Research Advances for the Extraction, Analysis and Uses of Anthraquinones: A Review. *Ind. Crops Prod.* **2016**, *94*, 812–833, doi:10.1016/j.indcrop.2016.09.056.
35. Ajila, C.M.; Brar, S.K.; Verma, M.; Tyagi, R.D.; Godbout, S.; Valéro, J.R. Extraction and Analysis of Polyphenols: Recent Trends. *Crit. Rev. Biotechnol.* **2011**, *31*, 227–249, doi:10.3109/07388551.2010.513677.
36. Parada, J.; Aguilera, J. m. Food Microstructure Affects the Bioavailability of Several Nutrients. *J. Food Sci.* **2007**, *72*, R21–R32, doi:10.1111/j.1750-3841.2007.00274.x.
37. Dima, C.; Assadpour, E.; Dima, S.; Jafari, S.M. Bioavailability and Bioaccessibility of Food Bioactive Compounds; Overview and Assessment by in Vitro Methods. *Compr. Rev. Food Sci. Food Saf.* **2020**, *19*, 2862–2884, doi:10.1111/1541-4337.12623.
38. Joye, I.J.; Davidov-Pardo, G.; McClements, D.J. Nanotechnology for Increased Micronutrient Bioavailability. *Trends Food Sci. Technol.* **2014**, *40*, 168–182, doi:10.1016/j.tifs.2014.08.006.
39. Nováková, L.; Vlčková, H. A Review of Current Trends and Advances in Modern Bio-Analytical Methods: Chromatography and Sample Preparation. *Anal. Chim. Acta* **2009**, *656*, 8–35, doi:10.1016/j.aca.2009.10.004.
40. Calvo-Castro, L.A.; Schiborr, C.; David, F.; Ehrt, H.; Voggel, J.; Sus, N.; Behnam, D.; Bosy-Westphal, A.; Frank, J. The Oral Bioavailability of Trans-Resveratrol from a Grapevine-Shoot Extract in Healthy Humans Is Significantly Increased by Micellar Solubilization. *Mol. Nutr. Food Res.* **2018**, *62*, 1701057, doi:10.1002/mnfr.201701057.
41. Flory, S.; Sus, N.; Haas, K.; Jehle, S.; Kienhöfer, E.; Waehler, R.; Adler, G.; Venturelli, S.; Frank, J. Increasing Post-Digestive Solubility of Curcumin Is the Most Successful Strategy to Improve Its Oral Bioavailability: A Randomized Cross-Over Trial in Healthy Adults and In Vitro Bioaccessibility Experiments. *Mol. Nutr. Food Res.* **2021**, *65*, 2100613, doi:10.1002/mnfr.202100613.
42. Food and Drug Administration Guidance for Industry: Bioavailability and Bioequivalence Studies Submitted in NDAs or INDs - General Considerations. **2014**.
43. Schulz, C.; Obermüller-Jevic, U.C.; Hasselwander, O.; Bernhardt, J.; Biesalski, H.K. Comparison of the Relative Bioavailability of Different Coenzyme Q_{10} Formulations with a Novel Solubilizate (Solu^{TM} Q10). *Int. J. Food Sci. Nutr.* **2006**, *57*, 546–555, doi:10.1080/09637480601058320.

44. Briskey, D.; Rao, A. Trans-Resveratrol Oral Bioavailability in Humans Using LipiSperse™ Dispersion Technology. *Pharmaceutics* **2020**, *12*, 1190, doi:10.3390/pharmaceutics12121190.
45. Schiborr, C.; Kocher, A.; Behnam, D.; Jandasek, J.; Toelstede, S.; Frank, J. The Oral Bioavailability of Curcumin from Micronized Powder and Liquid Micelles Is Significantly Increased in Healthy Humans and Differs between Sexes. *Mol. Nutr. Food Res.* **2014**, *58*, 516–527, doi:10.1002/mnfr.201300724.
46. Riva, A.; Ronchi, M.; Petrangolini, G.; Bosisio, S.; Allegrini, P. Improved Oral Absorption of Quercetin from Quercetin Phytosome®, a New Delivery System Based on Food Grade Lecithin. *Eur. J. Drug Metab. Pharmacokinet.* **2018**, *44*, 169–177, doi:10.1007/s13318-018-0517-3.
47. Shoba, G.; Joy, D.; Joseph, T.; Majeed, M.; Rajendran, R.; Srinivas, P. Influence of Piperine on the Pharmacokinetics of Curcumin in Animals and Human Volunteers. *Planta Med.* **1998**, *64*, 353–356, doi:10.1055/s-2006-957450.
48. Yue, G.G.L.; Cheng, S.-W.; Yu, H.; Xu, Z.-S.; Lee, J.K.M.; Hon, P.-M.; Lee, M.Y.H.; Kennelly, E.J.; Deng, G.; Yeung, S.K.; et al. The Role of Turmerones on Curcumin Transportation and P-Glycoprotein Activities in Intestinal Caco-2 Cells. *J. Med. Food* **2012**, *15*, 242–252, doi:10.1089/jmf.2011.1845.
49. Johnson, J.J.; Nihal, M.; Siddiqui, I.A.; Scarlett, C.O.; Bailey, H.H.; Mukhtar, H.; Ahmad, N. Enhancing the Bioavailability of Resveratrol by Combining It with Piperine. *Mol. Nutr. Food Res.* **2011**, *55*, 1169–1176, doi:10.1002/mnfr.201100117.
50. Thakore, S.D.; Sirvi, A.; Joshi, V.C.; Panigrahi, S.S.; Manna, A.; Singh, R.; Sangamwar, A.T.; Bansal, A.K. Biorelevant Dissolution Testing and Physiologically Based Absorption Modeling to Predict in Vivo Performance of Supersaturating Drug Delivery Systems. *Int. J. Pharm.* **2021**, *607*, 120958, doi:10.1016/j.ijpharm.2021.120958.
51. Tan, Y.; Zhou, H.; McClements, D.J. Application of Static in Vitro Digestion Models for Assessing the Bioaccessibility of Hydrophobic Bioactives: A Review. *Trends Food Sci. Technol.* **2022**, *122*, 314–327, doi:10.1016/j.tifs.2022.02.028.
52. Denninger, A.; Westedt, U.; Rosenberg, J.; Wagner, K.G. A Rational Design of a Biphasic DissolutionSetup-Modelling of Biorelevant Kinetics for a Ritonavir Hot-Melt Extruded Amorphous Solid Dispersion. *Pharmaceutics* **2020**, *12*, doi:10.3390/pharmaceutics12030237.
53. Denninger, A.; Westedt, U.; Wagner, K.G. Shared IVIVR for Five Commercial Enabling Formulations Using the BiPHa+ Biphasic Dissolution Assay. *Pharmaceutics* **2021**, *13*, doi:10.3390/pharmaceutics13020285.
54. Zhou, H.; Tan, Y.; McClements, D.J. Applications of the INFOGEST In Vitro Digestion Model to Foods: A Review. *Annu. Rev. Food Sci. Technol.* **2023**, *14*, 135–156, doi:10.1146/annurev-food-060721-012235.
55. Kataoka, M.; Masaoka, Y.; Yamazaki, Y.; Sakane, T.; Sezaki, H.; Yamashita, S. In Vitro System to Evaluate Oral Absorption of Poorly Water-Soluble Drugs: Simultaneous Analysis on Dissolution and Permeation of Drugs. *Pharm. Res.* **2003**, *20*, 1674–1680, doi:10.1023/A:1026107906191.
56. Abbas, M.; Saeed, F.; Anjum, F.M.; Afzaal, M.; Tufail, T.; Bashir, M.S.; Ishtiaq, A.; Hussain, S.; Suleria, H.A.R. Natural Polyphenols: An Overview. *Int. J. Food Prop.* **2017**, *20*, 1689–1699, doi:10.1080/10942912.2016.1220393.

57. Rana, A.; Samtiya, M.; Dhewa, T.; Mishra, V.; Aluko, R.E. Health Benefits of Polyphenols: A Concise Review. *J. Food Biochem.* **2022**, *46*, e14264, doi:10.1111/jfbc.14264.
58. Liu, S.; Liu, J.; He, L.; Liu, L.; Cheng, B.; Zhou, F.; Cao, D.; He, Y. A Comprehensive Review on the Benefits and Problems of Curcumin with Respect to Human Health. *Molecules* **2022**, *27*, 4400, doi:10.3390/molecules27144400.
59. Meng, T.; Xiao, D.; Muhammed, A.; Deng, J.; Chen, L.; He, J. Anti-Inflammatory Action and Mechanisms of Resveratrol. *Mol. Basel Switz.* **2021**, *26*, 229, doi:10.3390/molecules26010229.
60. Boots, A.W.; Haenen, G.R.M.M.; Bast, A. Health Effects of Quercetin: From Antioxidant to Nutraceutical. *Eur. J. Pharmacol.* **2008**, *585*, 325–337, doi:10.1016/j.ejphar.2008.03.008.
61. Pyrzynska, K.; Sentkowska, A. Chapter 21 - Chromatographic Analysis of Polyphenols. In *Polyphenols in Plants (Second Edition)*; Watson, R.R., Ed.; Academic Press, 2019; pp. 353–364 ISBN 978-0-12-813768-0.
62. Liu, X.; Xie, J.; Zhou, L.; Zhang, J.; Chen, Z.; Xiao, J.; Cao, Y.; Xiao, H. Recent Advances in Health Benefits and Bioavailability of Dietary Astaxanthin and Its Isomers. *Food Chem.* **2023**, *404*, 134605, doi:10.1016/j.foodchem.2022.134605.
63. Brenner, M.B.; Wüst, M.; Kuentz, M.; Wagner, K.G. High Loading of Lipophilic Compounds in Mesoporous Silica for Improved Solubility and Dissolution Performance. *Int. J. Pharm.* **2024**, *654*, 123946, doi:10.1016/j.ijpharm.2024.123946.
64. da Silveira Vasconcelos, M.; de Oliveira, L.M.N.; Nunes-Pinheiro, D.C.S.; da Silva Mendes, F.R.; de Sousa, F.D.; de Siqueira Oliveira, L.; de Aquino, A.C.; de Fátima Goebel de Souza, T.; Silva, A.S.; Nabavi, S.M.; et al. Chapter 12 - Analysis of Tetraterpenes and Tetraterpenoids (Carotenoids). In *Recent Advances in Natural Products Analysis*; Sanches Silva, A., Nabavi, S.F., Saeedi, M., Nabavi, S.M., Eds.; Elsevier, 2020; pp. 427–456 ISBN 978-0-12-816455-6.
65. Etzbach, L.; Pfeiffer, A.; Weber, F.; Schieber, A. Characterization of Carotenoid Profiles in Goldenberry (Physalis Peruviana L.) Fruits at Various Ripening Stages and in Different Plant Tissues by HPLC-DAD-APCI-MSn. *Food Chem.* **2018**, *245*, 508–517, doi:10.1016/j.foodchem.2017.10.120.
66. Brenner, M.B.; Wüst, M.; Frank, J.; Wagner, K.G. In Vivo Predictive Dissolution of the Lipophilic Phytochemicals Trans-Resveratrol, Coenzyme Q10 and Quercetin. *J. Drug Deliv. Sci. Technol.* **2024**, *95*, 105561, doi:10.1016/j.jddst.2024.105561.
67. Manufacturer Information on Quercefit® Composition. Available online: https://www.indena.com/product/quercefit/ (accessed on 31 October 2023).
68. Mihaylova, D.; Schalow, S. Antioxidant and Stabilization Activity of a Quercetin-Containing Flavonoid Extract Obtained from Bulgarian Sophora Japonica L. *Braz. Arch. Biol. Technol.* **2013**, *56*, 431–438, doi:10.1590/S1516-89132013000300011.
69. Brenner, M.B.; Flory, S.; Wüst, M.; Frank, J.; Wagner, K. Novel Biphasic In Vitro Dissolution Method Correctly Predicts the Oral Bioavailability of Curcumin in Humans. *J. Agric. Food Chem.* **2023**, doi:https://doi.org/10.1021/acs.jafc.3c04990.
70. Hanne Hjorth Tonnesen, Jan Karlsen Studies on Curcumin and Curcuminoids: VI. Kinetics of Curcumin Degradation in Aqueous Solution. *Z Leb. Unters Forsch* **1985**, *180*, 402–404.

71. Zimányi, L.; Thekkan, S.; Eckert, B.; Condren, A.R.; Dmitrenko, O.; Kuhn, L.R.; Alabugin, I.V.; Saltiel, J. Determination of the pKa Values of Trans-Resveratrol, a Triphenolic Stilbene, by Singular Value Decomposition. Comparison with Theory. *J. Phys. Chem. A* **2020**, *124*, 6294–6302, doi:10.1021/acs.jpca.0c04792.
72. Mano, C.M.; Guaratini, T.; Cardozo, K.H.M.; Colepicolo, P.; Bechara, E.J.H.; Barros, M.P. Astaxanthin Restrains Nitrative-Oxidative Peroxidation in Mitochondrial-Mimetic Liposomes: A Pre-Apoptosis Model. *Mar. Drugs* **2018**, *16*, 126, doi:10.3390/md16040126.
73. Herrero-Martínez, J.M.; Sanmartin, M.; Rosés, M.; Bosch, E.; Ràfols, C. Determination of Dissociation Constants of Flavonoids by Capillary Electrophoresis. *ELECTROPHORESIS* **2005**, *26*, 1886–1895, doi:10.1002/elps.200410258.
74. Trumpower, B. *Function of Quinones in Energy Conserving Systems*; Elsevier, 2012; ISBN 978-0-323-14468-1.
75. Tekin, E.D.; Erkoc, S. Structural and Electronic Features of the Ubiquinone and Ubiquinol Molecules: Molecular Dynamics and Quantum Chemical Treatments. *Mol. Simul.* **2010**, *36*, 763–771, doi:10.1080/08927021003752838.
76. Sy, C.; Gleize, B.; Dangles, O.; Landrier, J.-F.; Veyrat, C.C.; Borel, P. Effects of Physicochemical Properties of Carotenoids on Their Bioaccessibility, Intestinal Cell Uptake, and Blood and Tissue Concentrations. *Mol. Nutr. Food Res.* **2012**, *56*, 1385–1397, doi:10.1002/mnfr.201200041.
77. Rastogi, H.; Jana, S. Evaluation of Physicochemical Properties and Intestinal Permeability of Six Dietary Polyphenols in Human Intestinal Colon Adenocarcinoma Caco-2 Cells. *Eur. J. Drug Metab. Pharmacokinet.* **2016**, *41*, 33–43, doi:10.1007/s13318-014-0234-5.
78. Balakrishnan, P.; Lee, B.-J.; Oh, D.H.; Kim, J.O.; Lee, Y.-I.; Kim, D.-D.; Jee, J.-P.; Lee, Y.-B.; Woo, J.S.; Yong, C.S.; et al. Enhanced Oral Bioavailability of Coenzyme Q10 by Self-Emulsifying Drug Delivery Systems. *Int. J. Pharm.* **2009**, *374*, 66–72, doi:10.1016/j.ijpharm.2009.03.008.
79. Grady, H.; Elder, D.; Webster, G.K.; Mao, Y.; Lin, Y.; Flanagan, T.; Mann, J.; Blanchard, A.; Cohen, M.J.; Lin, J.; et al. Industry's View on Using Quality Control, Biorelevant, and Clinically Relevant Dissolution Tests for Pharmaceutical Development, Registration, and Commercialization. *J. Pharm. Sci.* **2018**, *107*, 34–41, doi:10.1016/j.xphs.2017.10.019.
80. McClements, D.J.; Zou, L.; Zhang, R.; Salvia-Trujillo, L.; Kumosani, T.; Xiao, H. Enhancing Nutraceutical Performance Using Excipient Foods: Designing Food Structures and Compositions to Increase Bioavailability. *Compr. Rev. Food Sci. Food Saf.* **2015**, *14*, 824–847, doi:10.1111/1541-4337.12170.
81. Food and Drug Administration Guidance for Industry; Dissolution Testing of Immediate Release Solid Oral Dosage Forms 1997.
82. Bevernage, J.; Brouwers, J.; Brewster, M.E.; Augustijns, P. Evaluation of Gastrointestinal Drug Supersaturation and Precipitation: Strategies and Issues. *Int. J. Pharm.* **2013**, *453*, 25–35, doi:10.1016/j.ijpharm.2012.11.026.
83. Phillips, D.J.; Pygall, S.R.; Cooper, V.B.; Mann, J.C. Overcoming Sink Limitations in Dissolution Testing: A Review of Traditional Methods and the Potential Utility of Biphasic Systems. *J. Pharm. Pharmacol.* **2012**, *64*, 1549–1559, doi:10.1111/j.2042-7158.2012.01523.x.

84. *Europäisches Arzneibuch 10. Ausgabe, Grundwerk 2020*; Deutscher Apotheker Verlag, 2020;
85. *USP 42 - NF 37 The United States Pharmacopeia and National Formulary*; Deutscher Apotheker Verlag, 2019;
86. Butler, J.; Hens, B.; Vertzoni, M.; Brouwers, J.; Berben, P.; Dressman, J.; Andreas, C.J.; Schaefer, K.J.; Mann, J.; McAllister, M.; et al. In Vitro Models for the Prediction of in Vivo Performance of Oral Dosage Forms: Recent Progress from Partnership through the IMI OrBiTo Collaboration. *Eur. J. Pharm. Biopharm.* **2019**, *136*, 70–83, doi:10.1016/j.ejpb.2018.12.010.
87. Vertzoni, M.; Augustijns, P.; Grimm, M.; Koziolek, M.; Lemmens, G.; Parrott, N.; Pentafragka, C.; Reppas, C.; Rubbens, J.; Van Den Abeele, J.; et al. Impact of Regional Differences along the Gastrointestinal Tract of Healthy Adults on Oral Drug Absorption: An UNGAP Review. *Eur. J. Pharm. Sci.* **2019**, *134*, 153–175, doi:10.1016/j.ejps.2019.04.013.
88. Heigoldt, U.; Sommer, F.; Daniels, R.; Wagner, K.-G. Predicting in Vivo Absorption Behavior of Oral Modified Release Dosage Forms Containing pH-Dependent Poorly Soluble Drugs Using a Novel pH-Adjusted Biphasic in Vitro Dissolution Test. *Eur. J. Pharm. Biopharm.* **2010**, *76*, 105–111, doi:10.1016/j.ejpb.2010.05.006.
89. Frank, K.J.; Locher, K.; Zecevic, D.E.; Fleth, J.; Wagner, K.G. In Vivo Predictive Mini-Scale Dissolution for Weak Bases: Advantages of pH-Shift in Combination with an Absorptive Compartment. *Eur. J. Pharm. Sci. Off. J. Eur. Fed. Pharm. Sci.* **2014**, *61*, 32–39, doi:10.1016/j.ejps.2013.12.015.
90. Locher, K.; Borghardt, J.M.; Frank, K.J.; Kloft, C.; Wagner, K.G. Evolution of a Mini-Scale Biphasic Dissolution Model: Impact of Model Parameters on Partitioning of Dissolved API and Modelling of in Vivo-Relevant Kinetics. *Eur. J. Pharm. Biopharm. Off. J. Arbeitsgemeinschaft Pharm. Verfahrenstechnik EV* **2016**, *105*, 166–175, doi:10.1016/j.ejpb.2016.06.008.
91. Marques, G.S.; Leão, W.F.; Lyra, M.A.M.; Peixoto, M.S.; Monteiro, R.P.M.; Rolim, L.A.; Xavier, H.S.; Neto, P.J.R.; Soares, L.A.L. Comparative Evaluation of UV/VIS and HPLC Analytical Methodologies Applied for Quantification of Flavonoids from Leaves of Bauhinia Forficata. *Rev. Bras. Farmacogn.* **2013**, *23*, 51–57, doi:10.1590/S0102-695X2012005000143.
92. Fuloria, S.; Sekar, M.; Khattulanuar, F.S.; Gan, S.H.; Rani, N.N.I.M.; Ravi, S.; Subramaniyan, V.; Jeyabalan, S.; Begum, M.Y.; Chidambaram, K.; et al. Chemistry, Biosynthesis and Pharmacology of Viniferin: Potential Resveratrol-Derived Molecules for New Drug Discovery, Development and Therapy. *Molecules* **2022**, *27*, 5072, doi:10.3390/molecules27165072.
93. Wang, R.; Han, J.; Jiang, A.; Huang, R.; Fu, T.; Wang, L.; Zheng, Q.; Li, W.; Li, J. Involvement of Metabolism-Permeability in Enhancing the Oral Bioavailability of Curcumin in Excipient-Free Solid Dispersions Co-Formed with Piperine. *Int. J. Pharm.* **2019**, *561*, 9–18, doi:10.1016/j.ijpharm.2019.02.027.
94. Jung, J.-Y.; Yoo, S.D.; Lee, S.-H.; Kim, K.-H.; Yoon, D.-S.; Lee, K.-H. Enhanced Solubility and Dissolution Rate of Itraconazole by a Solid Dispersion Technique. *Int. J. Pharm.* **1999**, *187*, 209–218, doi:10.1016/S0378-5173(99)00191-X.
95. Dizaj, S.M.; Vazifehasl, Zh.; Salatin, S.; Adibkia, Kh.; Javadzadeh, Y. Nanosizing of Drugs: Effect on Dissolution Rate. *Res. Pharm. Sci.* **2015**, *10*, 95–108.

96. Kohli, K.; Chopra, S.; Dhar, D.; Arora, S.; Khar, R.K. Self-Emulsifying Drug Delivery Systems: An Approach to Enhance Oral Bioavailability. *Drug Discov. Today* **2010**, *15*, 958–965, doi:10.1016/j.drudis.2010.08.007.
97. Jacob, S.; Nair, A.B. Cyclodextrin Complexes: Perspective from Drug Delivery and Formulation. *Drug Dev. Res.* **2018**, *79*, 201–217, doi:10.1002/ddr.21452.
98. Ainurofiq, A.; Putro, D.S.; Ramadhani, D.A.; Putra, G.M.; Do Espirito Santo, L.D.C. A Review on Solubility Enhancement Methods for Poorly Water-Soluble Drugs. *J. Rep. Pharm. Sci.* **2021**, *10*, 137, doi:10.4103/jrptps.JRPTPS_134_19.
99. Machado, T.C.; Kuminek, G.; Cardoso, S.G.; Rodríguez-Hornedo, N. The Role of pH and Dose/Solubility Ratio on Cocrystal Dissolution, Drug Supersaturation and Precipitation. *Eur. J. Pharm. Sci.* **2020**, *152*, 105422, doi:10.1016/j.ejps.2020.105422.
100. Chakravarthy, P.S.A.; Grandhi, S.; Swami, R.; Singh, I. Quality by Design Based Optimization and Development of Cyclodextrin Inclusion Complexes of Quercetin for Solubility Enhancement.
101. Gan, Y.; Baak, J.P.A.; Chen, T.; Ye, H.; Liao, W.; Lv, H.; Wen, C.; Zheng, S. Supersaturation and Precipitation Applicated in Drug Delivery Systems: Development Strategies and Evaluation Approaches. *Molecules* **2023**, *28*, 2212, doi:10.3390/molecules28052212.
102. Ajazuddin; Saraf, S. Applications of Novel Drug Delivery System for Herbal Formulations. *Fitoterapia* **2010**, *81*, 680–689, doi:10.1016/j.fitote.2010.05.001.
103. Mirzaei, H.; Shakeri, A.; Rashidi, B.; Jalili, A.; Banikazemi, Z.; Sahebkar, A. Phytosomal Curcumin: A Review of Pharmacokinetic, Experimental and Clinical Studies. *Biomed. Pharmacother.* **2017**, *85*, 102–112, doi:10.1016/j.biopha.2016.11.098.
104. Purpura, M.; Lowery, R.P.; Wilson, J.M.; Mannan, H.; Münch, G.; Razmovski-Naumovski, V. Analysis of Different Innovative Formulations of Curcumin for Improved Relative Oral Bioavailability in Human Subjects. *Eur. J. Nutr.* **2018**, *57*, 929–938, doi:10.1007/s00394-016-1376-9.
105. Dahan, A.; Miller, J.M.; Hoffman, A.; Amidon, G.E.; Amidon, G.L. The Solubility–Permeability Interplay in Using Cyclodextrins as Pharmaceutical Solubilizers: Mechanistic Modeling and Application to Progesterone. *J. Pharm. Sci.* **2010**, *99*, 2739–2749, doi:10.1002/jps.22033.
106. Sujja-areevath, J.; Munday, D.L.; Cox, P.J.; Khan, K.A. Relationship between Swelling, Erosion and Drug Release in Hydrophillic Natural Gum Mini-Matrix Formulations. *Eur. J. Pharm. Sci.* **1998**, *6*, 207–217, doi:10.1016/S0928-0987(97)00072-9.
107. Neslihan Gursoy, R.; Benita, S. Self-Emulsifying Drug Delivery Systems (SEDDS) for Improved Oral Delivery of Lipophilic Drugs. *Biomed. Pharmacother.* **2004**, *58*, 173–182, doi:10.1016/j.biopha.2004.02.001.
108. Miller, J.M.; Beig, A.; Krieg, B.J.; Carr, R.A.; Borchardt, T.B.; Amidon, G.E.; Amidon, G.L.; Dahan, A. The Solubility–Permeability Interplay: Mechanistic Modeling and Predictive Application of the Impact of Micellar Solubilization on Intestinal Permeation. *Mol. Pharm.* **2011**, *8*, 1848–1856, doi:10.1021/mp200181v.
109. Zhao, X.-H.; Tang, C.-H. Spray-Drying Microencapsulation of CoQ 10 in Olive Oil for Enhanced Water Dispersion, Stability and Bioaccessibility: Influence of Type of Emulsifiers and/or Wall Materials. *Food Hydrocoll.* **2016**, *61*, 20–30, doi:10.1016/j.foodhyd.2016.04.045.

110. Neuwirth, M.; Kappes, S.K.; Hartig, M.U.; Wagner, K.G. Amorphous Solid Dispersions Layered onto Pellets—An Alternative to Spray Drying? *Pharmaceutics* **2023**, *15*, 764, doi:10.3390/pharmaceutics15030764.
111. Nanavati, D.B. Phytosome: A Novel Approach to Enhance the Bioavailability of Phytoconstituent. *Asian J. Pharm. AJP* **2017**, *11*, doi:10.22377/ajp.v11i03.1445.
112. Cuomo, J.; Appendino, G.; Dern, A.S.; Schneider, E.; McKinnon, T.P.; Brown, M.J.; Togni, S.; Dixon, B.M. Comparative Absorption of a Standardized Curcuminoid Mixture and Its Lecithin Formulation. *J. Nat. Prod.* **2011**, *74*, 664–669, doi:10.1021/np1007262.
113. Singh, S.; Bajpai, M.; Mishra, P. Self-Emulsifying Drug Delivery System (SEDDS): An Emerging Dosage Form to Improve the Bioavailability of Poorly Absorbed Drugs. *Crit. Rev. Ther. Drug Carr. Syst.* **2020**, *37*, doi:10.1615/CritRevTherDrugCarrierSyst.2020033111.
114. Olejnik, A.; Goscianska, J.; Nowak, I. Active Compounds Release from Semisolid Dosage Forms. *J. Pharm. Sci.* **2012**, *101*, 4032–4045, doi:10.1002/jps.23289.
115. Aung, W.T.; Boonkanokwong, V. Preparation, Optimization Using a Mixture Design, and Characterization of a Novel Astaxanthin-Loaded Rice Bran Oil Self-Microemulsifying Delivery System Formulation. *J. Dispers. Sci. Technol.* **2023**, *44*, 1336–1349, doi:10.1080/01932691.2021.2016436.
116. Locher, K.; Borghardt, J.M.; Frank, K.J.; Kloft, C.; Wagner, K.G. Evolution of a Mini-Scale Biphasic Dissolution Model: Impact of Model Parameters on Partitioning of Dissolved API and Modelling of in Vivo-Relevant Kinetics. *Eur. J. Pharm. Biopharm.* **2016**, *105*, 166–175, doi:10.1016/j.ejpb.2016.06.008.
117. Teaima, M. et al. Comparative, Crossover, Single-Dose, Two-Way, Open-Label Study to Determine the Pharmacokinetic Parameters of Astaxanthin. *Eur J Drug Metab Pharmacokinet* **2024**, *49*.
118. Brenner, M.B.; Frank, J.; Wüst, M.; Wagner, K.G. Biphasische Freisetzung: Ein Schnelles Und Effizientes In-Vitro-Verfahren Zur Bewertung Der In-Vivo-Bioverfügbarkeit Curcumin-Haltiger Nahrungsergänzungsmittel. *Lebensmittelchemie* **2024**, *78*, 2–9, doi:10.1002/lemi.202400101.
119. López Mármol, Á.; Fischer, P.L.; Wahl, A.; Schwöbel, D.; Lenz, V.; Sauer, K.; Koziolek, M. Application of Tiny-TIM as a Mechanistic Tool to Investigate the in Vitro Performance of Different Itraconazole Formulations under Physiologically Relevant Conditions. *Eur. J. Pharm. Sci.* **2022**, *173*, 106165, doi:10.1016/j.ejps.2022.106165.
120. Monschke, M.; Wagner, K.G. Amorphous Solid Dispersions of Weak Bases with pH-Dependent Soluble Polymers to Overcome Limited Bioavailability Due to Gastric pH Variability – An in-Vitro Approach. *Int. J. Pharm.* **2019**, *564*, 162–170, doi:10.1016/j.ijpharm.2019.04.034.
121. Bhalani, D.V.; Nutan, B.; Kumar, A.; Singh Chandel, A.K. Bioavailability Enhancement Techniques for Poorly Aqueous Soluble Drugs and Therapeutics. *Biomedicines* **2022**, *10*, 2055, doi:10.3390/biomedicines10092055.
122. Repka, M.A.; Majumdar, S.; Kumar Battu, S.; Srirangam, R.; Upadhye, S.B. Applications of Hot-Melt Extrusion for Drug Delivery. *Expert Opin. Drug Deliv.* **2008**, *5*, 1357–1376, doi:10.1517/17425240802583421.
123. Zhao, J.; Yang, J.; Xie, Y. Improvement Strategies for the Oral Bioavailability of Poorly Water-Soluble Flavonoids: An Overview. *Int. J. Pharm.* **2019**, *570*, 118642, doi:10.1016/j.ijpharm.2019.118642.

124. Gómez-Guillén, M.C.; Montero, M.P. Enhancement of Oral Bioavailability of Natural Compounds and Probiotics by Mucoadhesive Tailored Biopolymer-Based Nanoparticles: A Review. *Food Hydrocoll.* **2021**, *118*, 106772, doi:10.1016/j.foodhyd.2021.106772.
125. Fasinu, P.; Pillay, V.; Ndesendo, V.M.K.; du Toit, L.C.; Choonara, Y.E. Diverse Approaches for the Enhancement of Oral Drug Bioavailability. *Biopharm. Drug Dispos.* **2011**, *32*, 185–209, doi:10.1002/bdd.750.
126. Denninger, A.; Becker, T.; Westedt, U.; Wagner, K.G. Advanced In Vivo Prediction by Introducing Biphasic Dissolution Data into PBPK Models. *Pharmaceutics* **2023**, *15*, 1978, doi:10.3390/pharmaceutics15071978.
127. Loisios-Konstantinidis, I.; Cristofoletti, R.; Fotaki, N.; Turner, D.B.; Dressman, J. Establishing Virtual Bioequivalence and Clinically Relevant Specifications Using in Vitro Biorelevant Dissolution Testing and Physiologically-Based Population Pharmacokinetic Modeling. Case Example: Naproxen. *Eur. J. Pharm. Sci.* **2020**, *143*, 105170, doi:10.1016/j.ejps.2019.105170.
128. Jamwal, R. Bioavailable Curcumin Formulations: A Review of Pharmacokinetic Studies in Healthy Volunteers. *J. Integr. Med.* **2018**, *16*, 367–374, doi:10.1016/j.joim.2018.07.001.
129. Chen, L.; Cao, H.; Huang, Q.; Xiao, J.; Teng, H. Absorption, Metabolism and Bioavailability of Flavonoids: A Review. *Crit. Rev. Food Sci. Nutr.* **2022**, *62*, 7730–7742, doi:10.1080/10408398.2021.1917508.
130. Crane, F.L.; Hatefi, Y.; Lester, R.L.; Widmer, C. Isolation of a Quinone from Beef Heart Mitochondria. *Biochim. Biophys. Acta* **1957**, *25*, 220–221, doi:10.1016/0006-3002(57)90457-2.
131. Vallee, B.L.; Rupley, J.A.; Coombs, T.L.; Neurath, H. THE RELEASE OF ZINC FROM CARBOXYPEPTIDASE AND ITS REPLACEMENT. *J. Am. Chem. Soc.* **1958**, *80*, 4750–4751, doi:10.1021/ja01550a094.
132. Villalba, J.M.; Parrado, C.; Santos-Gonzalez, M.; Alcain, F.J. Therapeutic Use of Coenzyme Q10 and Coenzyme Q10-Related Compounds and Formulations. *Expert Opin. Investig. Drugs* **2010**, *19*, 535–554, doi:10.1517/13543781003727495.
133. Crane, F.L. Biochemical Functions of Coenzyme Q10. *J. Am. Coll. Nutr.* **2001**, *20*, 591–598, doi:10.1080/07315724.2001.10719063.
134. Pöstges, F.; Kayser, K.; Stoyanov, E.; Wagner, K.G. Boost of Solubility and Supersaturation of Celecoxib via Synergistic Interactions of Methacrylic Acid-Ethyl Acrylate Copolymer (1:1) and Hydroxypropyl Cellulose in Ternary Amorphous Solid Dispersions. *Int. J. Pharm. X* **2022**, *4*, 100115, doi:10.1016/j.ijpx.2022.100115.
135. Bachmaier, R.D.; Monschke, M.; Faber, T.; Krome, A.K.; Pellequer, Y.; Stoyanov, E.; Lamprecht, A.; Wagner, K.G. In Vitro and in Vivo Assessment of Hydroxypropyl Cellulose as Functional Additive for Enabling Formulations Containing Itraconazole. *Int. J. Pharm. X* **2021**, *3*, 100076, doi:10.1016/j.ijpx.2021.100076.
136. Onoue, S.; Terasawa, N.; Nakamura, T.; Yuminoki, K.; Hashimoto, N.; Yamada, S. Biopharmaceutical Characterization of Nanocrystalline Solid Dispersion of Coenzyme Q10 Prepared with Cold Wet-Milling System. *Eur. J. Pharm. Sci.* **2014**, *53*, 118–125, doi:10.1016/j.ejps.2013.12.013.
137. Lopez Marmol, A. Supersaturation and solubilization to enhance the oral bioavailability of poorly soluble drug molecules: A mechanistic investigation of their potential and limitations, Univeristy of Bonn, 2021.

138. Fung, W.Y.; Liong, M.T.; Yuen, K.H. Preparation, in-Vitro and in-Vivo Characterisation of CoQ10 Microparticles: Electrospraying-Enhanced Bioavailability. *J. Pharm. Pharmacol.* **2016**, *68*, 159–169, doi:10.1111/jphp.12502.
139. Beg, S.; Javed, S.; JKohli, K. Bioavailability Enhancement of Coenzyme Q10: An Extensive Review of Patents. *Recent Pat. Drug Deliv. Formul.* **2010**, *4*, 245–257, doi:10.2174/187221110793237565.
140. Monschke, M.; Kayser, K.; Wagner, K.G. Influence of Particle Size and Drug Load on Amorphous Solid Dispersions Containing pH-Dependent Soluble Polymers and the Weak Base Ketoconazole. *AAPS PharmSciTech* **2021**, *22*, 44, doi:10.1208/s12249-020-01914-7.
141. Borde, S.; Paul, S.K.; Chauhan, H. Ternary Solid Dispersions: Classification and Formulation Considerations. *Drug Dev. Ind. Pharm.* **2021**, *47*, 1011–1028, doi:10.1080/03639045.2021.1908342.
142. Akram, A.; Irfan, M.; Abualsunun, W.A.; Bukhary, D.M.; Alissa, M. How to Improve Solubility and Dissolution of Irbesartan by Fabricating Ternary Solid Dispersions: Optimization and In-Vitro Characterization. *Pharmaceutics* **2022**, *14*, 2264, doi:10.3390/pharmaceutics14112264.
143. Kapote, D.N.; Wagner, K.G. Influence of Shellac on the Improvement of Solubility and Supersaturation of Loratadine Amorphous Solid Dispersion Using a New Grade of HPMC. *J. Drug Deliv. Sci. Technol.* **2021**, *61*, 102116, doi:10.1016/j.jddst.2020.102116.
144. Sun, Y.; Zhu, L.; Wu, T.; Cai, T.; Gunn, E.M.; Yu, L. Stability of Amorphous Pharmaceutical Solids: Crystal Growth Mechanisms and Effect of Polymer Additives. *AAPS J.* **2012**, *14*, 380–388, doi:10.1208/s12248-012-9345-6.
145. Hancock, B.C.; Parks, M. What Is the True Solubility Advantage for Amorphous Pharmaceuticals? *Pharm. Res.* **2000**, *17*, 397–404, doi:10.1023/A:1007516718048.
146. Monschke, M.; Kayser, K.; Wagner, K.G. Processing of Polyvinyl Acetate Phthalate in Hot-Melt Extrusion—Preparation of Amorphous Solid Dispersions. *Pharmaceutics* **2020**, *12*, 337, doi:10.3390/pharmaceutics12040337.
147. Seljak, K.B.; Kocbek, P.; Gašperlin, M. Mesoporous Silica Nanoparticles as Delivery Carriers: An Overview of Drug Loading Techniques. *J. Drug Deliv. Sci. Technol.* **2020**, *59*, 101906, doi:10.1016/j.jddst.2020.101906.
148. Ditzinger, F.; Price, D.J.; Nair, A.; Becker-Baldus, J.; Glaubitz, C.; Dressman, J.B.; Saal, C.; Kuentz, M. Opportunities for Successful Stabilization of Poor Glass-Forming Drugs: A Stability-Based Comparison of Mesoporous Silica Versus Hot Melt Extrusion Technologies. *Pharmaceutics* **2019**, *11*, 577, doi:10.3390/pharmaceutics11110577.
149. Ditzinger, F.; Price, D.J.; Ilie, A.-R.; Köhl, N.J.; Jankovic, S.; Tsakiridou, G.; Aleandri, S.; Kalantzi, L.; Holm, R.; Nair, A.; et al. Lipophilicity and Hydrophobicity Considerations in Bio-Enabling Oral Formulations Approaches – a PEARRL Review. *J. Pharm. Pharmacol.* **2019**, *71*, 464–482, doi:10.1111/jphp.12984.
150. Vraníková, B.; Niederquell, A.; Šklubalová, Z.; Kuentz, M. Relevance of the Theoretical Critical Pore Radius in Mesoporous Silica for Fast Crystallizing Drugs. *Int. J. Pharm.* **2020**, *591*, 120019, doi:10.1016/j.ijpharm.2020.120019.
151. Knapik, J.; Wojnarowska, Z.; Grzybowska, K.; Jurkiewicz, K.; Stankiewicz, A.; Paluch, M. Stabilization of the Amorphous Ezetimibe Drug by Confining Its Dimension. *Mol. Pharm.* **2016**, *13*, 1308–1316, doi:10.1021/acs.molpharmaceut.5b00903.

152. Jannel, S.; Caro, Y.; Bermudes, M.; Petit, T. Novel Insights into the Biotechnological Production of Haematococcus Pluvialis-Derived Astaxanthin: Advances and Key Challenges to Allow Its Industrial Use as Novel Food Ingredient. *J. Mar. Sci. Eng.* **2020**, *8*, 789, doi:10.3390/jmse8100789.
153. Gershkovich, P.; Hoffman, A. Uptake of Lipophilic Drugs by Plasma Derived Isolated Chylomicrons: Linear Correlation with Intestinal Lymphatic Bioavailability. *Eur. J. Pharm. Sci.* **2005**, *26*, 394–404, doi:10.1016/j.ejps.2005.07.011.
154. du Plessis, L.H.; Govender, K.; Denti, P.; Wiesner, L. In Vivo Efficacy and Bioavailability of Lumefantrine: Evaluating the Application of Pheroid Technology. *Eur. J. Pharm. Biopharm.* **2015**, *97*, 68–77, doi:10.1016/j.ejpb.2015.10.001.
155. Mano, C.M.; Guaratini, T.; Cardozo, K.H.M.; Colepicolo, P.; Bechara, E.J.H.; Barros, M.P. Astaxanthin Restrains Nitrative-Oxidative Peroxidation in Mitochondrial-Mimetic Liposomes: A Pre-Apoptosis Model. *Mar. Drugs* **2018**, *16*, 126, doi:10.3390/md16040126.
156. Patel, K.; Sarma, V.; Vavia, P. Design and Evaluation of Lumefantrine – Oleic Acid Self Nanoemulsifying Ionic Complex for Enhanced Dissolution. *DARU J. Pharm. Sci.* **2013**, *21*, 27, doi:10.1186/2008-2231-21-27.
157. Probucol: DrugBank Online. Available online: https://go.drugbank.com/drugs/DB01599 (accessed on 25 October 2023).
158. Katsikas, H.; Quinn, P.J. The Polyisoprenoid Chain Length Influences the Interaction of Ubiquinones with Phospholipid Bilayers. *Biochim. Biophys. Acta BBA - Biomembr.* **1982**, *689*, 363–369, doi:10.1016/0005-2736(82)90270-X.
159. Trzeciak, K.; Chotera-Ouda, A.; Bak-Sypien, I.I.; Potrzebowski, M.J. Mesoporous Silica Particles as Drug Delivery Systems—The State of the Art in Loading Methods and the Recent Progress in Analytical Techniques for Monitoring These Processes. *Pharmaceutics* **2021**, *13*, 950, doi:10.3390/pharmaceutics13070950.
160. Le, T.-T.; Elzhry Elyafi, A.K.; Mohammed, A.R.; Al-Khattawi, A. Delivery of Poorly Soluble Drugs via Mesoporous Silica: Impact of Drug Overloading on Release and Thermal Profiles. *Pharmaceutics* **2019**, *11*, 269, doi:10.3390/pharmaceutics11060269.
161. International council for harmonisation Impurities: Guidline for Residual Solvents Q3C (R8) 2021.
162. Kissi, E.O.; Ruggiero, M.T.; Hempel, N.-J.; Song, Z.; Grohganz, H.; Rades, T.; Löbmann, K. Characterising Glass Transition Temperatures and Glass Dynamics in Mesoporous Silica-Based Amorphous Drugs. *Phys. Chem. Chem. Phys.* **2019**, *21*, 19686–19694, doi:10.1039/C9CP01764J.
163. Willeit, E. Astaxanthin - the Red Diamond Amongst Antioxidants: A Powerful Ingredient to Support a Radiant and Healthy Skin. *SOFW J. Engl. Version* **2022**, *148*, 22–27.
164. Cokenakes, G. Liquid Imbibition into Mesoporous Silica, University of the Sciences: Philadelphia, 2021.
165. Waters, L.J.; Hanrahan, J.P.; Tobin, J.M.; Finch, C.V.; Parkes, G.M.B.; Ahmad, S.A.; Mohammad, F.; Saleem, M. Enhancing the Dissolution of Phenylbutazone Using Syloid® Based Mesoporous Silicas for Oral Equine Applications. *J. Pharm. Anal.* **2018**, *8*, 181–186, doi:10.1016/j.jpha.2018.01.004.

166. Kostelanská, K.; Prudilová, B.B.; Holešová, S.; Vlček, J.; Vetchý, D.; Gajdziok, J. Comparative Study of Powder Carriers Physical and Structural Properties. *Pharmaceutics* **2022**, *14*, 818, doi:10.3390/pharmaceutics14040818.
167. Shen, S.-C.; Dong, Y.-C.; Letchmanan, K.; Ng, W.K. Chapter 23 - Mesoporous Materials and Technologies for Development of Oral Medicine. In *Nanostructures for Oral Medicine*; Andronescu, E., Grumezescu, A.M., Eds.; Micro and Nano Technologies; Elsevier, 2017; pp. 699–749 ISBN 978-0-323-47720-8.
168. Hate, S.S.; Reutzel-Edens, S.M.; Taylor, L.S. Interplay of Adsorption, Supersaturation and the Presence of an Absorptive Sink on Drug Release from Mesoporous Silica-Based Formulations. *Pharm. Res.* **2020**, *37*, 163, doi:10.1007/s11095-020-02879-9.
169. Antonino, R.S.C.M.Q.; Ruggiero, M.; Song, Z.; Nascimento, T.L.; Lima, E.M.; Bohr, A.; Knopp, M.M.; Löbmann, K. Impact of Drug Loading in Mesoporous Silica-Amorphous Formulations on the Physical Stability of Drugs with High Recrystallization Tendency. *Int. J. Pharm. X* **2019**, *1*, 100026, doi:10.1016/j.ijpx.2019.100026.
170. Singh, A.; Van den Mooter, G. Spray Drying Formulation of Amorphous Solid Dispersions. *Adv. Drug Deliv. Rev.* **2016**, *100*, 27–50, doi:10.1016/j.addr.2015.12.010.
171. Dening, T.J.; Taylor, L.S. Supersaturation Potential of Ordered Mesoporous Silica Delivery Systems. Part 1: Dissolution Performance and Drug Membrane Transport Rates. *Mol. Pharm.* **2018**, *15*, 3489–3501, doi:10.1021/acs.molpharmaceut.8b00488.
172. Price, D.J.; Nair, A.; Kuentz, M.; Dressman, J.; Saal, C. Calculation of Drug-Polymer Mixing Enthalpy as a New Screening Method of Precipitation Inhibitors for Supersaturating Pharmaceutical Formulations. *Eur. J. Pharm. Sci.* **2019**, *132*, 142–156, doi:10.1016/j.ejps.2019.03.006.
173. Price, D.J.; Ditzinger, F.; Koehl, N.J.; Jankovic, S.; Tsakiridou, G.; Nair, A.; Holm, R.; Kuentz, M.; Dressman, J.B.; Saal, C. Approaches to Increase Mechanistic Understanding and Aid in the Selection of Precipitation Inhibitors for Supersaturating Formulations – a PEARRL Review. *J. Pharm. Pharmacol.* **2019**, *71*, 483–509, doi:10.1111/jphp.12927.
174. Mersmann, A. *Crystallization Technology Handbook*; CRC Press, 2001; ISBN 978-0-203-90828-0.
175. Laghezza, G.; Dietrich, E.; M. Yeomans, J.; Ledesma-Aguilar, R.; Stefan Kooij, E.; W. Zandvliet, H.J.; Lohse, D. Collective and Convective Effects Compete in Patterns of Dissolving Surface Droplets. *Soft Matter* **2016**, *12*, 5787–5796, doi:10.1039/C6SM00767H.
176. Kanaujia, P.; Poovizhi, P.; Ng, W.K.; Tan, R.B.H. Amorphous Formulations for Dissolution and Bioavailability Enhancement of Poorly Soluble APIs. *Powder Technol.* **2015**, *285*, 2–15, doi:10.1016/j.powtec.2015.05.012.
177. Frank, K.J.; Rosenblatt, K.M.; Westedt, U.; Hölig, P.; Rosenberg, J.; Mägerlein, M.; Fricker, G.; Brandl, M. Amorphous Solid Dispersion Enhances Permeation of Poorly Soluble ABT-102: True Supersaturation vs. Apparent Solubility Enhancement. *Int. J. Pharm.* **2012**, *437*, 288–293, doi:10.1016/j.ijpharm.2012.08.014.
178. Mellaerts, R.; Mols, R.; Jammaer, J.A.G.; Aerts, C.A.; Annaert, P.; Van Humbeeck, J.; Van den Mooter, G.; Augustijns, P.; Martens, J.A. Increasing the Oral Bioavailability

of the Poorly Water Soluble Drug Itraconazole with Ordered Mesoporous Silica. *Eur. J. Pharm. Biopharm.* **2008**, *69*, 223–230, doi:10.1016/j.ejpb.2007.11.006.

179. Dening, T.J.; Zemlyanov, D.; Taylor, L.S. Application of an Adsorption Isotherm to Explain Incomplete Drug Release from Ordered Mesoporous Silica Materials under Supersaturating Conditions. *J. Controlled Release* **2019**, *307*, 186–199, doi:10.1016/j.jconrel.2019.06.028.
180. McCarthy, C.A.; Ahern, R.J.; Devine, K.J.; Crean, A.M. Role of Drug Adsorption onto the Silica Surface in Drug Release from Mesoporous Silica Systems. *Mol. Pharm.* **2018**, *15*, 141–149, doi:10.1021/acs.molpharmaceut.7b00778.
181. Mellaerts, R.; Houthoofd, K.; Elen, K.; Chen, H.; Van Speybroeck, M.; Van Humbeeck, J.; Augustijns, P.; Mullens, J.; Van den Mooter, G.; Martens, J.A. Aging Behavior of Pharmaceutical Formulations of Itraconazole on SBA-15 Ordered Mesoporous Silica Carrier Material. *Microporous Mesoporous Mater.* **2010**, *130*, 154–161, doi:10.1016/j.micromeso.2009.10.026.
182. Mellaerts, R.; Jammaer, J.A.G.; Van Speybroeck, M.; Chen, H.; Humbeeck, J.V.; Augustijns, P.; Van den Mooter, G.; Martens, J.A. Physical State of Poorly Water Soluble Therapeutic Molecules Loaded into SBA-15 Ordered Mesoporous Silica Carriers: A Case Study with Itraconazole and Ibuprofen. *Langmuir* **2008**, *24*, 8651–8659, doi:10.1021/la801161g.
183. Schulz, C.; Obermüller-Jevic, U.C.; Hasselwander, O.; Bernhardt, J.; Biesalski, H.K. Comparison of the Relative Bioavailability of Different Coenzyme Q10 Formulations with a Novel Solubilizate (Solu^{TM} Q10). *Int. J. Food Sci. Nutr.* **2006**, *57*, 546–555, doi:10.1080/09637480601058320.
184. Ilevbare, G.A.; Taylor, L.S. Liquid–Liquid Phase Separation in Highly Supersaturated Aqueous Solutions of Poorly Water-Soluble Drugs: Implications for Solubility Enhancing Formulations. *Cryst. Growth Des.* **2013**, *13*, 1497–1509, doi:10.1021/cg301679h.
185. Indulkar, A.S.; Gao, Y.; Raina, S.A.; Zhang, G.G.Z.; Taylor, L.S. Exploiting the Phenomenon of Liquid–Liquid Phase Separation for Enhanced and Sustained Membrane Transport of a Poorly Water-Soluble Drug. *Mol. Pharm.* **2016**, *13*, 2059–2069, doi:10.1021/acs.molpharmaceut.6b00202.
186. Dokania, S.; Joshi, A.K. Self-Microemulsifying Drug Delivery System (SMEDDS) – Challenges and Road Ahead. *Drug Deliv.* **2015**, *22*, 675–690, doi:10.3109/10717544.2014.896058.
187. Lumefantrine: DrugBank Online. Available online: https://go.drugbank.com/drugs/DB06708 (accessed on 25 October 2023).
188. EUDRAGIT®: Technical Information. Available online: https://healthcare.evonik.com/en/drugdelivery/oral-drug-delivery/oral-excipients/eudragit-portfolio (accessed on 25 October 2023).
189. NISSO HPC Grades & Applications. Available online: https://www.nissoexcipients.com/hpc-e/medical_general.php (accessed on 25 October 2023).
190. Technical Information and Posters - For Pharmaceutical : Shin-Etsu Cellulose. Available online: https://www.shinetsu.co.jp/cellulose/en/pharmaceutical/technical.html#techinfo (accessed on 25 October 2023).

191. Kolliphor® P 407: Technical Information. Available online: https://pharma.basf.com/products/kolliphor-p-407-geismar (accessed on 25 October 2023).
192. Soluplus®: Technical Information. Available online: https://pharma.basf.com/products/soluplus (accessed on 25 October 2023).
193. Kollidon® 12 PF: Technical Information. Available online: https://pharma.basf.com/products/kollidon-12-pf (accessed on 25 October 2023).
194. Kollidon® VA 64: Technical Information. Available online: https://pharma.basf.com/products/kollidon-va-64 (accessed on 25 October 2023).
195. Mosca, F.; Fattorini, D.; Bompadre, S.; Littarru, G.P. Assay of Coenzyme Q10 in Plasma by a Single Dilution Step. *Anal. Biochem.* **2002**, *305*, 49–54, doi:10.1006/abio.2002.5653.
196. Xu, S.; Luo, H.; Chen, H.; Guo, J.; Yu, B.; Zhang, H.; Li, W.; Chen, W.; Zhou, X.; Huang, L.; et al. Optimization of Extraction of Total Trans-Resveratrol from Peanut Seeds and Its Determination by HPLC. *J. Sep. Sci.* **2020**, *43*, 1024–1031, doi:10.1002/jssc.201900915.
197. Careri, M.; Corradini, C.; Elviri, L.; Nicoletti, I.; Zagnoni, I. Direct HPLC Analysis of Quercetin and *Trans* -Resveratrol in Red Wine, Grape, and Winemaking Byproducts. *J. Agric. Food Chem.* **2003**, *51*, 5226–5231, doi:10.1021/jf034149g.
198. Kerns, E.H.; Di, L.; Petusky, S.; Kleintop, T.; Huryn, D.; McConnell, O.; Carter, G. Pharmaceutical Profiling Method for Lipophilicity and Integrity Using Liquid Chromatography–Mass Spectrometry. *J. Chromatogr. B* **2003**, *791*, 381–388, doi:10.1016/S1570-0232(03)00250-2.
199. Koziolek, M.; Grimm, M.; Becker, D.; Iordanov, V.; Zou, H.; Shimizu, J.; Wanke, C.; Garbacz, G.; Weitschies, W. Investigation of pH and Temperature Profiles in the GI Tract of Fasted Human Subjects Using the Intellicap® System. *J. Pharm. Sci.* **2015**, *104*, 2855–2863, doi:10.1002/jps.24274.
200. ICH International Conference on Harmonisation of Technical Requirements for Registration of Pharmaceuticals for Human Use (ICH). In *Wiley StatsRef: Statistics Reference Online*; Balakrishnan, N., Colton, T., Everitt, B., Piegorsch, W., Ruggeri, F., Teugels, J.L., Eds.; John Wiley & Sons, Ltd: Chichester, UK, 2014 ISBN 978-1-118-44511-2.
201. Loschen, C.; Klamt, A. COSMOquick: A Novel Interface for Fast σ-Profile Composition and Its Application to COSMO-RS Solvent Screening Using Multiple Reference Solvents. *Ind. Eng. Chem. Res.* **2012**, *51*, 14303–14308, doi:10.1021/ie3023675.